

**UNDERSTANDING TRANSFORMATIONS OF TREHALOSE
IN THE SOLID STATE**

BY

SARAH J. PYSZCZYNSKI

**Submitted to the graduate degree program in Pharmaceutical Chemistry and the
Graduate Faculty of the University of Kansas in partial fulfillment of the
requirements for the degree of Doctor of Philosophy.**

Jennifer S. Laurence

Sue M. Lunte

Eric J. Munson

Michael Z. Wang

Robert G. Carlson

Date Defended: April 19, 2013

The Dissertation Committee for Sarah J. Pyszczynski
certifies that this is the approved version of the following dissertation:

Understanding Transformations of Trehalose in the Solid State

Jennifer S. Laurence

Date approved: April 19, 2013

Abstract

Trehalose has many applications as an excipient in pharmaceutical formulations; however, its use is limited in part because the transformations among the solid forms of trehalose are not yet understood. Form changes that occur during manufacturing or storage of a pharmaceutical formulation can be detrimental to the stability of a drug product, and therefore, understanding the solid-state transformations of trehalose is critical to its increased use in the pharmaceutical industry. In this dissertation, the solid forms of trehalose and the transformations among them are investigated using a variety of techniques, most importantly, differential scanning calorimetry (DSC) and ^{13}C solid-state NMR spectroscopy (SSNMR).

Currently, trehalose is thought to exist in four solid forms: a crystalline dihydrate (T_h), the β -anhydrate (T_β), the α -anhydrate (T_α), and the amorphous form (T_{am}). Using SSNMR, we showed that there is a fifth solid form (T_δ) that is formed when T_h is dehydrated at or below 100 °C. This form is metastable, and like T_α , it rapidly reverts to T_h upon exposure to ambient conditions. T_δ was not detected using powder X-ray diffraction (PXRD), often considered the “gold standard” for polymorph identification, demonstrating the utility of SSNMR in analyzing pharmaceutically relevant systems.

There is significant confusion in the literature regarding which anhydrous forms of trehalose are generated when T_h is dehydrated, and we have demonstrated that source variability and lot-to-lot variability of T_h is a likely source of this confusion. Using DSC, we showed that when sieved T_h is heated at 10 °C/minute, three distinct behaviors are observed: 1) the sample will dehydrate to form T_β directly, 2) the sample will dehydrate to form T_{am} which crystallizes to T_β upon further heating, or 3) the sample will dehydrate

to form T_{am} that remains amorphous. The DSC results were used to develop a classification system that can be used to predict the products of dehydration of T_h under various conditions.

SSNMR was also used to analyze T_{am} prepared via lyophilization and dehydration of T_h , and the results indicate that the subtle structural differences between the samples are not consistent with polyamorphism. However, lyophilized T_{am} appears to be more homogeneous and at a higher energy state than dehydrated T_{am} . A SSNMR subtraction method was developed in order to determine if low levels of T_β or T_β nuclei are present in T_{am} samples, and for several samples with higher tendencies to crystallize to T_β , peaks corresponding to T_β were detected.

The greater understanding of the solid forms of trehalose that was achieved during the experiments described in this dissertation will:

1. Allow materials scientist to explicitly define the relationships among the solid forms of trehalose.
2. Assist pharmaceutical scientists in the development of more stable formulations that contain trehalose.
3. Aid biologists in determining the mechanism by which trehalose stabilizes biomolecules.

Dedicated to:

My Wonderful Family...Love You!

Acknowledgments

So many people have supported and inspired me during graduate school and throughout my life. I may have forgotten to include a few people by name, but I hope you all know how important you are.

I would first like to thank my advisor, Dr. Eric Munson, for his support, guidance, and enthusiasm during my graduate career. I admire his scientific curiosity and interest in tackling any problem that finds him (and as an expert in the field, a LOT of problems find him!). He suggested an “easy, 6-week project” during my second year, and that turned into 4.5 years of frustration and fun thanks to the magic of trehalose. Though his technical expertise was greatly appreciated, I am even more grateful that I always knew how much he cared about his students.

I would also like to thank the members of my dissertation committee: Dr. Jennifer Laurence, Dr. Sue Lunte, Dr. Michael Wang, and Dr. Robert Carlson. Special thanks go to Dr. Laurence for serving as the chair of my committee and for her help during this complicated process. I would also like to thank Dr. Valentino Stella; although scheduling conflicts prevented him from serving on my committee, I appreciate that he was willing to “adopt” the students in the Munson lab.

The members of the Munson lab have been an incredible source of mentoring and friendship: thank you to Dr. Dewey Barich, Dr. Joe Lubach, Dr. Loren Schieber, Dr. Ben Nelson, Dr. Diana Sperger, Dr. Bob Berendt, Dr. Eric Gorman, Dr. Elodie Dempah, Beau Pornputtapitak, and Donia Arthur. Dr. Chris Munson has also been a fantastic honorary member of the lab – from planning group parties to making sure the Kansas/Kentucky transition went as smoothly as possible, her presence has been greatly appreciated. When

Elodie and I started chatting during recruitment events in March 2007, I never would have imagined that we would both come to KU, join the same lab, and then follow Dr. Munson to UK. This has been a difficult process, and I absolutely would not have made it through this experience without Elodie. We have had so many fun times: attending KU basketball games, too many road trips to count (fueled by Twizzlers), a fabulous trip through Europe, lots of waffles and plantains (and champagne), and on and on and on... I am so thankful for our awesome friendship, and I can't wait until one of our career plans becomes a reality. ☺

I am very grateful to the Madison and Lila Self Graduate Fellowship for providing funding and professional development: the generosity of Al and Lila Self is inspiring. Thank you to Howard Mossberg, Cathy Dwigans, Sharon Graham, and Patty Dannenberg for their contributions to such an incredible program. I am especially thankful that I was able to continue as a Self Fellow after moving to Kentucky. I will never forget the friends I made through the SGF, especially Dr. Andrea Romero and Brian O'Neill.

Thank you to the staff members in the Department of Pharmaceutical Chemistry (KU) and the Department of Pharmaceutical Sciences (UK): Nancy Helm, Nicole Brooks, Ann Heptig, Karen Hall, Richard Walker, Catina Rossoll, Tonya Vance, and Todd Sizemore. You've all made life a little easier, and Nancy, Catina, and Todd were especially helpful with the KU/UK transition.

So many friends have made graduate school a much more pleasant experience: Sam and Bob, Katherine, Patrick, Kelly, Courtney, Maria and Matt, Mary, Barlas, Chuda, Supang, Prakash, Leon, Taryn, Josh, Ryan, Ahmed, Talia, Jess, Randy, Josh, Justin,

Shara, Chris, John, Kaci, Dayna, Lindsay, Andrei, Melissa, Carrie, Jen, Ann, Kyle, Nicki, Eleftheria, and so many more! I was lucky to make several friends through the Lexington chapter of the KU Alumni Association: Summer, Tim and Viki, Jana and James, and Aarin. You've all make the transition from one basketball town to another (inferior) basketball town much more fun.

Very, very special thanks to my family: I would not be where I am today without the love, support, and encouragement of my parents and my brother. My mom and dad are brilliant, quirky, and fun, and I'm lucky to be the perfect combination of the two of them. My brother Adam (Dr. Pyszczynski #3) is one of my favorite people in the entire world, and we've survived grad school together despite almost 2000 miles between us. His wife Angie has been a wonderful addition to the family, and I can't wait until we all live closer to each other. I love you all so much!

Table of Contents

	Page
Abstract.....	iii
Dedication.....	v
Acknowledgments.....	vi
Table of Contents.....	ix
Chapter 1. Introduction.....	1
1.1 Objectives.....	2
1.2 Introduction to Trehalose.....	2
1.3 Applications of Trehalose.....	4
1.3.1 Food, Cosmetic, and Medical Applications.....	4
1.3.2 Pharmaceutical Industry.....	5
1.4 Solid-State Stability of Trehalose.....	7
1.4.1 Solid-State Forms and Transformations of Trehalose.....	7
1.4.2 Trehalose as a Model Compound to Study the Amorphous State.....	9
1.5 Overview of Thesis Work.....	12
1.5.1 Solid-state Characterization Techniques.....	12
1.5.2 Literature Review.....	13
1.5.3 Initial Solid-State Characterization of Trehalose.....	13
1.5.4 Generation and Characterization of a New Solid Form of Trehalose.....	13

1.5.5 Dehydration of Trehalose Dihydrate: Part I	14
1.5.6 Dehydration of Trehalose Dihydrate: Part II	14
1.5.7 Characterization of Amorphous Trehalose Prepared By Lyophilization and Dehydration of Trehalose Dihydrate	15
1.5.9 Detection of Low Levels of Crystallinity Using SSNMR	15
1.5.10 Summary and Suggestions for Future Work.....	15
1.6 References.....	16
Chapter 2. Solid-State Characterization Techniques and Applications to the Trehalose System.....	22
2.1 Introduction.....	23
2.2 Polarized Light Microscopy (PLM).....	23
2.3 Powder X-Ray Diffraction (PXRD).....	25
2.4 Differential Scanning Calorimetry (DSC)	27
2.4.1 Conventional Differential Scanning Calorimetry	27
2.4.2 Modulated Differential Scanning Calorimetry (MDSC)	30
2.5 Thermogravimetric Analysis (TGA).....	30
2.6 Solid-State Nuclear Magnetic Resonance Spectroscopy (SSNMR).....	32
2.6.1 Basic NMR Theory	32
2.6.2 Methods for Signal Enhancement in Solid-state NMR Spectroscopy.....	35
2.6.3 SSNMR in the Analysis of Pharmaceutically Relevant Systems	39
2.7 Conclusions.....	43

2.8 References.....	44
Chapter 3. Literature Review	50
3.1 Introduction.....	51
3.2 Conformation and Structure of Trehalose in the Solid Forms	51
3.2.1 Crystalline Forms of Trehalose.....	51
3.2.2 Amorphous Trehalose.....	54
3.3 Dehydration of Trehalose Dihydrate	55
3.3.1 Isothermal Dehydrations of Trehalose Dihydrate.....	55
3.3.2 Non-Isothermal Dehydrations of Trehalose Dihydrate	58
3.3.2.1 Influence of Particle Size on the Dehydration of Trehalose Dihydrate.....	58
3.3.2.2 Influence of Heating Rate on the Dehydration of Trehalose Dihydrate.....	60
3.3.2.3 Influence of Sample Environment on the Dehydration of Trehalose Dihydrate	61
3.4 Physical Stability of Amorphous Trehalose	62
3.4.1 Effect of Aging on the Physical Stability of Amorphous Trehalose.....	62
3.4.2 Effect of Preparation Method on the Physical Stability of Amorphous Trehalose.....	63
3.5 Conclusion	64
3.6 References.....	66
Chapter 4. Initial Solid-State Characterization of Trehalose	71

4.1 Introduction.....	72
4.2 Materials and Methods.....	72
4.2.1 Materials	72
4.2.2 Dehydration	72
4.2.3 Lyophilization.....	73
4.2.4 Differential Scanning Calorimetry.....	73
4.2.5 ¹³ C Solid-State NMR Spectroscopy (SSNMR)	74
4.3 Results.....	74
4.3.1 Characterization of Trehalose Dihydrate (T _h)	74
4.3.2 Dehydration of Trehalose Dihydrate at 100 °C.....	76
4.3.4 Dehydration of Trehalose Dihydrate at 125 °C.....	83
4.3.5 Dehydration of Trehalose Dihydrate at 75 °C.....	83
4.4 Conclusions.....	86
4.5 References.....	87
Chapter 5. Generation and Characterization of a New Solid Form of Trehalose.....	89
5.2 Experimental.....	90
5.2.1 Materials	90
5.2.2 Sieving.....	90
5.2.3 Preparation of Dehydrated Samples	91
5.2.4 ¹³ C Solid-state Nuclear Magnetic Resonance (SSNMR)	
Spectroscopy.....	91
5.2.5 Variable-temperature SSNMR.....	94
5.2.6 Powder X-ray Diffraction (PXRD).....	94

5.2.7 Differential Scanning Calorimetry (DSC)	95
5.3 Results	95
5.3.1 Generation of T_{α} and the Discovery of Unknown Material in Samples of Dehydrated Trehalose	95
5.3.3 Exposure of T_{δ} to Ambient Temperature and Humidity	102
5.3.4 Thermal Behavior of T_{δ}	105
5.3.5 Generation of T_{δ}	109
5.4 Discussion	113
5.4.1 Identification of Unknown Peaks	113
5.4.2 Structure of T_{δ} and Its Role in the Solid-state Chemistry of Trehalose	116
5.5 Conclusion	119
5.6 References	120
Chapter 6. Dehydration of Trehalose Dihydrate: Part I	123
6.1 Introduction	124
6.2 Experimental	124
6.2.1 Materials	124
6.2.2 Sieving	126
6.2.3 Differential Scanning Calorimetry	126
6.2.4 Thermogravimetric Analysis	126
6.2.5 Polarized Light Microscopy	127
6.2.6 ^{13}C Solid-State NMR Spectroscopy	127
6.3 Results and Discussion	128

6.3.1 DSC and TGA Thermograms: Fluka 90210-1.....	128
6.3.2 DSC and TGA Thermograms: Sigma T9449-3	133
6.3.3 DSC and TGA Thermograms: Acros 18255-1	136
6.3.4 DSC and TGA Summary	139
6.3.5 Analysis of Endotherm Near 100 °C	139
6.3.5 Crystallization and Melting of T_{β}	142
6.3.6 Classification of Trehalose Dihydrate Samples.....	147
6.3.7 Visualization of Solid Form Changes During Dehydration of T_h Using Polarized Light Microscopy (PLM).....	148
6.3.8 Cause(s) of Differences in the Dehydration Behavior of Trehalose Dihydrate.....	151
6.3.8.1 Particle Morphology and Crystal Defects (PLM).....	152
6.3.8.2 Physical Impurities and Crystal Defects (SSNMR).....	155
6.3.8.3 Sample Purity.....	157
6.4 Conclusions.....	160
6.5 References.....	162
Chapter 7. Dehydration of Trehalose Dihydrate: Part II.....	165
7.1 Introduction.....	166
7.2 Experimental.....	167
7.2.1 Materials	167
7.2.2 Sieving.....	169
7.2.3 Dehydration	169
7.2.4 Differential Scanning Calorimetry.....	169

7.2.5 ^{13}C Solid-state NMR Spectroscopy	170
7.3 Results and Discussion	170
7.3.1 Non-Isothermal Dehydration of Trehalose Dihydrate	170
7.3.1.1 Dehydration of Trehalose Dihydrate at 2 °C/minute	171
7.3.1.2 Dehydration of Trehalose Dihydrate at 20 °C/minute	176
7.3.2 Isothermal Dehydrations of Trehalose Dihydrate: Vacuum Oven.....	180
7.3.2.1 Isothermal Dehydration of Trehalose Dihydrate in a Vacuum Oven: 75 °C	181
7.3.2.2 Isothermal Dehydration of Trehalose Dihydrate in a Vacuum Oven: 100 °C	185
7.3.2.3 Isothermal Dehydration of Trehalose Dihydrate in a Vacuum Oven: 125 °C	189
7.3.3 Dehydration of Trehalose Dihydrate at 68 °C: Variable-temperature ^{13}C SSNMR	193
7.4 Conclusion	198
7.5 References.....	199
Chapter 8. Characterization of Amorphous Trehalose Prepared by Lyophilization and Dehydration of Trehalose Dihydrate	202
8.1 Introduction.....	203
8.2 Experimental.....	204
8.2.1 Materials	204

8.2.2 Lyophilization.....	204
8.2.3 Dehydration	205
8.2.4 Polarized Light Microscopy.....	205
8.2.5 Differential Scanning Calorimetry (DSC).....	205
8.2.6 Solid-state NMR Spectroscopy.....	206
8.3 Results.....	206
8.3.1 Amorphous Trehalose Prepared by Lyophilization.....	207
8.3.3 Amorphous Trehalose Prepared by Dehydration of Trehalose Dihydrate.....	218
8.3.3 Comparison of ¹³ C SSNMR Spectra of Amorphous Trehalose.....	227
8.4 Discussion.....	229
8.4.1 Differences in the Glass Transitions of Amorphous Trehalose.....	230
8.4.2 Differences in the Crystallization Tendencies of Amorphous Trehalose.....	234
8.5 Conclusions.....	236
8.6 References.....	238
Chapter 9. Detection of Low Levels of Crystallinity Using SSNMR.....	241
9.1 Introduction.....	242
9.2 Experimental.....	242
9.2.1 Materials	242
9.2.2 Dehydration of T _h	243

9.2.3 Lyophilization	243
9.2.4 Aging	244
9.2.5 Differential Scanning Calorimetry (DSC)	244
9.2.6 Solid-State NMR Spectroscopy	244
9.3 Results and Discussion	245
9.3.1 SSNMR Parameters	245
9.3.1.1 Acquisition Length.....	245
9.3.1.2 Pulse Delay	248
9.3.1.3 Detection of Crystal Nuclei Using SSNMR	251
9.3.2 Assessment of Crystallization Tendency.....	254
9.3.2 SSNMR: Detection of Crystal Nuclei.....	256
9.4 Conclusions.....	264
9.5 References.....	267
Chapter 10. Summary and Suggestions for Future Work.....	269
10.1 Summary	270
10.1.1 Generation and Characterization of T_{δ} (Chapter 5)	270
10.1.2 Impact of Source and Lot-to-Lot Variability on the Dehydration of Trehalose Dihydrate (Chapters 6 and 7).....	271
10.1.3 Analysis of Physical Properties of Amorphous Trehalose (Chapters 8 and 9).....	272
10.2 Suggestions for Future Work	272
10.2.1 Additional Characterization of T_{δ}	273

10.2.2 Further Investigation of Variability in Trehalose	
Dihydrate	273
10.2.3 Characterization of Amorphous Trehalose	275
10.2.4 Other Questions from the Literature	275
10.3 References	277

Chapter 1

Introduction

1.1 Objectives

The overall purpose of the work described in this dissertation was to investigate the solid-state forms and transformations of trehalose, including the dehydration of trehalose dihydrate and the physical stability of amorphous trehalose. Trehalose is found in four known solid forms: a crystalline dihydrate (T_h), the β -anhydrate (T_β), the α -anhydrate (T_α), and the amorphous form (T_{am}). The anhydrous forms are often generated via dehydration of T_h , and the forms resulting from dehydrations of T_h are very sensitive to the rate of water removal; despite significant efforts, the factors controlling which forms are generated are still unclear.¹⁻¹⁴ The amorphous form of trehalose is able to crystallize to the most stable anhydrous crystalline form, T_β , but the factors controlling its physical stability have yet to be determined.^{9, 15, 16}

This work can be separated into three parts: 1) generation and characterization of a new solid form of trehalose, 2) determination of the effect of source and lot-to-lot variability on the dehydration behavior of trehalose dihydrate (T_h), and 3) analysis of the effect of preparation method on the physical properties of amorphous trehalose (T_{am}). In this chapter, background on the history, properties, and uses of trehalose are provided, and the relevance of trehalose to the pharmaceutical industry is presented.

1.2 Introduction to Trehalose

Trehalose is a non-reducing disaccharide composed of two glucose units joined by a 1 \rightarrow 1 linkage. The structure of the naturally occurring $\alpha\alpha$ conformer is shown in Figure 1.1. Trehalose was first isolated from ergot of rye, a fungus, by H.A.L. Wiggers in 1832.¹⁷ Mitscherlich isolated trehalose from mushrooms in 1858 and published one of the first accounts

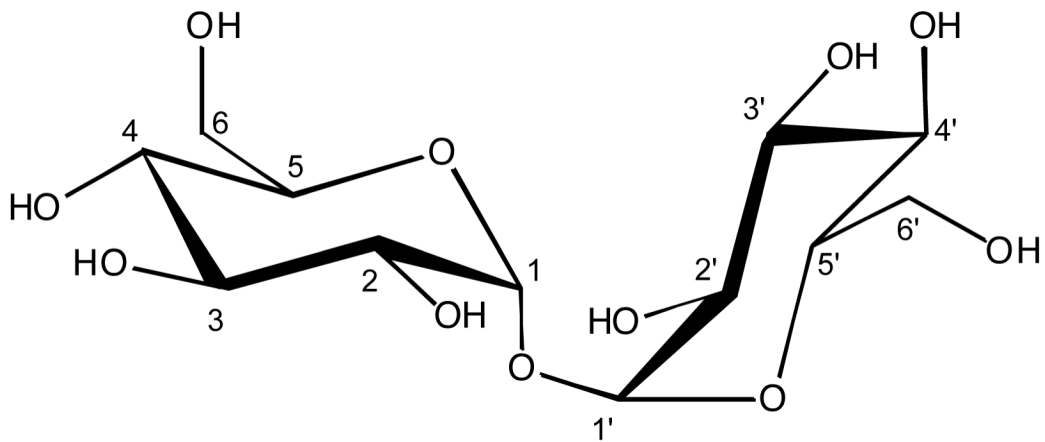


Figure 1.1. Structure of α,α -trehalose.

of its solid-state properties, reporting a melting point of 210 °C.¹⁸ Early studies revealed that it was resistant to hydrolysis and had a high capacity to polarize light.¹⁹ Many species, including insects, yeast, fungi, and bacteria, contain trehalose, and it can serve as a source of energy or a protector against environmental stresses.²⁰ Trehalose is found in familiar organisms that are tolerant to extremely dry conditions, including brine shrimp (more commonly known as sea monkeys), baker's yeast, shiitake mushrooms, and tardigrades. When these organisms are exposed to high heat or desert-like conditions, production of trehalose is induced, and they can exist in a desiccated state for years. Upon rehydration, biological activity resumes. Trehalose is thought to stabilize biological membranes in these organisms, and there is great interest in understanding the mechanism by which this stabilization occurs.²⁰⁻²⁴

1.3 Applications of Trehalose

Due to the unique stabilizing properties that trehalose displays in nature, many scientists have investigated its potential to stabilize other materials, such as foods, cosmetics, and pharmaceuticals. Many applications of trehalose have been described in recent review papers,^{20, 22, 24} and several are summarized in the following sections.

1.3.1 Food, Cosmetic, and Medical Applications

Trehalose is beneficial for food preservation, stabilization, odor suppression, and moisture retention, and in Japan, trehalose is present in over 8000 food products.²⁴ Trehalose is naturally present in foods such as mushrooms, lobster, honey, sunflower seeds, and various yeast-containing breads, but it is also added to many processed foods. In the cosmetics industry,

trehalose can be used to enhance the stability of certain oil-based products and mask odors from degradation products of cream-based products.²⁴ It is added to some creams in order to help retain moisture in the outer skin layer, and it is added to some deodorants and shower gels in order to suppress human body odor.

Trehalose has also shown promise in the treatment and/or prevention of some medical conditions. In mice, oral administration of trehalose inhibited bone weight loss, and with further research, it could be used to prevent osteoporosis.²⁵ Trehalose has been shown to inhibit aggregation of proteins with long polyglutamine chains, such as those found in Huntingtin protein.²⁶ Huntington's disease is caused by aggregation of Huntingtin protein, and trehalose is considered a candidate for therapeutic treatment of the disease. The efficacy of a 100-mM solution of trehalose in the treatment of dry eye has been demonstrated.²⁷ The preservative properties of trehalose also have applications in the field of medicine. Researchers at Kyoto University have developed a solution for organ preservation (for transplants) that is composed of more than 50% trehalose.²⁸ It has also been used in the cryopreservation of mammalian (including human) cells and tissues.

1.3.2 Pharmaceutical Industry

Trehalose is very stable and is not prone to degradation in solution or in the solid state,²⁹³⁰ and perhaps more importantly, it achieved “generally regarded as safe,” or GRAS, status from the US FDA in 2000.²² Trehalose is often used as a lyoprotectant in biopharmaceutical formulations and is present as an excipient in four products on the US pharmaceutical market.²⁴ Of these four formulations, two are lyophilized powders, and two are solutions for injection. In

these formulations, one role of trehalose is to interact with the active pharmaceutical ingredient (API), either a monoclonal antibody or a recombinant protein, and stabilize it. This stabilization mechanism is not yet understood, although it is thought that it occurs by one of two methods. In the first theory, a glassy trehalose matrix immobilizes biological components and helps preserve their structure. It has been suggested that the high glass transition temperature of trehalose, as compared to other disaccharides, is responsible for the enhanced efficacy of trehalose in stabilizing biomolecules.^{21, 31} Aldous has proposed that the ability of trehalose to act as an effective stabilizer is related to its ability to scavenge water from the amorphous matrix, crystallize as a dihydrate, and increase the glass transition of the remaining amorphous material.³² In the second theory, hydrogen bonds between trehalose molecules and biomolecules provide stabilization by helping to maintain the three-dimensional structure of the biomolecule; this is commonly referred to as the water-replacement theory. It has been suggested that the structure of trehalose, specifically its “clam shell conformation,” promotes interactions between trehalose and biomolecules.³³ Its mechanism of stabilization in formulations is likely similar to that which occurs in nature.

The number of patent applications listing trehalose as an excipient in quick-dissolving solid dosage forms is increasing.²⁴ Quick-dissolving tablets are in some ways superior to traditional tablets, which are often considered the preferred dosage form due to their high stability and ease of administration. Small children and the elderly are unable to take traditional tablets but can take quick-dissolving tablets. Additionally, the quick-dissolving tablets do not require the patient to drink water. Amorphous trehalose is specifically listed in a few of these patent applications; thus, inexpensive and efficient production of amorphous trehalose would be of interest to the pharmaceutical industry.

1.4 Solid-State Stability of Trehalose

A solid form conversion of an excipient may adversely affect the drug product in a pharmaceutical formulation. In this section, the current understanding of the solid-state forms of trehalose and their conversions is presented.

1.4.1 Solid-State Forms and Transformations of Trehalose

As stated earlier, there are four known solid forms of trehalose, and they readily interconvert. Upon water loss from T_h , one or more anhydrous forms of trehalose can be generated, and studies on the conditions governing which form(s) are generated have continued for decades. T_α forms during dehydrations in which water loss is slow, with minimal disruption of the intermolecular hydrogen bonds between trehalose molecules, and isothermal dehydrations leading to the formation of T_α are usually performed below 100 °C.^{5, 34-36} At higher temperatures, the speed at which the water molecules leave the crystal structure destroys the T_h lattice, and other forms (T_{am} or T_β) are generated.^{15, 34} When T_h is heated at slow rates (≤ 2 °C/minute), water loss occurs at low temperatures and results in the formation of T_α ; faster heating rates can produce T_{am} or T_β from T_h .¹⁴ Although most studies report on the formation of one anhydrous form during dehydration of T_h , it has been shown that mixtures of T_α and T_{am} can be simultaneously generated.³⁵ Recent studies have shown that T_h can crystallize and then undergo dehydration to form T_{am} during lyophilization, possibly impacting its ability to serve as an effective lyoprotectant;³⁷ in light of this, it is especially important to understand the ways in which T_h dehydrates.

T_α is a highly unusual polymorph in that it has a melting point of 132–139 °C,³⁴ which is only about 10–15 °C above the glass transition temperature (T_g) of T_{am} . The melting point of T_α is at least 60 °C lower than the melting point of T_β , which has been reported from 197 °C to 218 °C.^{34,38} The enthalpy of fusion for T_α was reported to be lower than that of T_β by about an order or magnitude,³⁹ reflecting the high energy and low ordering of this polymorph. Though larger values of the enthalpy of fusion have been reported,^{35,40} they are still much smaller than that of T_β . By the heat of fusion rule, T_α and T_β are related monotropically, with T_β more stable at all temperatures. A few observations have led to speculation that crystalline T_α is less stable than T_{am} . When exposed to 43% RH at 25 °C, T_α converted to T_h in less than an hour, as confirmed by XRD measurements, but under the same conditions, neither T_β nor T_{am} changed forms.⁴¹ Additionally, T_α undergoes vitrification below its melting temperature and below the T_g of amorphous trehalose. Rani et al. found that annealing mixtures of T_{am} and T_α at 100 °C and 110 °C did not increase the crystallinity of T_α .³⁵ Typically, this treatment would be expected to either facilitate crystallization of T_α from T_{am} or increase the crystallinity of T_α , and neither occurred. The thermal stability of T_α below the T_g of T_{am} was also investigated by Willart et al. using differential scanning calorimetry (DSC).¹⁴ Samples of T_α were held at 105, 110, and 117 °C for 5 to 376 hours, and in all cases, annealing resulted in a decrease in magnitude of the T_α melting peak. The disappearance of the melting peak was accompanied by a jump in the heat capacity, indicating that T_{am} was formed. Based on molecular and crystal energy calculations, Nagase et al. suggested that the intermolecular interactions between molecules of trehalose in T_α are likely weaker than those found in T_β and T_{am} .⁴² Kilburn et al. found that the free volume of T_α was higher than that of T_{am} and suggested that T_α may be more mobile than T_{am} .⁴³

In addition to the four known forms, two additional polymorphs of trehalose, T_γ and T_ϵ , have been suggested. Based on evidence from DSC experiments performed on T_h , T_γ was described as a transient form that melted a few degrees above its formation temperature.⁴⁴ T_γ formed via cold crystallization when T_h was heated at intermediate rates, and its presence was indicated by an exothermic peak immediately after the endotherm associated with water loss. T_γ was described as melting to form T_{am} at about 120 °C. Later, powder X-ray diffraction (PXRD) experiments showed that T_γ is actually a mixture of T_h and T_β , and it was hypothesized that an external layer of T_β forms upon dehydration and encapsulates the T_h core.⁴⁵ A second new form, the ϵ polymorph (T_ϵ), has also been proposed in the literature.⁴ This form was generated during simultaneous XRD-DSC experiments in which samples were heated at 2 °C/minute with a partial water vapor pressure of 3–5 kPa. The XRD pattern of this form is haloed, indicating that it has a low crystallinity. The XRD peaks were more intense at a partial water vapor pressure of 5 kPa, suggesting that the crystallinity of T_ϵ is dependent on the humidity. Upon heating to temperatures greater than 150 °C, this material transforms to T_β . The authors noted that T_ϵ with higher crystallinity transformed to T_β at a slightly lower temperature (157 °C for 3 kPa vs. 150 °C for 5 kPa). Upon exposure to $P_{H_2O} > 3\text{kPa}$ at room temperature, the material reverts to T_h . No other reports on this form have been published.

1.4.2 Trehalose as a Model Compound to Study the Amorphous State

Amorphous trehalose (T_{am}) has been studied extensively, both because it is an excellent model compound to study the amorphous state and because T_{am} is of specific interest as a pharmaceutical excipient.^{8, 43, 46-57} The amorphous state is important to the pharmaceutical industry because of the significant formulation advantage it offers if the crystalline form of an

API is poorly water-soluble. The amorphous form is less thermodynamically stable than the crystalline form(s), and it therefore displays faster dissolution and a higher apparent solubility, resulting in a higher bioavailability.^{58, 59} However, because the amorphous state is inherently unstable, it is energetically driven toward the crystalline state. The presence of crystalline material or crystal nuclei can facilitate the crystallization of amorphous materials, decreasing the physical stability of an amorphous API and eventually causing the loss of the bioavailability advantage.^{58, 59} An amorphous excipient may be used to stabilize an amorphous API and prevent crystallization of a formulation. Crystallization of an amorphous excipient, such as trehalose, whose purpose is to stabilize a protein can also be detrimental to a formulation.⁶⁰ For these reasons, it is necessary to develop an understanding of factors that control crystallization of the amorphous state.

Figure 1.2 depicts the energetics of a crystalline-liquid-amorphous system. As a crystalline solid is heated through its melting point, it undergoes a first-order phase transition to the liquid state. In the liquid state, molecules are more flexible and more mobile than in the crystalline state. One way to reach the amorphous state is to rapidly cool the liquid, effectively freezing the disorder of the liquid state into a solid. As the liquid is cooled, it first passes through the supercooled liquid region (rubbery state), and when it reaches the glass transition temperature (T_g), the mobility decreases significantly. Below the glass transition temperature, amorphous material is in the glassy state. Depending on the thermal history, i.e. how the amorphous material was prepared and stored, the glassy material can occupy many different energy states. As amorphous material is stored below its T_g (commonly referred to as aging or annealing), it loses excess enthalpy and slowly relaxes to a lower energy state. It is possible that nucleation can occur during storage below the T_g ; however, is thought crystallization occurs above the T_g .⁵⁸

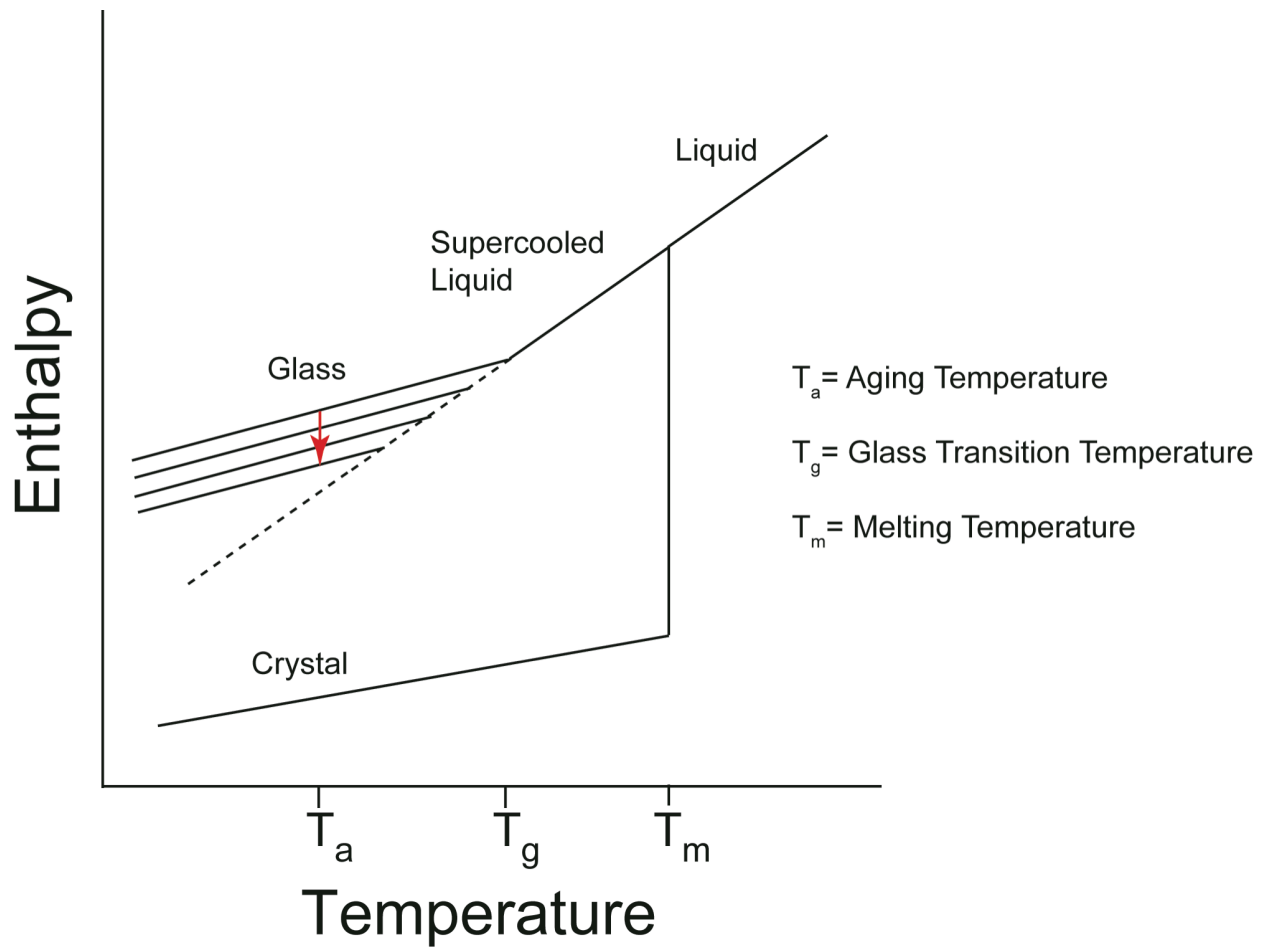


Figure 1.2. Diagram depicting the energetics of a crystalline-liquid-amorphous system. As an amorphous material is held below its glass transition temperature, it relaxes to a lower energy state during a process referred to as aging or annealing.

Amorphous materials can be generated using many different techniques, including milling or grinding of anhydrous crystalline forms, freeze-drying, spray-drying, and melt-quenching. The tendency of an amorphous material to crystallize can be evaluated using differential scanning calorimetry (DSC), where an increased tendency to crystallize is evidenced by a greater enthalpy of crystallization or a lower onset temperature of crystallization.^{15, 16} It has been reported that amorphous trehalose prepared using different techniques can display different tendencies to crystallize to T_{β} , and a few hypotheses have been proposed to explain this. Some have speculated that crystal nuclei are responsible when a higher degree of crystallization is observed for a particular sample.^{15, 16} However, direct evidence of T_{β} nuclei in samples of T_{am} has not been observed. Others have suggested that there are two structurally different glassy states of amorphous trehalose: one that crystallizes, and one that does not.⁹

1.5 Overview of Thesis Work

In the previous sections, an introduction to the solid-state forms and conversions of trehalose was presented, and the relevance of trehalose to the pharmaceutical industry was discussed. In this section, brief descriptions of the chapters in this dissertation are provided.

1.5.1 Solid-state Characterization Techniques

In Chapter 2, the solid-state characterization techniques used to analyze trehalose are discussed: DSC and ^{13}C solid-state NMR spectroscopy (SSNMR) are emphasized. The basic theory of each technique is provided, as well as examples of data that are obtained from each.

1.5.2 Literature Review

In Chapter 3, a more in-depth review of the trehalose literature is provided. Three key areas are highlighted: 1) the molecular structure of trehalose molecules in the solid forms, 2) factors influencing the dehydration of T_h , and 3) the physical stability of T_{am} .

1.5.3 Initial Solid-State Characterization of Trehalose

Chapter 4 describes the initial studies that were undertaken in an attempt to produce amorphous trehalose. First, T_h from four sources was characterized using DSC, and the thermograms indicated that the samples were dehydrating in different ways. Next, the four samples were dehydrated at 100 °C in order to produce amorphous trehalose.¹⁵ Instead of pure T_{am} , all samples contained T_β after dehydration. The T_h samples were analyzed after additional processing (grinding, lyophilization, dehydration at various temperatures), and differences among the samples as well as those reported in the literature were observed. During these investigations, unidentified peaks were observed in ^{13}C SSNMR spectra of samples of T_h that were dehydrated at 75 °C; these were attributed to a new form of trehalose whose characterization is described in Chapter 5. An investigation into the impact of source and lot-to-lot variability of T_h on its dehydration behavior continues in Chapters 6 and 7.

1.5.4 Generation and Characterization of a New Solid Form of Trehalose

In Chapter 5, the characterization of a previously unknown form of trehalose, the δ form (T_δ), is presented. T_δ is formed from dehydrations of trehalose dihydrate (T_h) performed at or

below 100 °C, and it is generated concurrently with T_α , T_{am} , and occasionally T_β . T_δ is detected with SSNMR, but DSC and powder X-ray diffraction (PXRD) studies of samples containing T_δ could not distinguish the presence of the new form. T_δ is metastable: upon exposure to temperatures above 80 °C, it converts to either T_α or T_{am} , and upon exposure to ambient humidity, it reverts to T_h .

1.5.5 Dehydration of Trehalose Dihydrate: Part I

Chapter 6 further explores the impact of source and lot-to-lot variability on the dehydration of T_h that was reported in Chapter 4. Sixteen samples of T_h from different sources and lots were sieved and characterized using DSC, thermogravimetric analysis (TGA), and polarized light microscopy (PLM). The results from the DSC analyses were used to develop a classification system that describes the behavior of T_h when heated at 10 °C/minute. Type 1 samples tend to form T_β , Type 2 samples tend to form T_{am} that crystallizes to T_β , and Type 3 samples tend to form T_{am} that remains amorphous. Potential sources of the differences in dehydration behavior, including particle morphology, crystal defects, and chemical/physical impurities, were also investigated.

1.5.6 Dehydration of Trehalose Dihydrate: Part II

Following the development of the classification system in Chapter 6, the dehydration of T_h was further investigated by dehydrating different types of T_h in the following ways: 1) at different rates (2 and 20 °C/minute), 2) isothermally in a vacuum oven (75 and 125 °C), and 3) in the SSNMR spectrometer at 68 °C. The differences among the three types of trehalose are

minimized when water loss is slow (2 °C/minute or 75 °C), and the differences are very apparent when water loss is fast (20 °C/minute or 125 °C).

1.5.7 Characterization of Amorphous Trehalose Prepared By Lyophilization and Dehydration of Trehalose Dihydrate

In Chapter 8, PLM, DSC, and SSNMR were used to investigate the structure and physical stability of T_{am} produced by lyophilization and dehydration of T_h . T_{am} produced by lyophilization has a lower tendency to crystallize to T_β , and the material appears to more homogeneous and at a higher energy level. T_{am} produced by dehydration of T_h appears to be more heterogeneous, possibly due to the formation of microscopic voids that are formed as water leaves the crystal structure.

1.5.9 Detection of Low Levels of Crystallinity Using SSNMR

In Chapter 9, a new SSNMR approach to detect low levels of crystallinity or crystal nuclei in seemingly amorphous samples of trehalose is demonstrated and discussed. Small peaks corresponding to T_β are detected in most samples that show a tendency to crystallize to T_β .

1.5.10 Summary and Suggestions for Future Work

In Chapter 10, the key insights on the solid-state transformations of trehalose are summarized, and some suggestions for future experiments are presented.

1.6 References

1. Willart, J.-F.; Descamps, M. Solid State Amorphization of Pharmaceuticals. *Mol. Pharmaceutics* **2008**, *5*, (6), 905-920.
2. Cesáro, A.; De Giacomo, O.; Sussich, F. Water interplay in trehalose polymorphism. *Food Chem.* **2008**, *106*, 1318-1328.
3. Ding, S.-P.; Fan, J.; Green, J. L.; Lu, Q.; Sanchez, E.; Angell, C. A. Vitrification of Trehalose by Water Loss from Its Crystalline Dihydrate. *J. Therm. Anal.* **1996**, *47*, 1391-1405.
4. Furuki, T.; Kishi, A.; Sakurai, M. De- and rehydration behavior of α,α -trehalose dihydrate under humidity-controlled atmospheres. *Carbohydr. Res.* **2005**, *340*, 429-438.
5. Gil, A. M.; Belton, P. S.; Felix, V. Spectroscopic studies of solid α,α trehalose. *Spectrochim. Acta A* **1996**, *52*, 1649 - 1659.
6. Jones, M. D.; Hooton, J. C.; Dawson, M. L.; Ferrie, A. R.; Price, R. Dehydration of trehalose dihydrate at low relative humidity and ambient temperature. *Int. J. Pharm.* **2006**, *313*, 87-98.
7. Kilburn, D.; Sokol, P. E. Structural Evolution of the Dihydrate to Anhydrate Crystalline Transition of Trehalose as Measured by Wide-angle X-ray Scattering. *J. Phys. Chem. B* **2009**, *113*, 2201-2206.
8. Macdonald, C.; Johari, G. P. Glass-softening of trehalose and calorimetric transformations in its liquid state. *J. Mol. Struct.* **2000**, *523*, 119-132.
9. Sussich, F.; Cesáro, A. Trehalose amorphization and recrystallization. *Carbohydr. Res.* **2008**, *343*, 2667-2674.
10. Sussich, F.; Skopec, C.; Brady, J.; Cesáro, A. Reversible dehydration of trehalose and anhydrobiosis: from solution state to an exotic crystal? *Carbohydr. Res.* **2001**, *334*, 165-176.
11. Sussich, F.; Urbani, R.; Princivalle, F.; Cesáro, A. Polymorphic Amorphous and Crystalline Forms of Trehalose. *J. Am. Chem. Soc.* **1998**, *120*, 7893-7899.

12. Taylor, L. S.; York, P. Effect of particle size and temperature on the dehydration kinetics of trehalose dihydrate. *Int. J. Pharm.* **1998**, *167*, 215-221.
13. Willart, J. F.; Danede, F.; De Gusseme, A.; Descamps, M.; Neves, C. Origin of the Dual Structural Transformation of Trehalose Dihydrate upon Dehydration. *J. Phys. Chem. B* **2003**, *107*, 11158-11162.
14. Willart, J. F.; De Gusseme, A.; Hemon, S.; Descamps, M.; Leveiller, F.; Rameau, A. Vitrification and Polymorphism of Trehalose Induced by Dehydration of Trehalose Dihydrate. *J. Phys. Chem. B* **2002**, *106*, 3365-3370.
15. Surana, R.; Pyne, A.; Suryanarayanan, R. Effect of preparation method on physical properties of amorphous trehalose. *Pharm. Res.* **2004**, *21*, (7), 1167-76.
16. Surana, R.; Pyne, A.; Suryanarayanan, R. Effect of aging on the physical properties of amorphous trehalose. *Pharm. Res.* **2004**, *21*, (5), 867-74.
17. Wiggers, H. A. L. Untersuchung über das Mutterkorn, Secale cornutum. *Liebigs Ann. Chem.* **1832**, *1*, (2), 129-182.
18. Mitscherlich, E. Ueber die Mycose, den Zucker des Mutterkorns. *Liebigs Ann. Chem.* **1858**, *106*, (1), 15-18.
19. Harding, T. S. History of trehalose, its discovery and methods of preparation. *Sugar* **1923**, *25*, 476-478.
20. Elbein, A. D.; Pan, Y. T.; Pastuszak, I.; Carroll, D. New insights on trehalose: a multifunctional molecule. *Glycobiology* **2003**, *13*, 17R-27R.
21. Crowe, L. M.; Reid, D. S.; Crowe, J. H. Is Trehalose Special for Preserving Dry Biomaterials. *Biophys. J.* **1996**, *71*, 2087-2093.
22. Richards, A. B.; Krakowka, S.; Dexter, L. B.; Schmid, H.; Wolterbeek, A. P. M.; Waalkens-Berendsen, D. H.; Shigoyuki, A.; Kurimoto, M. Trehalose: a review of properties,

history of use and human tolerance, and results of multiple safety studies. *Food Chem Toxicol.* **2002**, *40*, 871-898.

23. Jain, N. K.; Roy, I. Effect of trehalose on protein structure. *Protein Sci.* **2009**, *18*, 24-36.
24. Ohtake, S.; Wang, Y. J. Trehalose: Current Use and Future Applications. *J. Pharm. Sci.* **2011**, *100*, (6), 2020-2053.
25. Nishizaki, Y.; Yoshizane, C.; Toshimori, Y.; Arai, N.; Akamatsu, S.; Hanaya, T.; Arai, S.; Ikeda, M.; Kurimoto, M. Disaccharide-trehalose inhibits bone resorption in ovariectomized mice. *Nutr. Res.* **2000**, *20*, (5), 653-664.
26. Tanaka, M.; Machida, Y.; Niu, S.; Ikeda, T.; Jana, N. R.; Doi, H.; Kurosawa, M.; Nekooki, M.; Nukina, N. Trehalose alleviates polyglutamine-mediated pathology in a mouse model of Huntington disease. *Nat. Med.* **2004**, *10*, (2), 148-154.
27. Matsuo, T. Trehalose protects corneal epithelial cells from death by drying. *British J. Ophthalmol.* **2001**, *85*, (5), 610-612.
28. Yokomise, H.; Inui, K.; Wada, H.; Hasegawa, S.; Ohno, N.; Hitomi, S. Reliable cryopreservation of trachea for one month in a new trehalose solution. *J. Thorac. Cardiovasc. Sur.* **1995**, *110*, (2), 382-385.
29. Shafizadeh, F.; Lai, Y. Z. Thermal Rearrangements of Cellobiose and Trehalose. *Carbohydr. Res.* **1973**, *31*, 57-67.
30. Wolfenden, R.; Yuan, Y. Rates of Spontaneous Cleavage of Glucose, Fructose, Sucrose, and Trehalose in Water, and the Catalytic Proficiencies of Invertase and Trehalase. *J. Am. Chem. Soc.* **2008**, *130*, 7548-7549.
31. Green, J. L.; Angell, C. A. Phase Relations and Vitrification in Saccharide–Water Solutions and the Trehalose Anomaly. *J. Phys. Chem.* **1989**, *93*, 2880-2882.
32. Aldous, B. J.; Auffret, A. D.; Franks, F. The Crystallisation of Hydrates from Amorphous Carbohydrates. *Cryo-Lett.* **1995**, *16*, 181-186.

33. Albertorio, F.; Chapa, V. A.; Chen, X.; Diaz, A. J.; Cremer, P. S. The α,α -(1 \rightarrow 1) Linkage of Trehalose is Key to Anhydrobiotic Preservation. *J. Am. Chem. Soc.* **2007**, *129*, 10567-10574.
34. Reisener, H. J.; Goldschmid, H. R.; Ledingham, G. A.; Perlin, A. S. Formation of Trehalose and Polyols by Wheat Stem Rust (*Puccinia Graminis Tritici*) Uredospores. *Can. J. Biochem. Phys.* **1962**, *40*, 1248-1251.
35. Rani, M.; Govindarajan, R.; Surana, R.; Suryanarayanan, R. Structure in Dehydrated Trehalose Dihydrate—Evaluation of the Concept of Partial Crystallinity. *Pharm. Res.* **2006**, *23*, (10), 2356-2367.
36. Chakravarty, P.; Bhardwaj, S. P.; King, L.; Suryanarayanan, R. Monitoring Phase Transformations in Intact Tablets of Trehalose by FT-Raman Spectroscopy. *AAPS PharmSciTech* **2009**, *10*, (4), 1420-1426.
37. Sundaramurthi, P.; Suryanarayanan, R. Trehalose Crystallization During Freeze-Drying: Implications on Lyoprotection. *J. Phys. Chem. Lett.* **2010**, *1*, 510-514.
38. Ohashi, T.; Yoshii, H.; Furuta, T. Innovative crystal transformation of dihydrate trehalose to anhydrous trehalose using ethanol. *Carbohydr. Res.* **2007**, *342*, 819-825.
39. Sussich, F.; Cesáro, A. Transitions and Phenomenology of α,α -Trehalose Polymorphs Inter-conversion. *J. Therm. Anal. Calorim.* **2000**, *62*, 757-768.
40. Willart, J. F.; Hedoux, A.; Guinet, Y.; Danede, F.; Paccou, L.; Capet, F.; Descamps, M. Metastability Release of the Form α of Trehalose by Isothermal Solid State Vitrification. *J. Phys. Chem. B* **2006**, *110*, 11040-11043.
41. Nagase, H.; Endo, T.; Ueda, H.; Nakagaki, M. An anhydrous polymorphic form of trehalose. *Carbohydr. Res.* **2002**, *337*, 167-173.
42. Nagase, H.; Ogawa, N.; Endo, T.; Shiro, M.; Ueda, H.; Sakurai, M. Crystal Structure of an Anhydrous Form of Trehalose: Structure of Water Channels of Trehalose Polymorphism. *J. Phys. Chem. B* **2008**, *112*, 9105-9111.

43. Kilburn, D.; Townrow, S.; Meunier, V.; Richardson, R.; Alam, A.; Ubbink, J. Organization and mobility of water in amorphous and crystalline trehalose. *Nat. Mater.* **2006**, *5*, 632-635.
44. Sussich, F.; Urbani, R.; Cesáro, A.; Princivalle, F.; Bruckner, S. New Crystalline and Amorphous Forms of Trehalose. *Carbohydr. Lett.* **1997**, *2*, 403-408.
45. Sussich, F.; Princivalle, F.; Cesáro, A. The interplay of the rate of water removal in the dehydration of α,α -trehalose. *Carbohydr. Res.* **1999**, *322*, 113-119.
46. Zhang, P.; Klymachyov, A. N.; Brown, S.; Ellington, J. G.; Grandinetti, P. J. Solid-state ^{13}C NMR investigations of the glycosidic linkage in α,α' trehalose. *Solid State Nucl. Magn. Reson.* **1998**, *12*, 221-225.
47. Shamblin, S. L.; Tang, X.; Chang, L.; Hancock, B. C.; Pikal, M. J. Characterization of the Time Scales of Molecular Motion in Pharmaceutically Important Glasses. *J. Phys. Chem. B* **1999**, *103*, 4113-4121.
48. Ahlqvist, M. U. A.; Taylor, L. S. Water Diffusion in Hydrated Crystalline and Amorphous Sugars Monitored Using H/D Exchange. *J. Pharm. Sci.* **2002**, *91*, (3), 690-698.
49. De Gusseme, A.; Carpentier, L.; Willart, J. F.; Descamps, M. Molecular Mobility in Supercooled Trehalose. *J. Phys. Chem. B* **2003**, *107*, 10879-10886.
50. McGarvey, O. S.; Kett, V. L.; Craig, D. Q. M. An Investigation into the Crystallization of α,α - Trehalose from the Amorphous State. *J. Phys. Chem. B* **2003**, *107*, (27), 6614-6620.
51. Kawai, K.; Hagiwara, T.; Takai, R.; Suzuki, T. Comparative Investigation by Two Analytical Approaches of Enthalpy Relaxation for Glassy Glucose, Sucrose, Maltose, and Trehalose. *Pharm. Res.* **2005**, *22*, (3), 490-495.
52. Lefort, R.; Bordat, P.; Cesáro, A.; Descamps, M. Exploring the conformational energy landscape of glassy disaccharides by cross polarization magic angle spinning ^{13}C nuclear magnetic resonance and numerical simulations. II. Enhanced molecular flexibility in amorphous trehalose. *J. Chem. Phys.* **2007**, *126*, (1), 014511.

53. Moura Ramos, J. J.; Pinto, S. S.; Diogo, H. P. The Slow Molecular Mobility in Amorphous Trehalose. *ChemPhysChem* **2007**, *8*, 2391-2396.
54. Dranca, I.; Bhattacharya, S.; Vyazovkin, S.; Suryanarayanan, R. Implications of Global and Local Mobility in Amorphous Sucrose and Trehalose as Determined by Differential Scanning Calorimetry. *Pharm. Res.* **2009**, *26*, 1064.
55. Moran, A.; Buckton, G. Studies of the Crystallization of Amorphous Trehalose Using Simultaneous Gravimetric Vapor Sorption/Near IR (GVS/NIR) and "Modulated" GVS/NIR. *AAPS PharmSciTech* **2009**, *10*, (1), 297-302.
56. Bhardwaj, S. P.; Suryanarayanan, R. Subtraction of DC Conductivity and Annealing – Approaches to Identify Johari-Goldstein Relaxation in Amorphous Trehalose. *Mol. Pharmaceutics* **2011**.
57. Li, X.; Mansour, H. M. Physicochemical Characterization and Water Vapor Sorption of Organic Solution Advanced Spray-Dried Inhalable Trehalose Microparticles and Nanoparticles for Targeted Dry Powder Pulmonary Inhalation Delivery. *AAPS PharmSciTech* **2011**.
58. Bhugra, C.; Pikal, M. J. Role of Thermodynamic, Molecular, and Kinetic Factors in Crystallization From the Amorphous State. *J. Pharm. Sci.* **2008**, *97*, (4), 1329-1349.
59. Hancock, B. C.; Zografi, G. Characteristics and Significance of the Amorphous State in Pharmaceutical Systems. *J. Pharm. Sci.* **1997**, *86*, (1), 1-12.
60. Heljo, V.; Nordberg, A.; Tenho, M.; Virtanen, T.; Jouppila, K.; Salonen, J.; Maunu, S.; Juppo, A. The Effect of Water Plasticization on the Molecular Mobility and Crystallization Tendency of Amorphous Disaccharides. *Pharm. Res.* **2012**, *29*, (10), 2684-2697.

Chapter 2

Solid-State Characterization Techniques and Applications to the Trehalose System

2.1 Introduction

Multiple solid-state characterization methods are required to investigate the morphological, diffraction, thermal, and spectroscopic properties of the trehalose system. In this chapter, the basic theory of several techniques is described, and examples of the data that is generated from a few of these techniques are shown. Differential scanning calorimetry (DSC) and ^{13}C solid-state NMR spectroscopy (SSNMR) are the two primary techniques, and as such, in-depth descriptions of these techniques are presented. Polarized light microscopy (PLM), thermogravimetric analysis (TGA), and powder X-ray diffraction (PXRD) are used to complement and supplement the results from DSC and SSNMR; these are briefly discussed.

2.2 Polarized Light Microscopy (PLM)

With the addition of polarizers, an optical microscope can be used to produce images that can determine if a material is crystalline or amorphous. Plane-polarized light interacts with an anisotropic crystal to split the light into two components: this property is referred to as birefringence.¹ The velocities of the two components are different and result in different colors in images of crystalline materials, as is shown in Figure 2.1a. A single crystal will appear as either blue or yellow, and following a 90° rotation, the colors will invert. If a particle is composed of many small crystallites, it will appear green. Conversely, amorphous materials and liquids are isotropic and appear as the same color as the background of the image, as is shown in Figure 2.1b.

The utility of PLM extends beyond its ability to differentiate crystalline and amorphous materials. For example, PLM can also be used to assess the particle size and morphology of a

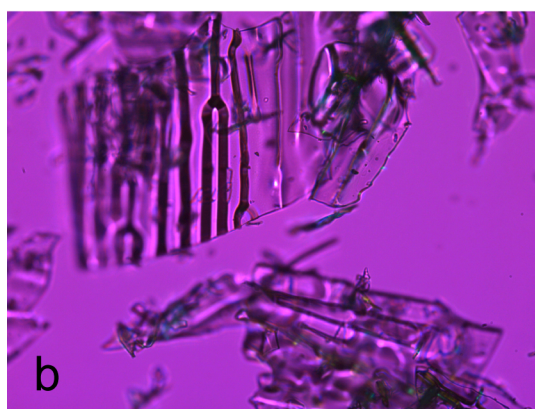
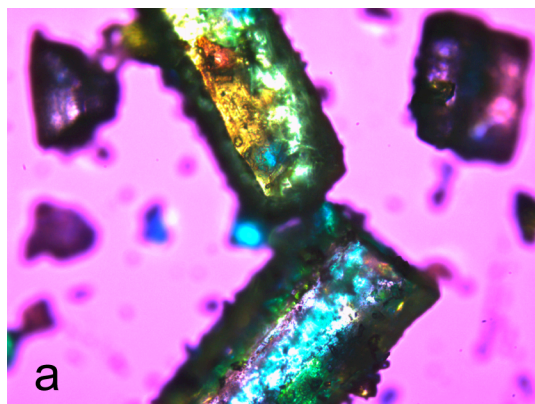


Figure 2.1. Images from polarized-light microscopy of crystalline trehalose dihydrate (a) and amorphous trehalose (b).

solid sample. Additionally, when coupled to a hot stage, the sample can be heated or cooled, and phase transformations can be observed. Examples of solid-state transformations that can be observed with hot-stage microscopy (HSM) include melting, crystallization, and desolvation. Thermomicroscopy has been used to investigate the forms of anhydrous trehalose generated upon dehydration of trehalose dihydrate (T_h).²⁻⁵

2.3 Powder X-Ray Diffraction (PXRD)

X-Ray diffraction techniques operate on the principle of coherent and incoherent scattering of X-rays (with wavelength λ) by a crystal lattice. The spacing between planes in the lattice (d) and the scattering angle (θ) determine if constructive or destructive interference occurs, in accordance with Bragg's Law:

$$n\lambda=2d(\sin\theta) \qquad \text{(Equation 2.1)}$$

When n is an integer, interference is constructive, and the result is a peak at a particular scattering angle. When exposed to X-rays, highly ordered crystalline materials diffract the X-rays to produce a diffraction pattern that is unique to each crystal structure. This can be seen in the PXRD pattern of the crystalline β anhydrate of trehalose (T_β), shown in Figure 2.2. Amorphous materials lack long-range order, resulting in a diffraction pattern that typically consists of a very broad peak with one to two maxima, as can be seen in the PXRD pattern of amorphous trehalose (T_{am}) shown in Figure 2.2. Peaks at characteristic diffraction angles can be used to identify a particular crystalline form, and the “amorphous halo” is used to identify an amorphous material. PXRD analyses can be performed quickly and with minimal sample preparation, but they may be inadequate for detecting low levels of crystallinity or identifying

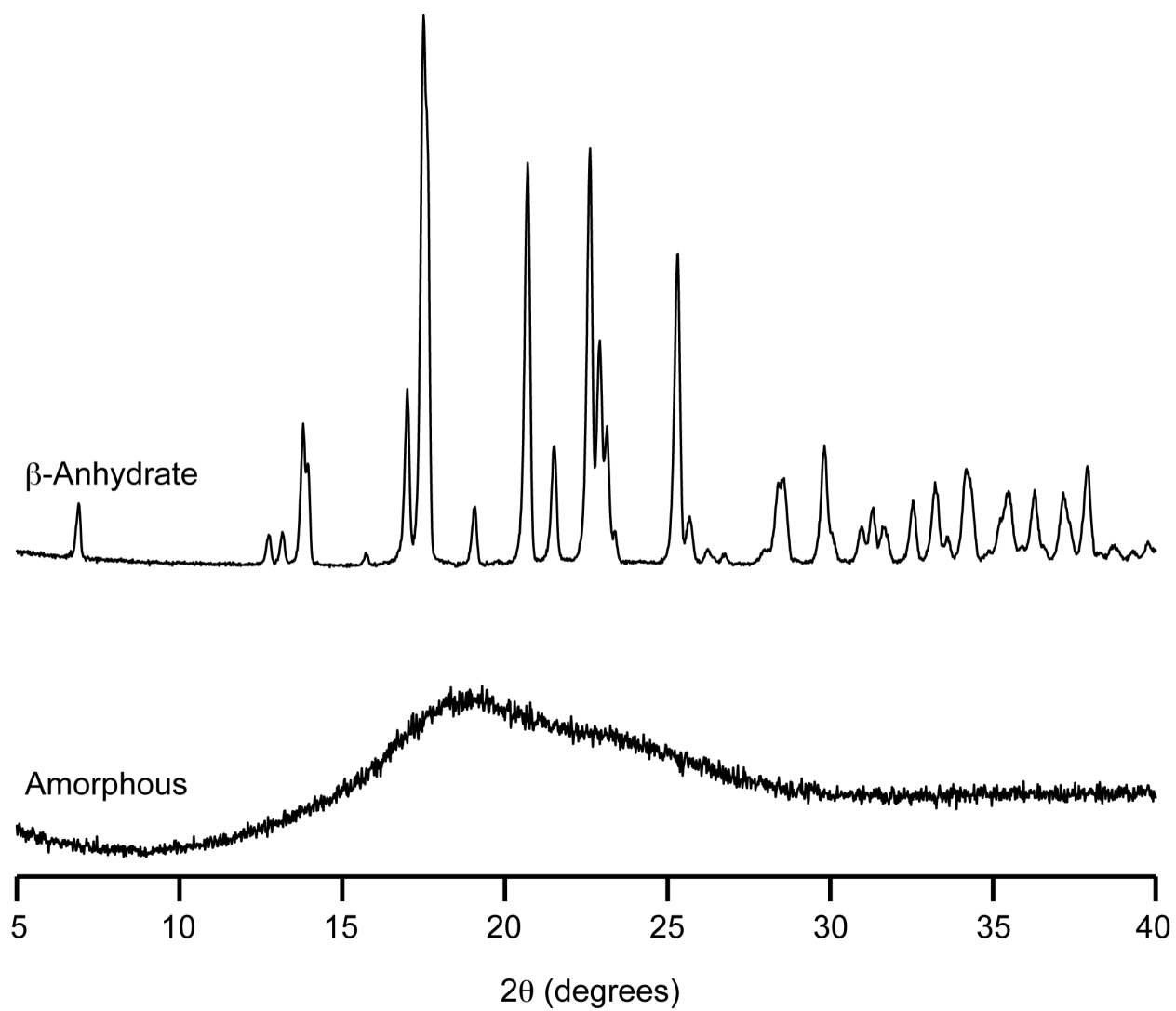


Figure 2.2. PXRD patterns of the crystalline β -anhydrate and amorphous forms of trehalose.

all components within a complex mixture. The trehalose system has been extensively characterized using PXRD, and therefore limited PXRD data is presented in this dissertation.⁵⁻¹⁶

2.4 Differential Scanning Calorimetry (DSC)

2.4.1 Conventional Differential Scanning Calorimetry

In a DSC experiment, the difference in heat flow between a reference and a sample is measured as they are heated, and the resulting thermograms contain exotherms, endotherms, and/or other events that can be used to identify thermal transformations of the sample.¹ The most commonly observed exothermic and endothermic events correspond to crystallization of an amorphous material and melting, respectively. A shift in the baseline of a DSC thermogram represents a change in the heat capacity, such as when an amorphous sample transitions from the rigid glassy state to the more mobile rubbery state. DSC has been used extensively to characterize the trehalose system,^{3-10, 17-35} and DSC analyses have been chosen as the preferred method of comparing the results in this dissertation to those in the literature. In the next few paragraphs, the basic features in DSC thermograms of trehalose are defined, and the applications of DSC to the trehalose system are highlighted.

Figure 2.3 contains thermograms of three different solid samples of trehalose and shows the transformations that can be used to determine which forms of trehalose are present in a sample. In these thermograms, endotherms are represented as downward peaks, and exotherms are represented as upward peaks. A large endotherm near 100 °C (**A**), as is seen in the top thermogram, corresponds to dehydration of trehalose dihydrate (T_h).^{5, 17} Dehydration is a complicated process that involves a number of steps, including loosening and evaporation of water molecules. The shape of this peak and the temperature at which dehydration occurs depend

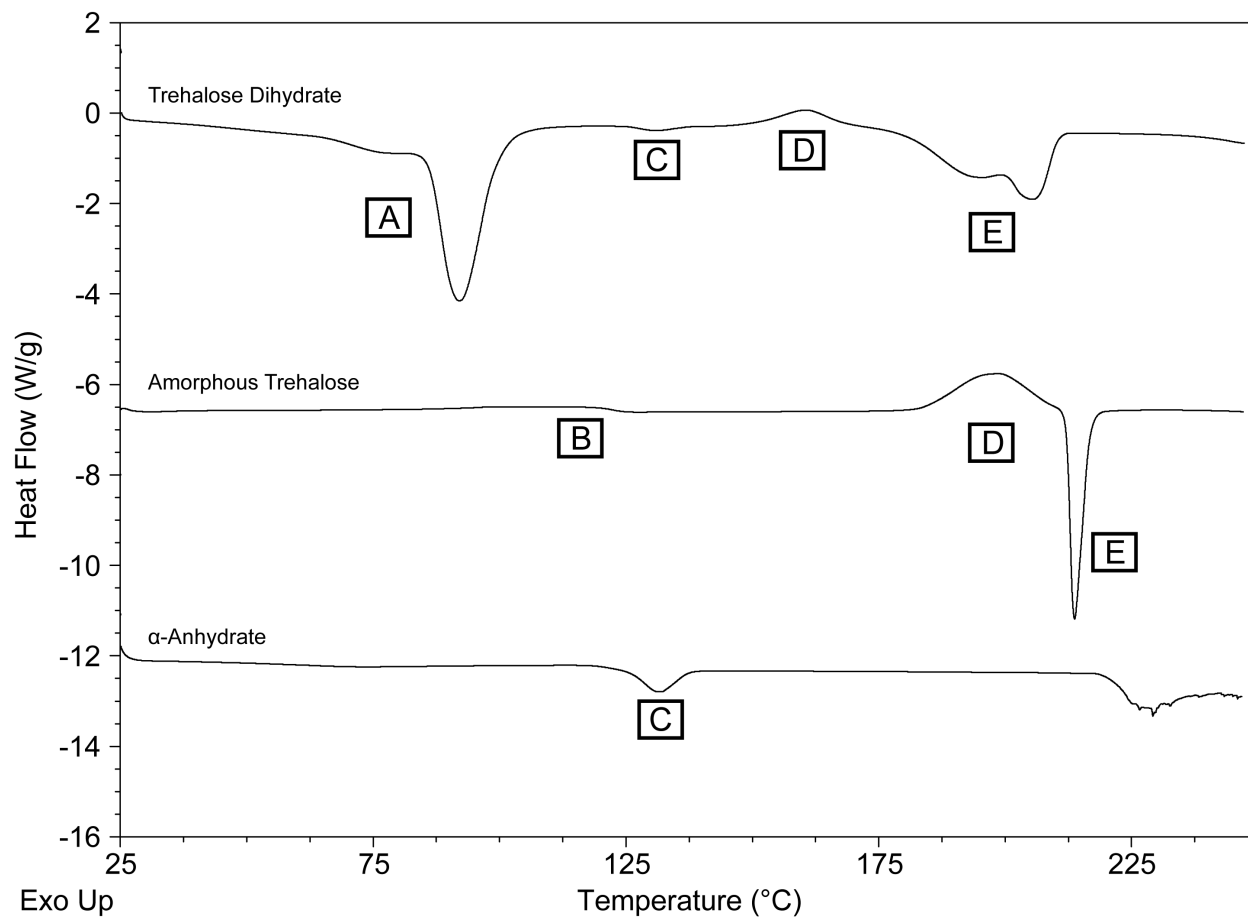


Figure 2.3. DSC thermograms illustrating the various thermal events observed for trehalose. The curves are offset in order to more clearly show the transitions.

upon not just the sample characteristics, but the experimental conditions as well. For example, both smaller particles and a slower heating rate are likely to result in dehydration at lower temperatures.⁵ The dehydration is also affected by the type of pan that is used and whether it is open, pinholed, or hermetically sealed; the sample environment, and therefore the thermal behavior, of a sample can change due to the pressure that results from vaporization of water in a hermetically sealed pan.^{7, 8, 23, 29} In the middle thermogram, the shift in the baseline near 120 °C (**B**) corresponds to the glass transition of amorphous trehalose. In the bottom thermogram, the endotherm at about 132 °C (**C**) represents the melting of T_α . This endotherm is also detected in the top thermogram. Crystallization of melted T_α or rubbery T_{am} can occur between the glass transition temperature of T_{am} and the melting temperature of T_β , and it is indicated by the exotherms in this region (**D**) in the top and middle thermograms. The crystallization temperature is influenced by the presence of crystal nuclei and the thermal history of a sample and is discussed in Chapters 6, 8, and 9. The β polymorph of trehalose (T_β) has reported melting points between 190 and 215 °C, and the endotherms above 175 °C (**E**) in the top and middle thermograms illustrate this variability.^{36, 37} This range appears to be unusually large because typical thermodynamic melting events are expected to occur at specific temperatures with minimal influence from outside factors. However, large ranges of melting temperatures have been reported for other sugars, and it is thought that they result from a kinetic loss of order rather than thermodynamic melting.³⁸ This phenomenon, as well as all other events in thermograms of trehalose, is discussed in greater detail in Chapter 6.

Significant advantages of DSC analyses include that only a few milligrams of material are required and that they can be completed quickly. However, as the complexity of a sample increases, the thermograms become significantly more difficult to interpret. Even for a one-

component system such as trehalose, the overlapping thermal events and variations in expected transition temperatures, as are shown in Figure 2.3, may make it nearly impossible to fully characterize the system using DSC.

2.4.2 Modulated Differential Scanning Calorimetry (MDSC)

MDSC differs from conventional DSC in that a sinusoidal modulation is applied to the temperature ramp, allowing the signals from reversible (thermodynamic) and non-reversible (kinetic) events to be separated. MDSC is particularly useful in the analysis of amorphous materials, and Figure 2.4 shows a typical MDSC thermogram of amorphous trehalose that was subjected to aging. In an MDSC thermogram, the glass transition appears in the reversing signal, and it is accompanied by an endotherm in the non-reversing signal. This endotherm corresponds to the recovery of the enthalpy that was lost during the aging process. The crystallization exotherm is found in the non-reversing signal, and a corresponding event representing the change in heat capacity as the material changes from a liquid to a solid is observed in the reversing signal. Melting endotherms can appear in both signals.

2.5 Thermogravimetric Analysis (TGA)

In a TGA experiment, a sample is placed on a microbalance and heated at a specified rate while the sample mass is monitored. Both the amount of weight loss and the temperature at which weight loss occurs are useful in characterizing solids, particularly hydrates and solvates. Trehalose dihydrate is composed of about 9.5% water,³⁹ and a TGA experiment can be used to determine the temperatures at which water loss is initiated and completed. Processes such as

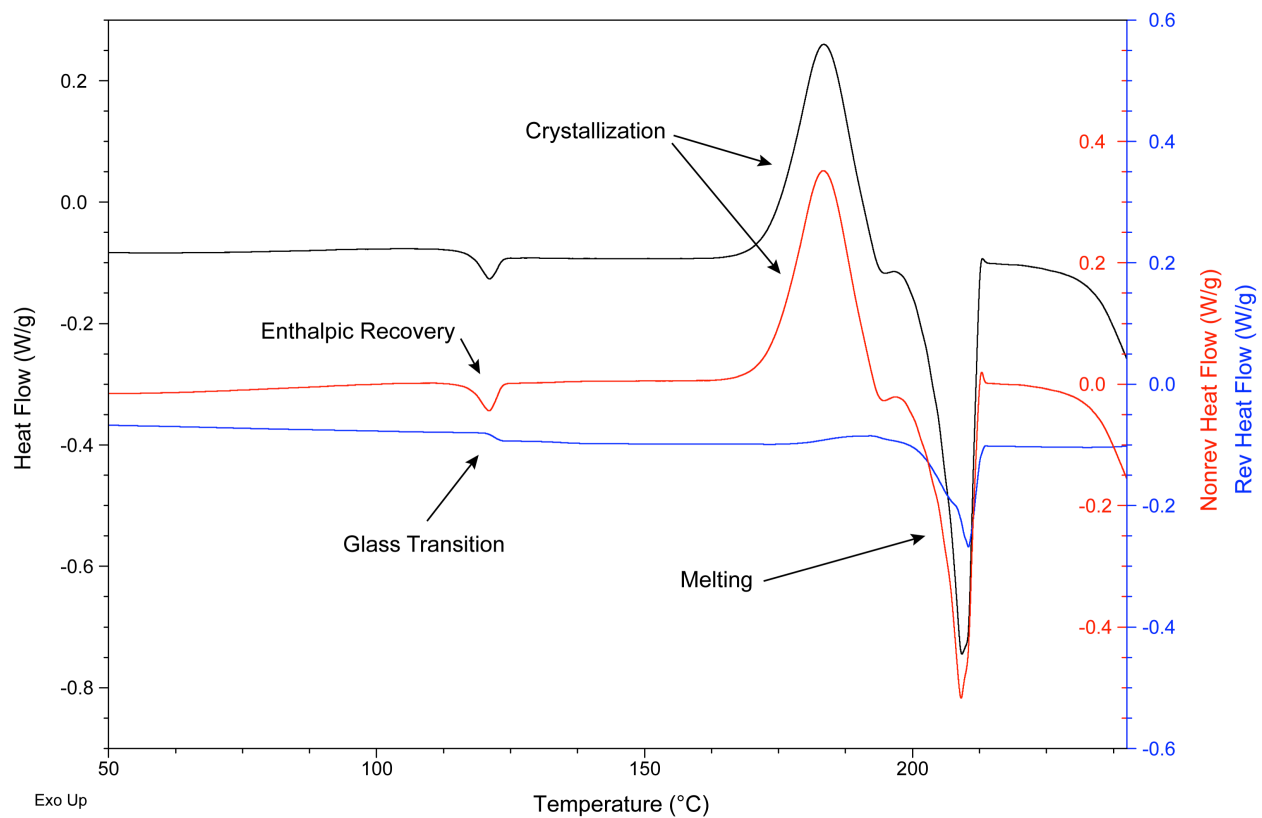


Figure 2.4. MDSC analysis of amorphous trehalose that has been aged.

thermal decomposition can also result in weight loss. By choosing DSC and TGA parameters that are the same (heating rate, sample environment, etc.), results from TGA can be used in the interpretation of thermal events in a DSC thermogram.

2.6 Solid-State Nuclear Magnetic Resonance Spectroscopy (SSNMR)

In a nuclear magnetic resonance (NMR) experiment, NMR-active nuclei are excited, and a signal is recorded as the sample returns to equilibrium. From this signal, detailed structural, chemical, and electronic information on solutions and solids can be obtained. The following sections provide the reader with an understanding of basic NMR theory, identify the challenges associated with NMR experiments performed on solids, and highlight applications of SSNMR to pharmaceutical systems, in particular, those containing trehalose.

2.6.1 Basic NMR Theory

Nuclei are composed of protons and neutrons and have an inherent spin associated with them. Not all nuclei are NMR-active, as this property is dependent upon the nuclear spin. Each nucleus has a spin quantum number, I , which can be zero, an integer, or a half-integer. Nuclei with $I=0$ are NMR inactive. For this work, only two NMR-active nuclei, ^1H and ^{13}C , are of interest. Each has $I=1/2$, which leads to two spin states of $+1/2$ and $-1/2$. In the absence of a magnetic field, these two spins states are degenerate; however, when placed in a static magnetic field, spins aligning with the magnetic field occupy a lower energy state than those aligned against the magnetic field. This is illustrated in Figure 2.5. The intensity of the NMR signal that is observed is proportional to the population difference between the two spin states, and this population difference is governed by the Boltzmann distribution:

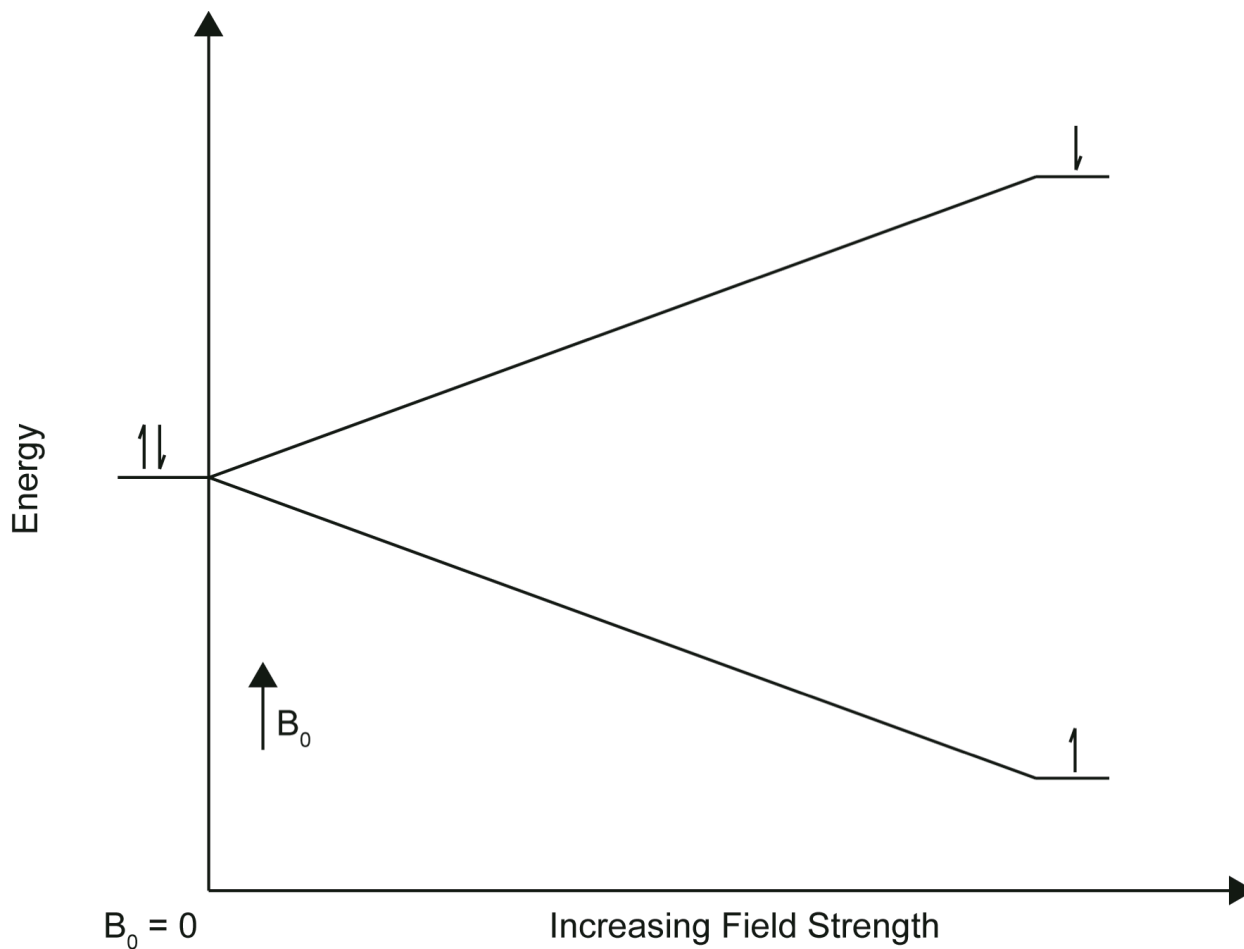


Figure 2.5. Diagram depicting the splitting of nuclear spin states when placed in an external magnetic field. Increasing the strength of the magnetic field increases the population difference between the two energy states and results in a stronger NMR signal.

$$\Delta N = N \left(\frac{\Delta E}{k_B T} \right) \quad (\text{Equation 2.2})$$

where ΔN is the population difference, N is the number of nuclei, $\Delta E = \hbar \gamma B_0$, k_B is the Boltzmann constant, and T is the temperature. The difference in energy, ΔE , between the two states is dictated by the magnetogyric ratio, γ , and the strength of the static magnetic field, B_0 . The magnetogyric ratio is a constant that relates the magnetic moment, μ , and the spin quantum number, and it is inherent to each nucleus.

The external magnetic field, B_0 , exerts a torque on the magnetic moments of the individual nuclei, causing them to precess. The frequency of the precession is known as the Larmor frequency, and it is described by the following equation:

$$\nu = \frac{\gamma}{2\pi} B_0 \quad (\text{Equation 2.3})$$

For a magnetic field strength of 7.05 tesla (T), ^1H nuclei resonate at a frequency of about 300 MHz and ^{13}C nuclei resonate at a frequency of about 75 MHz.

During an NMR experiment, the spin states are perturbed by a sequence of RF pulses at the appropriate Larmor frequency, and as the spins return to equilibrium, they produce a current that is detected in a coil surrounding the sample. Data are acquired as a free induction decay (FID) in the time domain, and the FID is then converted to an NMR spectrum (frequency domain) via a Fourier transform (FT). Spectra with sufficient signal-to-noise ratios are achieved by summation of FIDs acquired after numerous pulses. Very small differences in resonance frequencies (Hz) are compared to a reference frequency (MHz) and are then converted to a parts-per-million (ppm) scale. For a ^1H spectrum, all peaks can usually be found in a 10-ppm range, while ^{13}C spectra require a range of about 200 ppm.

2.6.2 Methods for Signal Enhancement in Solid-state NMR Spectroscopy

Solution and solid-state ^{13}C NMR spectra of 3-methylglutaric acid are shown in Figure 2.6. While the solution spectrum contains well-resolved peaks with narrow lines, the solid-state spectrum contains very broad peaks. In order to acquire an informative NMR spectrum in the solid state, special techniques are required to decrease the linewidth. The application of cross polarization (CP), high-power decoupling, and magic angle spinning (MAS) to solid samples yields high-resolution spectra that provide a wealth of information about these samples.⁴⁰

During cross polarization, magnetization of the abundant ^1H nuclei is transferred to the dilute ^{13}C nuclei. This results in a signal enhancement of about four because the magnetogyric ratio of ^1H is approximately 4x the magnetogyric ratio of ^{13}C . After CP, the relaxation dynamics of the sample are determined by the ^1H nuclei rather than the ^{13}C nuclei. Due to their larger γ , the ^1H nuclei typically relax faster than the ^{13}C nuclei, allowing for shorter delays between pulses.⁴¹ Because of the low natural abundance ($\sim 1.1\%$) of ^{13}C , many scans must be acquired in order to generate a spectrum with a sufficient signal-to-noise ratio. With CP, the large number of scans required for a good ^{13}C SSNMR spectrum can be acquired in a shorter amount of time.

In a solid sample, the molecules have many different fixed orientations with respect to the magnetic field, resulting in different chemical shifts for each orientation. The range of chemical shifts for each nucleus in a solid sample is referred to as chemical shift anisotropy (CSA). The observed chemical shift is represented by the following equation:

$$\sigma_{obs} = \sigma_{iso} + \sigma_{aniso}(3 \cos^2 \theta - 1) \quad (\text{Equation 2.4})$$

where σ_{obs} is the observed chemical shift and σ_{iso} and σ_{aniso} are the isotropic and anisotropic components of the chemical shift, respectively. When $\theta=54.74^\circ$, $\sigma_{obs}=\sigma_{iso}$, and therefore, rotating

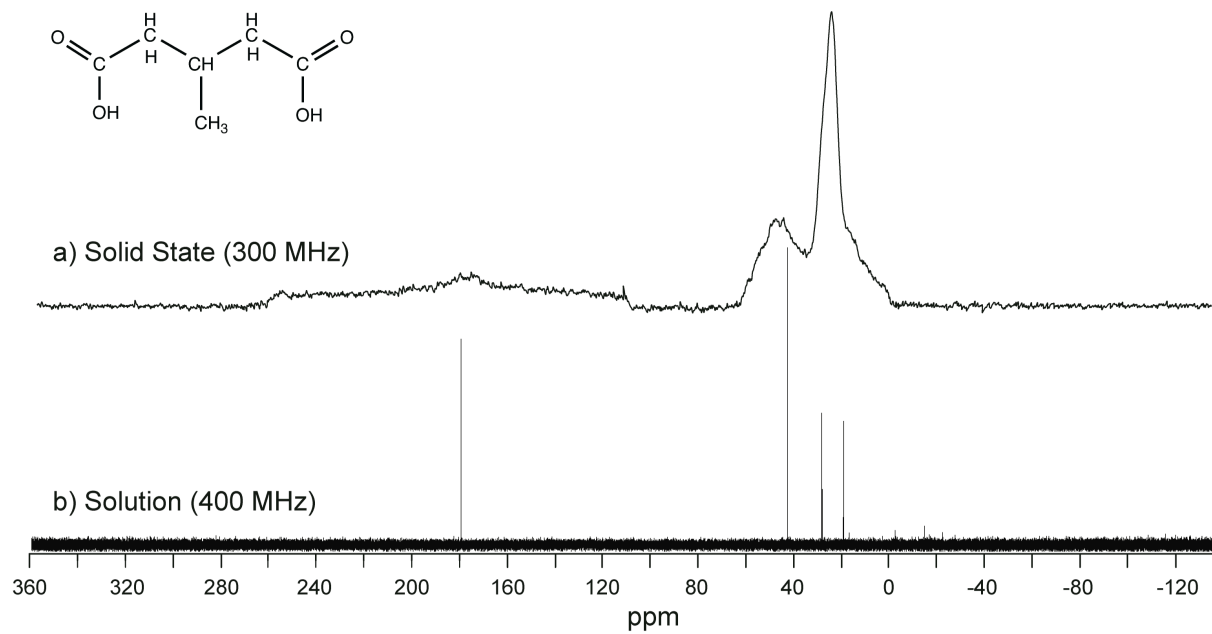


Figure 2.6. Structure of 3-methylglutaric acid and its solid-state (a) and solution (b) NMR spectra.

samples about the magic angle of 54.74° with respect to the magnetic field continuously changes a molecule's orientation in such a way that the effects of CSA are minimized and only the isotropic component is observed.^{42, 43} A side effect of magic angle spinning is the appearance of spinning sidebands in SSNMR spectra. The spinning sidebands result from the periodic variation of the resonance frequencies of the nuclei with the spinning speed. These peaks appear on both sides of the isotropic chemical shifts at multiples of the spinning speed and can be suppressed using a pulse sequence such as TOSS (**T**otal **S**uppression of **S**idebands).⁴⁴

The magnetic moments of the nuclei within a sample can interact with each other via a process referred to as dipolar coupling. Homonuclear coupling occurs between nuclei of the same type, and heteronuclear coupling occurs between nuclei of different types. The strength of these interactions is dependent upon the distance between the nuclei and the product of their magnetogyric ratios. ^{13}C is only about 1.1% naturally abundant, and the probability of finding two ^{13}C nuclei in close enough proximity to interact is low; therefore, ^{13}C - ^{13}C coupling is not usually a concern in unlabeled samples. However, ^1H - ^{13}C interactions are common and significant. This strong heteronuclear dipolar coupling results in very broad SSNMR lines in a ^{13}C SSNMR spectrum. High-power ^1H decoupling prevents the ^1H magnetic moments from interacting with the ^{13}C nuclei, producing narrower peaks and greater spectral resolution in ^{13}C SSNMR spectra. Magic angle spinning also helps remove the effects of dipolar coupling and improve the quality of a SSNMR spectrum.

Figure 2.7 shows the combined effects of CP, MAS, high-power ^1H decoupling, and TOSS. When only CP is applied to a solid sample, as in Figure 2.7a, the spectrum contains very broad peaks, and little structural information can be obtained. As is seen in Figure 2.7b, with the

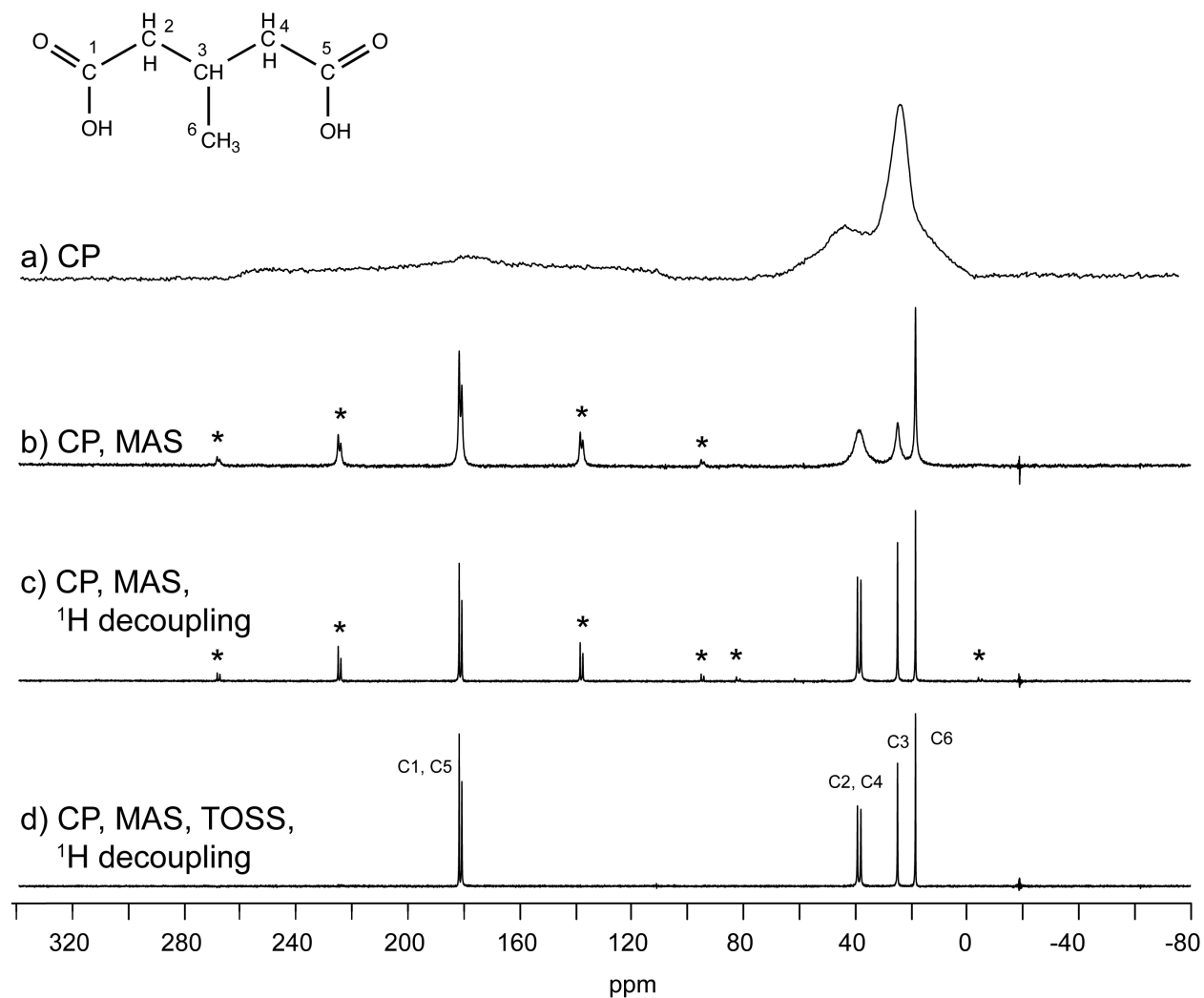


Figure 2.7. Structure and ^{13}C SSNMR spectra of 3-methylglutaric acid: with cross polarization and no spinning (a), with cross polarization and magic angle spinning (b), with cross polarization, magic angle spinning, and high-power ^1H decoupling (c), and with cross polarization, magic angle spinning, suppression of spinning sidebands, and high-power ^1H decoupling (d). Spinning sidebands are marked with an asterisk (*).

addition of MAS, the peaks become much sharper, and spinning sidebands can be seen. When high-power ^1H decoupling is performed in addition to CP and MAS, as is seen in Figure 2.7c, the peaks become even narrower, with the most significant effect observed for C2 and C4. Figure 2.7d shows the effect of adding the TOSS sequence: the spinning sidebands are removed, and a well-resolved spectrum is achieved. The high quality SSNMR spectra acquired using these techniques can be used for the applications described in the next section.

2.6.3 SSNMR in the Analysis of Pharmaceutically Relevant Systems

The application of SSNMR to the analysis of pharmaceutical systems has been described in several excellent review articles.⁴⁵⁻⁴⁹ Unlike the previously described solid-state characterization techniques, SSNMR can be used to characterize both the structure and dynamics of many solid pharmaceutical systems, including solid dispersions, biopharmaceutical formulations, and cocrystals.⁴⁹ Other advantages of SSNMR include:

1. It is non-destructive and non-invasive, allowing for samples to be reclaimed after analysis and further testing to be performed or for intact dosage forms to be analyzed.
2. It is sensitive to short-range order, and structural information about both crystalline and amorphous systems can be obtained.
3. The selectivity of SSNMR enables one to study a specific part of a molecule or different components within a mixture.
4. SSNMR relaxation times can be used to study the mobility of solid systems.
5. SSNMR is inherently a quantitative technique, and when experimental conditions are carefully chosen, a standard is not required.

The wealth of information provided by SSNMR experiments ensures that its presence will continue to increase in the pharmaceutical industry despite the expense of the equipment, long analysis times, and the high level of expertise required to acquire and analyze the data.

The resonance frequency of a particular nucleus, and therefore the chemical shift, is sensitive to the electron density, or electronic environment, surrounding that nucleus. The electronic environment is determined by several factors, including the electronegativity of neighboring atoms/groups, the conformation of the molecule, and interactions with surrounding molecules. The largest differences in chemical shift are determined by the neighboring atoms: for example, a ^{13}C nucleus that is attached to an electronegative oxygen atom experiences reduced electron density and is deshielded from the applied magnetic field. The peak for this nucleus moves upfield to a higher chemical shift that may be tens of ppm from peaks corresponding to other types of ^{13}C nuclei in the molecule. Smaller differences in chemical shifts result from the differences in molecular conformations and interactions, and as a result, different crystalline forms of the same compound have different SSNMR spectra. Addition changes in chemical shifts and linewidths among solid forms result from the conformational flexibility and lack of long-range order in the amorphous state: peaks from amorphous material in a SSNMR spectrum can be at least ten times broader than peaks from crystalline material. Differences in chemical shifts and linewidths provide information about structure and intermolecular interactions: it is this property that makes NMR spectroscopy so important to pharmaceutical scientists.⁴⁵

Figure 2.8 shows the ability of SSNMR to distinguish among the solid forms of trehalose. The spectrum of trehalose dihydrate (Figure 2.8a) and the β -anhydrate form of trehalose (Figure 2.8b) differ in several ways, most notably in the region of the spectrum between 90 and 95 ppm. The high degree of order in crystalline materials results in SSNMR spectra with sharp peaks

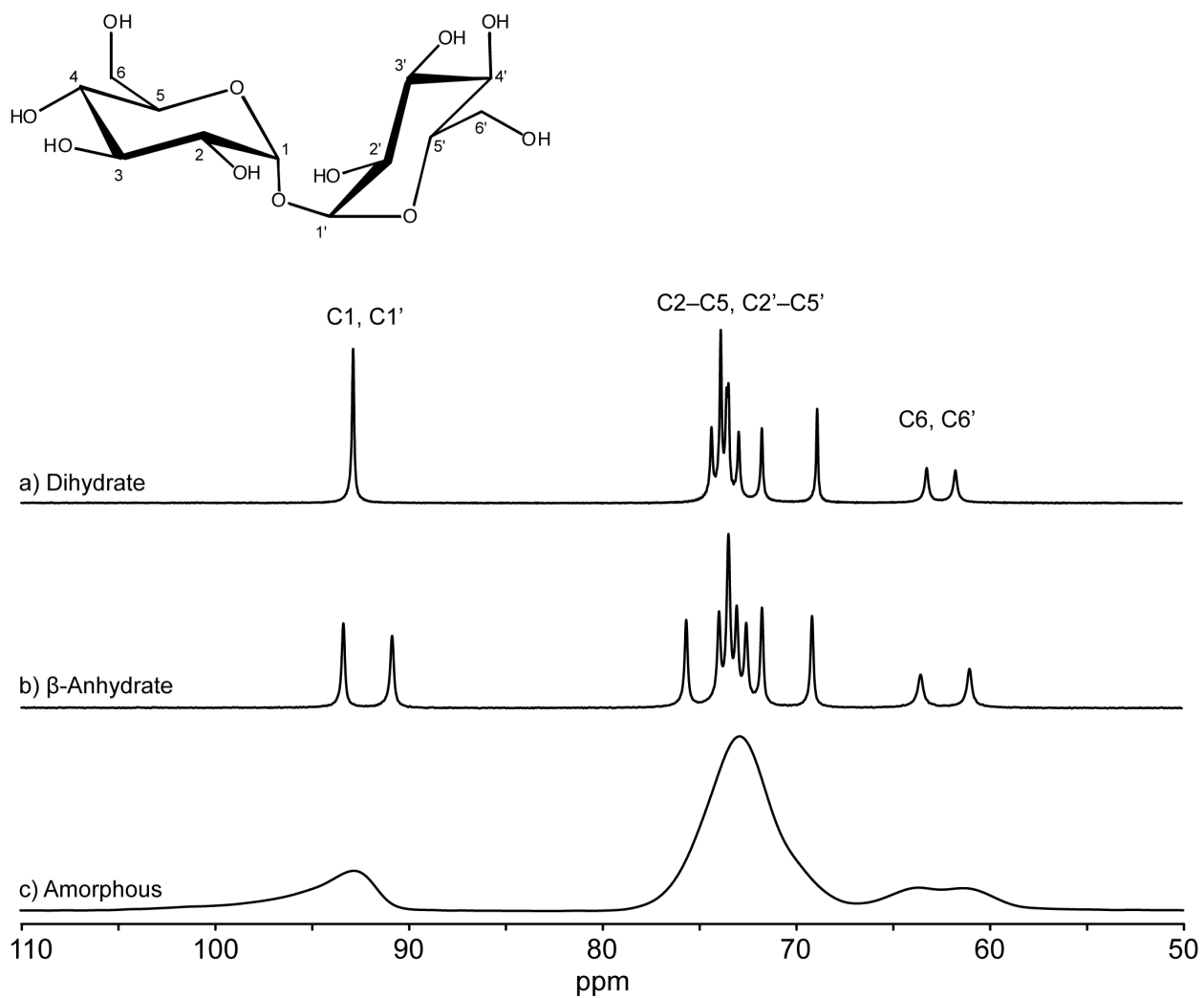


Figure 2.8. Structure of trehalose and ^{13}C SSNMR spectra of three solid forms.

(Figure 2.8a and b), while broad lines are characteristic of SSNMR spectra of amorphous materials (Figure 2.8c). All trehalose peaks are between 50 and 110 ppm, a region of the spectrum that is unoccupied by peaks corresponding to many of the types of carbons that are found in active pharmaceutical ingredients (API): aromatic, olefinic, and carbonyl carbons are found above 120 ppm, and aliphatic carbons are usually found below 40 ppm. This selectivity is especially advantageous when analyzing formulations containing trehalose: many peaks corresponding to trehalose and the API will be well resolved, and each component can be analyzed individually.

In addition to the chemical shifts and linewidths, SSNMR relaxation times are used as a method of characterizing a solid sample. Relaxation times describe the time that it takes spins to return to equilibrium after an RF pulse and are correlated to the molecular mobility. Several relaxation processes exist: spins can lose energy during interactions with other spins (spin-spin relaxation) and by interacting with the surroundings (spin-lattice relaxation). Both ^1H and ^{13}C spin-lattice relaxation times (T_1) have been reported for amorphous trehalose,⁵⁰ but to the best of our knowledge, relaxation times of crystalline forms of trehalose have not been reported in the literature. The spin-lattice relaxation times ($^1\text{H } T_1$) of lactose, another disaccharide, were measured by Lubach et al.⁵¹ Crystalline lactose monohydrate (α -form) had a $^1\text{H } T_1$ relaxation time of 243 seconds, while amorphous lactose produced by lyophilization and spray drying had $^1\text{H } T_1$ relaxation times of about 4 seconds. Crystal defects, introduced via compaction and cryogrinding, reduced the $^1\text{H } T_1$ relaxation times of crystalline lactose in monohydrate and anhydrate forms. The ability of SSNMR relaxation times to distinguish among solid forms was also demonstrated using neotame. Offerdahl et al. measured spin-lattice relaxation times in the rotating frame ($^1\text{H } T_{1\rho}$) of three solid forms of neotame, two crystalline and one amorphous.⁵² A

^1H $T_{1\rho}$ relaxation time of about 70 milliseconds was measured for Form G. ^1H $T_{1\rho}$ relaxation times of Form A and amorphous neotame were approximately 7 and 11 milliseconds, respectively.

Lefort et al. measured the amounts of amorphous trehalose and the β anhydrate in ball-milled samples using SSNMR: quantitation of these samples using DSC was not possible due to overlapping, broad transitions.⁵³ NMR is inherently a quantitative technique, and the integral of an NMR signal is directly proportional to the number of carbons contributing to that signal.

2.7 Conclusions

By using combinations of the techniques described in this chapter, a clearer picture of the transformations among the solid forms of trehalose has emerged. SSNMR, DSC, and PXRD were used in the characterization of mixtures containing a new solid form of trehalose, T_δ (Chapter 5). DSC, TGA, HSM, PLM, and SSNMR were used to investigate the dehydration of T_h (Chapters 6 and 7). Finally, PLM, DSC, and SSNMR were used to investigate the physical properties and stability of amorphous trehalose (Chapters 8 and 9). SSNMR is not yet considered a routine technique, and previously, it was used in a very limited number of studies on trehalose; the results in this dissertation demonstrate its significant contributions to the understanding of this complicated system. Most notably, only SSNMR indicated the presence of T_δ in dehydrated T_h samples and the presence of T_β nuclei in T_{am} samples with decreased physical stability.

2.8 References

1. Byrn, S. R.; Pfeiffer, R. R.; Stowell, J. G., *Solid-state chemistry of drugs*. SSCI, Inc.: 1999.
2. Berton, B.; Dupray, V.; Atmani, H.; Coquerel, G. Gas vacuoles formation during the dehydration of trehalose dihydrate: a Raman microspectroscopy approach. *J. Therm. Anal. Calorim.* **2007**, *90*, 325-328.
3. Dupray, V.; Berton, B.; Ossart, S.; Atmani, H.; Petit, M.-N. Concomitant dehydration mechanisms in single crystals of α,α -trehalose. *Carbohydr. Res.* **2009**, *344*, 2539-2546.
4. Sussich, F.; Urbani, R.; Princivale, F.; Cesáro, A. Polymorphic Amorphous and Crystalline Forms of Trehalose. *J. Am. Chem. Soc.* **1998**, *120*, 7893-7899.
5. Taylor, L. S.; York, P. Characterization of the Phase Transitions of Trehalose Dihydrate on Heating and Subsequent Dehydration. *J. Pharm. Sci.* **1998**, *87*, (3), 347-355.
6. Sussich, F.; Urbani, R.; Cesáro, A.; Princivale, F.; Bruckner, S. New Crystalline and Amorphous Forms of Trehalose. *Carbohydr. Lett.* **1997**, *2*, 403-408.
7. Nagase, H.; Endo, T.; Ueda, H.; Nakagaki, M. An anhydrous polymorphic form of trehalose. *Carbohydr. Res.* **2002**, *337*, 167-173.
8. Willart, J. F.; De Gusseme, A.; Hemon, S.; Descamps, M.; Leveiller, F.; Rameau, A. Vittrification and Polymorphism of Trehalose Induced by Dehydration of Trehalose Dihydrate. *J. Phys. Chem. B* **2002**, *106*, 3365-3370.
9. McGarvey, O. S.; Kett, V. L.; Craig, D. Q. M. An Investigation into the Crystallization of α,α - Trehalose from the Amorphous State. *J. Phys. Chem. B* **2003**, *107*, (27), 6614-6620.
10. Furuki, T.; Kishi, A.; Sakurai, M. De- and rehydration behavior of α,α -trehalose dihydrate under humidity-controlled atmospheres. *Carbohydr. Res.* **2005**, *340*, 429-438.

11. Kilburn, D.; Townrow, S.; Meunier, V.; Richardson, R.; Alam, A.; Ubbink, J. Organization and mobility of water in amorphous and crystalline trehalose. *Nat. Mater.* **2006**, *5*, 632-635.
12. Rani, M.; Govindarajan, R.; Surana, R.; Suryanarayanan, R. Structure in Dehydrated Trehalose Dihydrate—Evaluation of the Concept of Partial Crystallinity. *Pharm. Res.* **2006**, *23*, (10), 2356-2367.
13. Willart, J. F.; Hedoux, A.; Guinet, Y.; Danede, F.; Paccou, L.; Capet, F.; Descamps, M. Metastability Release of the Form α of Trehalose by Isothermal Solid State Vitrification. *J. Phys. Chem. B* **2006**, *110*, 11040-11043.
14. Nagase, H.; Ogawa, N.; Endo, T.; Shiro, M.; Ueda, H.; Sakurai, M. Crystal Structure of an Anhydrous Form of Trehalose: Structure of Water Channels of Trehalose Polymorphism. *J. Phys. Chem. B* **2008**, *112*, 9105-9111.
15. Ballirano, P.; Sadun, C. Thermal behavior of trehalose dihydrate (Th) and b-anhydrous trehalose (Tb) by in-situ laboratory parallel-beam X-ray powder diffraction. *Struct. Chem.* **2009**, *20*, 815-823.
16. Kilburn, D.; Sokol, P. E. Structural Evolution of the Dihydrate to Anhydrate Crystalline Transition of Trehalose as Measured by Wide-angle X-ray Scattering. *J. Phys. Chem. B* **2009**, *113*, 2201-2206.
17. Shafizadeh, F.; Lai, Y. Z. Thermal Rearrangements of Cellobiose and Trehalose. *Carbohydr. Res.* **1973**, *31*, 57-67.
18. Shafizadeh, F.; Susott, R. A. Crystalline Transformations of Carbohydrates. *J. Org. Chem.* **1973**, *38*, (21), 3710-3715.
19. Sussich, F.; Princivalle, F.; Cesáro, A. The interplay of the rate of water removal in the dehydration of α,α -trehalose. *Carbohydr. Res.* **1999**, *322*, 113-119.
20. Macdonald, C.; Johari, G. P. Glass-softening of trehalose and calorimetric transformations in its liquid state. *J. Mol. Struct.* **2000**, *523*, 119-132.

21. Sussich, F.; Skopec, C.; Brady, J.; Cesáro, A. Reversible dehydration of trehalose and anhydrobiosis: from solution state to an exotic crystal? *Carbohydr. Res.* **2001**, *334*, 165-176.
22. Willart, J. F.; De Gusseme, A.; Hemon, S.; Odou, G.; Danede, F.; Descamps, M. Direct crystal to glass transformation of trehalose induced by ball milling. *Solid State Commun.* **2001**, *119*, 501-505.
23. Sussich, F.; Bortoluzzi, S.; Cesáro, A. Trehalose dehydration under confined conditions. *Thermochim. Acta* **2002**, *391*, 137-150.
24. Surana, R.; Pyne, A.; Suryanarayanan, R. Effect of preparation method on physical properties of amorphous trehalose. *Pharm. Res.* **2004**, *21*, (7), 1167-76.
25. Surana, R.; Pyne, A.; Suryanarayanan, R. Effect of aging on the physical properties of amorphous trehalose. *Pharm. Res.* **2004**, *21*, (5), 867-74.
26. Surana, R.; Pyne, A.; Rani, M.; Suryanarayanan, R. Measurement of enthalpic relaxation by differential scanning calorimetry - effect of experimental conditions. *Thermochim. Acta* **2005**, *433*, 173-182.
27. Jones, M. D.; Hooton, J. C.; Dawson, M. L.; Ferrie, A. R.; Price, R. Dehydration of trehalose dihydrate at low relative humidity and ambient temperature. *Int. J. Pharm.* **2006**, *313*, 87-98.
28. Simperler, A.; Kornherr, A.; Chopra, R.; Jones, W.; Motherwell, W. D. S.; Zifferer, G. The glass transition temperatures of amorphous trehalose-water mixtures and the mobility of water: an experimental and in silico study. *Carbohydr. Res.* **2007**, *342*, 1470-1479.
29. Cesáro, A.; De Giacomo, O.; Sussich, F. Water interplay in trehalose polymorphism. *Food Chem.* **2008**, *106*, 1318-1328.
30. Furuki, T.; Abe, R.; Kawaji, H.; Atake, T.; Sakurai, M. Effect of Atmospheric Pressure on the Phase Transitions of α,α -Trehalose Dihydrate: DTA study of the dehydration behavior in open systems. *J. Therm. Anal. Calorim.* **2008**, *93*, (2), 561-567.

31. Luthra, S. A.; Hodge, I. M.; Pikal, M. J. Effects of Annealing on Enthalpy Relaxation in Lyophilized Disaccharide Formulations: Mathematical Modeling of DSC Curves. *J. Pharm. Sci.* **2008**, *97*, 3084-3099.
32. Dranca, I.; Bhattacharya, S.; Vyazovkin, S.; Suryanarayanan, R. Implications of Global and Local Mobility in Amorphous Sucrose and Trehalose as Determined by Differential Scanning Calorimetry. *Pharm. Res.* **2009**, *26*, 1064.
33. Schebor, C.; Mazzobre, M. F.; Buera, M. d. P. Glass transition and time-dependent crystallization behavior of dehydration bioprotectant sugars. *Carbohydr. Res.* **2010**, *345*, 303-308.
34. Sussich, F.; Skopec, C. E.; Brady, J. W.; Cesáro, A. Water mobility in the dehydration of crystalline trehalose. *Food Chem.* **2010**, *122*, 388-393.
35. Li, X.; Mansour, H. M. Physicochemical Characterization and Water Vapor Sorption of Organic Solution Advanced Spray-Dried Inhalable Trehalose Microparticles and Nanoparticles for Targeted Dry Powder Pulmonary Inhalation Delivery. *AAPS PharmSciTech* **2011**.
36. Reisener, H. J.; Goldschmid, H. R.; Ledingham, G. A.; Perlin, A. S. Formation of Trehalose and Polyols by Wheat Stem Rust (*Puccinia Graminis Tritici*) Uredospores. *Can. J. Biochem. Phys.* **1962**, *40*, 1248-1251.
37. Ohashi, T.; Yoshii, H.; Furuta, T. Innovative crystal transformation of dihydrate trehalose to anhydrous trehalose using ethanol. *Carbohydr. Res.* **2007**, *342*, 819-825.
38. Lee, J. W.; Thomas, L. C.; Schmidt, S. J. Investigation of the Heating Rate Dependence Associated with the Loss of Crystalline Structure in Sucrose, Glucose, and Fructose Using a Thermal Analysis Approach (Part I). *J. Agr. Food Chem.* **2011**, *59*, 684-701.
39. Mitscherlich, E. Ueber die Mycose, den Zucker des Mutterkorns. *Liebigs Ann. Chem.* **1858**, *106*, (1), 15-18.
40. Stejskal, E. O.; Schaefer, J. Magic-Angle Spinning and Polarization Transfer in Proton-Enhanced NMR. *J. Magn. Reson.* **1977**, *28*, 105-112.

41. Pines, A.; Gibby, M. G.; Waugh, J. S. Proton-enhanced NMR of Dilute Spins. *J. Chem. Phys.* **1973**, *59*, 569-590.
42. Andrew, A. R.; Bradbury, A.; Eades, R. G. Removal of dipolar broadening of nuclear magnetic resonance spectra of solids by specimen rotation. *Nature* **1958**, *183*, 1802-1803.
43. Lowe, I. J. Free Induction Decays of Rotating Solids. *Phys. Rev. Lett.* **1959**, *2*, (7), 285-287.
44. Dixon, W. T.; Schaefer, J.; Sefcik, M. D. Total suppression of sidebands in CPMAS carbon-13 NMR. *J. Magn. Reson.* **1982**, *49*, (2), 341-345.
45. Tishmack, P. A.; Bugay, D. E.; Byrn, S. R. Solid-state nuclear magnetic resonance spectroscopy--pharmaceutical applications. *J. Pharm. Sci.* **2003**, *92*, (3), 441-74.
46. Offerdahl, T. J.; Munson, E. J. Solid state NMR spectroscopy of pharmaceutical materials. *Amer. Pharm. Rev.* **2004**, *7*, (1), 109-112.
47. Berendt, R. T.; Sperger, D. M.; Munson, E. J.; Isbester, P. K. Solid-state NMR spectroscopy in pharmaceutical research and analysis. *TrAC* **2006**, *25*, (10), 977-984.
48. Geppi, M.; Mollica, G.; Borsacchi, S.; Veracini, C. A. Solid-State NMR Studies of Pharmaceutical Systems. *Appl. Spectrosc. Rev.* **2008**, *43*, 202-302.
49. Vogt, F. G. Evolution of solid-state NMR in pharmaceutical analysis. *Future Med. Chem.* **2010**, *2*, (6), 915-21.
50. Luthra, S. A.; Pikal, M. J.; Utz, M. Solid State ¹³C NMR Investigation of Impact of Annealing in Lyophilized Glasses. *J. Pharm. Sci.* **2008**, *97*, (10), 4336-4346.
51. Lubach, J. W.; Xu, D.; Segmuller, B. E.; Munson, E. J. Investigation of the effects of pharmaceutical processing upon solid-state NMR relaxation times and implications to solid-state formulation stability. *J. Pharm. Sci.* **2007**, *96*, (4), 777-787.
52. Offerdahl, T. J.; Salsbury, J. S.; Dong, Z.; Grant, D. J. W.; Schroeder, S. A.; Prakash, I.; Gorman, E. M.; Barich, D. H.; Munson, E. J. Quantitation of Crystalline and Amorphous Forms

of Anhydrous Neotame using ^{13}C CPMAS NMR Spectroscopy. *J. Pharm. Sci.* **2005**, *94*, (12), 2591-2605.

53. Lefort, R.; De Gusseme, A.; Willart, J. F.; Danede, F.; Descamps, M. Solid state NMR and DSC methods for quantifying the amorphous content in solid dosage forms: an application to ball-milling of trehalose. *Int. J. Pharm.* **2004**, *280*, (1-2), 209-19.

Chapter 3
Literature Review

3.1 Introduction

The properties of the solid forms of trehalose and the interconversions among the forms are the subject of more than 75 published papers. This chapter highlights three key areas from the literature: 1) the structure of the solid forms of trehalose, 2) the dehydration of trehalose dihydrate, and 3) the physical stability of amorphous trehalose. A discussion of these areas of interest provides some perspective on the extent of confusion and disagreement in the literature and acts as a testimony to the complexity of the trehalose system.

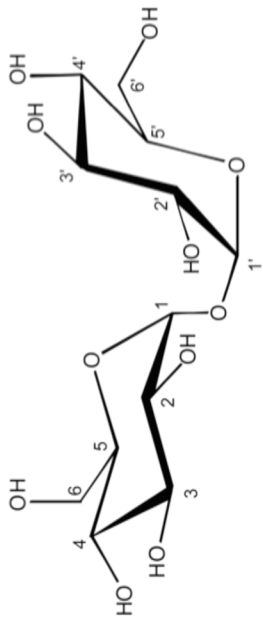
3.2 Conformation and Structure of Trehalose in the Solid Forms

Numerous studies have addressed the conformation and structure of trehalose in the four known forms, three crystalline and one amorphous, in order to gain insight into not just the stabilities of the solid forms, but also the possible mechanisms by which trehalose stabilizes biomolecules in nature and in pharmaceutical formulations. Data from these studies are summarized in the following sections.

3.2.1 Crystalline Forms of Trehalose

Trehalose is found in three crystalline forms: the dihydrate (T_h), the β -anhydrate (T_β), and the α -anhydrate (T_α). The crystal structures of T_h , T_β , and T_α have been solved,¹⁻⁵ and selected data from the crystal structure determinations are presented in Table 3.1. The trehalose molecules have roughly C2 symmetry, and the approximate conformation of the glucopyranose residues is 4C_1 (chair).³ The glycosidic linkage angles (C1-O1-C1') are similar, ranging from about 113° in T_α and T_β to about 116° in T_h . In comparing the

Table 3.1. Data from crystal structure determinations of the dihydrate, β -anhydrate, and α -anhydrate forms of trehalose.



Form	T _h ¹	T _h ¹	T _h ¹	T _h ²	T _h ³	T _h ⁴	T _h ⁵	T _h ⁶	T _h ⁷	T _h ⁸	T _h ⁹	T _h ¹⁰	T _h ¹¹	T _h ¹²
Reference	Brown ¹	Brown ¹	Brown ¹	Taga ²	Nagase ⁴	Nagase ⁴	Stevens ⁵	Jeffrey ³	Nagase ⁴					
Temperature (°C)	23.5±0.5		18.0±1.0		2.5		100 K	-150	-180					
a (Å)	12.229(2)	12.230(2)	12.233(3)	17.90±0.02	7.5969(10)	7.5609(2)	7.5609(2)	12.971(5)	6.7999(15)					
b (Å)	17.890(3)	17.890(3)	17.889(4)	12.21±0.01	12.2305(10)	12.2002(3)	12.2002(3)	8.229(4)	11.638(3)					
c (Å)	7.597(1)	7.595(1)	7.596(2)	7.586±0.008	17.887(5)	17.8482(4)	17.8482(4)	6.789(7)	18.583(5)					
Crystal System		Orthorhombic			Orthorhombic	Orthorhombic	Orthorhombic	Monoclinic	Orthorhombic					
Space Group		P2 ₁ -2 ₁ -2 ₁		P2 ₁ -2 ₁ -2 ₁	P2 ₁ -2 ₁ -2 ₁	P2 ₁ -2 ₁ -2 ₁	P2 ₁ -2 ₁ -2 ₁	P2 ₁	P2 ₁ -2 ₁ -2 ₁					
Z		4		4	4	4	4	2	4					
C1-O1-C1' (°)		115.8		115.7(3)	115.87(13)			113.3(4)	113.0(9)					
O5-C1-O1-C1' (°)		74.8		75				60.8(6)						
O5'-C1'-O1-C1 (°)		61.7		61.7				60.1(6)						
O5-C5-C6-O6 (°)		-75.6		-75.3	69.83(19)			-72.1(6)	-63.4(11)					
O5'-C5'-C6'-O6' (°)		69.8		69.8	-75.67(9)			71.0(6)	-61.0(12)					

O5-C1-O1-C1' and O5'-C1'-O1-C1 angles in the T_h and T_β forms, the glucopyranose residues are oriented around O1 more symmetrically in T_β . Although the crystal structure data indicate that the conformations surrounding C1 and C1' are more symmetric in T_β , the ^{13}C SSNMR spectra contradict this: in the spectrum of T_h , a single resonance appears for C1 and C1', but in the spectra of T_β , the C1 and C1' resonances are separated. Stevens suggested that this discrepancy is because chemical shifts are sensitive to both conformational differences and crystal packing effects.⁵

The exception to the twofold symmetry of the trehalose molecules in each crystalline form lies in the orientations of the primary alcohol groups: the O5-C5-C6-O6 and O5'-C5'-C6'-O6' angles indicate that the primary alcohol groups are gauche-trans and gauche-gauche in T_h and T_β , and they are both gauche-gauche in T_α . Although T_α and T_h are considered to be structurally similar,⁶ the difference in these angles demonstrate that T_α is not a true isomorphous desolvate. The difference in the orientations of the primary alcohol groups is reflected in the ^{13}C SSNMR spectra: the spectra of T_h and T_β contain two well-resolved resonances for C6 and C6' (≥ 1.3 ppm) that are farther upfield than the peaks for T_α , which are only separated by 0.2 ppm. Previously, it was reported that the C6 and C6' peaks in T_α appeared as a singlet.⁷ When comparing T_h and T_β , the asymmetry within T_h is greater than that within T_β .⁷ Despite this, the difference in chemical shifts of the C6 and C6' peaks is larger in T_β (2.3 ppm) than it is in T_h (1.3 ppm).

The three crystalline forms of trehalose contain many intermolecular hydrogen bonds but no intramolecular hydrogen bonds.⁸ In T_h , trehalose and two water molecules are bound by twelve crystallographically independent hydrogen bonds.^{1,2,4,5} In T_h , Nagase et al. found seven hydroxyl groups bonded to crystal waters (W1 and W2) and five hydroxyl groups bonded to O1

and hydroxyl groups from an adjacent molecule of trehalose; four of the five hydrogen bonds that do not involve water molecules are maintained when T_h transforms to T_α .⁴ During the transformation, five hydrogen bond sequences form, resulting in a total of nine hydrogen bonds in T_α . In T_β , there are eleven hydrogen bonds.³ Of the three forms, T_α has the fewest hydrogen bonds, and it has been reported that the intermolecular interactions are weakest in this form.⁴

The release of water molecules from the crystal structure of T_h to form T_α results in holes in the crystal structure of T_α . Nagase et al. identified two different types of holes in T_α , both with a diameter of 4.3 Å.⁴ One hole is large and corresponds to the vacant position of W1 (Hole 1); the other is small and corresponds to W2's position (Hole 2). Sussich et al. used DSC to confirm the non-equivalent positions of W1 and W2 and that the water molecules can interchange their positions.⁹ Hole 1 is considered to be a one-dimensional water channel, and it is thought that water molecules in the channel can move to the W2 position reversibly. Petit and Coquerel proposed that water must leave through a channel in order for the structure of the starting material to be maintained, as occurs when T_h transforms to T_α .¹⁰ The formation of T_α via the reversible loss of water from T_h via channels is thought to play an important role in the ability of trehalose to act as a desiccation protectant in nature.⁶

3.2.2 Amorphous Trehalose

It is difficult to study the local structure of trehalose in the amorphous state, and SSNMR has proved exceptionally useful in this area of research. In the SSNMR spectrum of T_{am} , the C1 peak is very broad (> 15 ppm) and asymmetric, and the breadth is associated with variations in the glycosidic linkage torsion angles ϕ and φ (O5-C1-O1-C1' and O5'-C1'-O1-C1, respectively).¹¹ In SSNMR spectra of amorphous sucrose and lactose, the peak for the glycosidic

carbons (C1) is about 10 ppm wide, suggesting that the trehalose molecules in T_{am} are more flexible than other disaccharides.¹² Using ab initio quantum mechanical methods, Zhang et al. showed that the distribution of glycosidic torsion angles in T_{am} is centered around $(\phi, \varphi) = (76^\circ, 76^\circ)$,¹¹ which is different from the torsion angles in the crystalline forms (Table 3.1). The glycosidic torsion angles could vary by as much as 50° , which may contribute to the stabilizing power of trehalose.¹²

3.3 Dehydration of Trehalose Dihydrate

Anhydrous forms of trehalose are generated by dehydrating trehalose, but the conditions governing which form (or forms) is generated are not yet understood. In this section, several factors that have been shown to influence the dehydration behavior are discussed, including the temperature, heating rate, particle size, and sample environment.

3.3.1 Isothermal Dehydrations of Trehalose Dihydrate

Isothermal dehydration conditions that have been reported to produce anhydrous forms of trehalose from T_h are listed in Table 3.2. Dehydration temperatures as low as 60°C and as high as 170°C have been reported to generate T_β from T_h .^{13, 14} T_β formed by dehydration of T_h could proceed through an amorphous intermediate or may be formed directly, but a direct transformation from T_h to T_β was ignored in two diagrams that claim to outline the transformations among the solid forms of trehalose.^{6, 15} Sussich et al. dehydrated T_h at 130°C for

Table 3.2. Isothermal dehydrations of trehalose dihydrate. The table is sorted by increasing temperature in order to more effectively demonstrate that low temperatures do not always result in T_α, high temperatures do not always result in T_β, etc.

Reference	Dehydration Conditions	Resulting Form
Willart et al. ¹⁶	50 °C under dry nitrogen for 3 hours	α
Gil et al. ⁷	50 °C under vacuum for 48 hours	α
Chakravarty et al. ¹³	60 °C	α
Surana et al. ¹⁷	60 °C at 20% RH for ≥ 24 hours	β
Rani et al. ¹⁸	60 °C at 20% RH for several hours	β
Ding et al. ¹⁹	70 °C under vacuum for 3 days	Amorphous
Gil et al. ⁷	85 °C in an NMR rotor	β
Reisener et al. ²⁰	85 °C under vacuum for 4 hours	α
Sussich et al. ²¹	85 °C under vacuum for 4 hours	α
Surana et al. ¹⁷	97 °C in N ₂ atmosphere at ~400 Torr for 24 hours	Amorphous
Surana et al. ¹⁷	100 °C under vacuum for 24 hours	Amorphous
Taylor and York ²²	120 °C for 5 minutes	β
Dranca et al. ²³	125 °C in N ₂ atmosphere at ~400 Torr for 1 hour	Amorphous
Mitscherlich ²⁴	130 °C	β
Sussich et al. ²¹	130 °C for 4 hours	β
Berton et al. ²⁵	130 °C for 4 hours	β
Reisener et al. ²⁰	130 °C in an open flask for 4 hours	β
Lefort et al. ¹⁴	170 °C under vacuum for 2 hours	β

periods of time ranging from 15 to 240 minutes and used differential scanning calorimetry (DSC) to monitor the progress of the dehydration.²⁶ After 30 minutes, the dehydration was complete, but the DSC thermograms indicated that the sample contained both T_{am} and T_{β} . After 100 minutes, T_{am} was not present in the dehydrated samples, indicating that any T_{am} formed upon dehydration was able to crystallize to T_{β} . While these results demonstrate that a fraction of T_{β} generated from dehydration of T_h is formed from an amorphous intermediate, it is not clear if a direct transformation is occurring concurrently. Chakravarty et al. monitored the direct formation of T_{β} as a sample of T_h was held at 60 °C and 11% relative humidity (RH) using FT-Raman spectroscopy.¹³ This low-temperature transition to T_{β} was explained using a “bridge effect” mechanism in which the surrounding water vapor traps the water molecules that escape from the crystal structure of T_h and promotes the molecular rearrangement to T_{β} .²⁷

Isothermal dehydration temperatures that have been reported to result in the formation of T_{α} from T_h are lower than those that form T_{β} and range from 50 °C to 85 °C (Table 3.2). As discussed previously, crystal structures of T_h and T_{α} are similar, and as water leaves T_h slowly, as occurs during dehydration at lower temperatures, much of the structure is maintained.²⁸ Willart et al. reported on a critical rate of water removal (1.14×10^{-5} mL/(min•g)), above which T_{am} is formed and below which T_{α} is formed.¹⁶ Interestingly, Rani et al. found that dehydration of T_h at 40 °C, 60 °C, and 85 °C produced mixtures of T_{α} and T_{am} and that the fraction of T_{α} decreased with increasing temperature.¹⁸

Isothermal dehydration temperatures that reportedly lead to the generation of T_{am} range from 70 °C to 125 °C.^{19,23} Ding et al. first reported upon the formation of T_{am} from dehydration of T_h at 70 °C,¹⁹ but Willart et al. suggested that the form they observed was actually T_{α} .¹⁶ Rani et al. showed that dehydration of T_h at 40 °C results in a sample with ~40% amorphous content,

and that the amorphous content increases as the dehydration temperature increases.¹⁸ Recent studies have shown that T_h can crystallize during the lyophilization process and then undergo dehydration to form T_{am} during primary and secondary drying in the temperature range of -25 °C to 10 °C.²⁹ T_{am} has also been produced when the water molecules in T_h are removed via alternative treatments such as microwave treatment or supercritical CO_2 fluid extraction.^{30, 31}

3.3.2 Non-Isothermal Dehydrations of Trehalose Dihydrate

Table 3.3 summarizes the non-isothermal conditions that have been used to analyze the dehydration of T_h via DSC and illustrates the difficulty in interpreting the thermograms: transitions occur at different temperatures, and the identification of thermal events is not consistent. In the ten years that have passed since McGarvey et al. addressed the confusion regarding the interpretation of DSC thermograms of T_h ,³² little progress has been made. In the next few sections, some of the factors that have been shown to influence the thermal transformations of T_h are summarized.

3.3.2.1 Influence of Particle Size on the Dehydration of Trehalose Dihydrate

Taylor and York analyzed fractionated particles of T_h (<45 , $45-75$, $75-150$, $150-250$, $250-425$, and >425 - μm) and observed DSC and TGA thermograms that were different from each other and from the thermograms of the unfractionated sample.²² The effects were thought to be unrelated to thermal lag associated with differences in particle size. The authors concluded that T_h can be crystallized to T_β via two routes that depend primarily upon the particle size. Smaller

Table 3.3. Observations from Non-Isothermal Dehydrations of Trehalose Dihydrate Performed by DSC. The table is sorted chronologically.

Reference	Sample Description	Heating Rate (°C/minute)	Sample Environment	Key Observations
Shafizadeh and Lai ³³		15		Two endotherms: 100 and 215 °C
Shafizadeh and Susott ³⁴		5, 15	Hermetic, covered, open pans	Closed: Simultaneous melting of T _h and crystallization of T _β Open: T _h forms T _{am} which melts at 135 °C and then crystallizes
Green and Angell ³⁵		10		Endotherm (90–100 °C): T _h melt Well-defined melting event only when Zn < 4 ppm
Sussich et al. ³⁶		20	Pinholed pan	Three endotherms: water loss, T _γ →T _β , T _β melt
Sussich et al. ²¹		1, 2, 5, 10, 20, 30, 40, 60	Pinholed pan	Slow heating: T _h →T _{am} All heating rates: T _β melt
Taylor and York ²²	Sieved particles (<45, 45–75, 75–150, 150–250, 250–425, >425 μm)	1, 2, 4, 6, 8, 10	Vented pan	Small particles: T _h →T _{am} →T _β Large particles: T _h →T _β , formation of anhydrous outer layer around a T _h core
Sussich et al. ²⁶	<100-μm particles	5–50	Pinholed pan	T _γ =T _h +T _β
Macdonald and Johari ³⁷		20	Open pan	Endotherm at 100 °C: dehydration, dissolution, evaporation, tautomerization, crystallization
Nagase et al. ²⁸	Ground, sieved (<150 μm)	2	Open pan (no gas flow)	Two endotherms: 100 and 210 °C One exotherm: 166 °C
Sussich et al. ³⁸		1	Pinholed (0.1, 0.5, 0.9, 1.2 mm), open, hermetic pans	Two events are constantly present: dehydration and melting of T _β
Willart et al. ¹⁶		1, 5, 10, 20, 50	Open pan	Fast heating rate: T _h →T _{am} Slow heating rate: T _h →T _α
McGarvey et al. ³²	50–100-μm particles	10	Pinholed pan	Three endotherms: 100, 122, 211 °C “There is still considerable debate regarding the interpretation of the DSC data for the dihydrate”
Furuki et al. ²⁷	Ground, sieved (<45 μm)	2	Dry N ₂ , P _{H2O} = 3 and 5 kPa	Dry N ₂ atmosphere: T _h →T _α Humid atmosphere: T _h →T _β Existence of T _ε suggested
Jones et al. ³⁹	Sieved (<63 μm); Recrystallized	5	Open pan	Large particle: broad, irregular event (122–175 °C) and no T _β melt
Furuki et al. ⁴⁰	~63-μm particles	2	Pressure = 101, 75, 61, 48, 35 kPa	Endotherm at 100 °C: T _h melt Endotherm at 122 °C: dehydration
Dupray et al. ⁴¹	Recrystallized (large particles)	1		Particle surface: T _h →T _{am} →T _β (100–118 °C) Fluid phase then migrates to surface
Sussich et al. ⁹		0.025, 0.05, 0.1, 0.25	Pinholed pan	Splitting of endotherm (60–100 °C): removal of non-equivalent H ₂ O molecules
Li and Mansour ⁴²	~60-μm particles		Hermetic pan	Endotherm at 100 °C: loss of unbound H ₂ O Endotherm at 140 °C: loss of bound H ₂ O Endotherm at 210 °C: T _β melt
Megarry et al. ⁴³		10	Hermetic pan	Small endotherm at 93 °C: humidity in pan Large endotherm at 96 °C: water loss

particles of T_h dehydrate to form an amorphous phase that crystallizes above the glass transition temperature, and larger particles of T_h dehydrate and directly form T_β via a solid-solid conversion. Faster dehydration of smaller particles was attributed to their larger surface area-to-volume ratio and the presence of crystal defects. A decrease in activation energy for the dehydration of smaller particles was observed, reflecting greater disorder in the lattice of these particles.⁴⁴ One theory proposed to explain the direct transformation of T_h to T_β for larger particles was the higher degree of order in the larger particles. The different dehydration behaviors of small and large particles were confirmed using hot stage microscopy (HSM).²² During HSM experiments, the authors observed bubbles migrating through larger particles and hypothesized that an impermeable anhydrous outer layer was forming. This layer could not be penetrated until sufficient pressure from water inside the particle was generated.

3.3.2.2 Influence of Heating Rate on the Dehydration of Trehalose Dihydrate

Taylor and York analyzed small (<45 μm) and large (>425 μm) particles of T_h with several heating rates (1–10 $^\circ\text{C}/\text{minute}$) and showed that several thermal events in the DSC and TGA thermograms were affected by the heating rate. For the smallest particles, as the heating rate was decreased, water loss occurred at lower temperatures. When the largest particles were heated at rates of 1 $^\circ\text{C}/\text{minute}$ and above, water was lost in an apparent two-step process that the authors concluded was consistent with the hypothesis that an impermeable, anhydrous shell was formed on the surface of the particles. As the heating rate was decreased, the material formed from dehydration of the small particles crystallized to T_β at lower temperatures.

Sussich et al. heated T_h at rates ranging from 1 $^\circ\text{C}/\text{minute}$ to 60 $^\circ\text{C}/\text{minute}$ using DSC and showed that the dehydration process is significantly impacted by the heating rate.²¹ Differences

in the DSC thermograms and the transformations of T_h were attributed to differences in the rate of water loss. At slower scan rates, the authors concluded that T_{am} was generated upon dehydration, and it crystallized to T_β around 180 °C. As the scan rate was increased, the dehydration endotherm at ~100 °C shifted to slightly higher temperatures. The authors acknowledged that not all thermograms recorded at higher scan rates were reproducible, and they attributed this to differences in the sample grains.

Willart et al. investigated the underlying factors controlling the dehydration of T_h by heating samples at rates ranging from 1 °C/minute to 50 °C/minute, and they determined that the dehydration products were dictated by a threshold rate of water loss and not a threshold temperature.⁴⁵ In general, they found that fast heating rates lead to formation of T_{am} and slower heating rates leading to formation of T_α . The authors describe the dual nature of the dehydration (formation of T_α or T_{am}) and do not comment on direct formation of T_β from T_h .

3.3.2.3 Influence of Sample Environment on the Dehydration of Trehalose Dihydrate

Sussich et al. determined that the dehydration of T_h changed as a result of how easily water could escape the sample environment during a DSC experiment, i.e. if an open pan, hermetically sealed pan, or pinholed pan was used.³⁸ Thermograms of T_h in an open cell and with orifices of 1.2 and 0.9 mm were similar, but the thermal events significantly changed as the size of the orifice decreased. For example, while the endotherm near 100 °C was broad when open pans were used, it shifted to higher temperatures and sharpened when the size of the orifice was 0.5 mm. With an orifice size of 0.1 mm, the shape of this endotherm change dramatically to a sharp spike at about 90 °C followed by a smaller, broader endotherm that ends at about 110 °C. While crystallization and melting of T_β was observed for all pans with a path for water to escape,

these two events were not present in thermograms of pans that were hermetically sealed. The authors concluded that modulation of the heating rate and the flow of water out of the pan will determine which anhydrous form of trehalose is generated upon dehydration of T_h .

3.4 Physical Stability of Amorphous Trehalose

Amorphous trehalose (T_{am}) is the subject of several studies, and its physical stability has been shown to be influenced by both the thermal history and the preparation method. In this section, the most comprehensive studies of these areas are summarized.

3.4.1 Effect of Aging on the Physical Stability of Amorphous Trehalose

Surana et al. observed an increased tendency of T_{am} to crystallization after aging and attributed this to the formation of T_β nuclei during the aging process.⁴⁶ T_{am} was prepared via lyophilization, aged ~ 20 °C below the glass transition temperature for varying lengths of time, and analyzed using DSC. They observed an increase in the enthalpic recovery peak after aging, demonstrating that structural relaxation occurred during the aging process. Prior to aging, the onset of crystallization occurred at 174 °C, and a decrease in the onset temperature after aging demonstrated the increased crystallization tendency of the aged T_{am} . The authors concluded that nucleation of T_β must have occurred during aging, as the effects of structural relaxation would have been erased in the temperature range where crystallization occurs. If nuclei formed during aging, heating the material through the T_g would not be likely to erase nucleation. PXRD indicated that all samples were amorphous, and no direct evidence of the nuclei was detected.

3.4.2 Effect of Preparation Method on the Physical Stability of Amorphous Trehalose

Surana et al. prepared T_{am} via spray-drying, freeze-drying, melt-quenching of T_{β} , and dehydration of T_h (two methods), and they observed differences in the physical properties of these samples.¹⁷ The morphologies of the samples were examined: spray-dried T_{am} was flaky, spray-dried T_{am} was spherical, and dehydrated T_{am} was either prismatic (retained from T_h) or irregular. Thermograms of all samples contained a glass transition at ~ 117 °C, indicating that the T_g was not affected by the preparation methods. Thermograms of all samples contained an enthalpic recovery peak, though the extent of structural relaxation varied among the samples. The dehydrated T_{am} samples underwent the most relaxation during preparation. T_{am} prepared by spray-drying did not crystallize during a DSC experiment, and for the remaining samples, the crystallization onset temperatures are as follows: freeze-dried $T_{am} >$ melt-quenched $T_{am} >$ dehydrated T_{am} . The impact of morphology and structural relaxation on the crystallization tendency was deemed irrelevant because crystallization occurs above the T_g (where the material has softened and the effects of structural relaxation have been erased), and the authors concluded that differences in crystallization result from variations in nucleation of T_{β} during preparation. Therefore, the authors concluded that the highest concentration of nuclei must have been generated during dehydration. Crystallization of the spray-dried T_{am} was not observed initially, but it was observed after storage for 30 days at room temperature, indicating that nucleation occurred ~ 100 °C below the T_g . While crystallization below the T_g has been observed in other systems, it is still surprising that there is sufficient motion for nucleation so far below the T_g .⁴⁷ As in the study described in §3.4.1, PXRD was used to verify that the samples were amorphous, and no direct evidence of the nuclei was observed.

Sussich and Cesàro also observed that different preparation methods yield T_{am} samples with different tendencies to crystallize to T_{β} .³¹ T_{am} was prepared via melt-quenching of T_{β} , melting of T_{α} , dehydration of T_h , microwave treatment of T_h , drying of a trehalose solution, and lyophilization. For comparison, they also included results for milling of T_{β} and supercritical fluid extraction of T_h .^{30, 48} The authors suggest that two different amorphous states of trehalose exist: TRE-am1 (non-crystallizable) and TRE-am2 (crystallizable). Methods that were classified as “non-crystallizable” include melt-quenching of T_{β} , freeze-drying, drying of a trehalose solution, and milling of T_{β} . “Crystallizable” methods of preparation include melting of T_{α} , microwave treatment of T_h , and supercritical fluid extraction of T_h . Dehydration of T_h was included in both categories. In proposing the existence of two amorphous states, they state that interpreting different tendencies to crystallize using the presence (or absence) of crystal nuclei is “naïve.” They believe that crystallization is related to higher mobility of T_{am} that is prepared from T_{α} and that there is a specific relationship between T_{α} and the tendency of T_{am} to crystallize. They do not present additional evidence in support of this hypothesis.

3.5 Conclusion

The information presented in this chapter demonstrates the interest in studying the solid forms and solid-state transformations of trehalose, and it introduces the confusion surrounding the relationships among the forms. Although some authors have stated that the dehydration pathways and other solid-state transitions can be defined with careful control of the operational parameters,^{31, 41} the data in the literature appear to contradict this. With the exception of particle size, most studies seem to focus on the external factors that affect the dehydration, and in Chapter 4, an exploration of the effects of source variability and lot-to-lot variability of T_h on the

dehydration pathways is initiated. These investigations are continued in Chapters 6 and 7. SSNMR provided a wealth of information about the structure of amorphous trehalose, but it has not yet been used to investigate the crystallization tendencies of different samples of amorphous trehalose. In Chapters 8 and 9, SSNMR is used to analyze the structure of T_{am} prepared via lyophilization and dehydration of T_h , and it is used to detect low levels of T_β or T_β nuclei in these samples.

3.6 References

1. Brown, G. M.; Rohrer, D. C.; Berking, B.; Beevers, C. A.; Gould, R. O.; Simpson, R. The Crystal Structure of α,α -Trehalose Dihydrate from Three Independent X-ray Determinations. *Acta Crystallogr. B* **1972**, *B28*, 3145-3158.
2. Taga, T.; Senma, M.; Osaki, K. The Crystal and Molecular Structure of Trehalose Dihydrate. *Acta Crystallogr. B* **1972**, *28*, 3258-3263.
3. Jeffrey, G. A.; Nanni, R. The Crystal Structure of Anhydrous α,α -Trehalose at -150° . *Carbohydr. Res.* **1985**, *137*, 21-30.
4. Nagase, H.; Ogawa, N.; Endo, T.; Shiro, M.; Ueda, H.; Sakurai, M. Crystal Structure of an Anhydrous Form of Trehalose: Structure of Water Channels of Trehalose Polymorphism. *J. Phys. Chem. B* **2008**, *112*, 9105-9111.
5. Stevens, E. D.; Down, M. K.; Johnson, G. P.; French, A. D. Experimental and theoretical electron density distribution of α,α -trehalose dihydrate. *Carbohydr. Res.* **2010**, *345*, 1469-1481.
6. Sussich, F.; Skopec, C.; Brady, J.; Cesáro, A. Reversible dehydration of trehalose and anhydrobiosis: from solution state to an exotic crystal? *Carbohydr. Res.* **2001**, *334*, 165-176.
7. Gil, A. M.; Belton, P. S.; Felix, V. Spectroscopic studies of solid α - α trehalose. *Spectrochim. Acta A* **1996**, *52*, 1649 - 1659.
8. Cesáro, A.; De Giacomo, O.; Sussich, F. Water interplay in trehalose polymorphism. *Food Chem.* **2008**, *106*, 1318-1328.
9. Sussich, F.; Skopec, C. E.; Brady, J. W.; Cesáro, A. Water mobility in the dehydration of crystalline trehalose. *Food Chem.* **2010**, *122*, 388-393.
10. Petit, S.; Coquerel, G. Mechanism of Several Solid-Solid Transformations between Dihydrated and Anhydrous Copper(II) 8-Hydroxyquinolates. Proposition for a Unified Model for the Dehydration of Molecular Crystals. *Chem. Mater.* **1996**, *8*, (9), 2247-2258.

11. Zhang, P.; Klymachyov, A. N.; Brown, S.; Ellington, J. G.; Grandinetti, P. J. Solid-state ^{13}C NMR investigations of the glycosidic linkage in α,α' trehalose. *Solid State Nucl. Magn. Reson.* **1998**, *12*, 221-225.
12. Lefort, R.; Bordat, P.; Cesáro, A.; Descamps, M. Exploring the conformational energy landscape of glassy disaccharides by cross polarization magic angle spinning ^{13}C nuclear magnetic resonance and numerical simulations. II. Enhanced molecular flexibility in amorphous trehalose. *J. Chem. Phys.* **2007**, *126*, (1), 014511.
13. Chakravarty, P.; Bhardwaj, S. P.; King, L.; Suryanarayanan, R. Monitoring Phase Transformations in Intact Tablets of Trehalose by FT-Raman Spectroscopy. *AAPS PharmSciTech* **2009**, *10*, (4), 1420-1426.
14. Lefort, R.; De Gusseme, A.; Willart, J. F.; Danede, F.; Descamps, M. Solid state NMR and DSC methods for quantifying the amorphous content in solid dosage forms: an application to ball-milling of trehalose. *Int. J. Pharm.* **2004**, *280*, (1-2), 209-19.
15. Kilburn, D.; Sokol, P. E. Structural Evolution of the Dihydrate to Anhydrate Crystalline Transition of Trehalose as Measured by Wide-angle X-ray Scattering. *J. Phys. Chem. B* **2009**, *113*, 2201-2206.
16. Willart, J. F.; De Gusseme, A.; Hemon, S.; Descamps, M.; Leveiller, F.; Rameau, A. Vitrification and Polymorphism of Trehalose Induced by Dehydration of Trehalose Dihydrate. *J. Phys. Chem. B* **2002**, *106*, 3365-3370.
17. Surana, R.; Pyne, A.; Suryanarayanan, R. Effect of preparation method on physical properties of amorphous trehalose. *Pharm. Res.* **2004**, *21*, (7), 1167-76.
18. Rani, M.; Govindarajan, R.; Surana, R.; Suryanarayanan, R. Structure in Dehydrated Trehalose Dihydrate—Evaluation of the Concept of Partial Crystallinity. *Pharm. Res.* **2006**, *23*, (10), 2356-2367.
19. Ding, S.-P.; Fan, J.; Green, J. L.; Lu, Q.; Sanchez, E.; Angell, C. A. Vitrification of Trehalose by Water Loss from Its Crystalline Dihydrate. *J. Therm. Anal.* **1996**, *47*, 1391-1405.

20. Reisener, H. J.; Goldschmid, H. R.; Ledingham, G. A.; Perlin, A. S. Formation of Trehalose and Polyols by Wheat Stem Rust (*Puccinia Graminis Tritici*) Uredospores. *Can. J. Biochem. Phys.* **1962**, *40*, 1248-1251.
21. Sussich, F.; Urbani, R.; Princivalle, F.; Cesáro, A. Polymorphic Amorphous and Crystalline Forms of Trehalose. *J. Am. Chem. Soc.* **1998**, *120*, 7893-7899.
22. Taylor, L. S.; York, P. Characterization of the Phase Transitions of Trehalose Dihydrate on Heating and Subsequent Dehydration. *J. Pharm. Sci.* **1998**, *87*, (3), 347-355.
23. Dranca, I.; Bhattacharya, S.; Vyazovkin, S.; Suryanarayanan, R. Implications of Global and Local Mobility in Amorphous Sucrose and Trehalose as Determined by Differential Scanning Calorimetry. *Pharm. Res.* **2009**, *26*, 1064.
24. Mitscherlich, E. Ueber die Mycose, den Zucker des Mutterkorns. *Liebigs Ann. Chem.* **1858**, *106*, (1), 15-18.
25. Berton, B.; Dupray, V.; Atmani, H.; Coquerel, G. Gas vacuoles formation during the dehydration of trehalose dihydrate: a Raman microspectroscopy approach. *J. Therm. Anal. Calorim.* **2007**, *90*, 325-328.
26. Sussich, F.; Princivalle, F.; Cesáro, A. The interplay of the rate of water removal in the dehydration of α,α -trehalose. *Carbohydr. Res.* **1999**, *322*, 113-119.
27. Furuki, T.; Kishi, A.; Sakurai, M. De- and rehydration behavior of α,α -trehalose dihydrate under humidity-controlled atmospheres. *Carbohydr. Res.* **2005**, *340*, 429-438.
28. Nagase, H.; Endo, T.; Ueda, H.; Nakagaki, M. An anhydrous polymorphic form of trehalose. *Carbohydr. Res.* **2002**, *337*, 167-173.
29. Sundaramurthi, P.; Patapoff, T. W.; Suryanarayanan, R. Crystallization of Trehalose in Frozen Solutions and its Phase Behavior during Drying. *Pharm. Res.* **2010**, *27*, 2374-2383.

30. Akao, K.-i.; Okubo, Y.; Inoue, Y.; Sakurai, M. Supercritical CO₂ fluid extraction of crystal water from trehalose dihydrate. Efficient production of form II (Ta) phase. *Carbohydr. Res.* **2002**, *337*, 1729-1735.
31. Sussich, F.; Cesáro, A. Trehalose amorphization and recrystallization. *Carbohydr. Res.* **2008**, *343*, 2667-2674.
32. McGarvey, O. S.; Kett, V. L.; Craig, D. Q. M. An Investigation into the Crystallization of α,α - Trehalose from the Amorphous State. *J. Phys. Chem. B* **2003**, *107*, (27), 6614-6620.
33. Shafizadeh, F.; Lai, Y. Z. Thermal Rearrangements of Cellobiose and Trehalose. *Carbohydr. Res.* **1973**, *31*, 57-67.
34. Shafizadeh, F.; Susott, R. A. Crystalline Transformations of Carbohydrates. *J. Org. Chem.* **1973**, *38*, (21), 3710-3715.
35. Green, J. L.; Angell, C. A. Phase Relations and Vitrification in Saccharide–Water Solutions and the Trehalose Anomoly. *J. Phys. Chem.* **1989**, *93*, 2880-2882.
36. Sussich, F.; Urbani, R.; Cesáro, A.; Princivalle, F.; Bruckner, S. New Crystalline and Amorphous Forms of Trehalose. *Carbohydr. Lett.* **1997**, *2*, 403-408.
37. Macdonald, C.; Johari, G. P. Glass-softening of trehalose and calorimetric transformations in its liquid state. *J. Mol. Struct.* **2000**, *523*, 119-132.
38. Sussich, F.; Bortoluzzi, S.; Cesáro, A. Trehalose dehydration under confined conditions. *Thermochim. Acta* **2002**, *391*, 137-150.
39. Jones, M. D.; Hooton, J. C.; Dawson, M. L.; Ferrie, A. R.; Price, R. Dehydration of trehalose dihydrate at low relative humidity and ambient temperature. *Int. J. Pharm.* **2006**, *313*, 87-98.
40. Furuki, T.; Abe, R.; Kawaji, H.; Atake, T.; Sakurai, M. Effect of Atmospheric Pressure on the Phase Transitions of α,α -Trehalose Dihydrate: DTA study of the dehydration behavior in open systems. *J. Therm. Anal. Calorim.* **2008**, *93*, (2), 561-567.

41. Dupray, V.; Berton, B.; Ossart, S.; Atmani, H.; Petit, M.-N. Concomitant dehydration mechanisms in single crystals of α,α -trehalose. *Carbohydr. Res.* **2009**, *344*, 2539-2546.
42. Li, X.; Mansour, H. M. Physicochemical Characterization and Water Vapor Sorption of Organic Solution Advanced Spray-Dried Inhalable Trehalose Microparticles and Nanoparticles for Targeted Dry Powder Pulmonary Inhalation Delivery. *AAPS PharmSciTech* **2011**.
43. Megarry, A. J.; Booth, J.; Burley, J. Amorphous trehalose dihydrate by cryogenic milling. *Carbohydr. Res.* **2011**, *346*, 1061-1064.
44. Taylor, L. S.; York, P. Effect of particle size and temperature on the dehydration kinetics of trehalose dihydrate. *Int. J. Pharm.* **1998**, *167*, 215-221.
45. Willart, J. F.; Danede, F.; De Gusseme, A.; Descamps, M.; Neves, C. Origin of the Dual Structural Transformation of Trehalose Dihydrate upon Dehydration. *J. Phys. Chem. B* **2003**, *107*, 11158-11162.
46. Surana, R.; Pyne, A.; Suryanarayanan, R. Effect of aging on the physical properties of amorphous trehalose. *Pharm. Res.* **2004**, *21*, (5), 867-74.
47. Andronis, V.; Zografi, G. Crystal nucleation and growth of indomethacin polymorphs from the amorphous state. *J. Non-Cryst. Solids* **2000**, *271*, (3), 236-248.
48. Willart, J. F.; De Gusseme, A.; Hemon, S.; Odou, G.; Danede, F.; Descamps, M. Direct crystal to glass transformation of trehalose induced by ball milling. *Solid State Commun.* **2001**, *119*, 501-505.

Chapter 4

Initial Solid-State Characterization of Trehalose

4.1 Introduction

Four samples of trehalose dihydrate (T_h) from Fluka and Sigma were analyzed using differential scanning calorimetry (DSC), and the thermograms indicated that the samples may dehydrate in different ways. The samples were then dehydrated using conditions that were expected to generate amorphous trehalose (T_{am});¹ however, mixtures of the β -anhydrate form of trehalose (T_β) and T_{am} were generated. The samples of T_h were then lyophilized in a second attempt at generating T_{am} ; while this method was successful, the T_{am} samples unexpectedly displayed different tendencies to crystallize to T_β . Additional dehydrations of T_h were performed at 75 °C and 125 °C, and the compositions of these dehydrated samples were analyzed using ^{13}C solid-state NMR spectroscopy (SSNMR). These results motivated many of the studies in this dissertation.

4.2 Materials and Methods

4.2.1 Materials

D-(+)-trehalose dihydrate was purchased from Fluka (Buchs, Switzerland) and Sigma (St. Louis, MO) and used without further purification. A portion of each sample was gently ground with a mortar and pestle for approximately one minute.

4.2.2 Dehydration

As-received and ground samples of trehalose dihydrate were dehydrated at 100 °C for 24 hours under vacuum, 75 °C for 48 hours under vacuum, and 125 °C for 1 hour under vacuum. Each sample was spread in a single layer in a Pyrex dish and placed in a vacuum oven. A Baxter

DP-32 vacuum drying oven (Deerfield, IL) was used for the dehydrations, and the temperature was verified with a calibrated thermometer.

4.2.3 Lyophilization

Amorphous trehalose was prepared by lyophilization of a 10 % w/v aqueous solution of trehalose dihydrate using a VirTis AdVantage lyophilizer (SP Scientific, Warminster, PA) and the procedure of Surana et al.¹ Approximately 10 mL of solution was placed in 25 mL scintillation vials and cooled to -45 °C. Samples were subjected to primary drying at -45 °C and ~100 mTorr for 48 hours. The temperature was then increased to 50 °C over the next 24 hours, and then secondary drying proceeded at 50 °C for 24 hours. The temperature was increased to 60 °C over 24 hours and then held at 60 °C for 24 hours.

4.2.4 Differential Scanning Calorimetry

Differential scanning calorimetry was performed using a Thermal Analysis DSC Q100 (TA Instruments; New Castle, DE). Trehalose dihydrate samples were weighed into open aluminum pans, and dehydrated trehalose samples were weighed into aluminum hermetic pans with 3 pinholes in each lid. All samples were analyzed using a standard ramp method and were heated from 25 °C to 250 °C at a rate of 10 °C/min. under a dry nitrogen purge at 50 mL/min.

4.2.5 ^{13}C Solid-State NMR Spectroscopy (SSNMR)

^{13}C SSNMR spectroscopy was performed using a Chemagnetics CMX-300 spectrometer (Varian, Inc) operating at approximately 300 MHz for ^1H and 75 MHz for ^{13}C . Samples were packed into zirconia rotors and spun at the magic angle.² The spinning speed was 4kHz. Peaks were referenced to the methyl peak of 3-methylglutaric acid, which was set to 18.84 ppm.³ Spectra were acquired using ramped cross polarization, Spinal 64 decoupling, and sideband suppression.^{4,6} A contact time of 1 ms was used for all samples.

4.3 Results

4.3.1 Characterization of Trehalose Dihydrate (T_h)

Figure 4.1 shows DSC thermograms of four samples of T_h . All thermograms contain an endotherm near 100 °C that is associated with dehydration. The peak temperatures of this endotherm vary from about 99 °C for the Sigma 114K7064 sample to about 105 °C for the Fluka sample. The reason for the variability is not known, though studies have shown that the particle size can significantly affect the dehydration of T_h and therefore the DSC thermograms.⁷ For the Fluka sample, the first endotherm is followed immediately by an exotherm and then another endotherm. These events have been assigned to the formation and melting of the γ form of trehalose,⁸ but this form is now known to be a mixture of T_h and T_β .⁹ For the Sigma 114K7064 and Sigma 127K7350 samples, the first exotherm is followed by an irregular, “noisy” area between 125 °C and 175 °C. A similar event has been described in the literature, but an explanation has not been provided.¹⁰ The thermogram of the Sigma 127K7355 sample contains

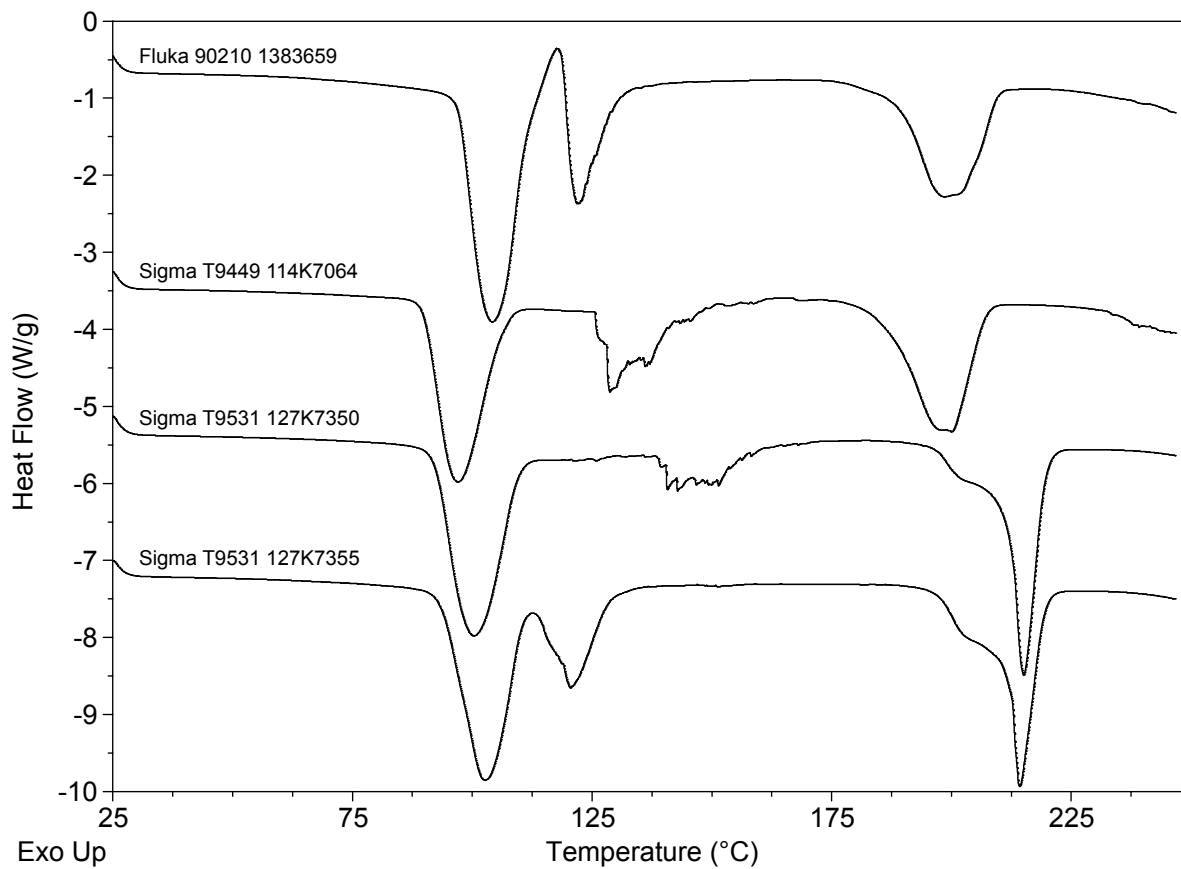


Figure 4.1. DSC thermograms of as-received samples of trehalose dihydrate.

a second exotherm with a peak temperature of about 120 °C, but the transition associated with this thermal event is unknown. In Chapter 6, the DSC thermograms of T_h are more thoroughly investigated, and the identities of previously unknown thermal events are determined.

Each thermogram in Figure 4.1 also contains an endotherm above 190 °C that corresponds to melting of T_β . For the Fluka and Sigma 114K7064 samples, the onset of melting is about 175 °C, and the endotherm peaks at about 200 °C. For the Sigma 127K7350 and Sigma 127K7355 samples, the melting begins at about 190 °C, and after a broad, shallow peak, there is a much sharper peak with a peak temperature of about 213 °C. Reported melting temperatures of T_β range from 197 to 218 °C,^{11, 12} and the shape of this endotherm ranges from a sharp peak, to a broader peak with multiple maxima, to a combination of the two shapes.^{7, 13, 14} Although some of the results in the literature were obtained under different experimental conditions, e.g. different heating rates or pan types, the thermograms in Figure 4.1 only differ in the starting material. Interestingly, the thermogram of the Sigma 114K7064 sample is similar to the thermogram of the Sigma 127K7350 sample below 175 °C and similar to the thermogram of the Fluka sample above 175 °C, suggesting that the dehydration events may not be directly correlated with the melting events.

4.3.2 Dehydration of Trehalose Dihydrate at 100 °C

Figure 4.2 shows the DSC thermograms of four samples of trehalose dihydrate after dehydration at 100 °C for 24 hours under vacuum. These dehydration conditions reportedly lead to the formation of T_{am} .¹ A glass transition near 120 °C is present in the thermograms of the Fluka, Sigma 127K7350, and Sigma 127K7355 samples; this is consistent with the expected glass transition temperature (T_g) of amorphous trehalose. The change in heat capacity is larger

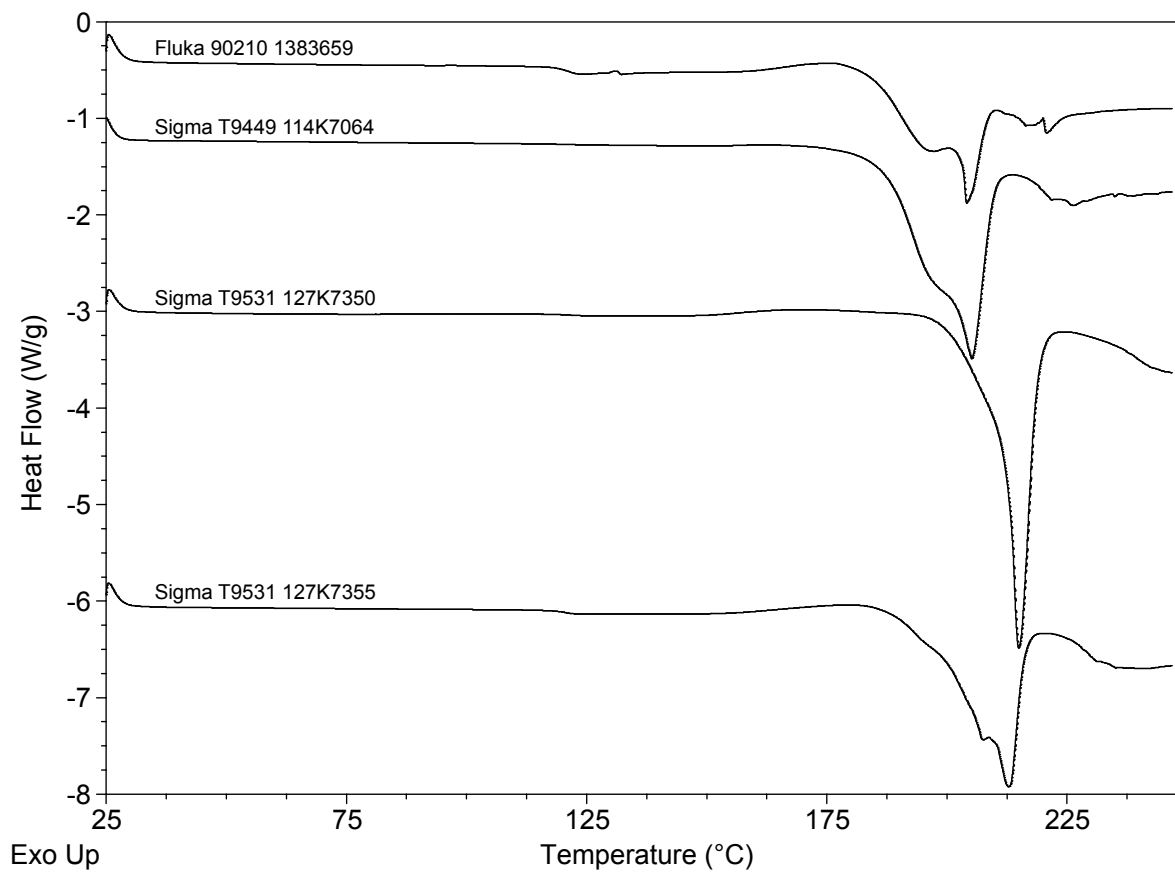


Figure 4.2. DSC thermograms of trehalose dihydrate samples that were dehydrated at 100 °C for 24 hours under vacuum.

for the Fluka sample than for the Sigma samples, but for all three samples, the change in heat capacity at the T_g is smaller than expected for a sample of trehalose that is fully amorphous.¹ The changes in heat capacity suggest that more T_{am} was formed in the Fluka samples than in the Sigma 127K7350 and 127K7355 samples. A glass transition is not present in the thermogram of the dehydrated Sigma 114K7064 sample, indicating that T_{am} was not formed in this sample. Small exotherms at about 175 °C correspond to crystallization of T_β and are present in the thermograms of the Fluka and Sigma 127K7355 samples. All thermograms contain an endotherm between 190 and 215 °C that corresponds to melting of T_β , but they differ in magnitude, shape, and onset temperature. From these thermograms, it appears that the Sigma 114K7064 sample formed T_β following dehydration at 100 °C, and the other samples formed mixtures of T_{am} and T_β . These results are not consistent with the literature, and furthermore, the results differ for the four samples of T_h .

Figure 4.3 shows DSC thermograms of T_h samples that were ground and then dehydrated at 100 °C. Grinding was expected to minimize any differences in particle size among the samples, as it has been shown that particle size can impact the forms obtained from dehydration of T_h .⁷ Additionally, creating defects in the starting material via grinding might facilitate formation of the disordered amorphous state.¹⁵ In contrast to the thermograms of the dehydrated as-received samples (Figure 4.2), each thermogram in Figure 4.3 contains a glass transition near 120 °C, demonstrating that amorphous trehalose was formed in each sample. Each thermogram also contains an endotherm near 130 °C that corresponds to melting of the α -anhydrate form of trehalose (T_α). The exotherms between 150 °C and 200 °C correspond to crystallization of T_β from either rubbery T_{am} or melted T_α . The magnitude of the endotherm at about 210 °C in the thermogram of the Fluka sample is smaller than the endotherms in the thermograms of the Sigma

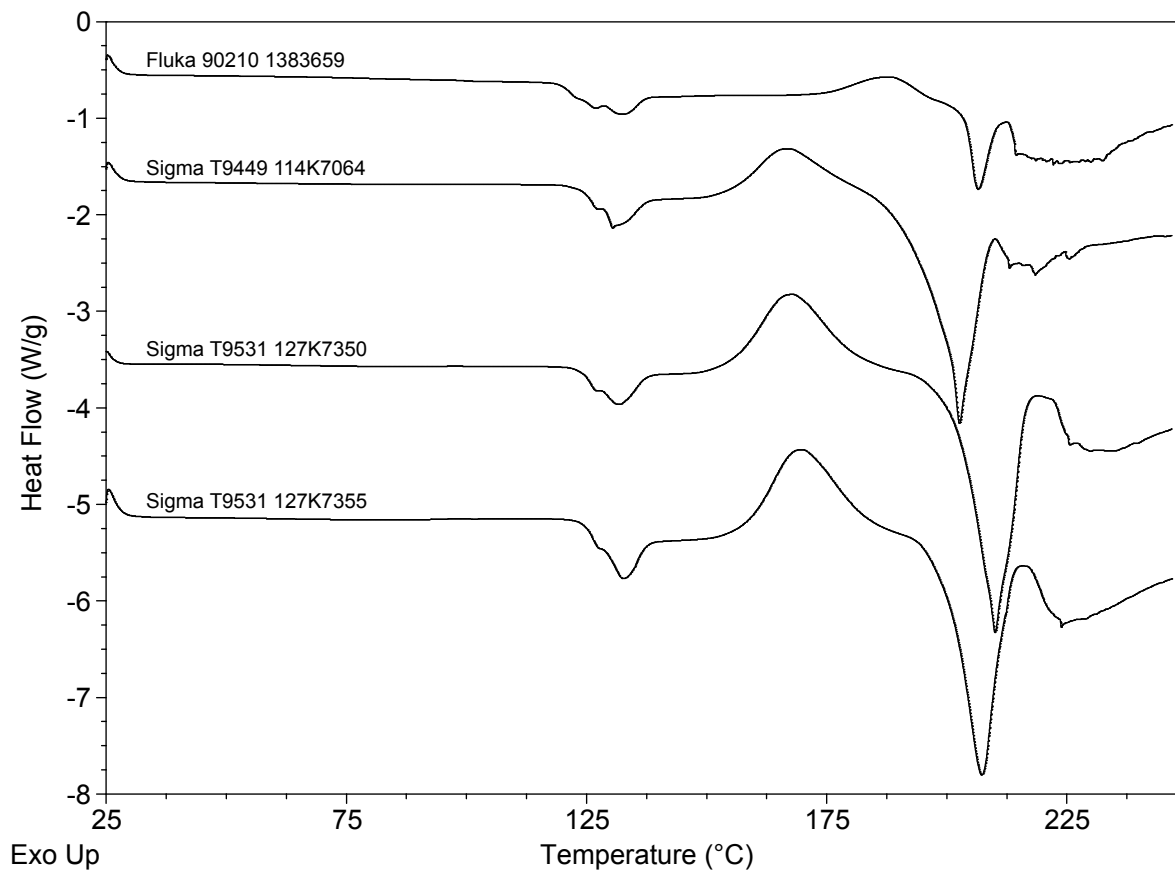


Figure 4.3. DSC thermograms of ground trehalose dihydrate samples that were dehydrated at 100 °C for 24 hours under vacuum.

samples, indicating that crystallization of T_{β} occurred to a lesser extent in the Fluka sample. The DSC thermograms in Figure 4.3 show that grinding changed the T_h samples in such a way that formation of metastable forms of trehalose, T_{am} and T_{α} , was favored.

4.3.3 Lyophilization of Trehalose Dihydrate

Figure 4.4 shows DSC thermograms of four samples of T_h that were lyophilized. Each contains a glass transition at about 120 °C, indicating that freeze-drying successfully produced T_{am} . Each also contains an exotherm at temperatures greater than 175 °C that corresponds to crystallization of T_{β} . The Fluka sample has the lowest tendency to crystallize to T_{β} , as evidenced by the highest onset of crystallization and the smallest exotherm. The thermogram of the Sigma 127K7350 sample has the lowest onset of crystallization and the largest exotherm, demonstrating that this sample has the highest tendency to crystallize. Unlike the thermograms in Figures 4.1, 4.2, and 4.3 that contained broad endotherms corresponding to melting of T_{β} , the thermograms in Figure 4.4 all contain sharp endotherms at 213 °C. When compared to previously published results,¹ the DSC thermogram of the Fluka T_{am} is similar to that obtained from spray-drying, and the DSC thermogram of the Sigma 127K7350 lyophilized T_{am} is similar to the thermogram of dehydrated T_{am} . These results demonstrate that samples of T_{am} with different physical stabilities can be generated with only one preparation method.

Figure 4.5 shows the ^{13}C SSNMR spectra of the lyophilized samples with the highest and lowest crystallization tendencies. Both are consistent with the published spectra of T_{am} .¹⁶⁻¹⁸ The spectra are nearly identical, and any features that might help to understand the different crystallization tendencies of the samples are not apparent. This highlights the need for more

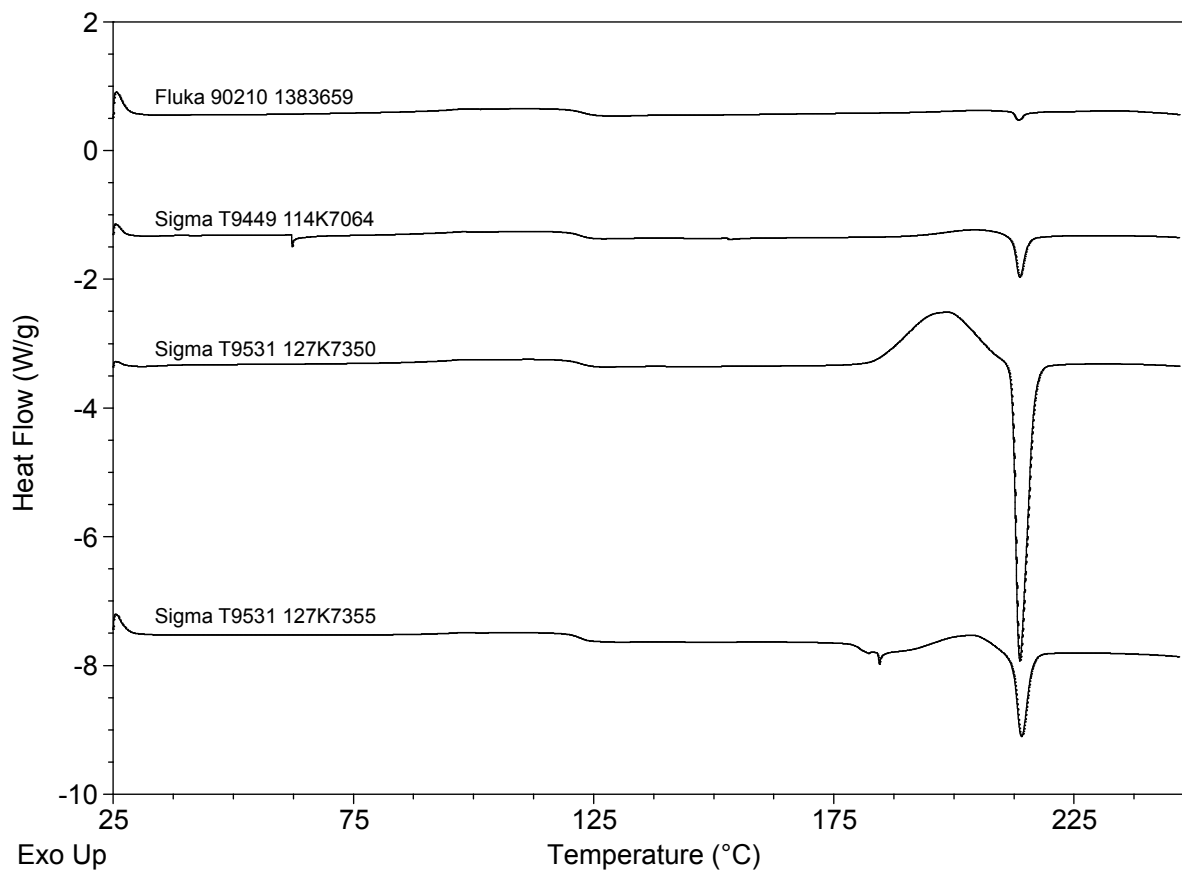


Figure 4.4. DSC thermograms of lyophilized trehalose.

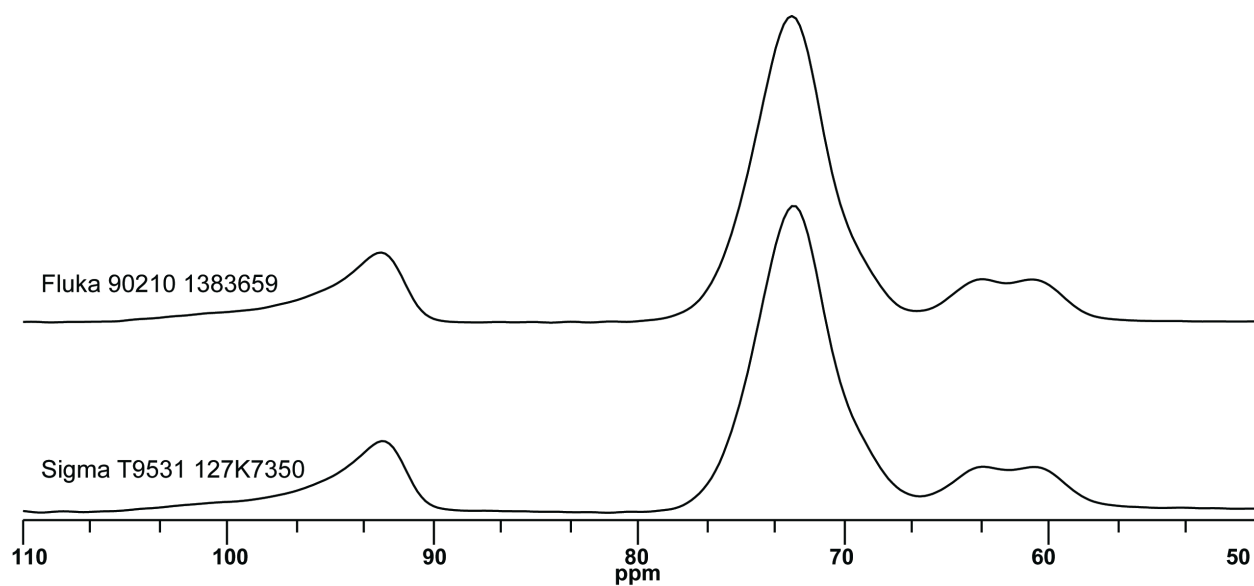


Figure 4.5. ¹³C SSNMR spectra of amorphous trehalose prepared by lyophilization. The DSC analyses of these samples showed that the Fluka sample had the lowest tendency to crystallize to T_{β} , and the Sigma 127K7350 sample had the highest tendency to crystallize to T_{β} . The spectra are essentially identical, indicating that any structural differences between the two samples are very small.

sophisticated techniques to analyze amorphous materials; this topic is addressed in Chapters 8 and 9.

4.3.4 Dehydration of Trehalose Dihydrate at 125 °C

Figure 4.6 shows ^{13}C SSNMR spectra of the four as-received T_h samples following dehydration at 125 °C for one hour under vacuum, as well as the spectra of T_β and T_{am} . Dehydration of T_h at 120 °C for 5 minutes has been reported to form T_β ,⁷ but dehydration of T_h at 125 °C for 1 hour under partial vacuum has been reported to form T_{am} . The spectrum of each dehydrated sample is a combination of the spectra of T_β and T_{am} . Of the four dehydrated samples, the T_β peaks are largest in the spectrum of the Sigma 114K7064 sample, indicating that it contains the most T_β . Following dehydration at 100 °C, the DSC thermogram indicated that this sample contained the most T_β . The spectra of the remaining three samples are nearly identical and suggest that similar mixtures of T_{am} and T_β were formed in each. Again, not only are the results from this dehydration inconsistent with the literature, they also differ among four samples of T_h that were subjected to the same treatment.

4.3.5 Dehydration of Trehalose Dihydrate at 75 °C

Figure 4.7 shows ^{13}C SSNMR spectra of two as-received samples of T_h following dehydration at 75 °C for 48 hours under vacuum. These dehydration conditions are similar to those that have been reported to form T_α .¹² The solid forms of trehalose are easily identified by examining the C1,C1' region (96–90 ppm), and the expanded region of each spectrum shows that

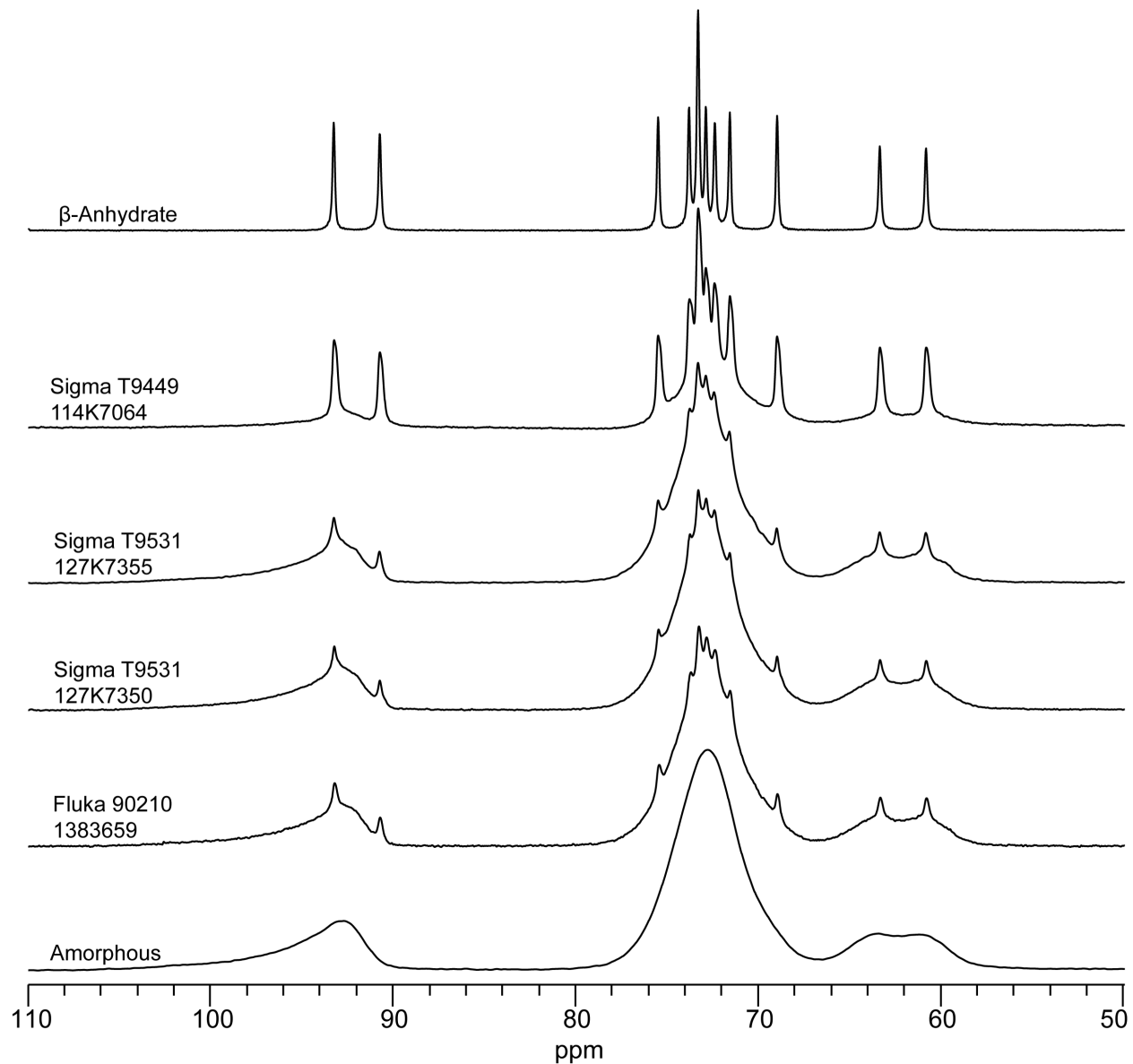


Figure 4.6. ^{13}C SSNMR spectra of T_{β} , trehalose dihydrate samples that were dehydrated at 125 $^{\circ}\text{C}$ for one hour under vacuum, and T_{am} .

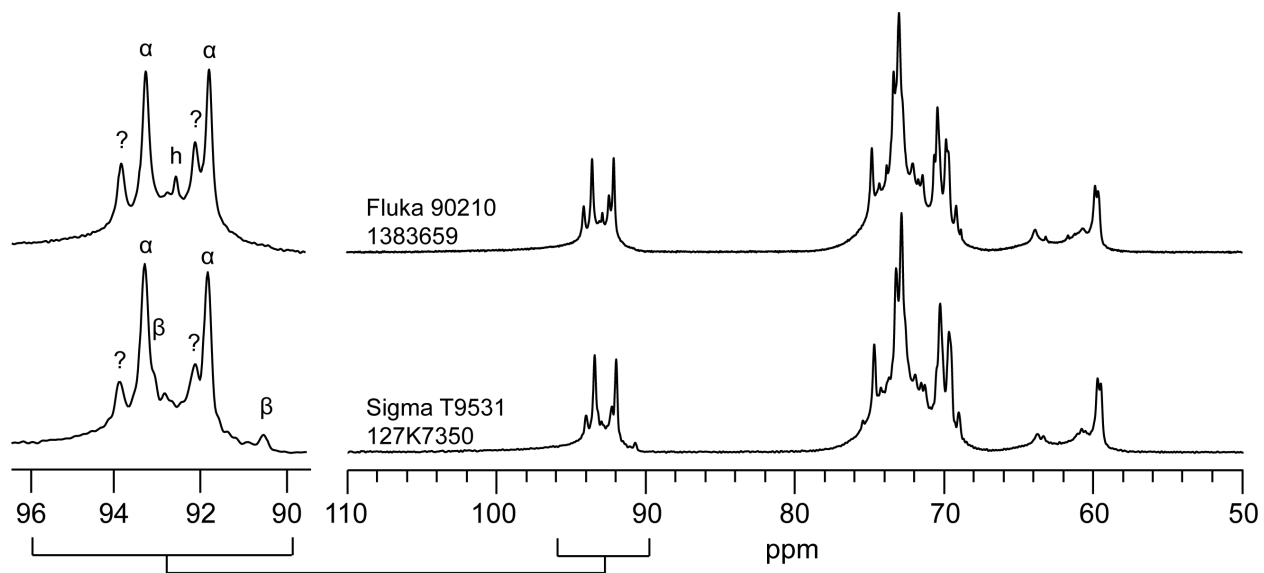


Figure 4.7. ^{13}C SSNMR spectra of trehalose dihydrate samples that were dehydrated at 75 °C. Unidentified peaks are labeled with a question mark (?).

each sample contains several forms of trehalose. The presence of a peak corresponding to T_h in the spectrum of the dehydrated Fluka sample shows that the dehydration was incomplete for that sample. Both spectra have a broad, underlying peak that indicates that T_{am} is present in the samples, and both spectra also contain peaks corresponding to T_α . Previously, dehydrations of T_h at 60 and 80 °C were reported to form mixtures of T_{am} and T_α ,¹⁹ but the SSNMR spectra in Figure 4.7 show that additional forms were generated upon dehydration at 75 °C. The spectrum of the dehydrated Sigma 127K7350 sample shows that T_β was generated, and both spectra contain unknown peaks that are not consistent with peaks from any of the solid forms of trehalose. These peaks have been attributed to a new solid form of trehalose whose characterization is described in Chapter 5.

4.4 Conclusions

The inconsistencies among the T_h samples both before and after processing, as evidenced by differences among the DSC thermograms and ^{13}C SSNMR spectra, indicate that both source variability and lot-to-lot variability of trehalose dihydrate are present and that variability affects the physicochemical properties of the samples. In Chapter 6, these four samples of T_h , in addition to twelve more samples of T_h , are subjected to analyses by DSC, thermogravimetric analysis (TGA), and polarized light microscopy (PLM) in order to qualitatively and quantitatively describe these differences. In Chapter 7, isothermal dehydrations of T_h are repeated, and the conditions that can be used to generate T_{am} via dehydration of T_h are determined. In Chapters 8 and 9, amorphous trehalose is prepared via lyophilization and dehydration of T_h , and its physical properties are studied using PLM, DSC, and SSNMR in order to understand the different crystallization tendencies of the samples.

4.5 References

1. Surana, R.; Pyne, A.; Suryanarayanan, R. Effect of preparation method on physical properties of amorphous trehalose. *Pharm. Res.* **2004**, *21*, (7), 1167-76.
2. Andrew, A. R.; Bradbury, A.; Eades, R. G. Removal of dipolar broadening of nuclear magnetic resonance spectra of solids by specimen rotation. *Nature* **1958**, *183*, 1802-1803.
3. Barich, D. H.; Gorman, E. M.; Zell, M. T.; Munson, E. J. 3-Methylglutaric acid as a ¹³C solid-state NMR standard. *Solid State Nucl. Magn. Reson.* **2006**, *30*, (3-4), 125-129.
4. Dixon, W. T.; Schaefer, J.; Sefcik, M. D. Total suppression of sidebands in CPMAS carbon-13 NMR. *J. Magn. Reson.* **1982**, *49*, (2), 341-345.
5. Fung, B.; Khittrin, A.; Ermolaev, K. An improved broadband decoupling sequence for liquid crystals and solids. *J. Magn. Reson.* **2000**, *142*, (1), 97-101.
6. Pines, A.; Gibby, M. G.; Waugh, J. S. Proton-enhanced NMR of Dilute Spins. *J. Chem. Phys.* **1973**, *59*, 569-590.
7. Taylor, L. S.; York, P. Characterization of the Phase Transitions of Trehalose Dihydrate on Heating and Subsequent Dehydration. *J. Pharm. Sci.* **1998**, *87*, (3), 347-355.
8. Sussich, F.; Urbani, R.; Cesáro, A.; Princivalle, F.; Bruckner, S. New Crystalline and Amorphous Forms of Trehalose. *Carbohydr. Lett.* **1997**, *2*, 403-408.
9. Sussich, F.; Princivalle, F.; Cesáro, A. The interplay of the rate of water removal in the dehydration of α,α -trehalose. *Carbohydr. Res.* **1999**, *322*, 113-119.
10. Jones, M. D.; Hooton, J. C.; Dawson, M. L.; Ferrie, A. R.; Price, R. Dehydration of trehalose dihydrate at low relative humidity and ambient temperature. *Int. J. Pharm.* **2006**, *313*, 87-98.
11. Ohashi, T.; Yoshii, H.; Furuta, T. Innovative crystal transformation of dihydrate trehalose to anhydrous trehalose using ethanol. *Carbohydr. Res.* **2007**, *342*, 819-825.

12. Reisener, H. J.; Goldschmid, H. R.; Ledingham, G. A.; Perlin, A. S. Formation of Trehalose and Polyols by Wheat Stem Rust (*Puccinia Graminis Triticis*) Uredospores. *Can. J. Biochem. Phys.* **1962**, *40*, 1248-1251.
13. Shafizadeh, F.; Susott, R. A. Crystalline Transformations of Carbohydrates. *J. Org. Chem.* **1973**, *38*, (21), 3710-3715.
14. Sussich, F.; Urbani, R.; Princivalle, F.; Cesáro, A. Polymorphic Amorphous and Crystalline Forms of Trehalose. *J. Am. Chem. Soc.* **1998**, *120*, 7893-7899.
15. Taylor, L. S.; Williams, A. C.; York, P. Particle size dependent molecular rearrangements during the dehydration of trehalose dihydrate in situ FT-Raman spectroscopy. *Pharm. Res.* **1998**, *15*, (8), 1207-14.
16. Lefort, R.; Bordat, P.; Cesáro, A.; Descamps, M. Exploring the conformational energy landscape of glassy disaccharides by cross polarization magic angle spinning ¹³C nuclear magnetic resonance and numerical simulations. II. Enhanced molecular flexibility in amorphous trehalose. *J. Chem. Phys.* **2007**, *126*, (1), 014511.
17. Lefort, R.; De Gusseme, A.; Willart, J. F.; Danede, F.; Descamps, M. Solid state NMR and DSC methods for quantifying the amorphous content in solid dosage forms: an application to ball-milling of trehalose. *Int. J. Pharm.* **2004**, *280*, (1-2), 209-19.
18. Zhang, P.; Klymachyov, A. N.; Brown, S.; Ellington, J. G.; Grandinetti, P. J. Solid-state ¹³C NMR investigations of the glycosidic linkage in α,α' trehalose. *Solid State Nucl. Magn. Reson.* **1998**, *12*, 221-225.
19. Rani, M.; Govindarajan, R.; Surana, R.; Suryanarayanan, R. Structure in Dehydrated Trehalose Dihydrate—Evaluation of the Concept of Partial Crystallinity. *Pharm. Res.* **2006**, *23*, (10), 2356-2367.

Chapter 5

Generation and Characterization of a New Solid Form of Trehalose

5.1 Introduction

In this chapter, evidence for a previously undiscovered form of trehalose, the δ form (T_δ), is provided. This form was generated while performing low-temperature dehydrations of trehalose dihydrate (T_h) in an effort to generate the α -anhydrate (T_α). These low-temperature dehydrations of T_h result in mixtures of a minimum of three forms: amorphous trehalose (T_{am}), T_α , and the new form. Samples containing the new form were analyzed using ^{13}C solid-state NMR spectroscopy (SSNMR), differential scanning calorimetry (DSC), and powder X-ray diffractometry (PXRD), but only SSNMR indicates the presence of the new form. Its stability upon exposure to heat and humidity were investigated, and its tendency to convert to other solid forms of trehalose during these experiments indicates that it is not a thermal degradant.

5.2 Experimental

5.2.1 Materials

Trehalose dihydrate (T_h) was purchased from Acros (Geel, Belgium) and Sigma (St. Louis, MO, USA) and used without further purification. Reported purities were 99%.

5.2.2 Sieving

Bulk materials were sieved to obtain particle size fractions of $<75\ \mu\text{m}$, $75\text{--}125\ \mu\text{m}$, $125\text{--}180\ \mu\text{m}$, $180\text{--}425\ \mu\text{m}$, $425\text{--}850\ \mu\text{m}$, and $>850\ \mu\text{m}$. A set of U.S.A. Standard Test Sieves (Hogentogler&Co., Inc., Columbia, MD) was stacked and shaken manually or using a Performer III Model SS-3 mechanical sieve shaker (Gilson Company, Inc., Lewis Center, OH).

5.2.3 Preparation of Dehydrated Samples

Dehydrated samples were prepared by either dehydrating T_h in a vacuum oven or by exposing the sample to hot air during solid-state NMR experiments. A VWR Scientific Products vacuum oven (Model 1410M) was used, and the temperature was verified with a calibrated thermometer. The temperature of the sample during SSNMR experiments was calibrated using lead nitrate.¹ Sample descriptions and dehydration conditions are listed in Table 5.1.

5.2.4 ^{13}C Solid-state Nuclear Magnetic Resonance (SSNMR) Spectroscopy

^{13}C SSNMR spectra were acquired using a Tecmag Redstone spectrometer (Tecmag Inc., Houston, TX) operating at approximately 300 MHz for ^1H and 75 MHz for ^{13}C . Samples were packed into 7.5-mm zirconia rotors and spun at the magic angle.² The spinning speed was 4kHz. Peaks were referenced to the methyl peak of 3-methylglutaric acid, which was set to 18.84 ppm.³ Spectra were acquired using ramped cross polarization, Spinal 64 decoupling, and sideband suppression.^{4,6} A contact time of 1 ms was used for all samples.

^1H T_1 relaxation times were measured using a saturation recovery experiment. Peaks in the C1-C1' region were deconvoluted so that relaxation times of each form in the mixture could be measured. Integrated peak areas resulting from the signal from only one form were fit to the following monoexponential equation:

$$I_\tau = I_\infty \left(1 - e^{-\frac{\tau}{T_1}} \right) \quad (\text{Equation 5.1})$$

where I_τ is the integrated peak area at a saturation recovery time, τ ; I_∞ is the maximum signal;

Table 5.1. Sample descriptions and dehydration conditions. Dehydrations by hot air were performed by packing the starting material (T_h) into a rotor for SSNMR analysis and heating in the NMR spectrometer.

ID	Source	Lot	Particle Size (μm)	Method of Dehydration	Temperature	Duration	Figure
A	Acros 18255	A0285874	As Received	Vacuum oven	60 °C	5 days	5.2a
B	Sigma T9449	099K7352	As Received	Vacuum oven	60 °C	5 days	5.2b
C	Acros 18255	A0285874	As Received	Vacuum oven	75 °C	2 days	5.2c
D	Sigma T9449	099K7352	As Received	Vacuum oven	75 °C	2 days	5.1, 5.2d, 5.5
E	Acros 18255	A0264819	180–425	Hot air	65 °C		5.2e
F	Sigma T9449	099K7352	75–125	Hot air	68 °C		5.2f, 5.4
G	Sigma T9449	099K7352	As Received	Hot air	75 °C		5.2g, 5.9
H	Acros 18255	A0285874	300–425	Vacuum oven	75 °C	2 days	5.5, 5.6
J	Sigma T9449	099K7352	180-425	Hot air	68 °C		5.7, 5.8

and T_1 is the ^1H spin-lattice relaxation time. Integrated peak areas resulting from more than one form were fit to the following biexponential equation:

$$I_\tau = I_{a\infty} \left(1 - e^{-\frac{\tau}{T_{1a}}}\right) + I_{b\infty} \left(1 - e^{-\frac{\tau}{T_{1b}}}\right) \quad (\text{Equation 5.2})$$

where I_τ is the integrated peak area at a saturation recovery time, τ ; $I_{a\infty}$ and $I_{b\infty}$ are the maximum signals corresponding to the a and b components, respectively; and T_{1a} and T_{1b} are the ^1H spin-lattice relaxation times corresponding to the a and b components, respectively. Data were plotted and fitted to Equations 1 and 2 using KaleidaGraph (Version 4.01, Synergy Software), which employs a Levenberg-Marquardt algorithm for curve fitting.

^1H $T_{1\rho}$ relaxation times were measured by varying the spin-lock duration. As with the ^1H T_1 data, deconvoluted peak areas were used when analyzing a mixture. Integrated peak areas resulting from the signal from only one form were fit to the following monoexponential equation:

$$M_\tau = M_0 \left(e^{-\frac{\tau}{T_{1\rho}}}\right) \quad (\text{Equation 5.3})$$

where M_τ is the integrated peak area at each spin-lock time, τ ; M_0 is the initial magnetization; and $T_{1\rho}$ is the spin-lattice relaxation time in the rotating frame. Integrated peak areas resulting from more than one form were fit to the following biexponential equation:

$$M_\tau = M_0 \left(e^{-\frac{\tau}{T_{1\rho a}}} + e^{-\frac{\tau}{T_{1\rho b}}}\right) \quad (\text{Equation 5.4})$$

where M_τ is the integrated peak area at each spin-lock time, τ ; M_0 is the initial magnetization; and $T_{1\rho a}$ and $T_{1\rho b}$ are the spin-lattice relaxation times of the a and b components in the rotating frame. Data were plotted and fitted to Equations 3 and 4 using KaleidaGraph.

5.2.5 Variable-temperature SSNMR

Variable-temperature experiments were performed by heating a sample to 80 °C and allowing it to equilibrate for about 10 minutes in the magnet. After equilibration, 512 acquisitions were collected with a pulse delay of 10 seconds. Though not quantitative, these parameters could be used to detect all forms of trehalose in the mixture. Upon completion of the first data set, the temperature was increased to 90 °C, the sample was allowed to equilibrate for 5 minutes, and the same acquisition conditions were used to acquire a second data set. This procedure was repeated at 100 and 110 °C. After being held at 110 °C for 1.5 hours, the material was cooled to room temperature, and a final spectrum was acquired.

Additional variable-temperature SSNMR experiments were performed by dehydrating a sample of T_h consisting of 180-425- μm particles in the magnet as spectra were acquired. The sample was packed into a zirconia rotor fitted with a top endcap with a small hole (~2-mm) to allow water vapor to escape from the rotor, and it was heated to 68 °C in the magnet. Data acquisition commenced after equilibrating for about 10 minutes. For each spectrum, 512 acquisitions were collected with a pulse delay of 14 seconds. These conditions yielded spectra that represented the composition of the material over a 2-hour period. This sample was held at 68 °C for about 28 hours.

5.2.6 Powder X-ray Diffraction (PXRD)

Dehydrated trehalose (Sample F in Table 5.1) was filled into a quartz sample holder and exposed to Cu $K\alpha$ radiation (40 kV and 44mA) in a powder X-ray diffractometer (Multiflex, Rigaku Co., The Woodlands, TX). Samples were scanned over a 2θ range of 10 to 30° in the

step-scan mode. At each increment of 0.050° , counts were accumulated for 1 s. The chamber was not environmentally controlled.

5.2.7 Differential Scanning Calorimetry (DSC)

DSC was performed using a Thermal Analysis DSC Q2000 (TA Instruments, New Castle, DE). Approximately 3 mg of dehydrated materials (Sample H in Table 5.1) were weighed into hermetic aluminum pans and sealed with lids with three pinholes. Samples were analyzed using a standard ramp method and were heated from 25°C to 250°C at $10^\circ\text{C}/\text{minute}$.

5.3 Results

5.3.1 Generation of T_α and the Discovery of Unknown Material in Samples of Dehydrated Trehalose

Figure 5.1 shows the structure of trehalose and the ^{13}C SSNMR spectra of four samples of trehalose: T_h , T_β , T_{am} , and Sample D. The spectra of T_h , T_β , and T_{am} in Figure 5.1 are consistent with the previously published spectra.^{7, 8} The conditions used to dehydrate Sample D were expected to form T_α , but the SSNMR spectrum of this sample is not consistent with the spectrum of T_α . For the trehalose system, the C1, C1' region of the spectrum, between 90 and 110 ppm, is particularly useful for form identification. Peaks at 93.4 and 92.0 ppm in the spectrum of Sample D show that T_α was formed during the dehydration, but the underlying broad, asymmetric peak spanning from 110 to 90 ppm indicates that T_{am} is also present in the dehydrated sample. The peaks at 94.0 and 92.3 ppm do not correspond to either T_h or T_β . In examining other regions of the spectrum, small peaks at 74.2, 71.9, 71.3, and 69.0 ppm are also unidentified.

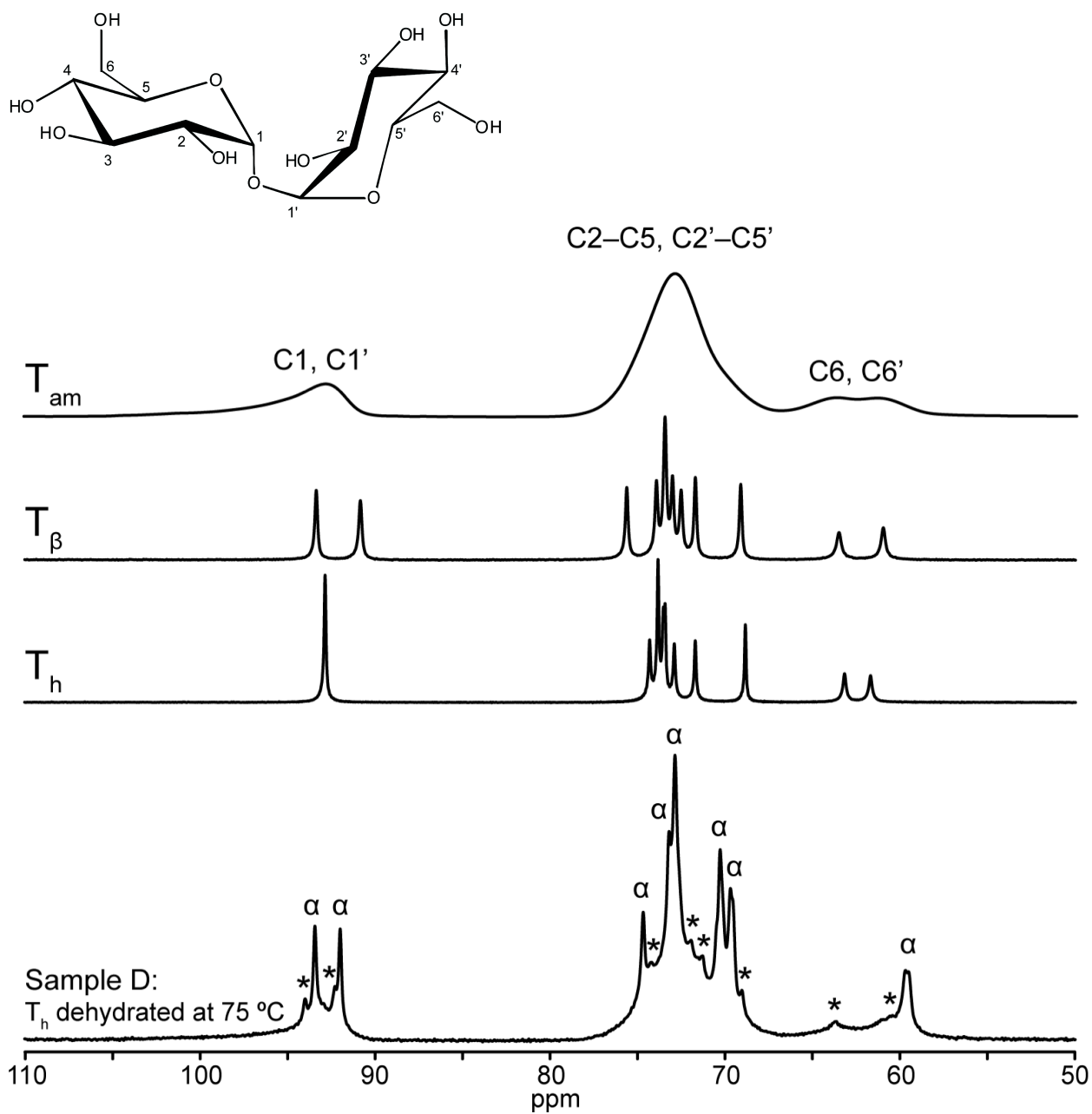


Figure 5.1. Structure of trehalose and ¹³C SSNMR spectra of T_α, T_β, T_h, and a sample that was dehydrated at 75 °C (Sample D in Table 5.1). In the spectrum of the dehydrated sample, peaks corresponding to T_α and T_{am} are present. Unidentified peaks are marked with an asterisk (*).

Figure 5.2 shows ^{13}C SSNMR spectra of other dehydrated samples (Samples A–G in Table 5.1) that were prepared in order to determine if the unknown peaks could be reproducibly generated. The samples whose spectra are shown in Figure 5.2 were dehydrated at or below 75 °C; the unknown peaks have not appeared in spectra of samples dehydrated above 100 °C. For all samples, peaks corresponding to T_{am} , T_{α} , and the unknown material(s) are present in the spectra, and in some samples, T_{β} peaks are also present. In addition to the two peaks in the C1, C1' region, three small peaks in the region corresponding to C2–C5 and C2'–C5' are assigned to the unknown material: these appear at 71.9, 71.3, and 69.0 ppm. In the spectrum shown in Figure 5.1, it appeared that a fourth peak in this region, at 74.2 ppm, may correspond to the unknown material, but this peak is not detected in the spectra shown in Figures 3f and 3g. The amount of unknown material is highest in these samples (as evidenced by the intensities of the peaks at 94.0 and 92.3 ppm), and the absence of the peak at 74.2 ppm likely indicates that it does not result from the unknown material(s). Some spectra also contain a very small peak near 92.8 ppm. The SSNMR spectrum of T_{h} contains peaks near 92.8 and 74.2 ppm, and the presence of these two peaks in the spectra of dehydrated samples may indicate that residual T_{h} is present. Peaks at 63.8 and 60.5 ppm in the C6, C6' region are also assigned to the unknown material. In all spectra containing the unknown peaks, the T_{α} peaks are larger than the unknown peaks, though the ratio is not the same in each spectrum. The largest unknown peaks are observed during dehydrations via VT-SSNMR (Samples E–G in Table 5.1). Samples D and G were dehydrated at the same temperature (75 °C) using the same starting material, yet they have different SSNMR spectra. The unknown peaks are larger in the spectrum of Sample G, and this sample also contains T_{β} . This highlights the sensitivity of the dehydration to the sample environment. Sample D was

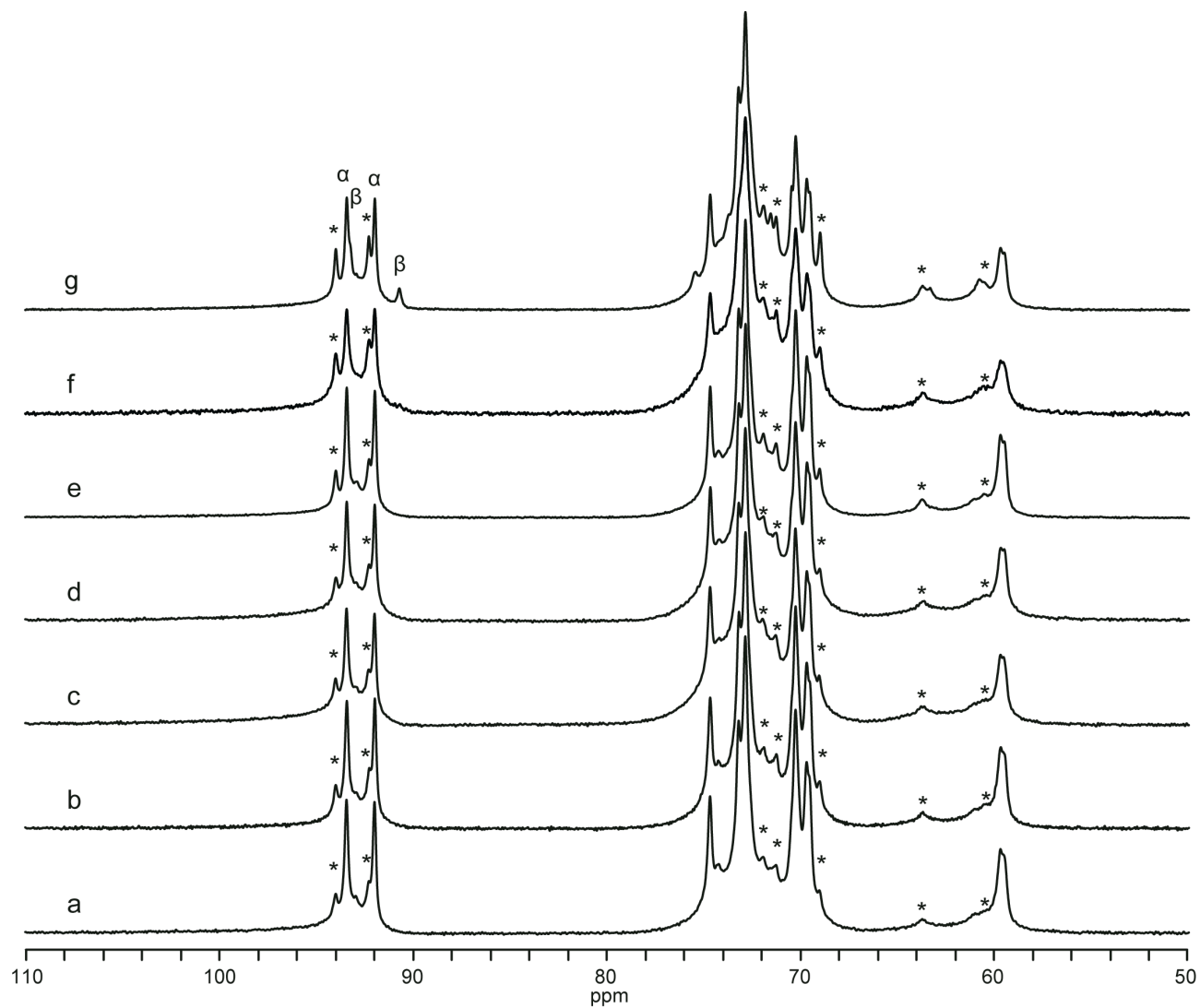


Figure 5.2. ^{13}C SSNMR spectra of Samples A–G (Table 5.1). Peaks corresponding to the unknown material are labeled with an asterisk (*).

dehydrated in a vacuum oven, and Sample G was dehydrated in a SSNMR rotor. In the vacuum oven, the water is able to freely escape, and in a rotor, the flow of water is impeded; this difference is expected to affect the forms that are generated. It has also been suggested that the rapid spinning of samples during VT-SSNMR dehydration can impact the anhydrous forms that are generated.⁹ These two factors may increase the tendency of the sample to form the unknown material(s).

Several possible explanations were considered to explain the presence of the unknown peaks. One explanation is that the peaks are due to a new polymorphic form of trehalose. A second explanation is that they are due to a degradation product. The following observations were made to try to determine which explanation is correct. First, the unknown peaks in the C1, C1' region always appear together with similar areas, suggesting that they result from only one substance, and the sharpness of these peaks shows that they result from crystalline material. Second, these peaks are located well within the broad peaks corresponding to amorphous trehalose, and their chemical shifts are close to those of the other solid forms of trehalose; this indicates that the structure of the unknown material is similar to the other solid forms of trehalose. Based on this, it appears that these peaks result from a previously undiscovered solid form of trehalose, which has been named the δ polymorph (T_δ). The following sections describe additional experiments that were performed in order to provide support for this conclusion.

5.3.2 ¹³C Solid-state NMR Relaxation Times of Trehalose Solid Forms

SSNMR relaxation times of different solid forms often differ due to conformational and packing differences among the solid forms of a compound.¹⁰⁻¹² As a result of rapid ¹H spin diffusion, the relaxation time of each peak corresponding to a particular form is expected to be

the same, and this property can be used to confirm that the T_δ peaks result from only one component. In complex mixtures of forms, such as those containing T_δ , the observation of different relaxation times of the individual components also enables one to conclude that the components are present in distinct phases.¹³

The SSNMR spectrum of Sample E (Table 5.1) is shown in Figure 5.2e, and the $^1\text{H } T_1$ and $^1\text{H } T_{1\rho}$ relaxation times in this sample are listed in Table 5.2. Areas of the peaks at 94.0 and 92.3 ppm (T_δ) and 93.4 and 92.0 ppm (T_α) from a $^1\text{H } T_1$ experiment were fit to Equation 5.1. In addition, the total peak area of the C1, C1' region (89–110 ppm) was fit to Equation 5.2. Areas of these peaks from a $^1\text{H } T_{1\rho}$ experiment were fit to Equation 5.3 (T_α and T_δ) and Equation 5.4 (89–110 ppm). The two peaks corresponding to T_α have a common $^1\text{H } T_1$ relaxation time of about 15 seconds, and the two peaks corresponding to T_δ have a common $^1\text{H } T_1$ relaxation time of about 12 seconds. Amorphous trehalose has a $^1\text{H } T_1$ relaxation time of 5–8 seconds, and the shorter relaxation time from the biexponential fit of the C1, C1' region is consistent with this. The longer value likely corresponds to an approximate $^1\text{H } T_1$ relaxation time of the crystalline material in the sample. The similar $^1\text{H } T_1$ relaxation times that were observed for the T_δ peaks support the conclusion that they result from one material. Though the $^1\text{H } T_1$ relaxation times of T_α and T_δ are different, the difference may not be large enough to conclusively show that the two forms are present in separate domains. The two peaks corresponding to T_α have a common $^1\text{H } T_{1\rho}$ relaxation time of about 110 ms, and the two peaks corresponding to T_δ have a common $^1\text{H } T_{1\rho}$ relaxation time of about 40 ms. Similar to the $^1\text{H } T_1$ results, the shorter $^1\text{H } T_{1\rho}$ relaxation time from the biexponential fit of the C1, C1' region is close to the $^1\text{H } T_{1\rho}$ relaxation time of amorphous trehalose, which has been measured in a pure sample and is on the order of a few milliseconds. The longer component corresponds to an approximate relaxation time of the crystalline material

Table 5.2. Calculated $^1\text{H } T_1$ and $^1\text{H } T_{1\rho}$ relaxation times of Sample E (Table 5.1). The error of the fit is shown in parentheses.

Peak (ppm)	$^1\text{H } T_1$ (s)	$^1\text{H } T_{1\rho}$ (ms)
110–89	5.2 (2.5), 16.5 (4.1)	7.3 (0.9), 120.0 (10.9)
93.4 (α)	15.3 (0.4)	117.3 (11.5)
92.0 (α)	14.6 (0.3)	103.7 (8.8)
94.0 (δ)	11.6 (0.7)	41.6 (4.4)
92.3 (δ)	12.7 (0.8)	42.2 (3.3)

in the sample. It is much closer to the ^1H $T_{1\rho}$ relaxation time of T_α , probably because the amount of T_α in the sample is higher than the amount of T_δ . The ^1H $T_{1\rho}$ relaxation time of T_α is almost three times longer than the ^1H $T_{1\rho}$ relaxation time of T_δ , clearly demonstrating that T_α and T_δ exist in separate domains.

5.3.3 Exposure of T_δ to Ambient Temperature and Humidity

T_α quickly reverts to T_h upon exposure to ambient humidity,¹⁴ and if T_δ is a metastable form, it may also easily convert to T_h . A portion of a dehydrated sample containing T_α , T_{am} , and T_δ (Sample D in Table 5.1) was spread on a weighing dish and left uncovered for 24 hours. Figure 5.3 shows the ^{13}C SSNMR spectra of T_h before dehydration, the dehydrated sample, and the dehydrated sample after exposure to ambient conditions. The SSNMR spectrum of the starting material is consistent with that of T_h , and the spectrum of Sample D indicates that T_α , T_{am} , and T_δ are present in the dehydrated sample. The spectrum of the material that was exposed to ambient conditions is also consistent with that of T_h , demonstrating that T_α , T_{am} , and T_δ all convert to T_h after exposure to ambient temperature and humidity for 24 hours.

Figure 5.4 shows PXRD patterns of Sample F over the course of two hours as it was exposed to ambient conditions. In the first scan, characteristic peaks of T_α are detected at $16^\circ 2\theta$ and $17.8^\circ 2\theta$, and characteristic peaks of T_h are detected at $13.6^\circ 2\theta$ and $23.9^\circ 2\theta$. Unidentified peaks that could be attributed to T_δ are not obviously present, though the material could have transformed to T_h prior to analysis. As the sample is exposed to ambient conditions, the characteristic peaks of T_α decrease in intensity, and the characteristic peaks of T_h increase in

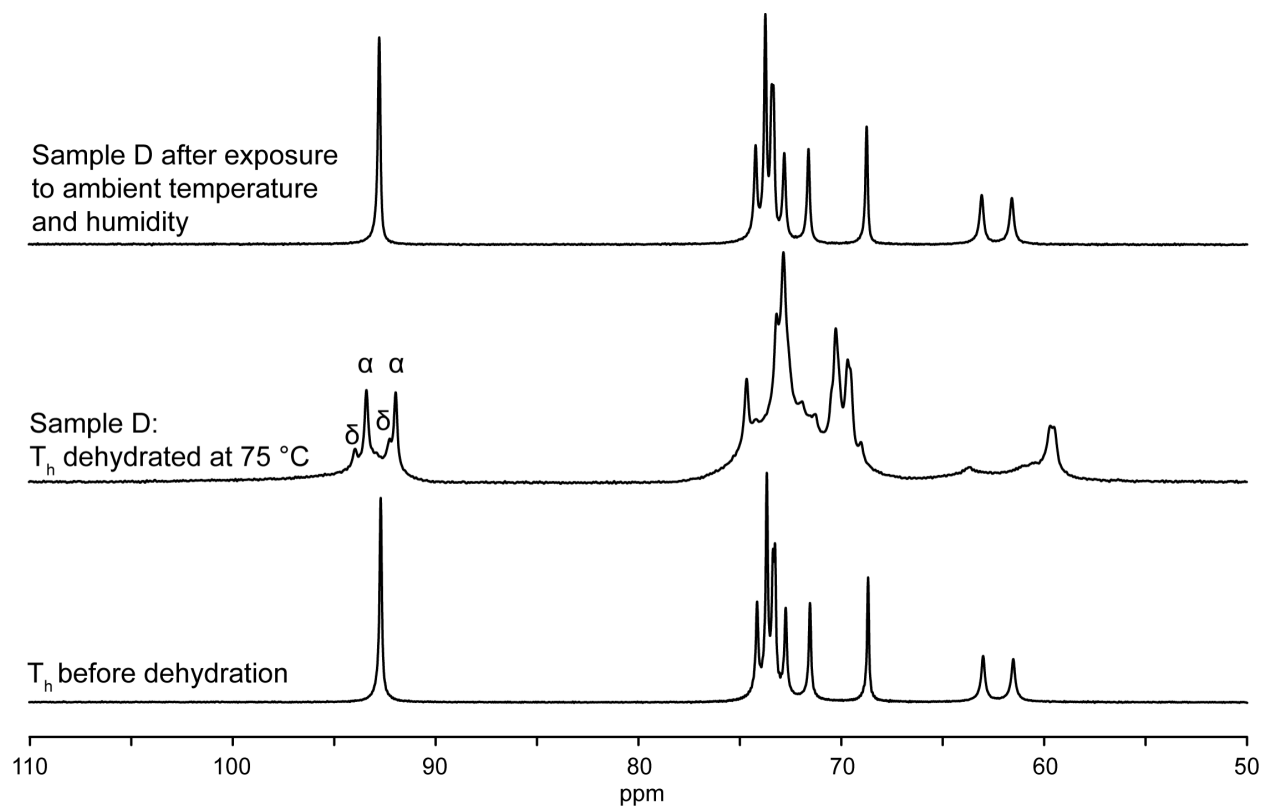


Figure 5.3. ^{13}C SSNMR spectra of T_h , Sample D (Table 5.1), and the dehydrated material after exposure to ambient conditions.

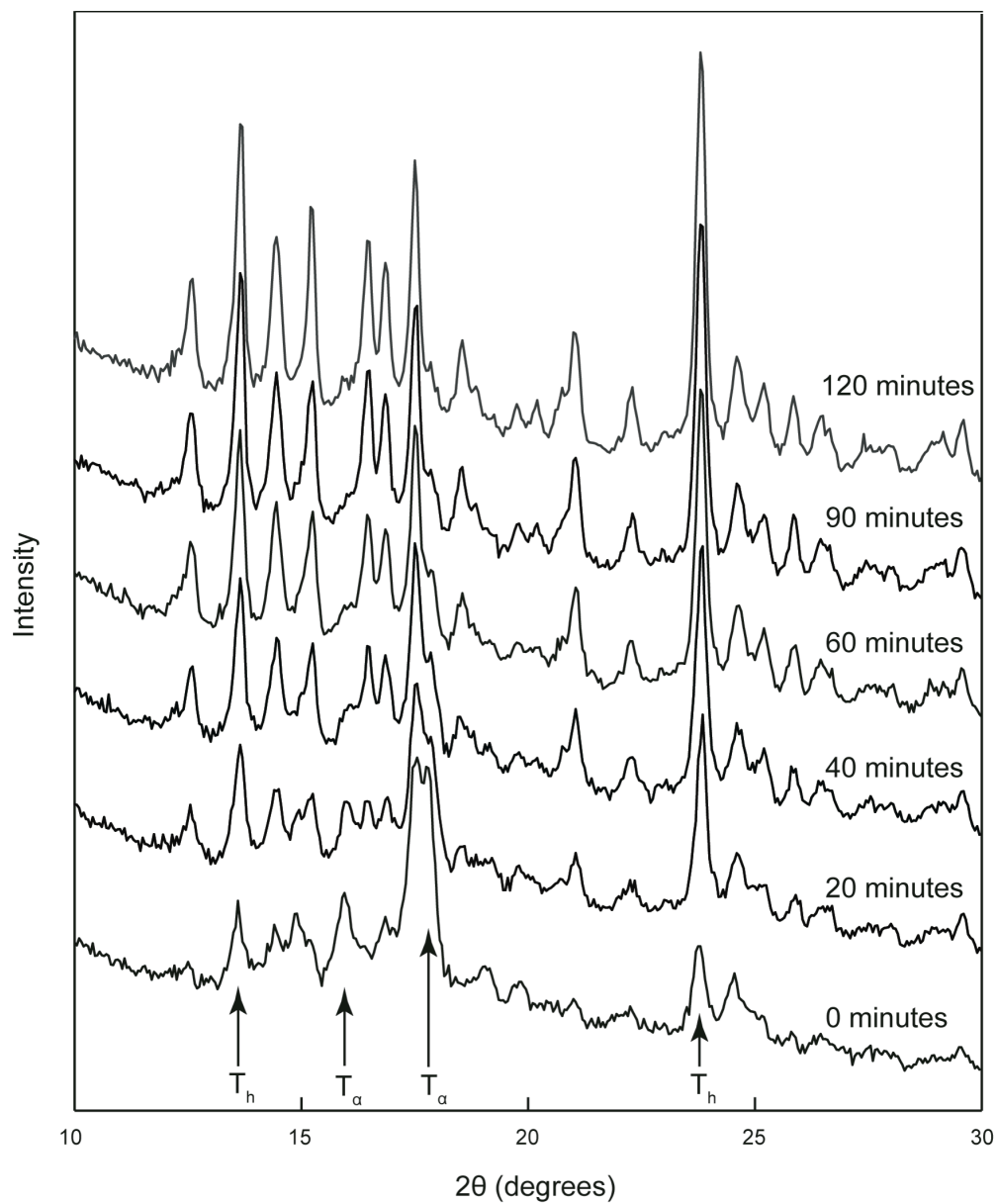


Figure 5.4. PXR D patterns of a sample containing T_α , T_{am} , and T_δ (Sample F in Table 5.1) as it was held at ambient temperature and humidity. Characteristic peaks of T_α and T_h are labeled and were monitored during the experiment.

intensity. Most peaks appear to either decrease (T_α) or increase (T_h) in intensity during the experiment, but the behavior of the peak at $17.5^\circ 2\theta$, assigned to T_h , does not follow this pattern. It decreases in intensity after 20 minutes and then increases in intensity after 40 minutes. Peaks corresponding to T_α are broad, and the T_α peak at $17.8^\circ 2\theta$ is not resolved from the T_h peak at $17.5^\circ 2\theta$. Though we considered that a peak in this region could be attributed to unknown material, we believe that the unusual behavior in this region results from the poor resolution of the T_h and T_α peaks. The pattern collected after 120 minutes is consistent with that of T_h , indicating that all materials in the original sample, T_α , T_{am} , and T_δ , converted to T_h after only two hours. If the material that is now identified as the new δ form of trehalose resulted from irreversible thermal degradation, exposure to ambient temperature and humidity would not be expected to cause a conversion to T_h .

5.3.4 Thermal Behavior of T_δ

^{13}C SSNMR spectra of Sample H (Table 5.1) were acquired at room temperature, 80, 90, 100, and 110 °C and are shown in Figure 5.5. The spectrum of the material after it was cooled to room temperature is also shown. The SSNMR spectra of Sample H at room temperature and 80 °C are very similar. At 90 °C, there appears to be only one peak for the carbons in the 6 and 6' positions of T_α (~60 ppm), whereas two overlapping peaks are visible in the spectra at room temperature and 80 °C. These carbons are outside the ring and would be expected to be more mobile as the temperature increases, leading to coalescence of these peaks. Also at 90 °C, there appears to be a slight decrease in the intensity of the T_δ peaks near 92.3 and 94.0 ppm. These peaks continue to decrease in intensity as the material is held at 100 °C, and they are no longer

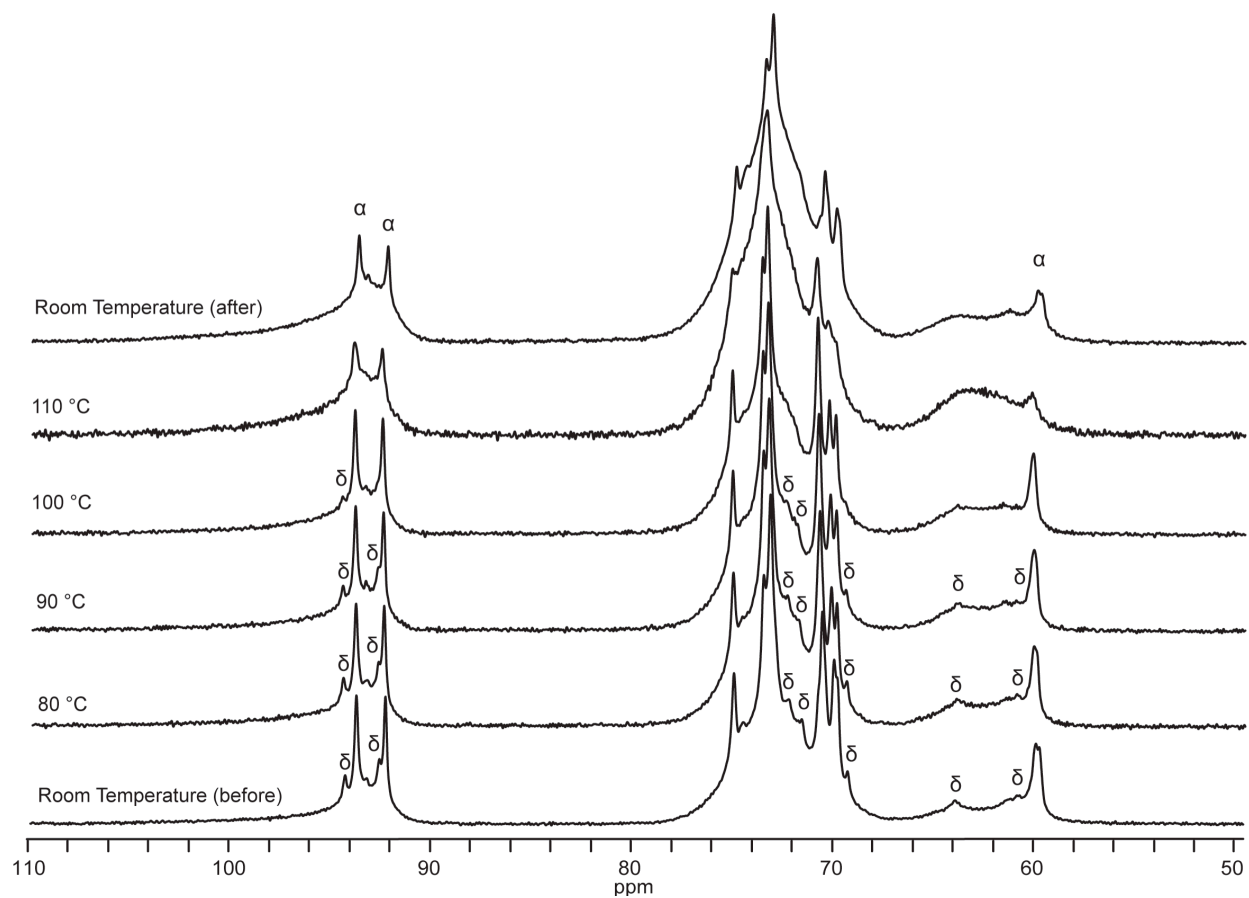


Figure 5.5. ^{13}C SSNMR spectra acquired as Sample H (Table 5.1) was held at elevated temperatures. Peaks corresponding to the unknown material are labeled with an asterisk (*).

visible in the spectrum acquired at 110 °C. T_δ peaks at 71.9, 71.3, 69.0, 63.8, and 60.8 ppm also disappear at 110 °C, confirming that they all result from one component, the δ form. This transformation helps to explain why T_δ has not been observed in dehydrations performed above 100 °C. In addition to the disappearance of the T_δ peaks in the spectrum acquired at 110 °C, other significant changes to the spectrum have occurred. As the glass transition temperature of T_{am} (~120 °C) is approached, the signal from T_{am} decreases as the amorphous material becomes more mobile and cross-polarization between ^1H and ^{13}C becomes less efficient. The intensities of the C1 and C1' peaks for T_α also decrease in intensity at 110 °C, illustrating the sub-melting-temperature conversion of T_α to T_{am} . The spectrum acquired at room temperature after heating shows that T_δ is no longer present, indicating that it converted to T_α or T_{am} . SSNMR is inherently quantitative, which should allow us to determine if T_δ transforms to T_{am} or T_α ; however, because T_α converts to T_{am} as T_δ is transforming, it is not possible to determine conclusively if T_α or T_{am} is generated from T_δ .

Figure 5.6 shows DSC thermograms of Sample H before and after heating to 110 °C in the magnet. In both thermograms, there is a slight downward drift in the baseline below 110 °C. This is likely due to the loss of loosely bound water that was adsorbed as the samples were prepared for analyses and as the heated sample was packed into and unpacked from the SSNMR rotor. In both thermograms, significant overlap between the glass transition of T_{am} and the melting of T_α is evident. In the thermogram of the material before heating, the glass transition appears as a shoulder on the low-temperature side of the endotherm corresponding to the melt of T_α . Aging (or annealing) of T_{am} occurs as it is held at temperatures below T_g , which results in a peak for enthalpic recovery accompanying the glass transition of the heated sample. In the thermogram of the heated sample, the glass transition with enthalpic recovery is better resolved

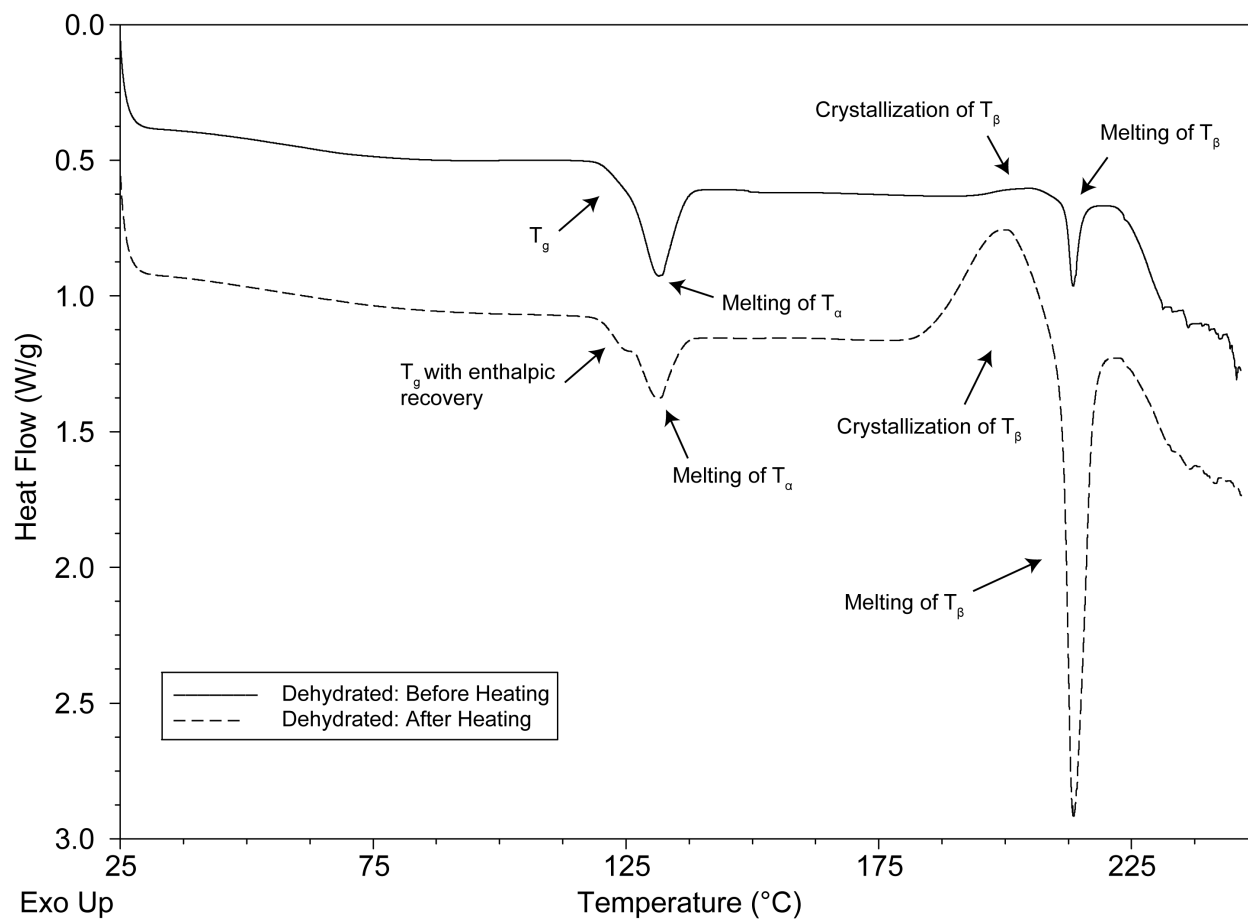


Figure 5.6. DSC thermograms of Sample H (Table 5.1) before and after heating to 110 °C. SSNMR spectra of these samples are shown in Figure 5.5. Prior to heating, the sample contained T_δ , T_{am} , and T_α .

from the melting of T_α . SSNMR shows a decrease in intensity of the T_α peaks as the sample is heated, and accordingly, the melting endotherm of T_α is smaller in the thermogram of the heated sample. T_δ may also melt in this region, but it cannot be detected due to overlapping thermal events. Exotherms above 175 °C correspond to crystallization of T_β . After exposure to elevated temperatures, the dehydrated sample has a higher tendency to crystallize, as evidenced by a lower onset of crystallization and a larger endotherm. The melting endotherm with a peak temperature at 213 °C corresponds to melting of T_β . Although the heated sample has a higher tendency to crystallize, the SSNMR spectra do not indicate that T_β is present in either sample. An investigation into this increased tendency to crystallize upon storage below T_g is addressed in Chapter 9. The absence of a thermal event between 80 and 110 °C in the DSC thermogram of the dehydrated sample prior to heating suggests that the transformation of T_δ below 110 °C is not a typical melting or decomposition. It may not be possible to use DSC to identify or characterize T_δ unless a pure sample of T_δ is generated and analyzed.

5.3.5 Generation of T_δ

Figure 5.7 shows ^{13}C SSNMR spectra (C1, C1' region) acquired as a sample of T_h was held at 68 °C in the NMR spectrometer (Sample J in Table 5.1). As water molecules leave the crystal structure, the peak corresponding to T_h decreases in magnitude. This decrease is accompanied by the appearance and growth of peaks corresponding to T_{am} , T_α , T_δ , and T_β . Peaks corresponding to T_α are first detected after 2 hours, and peaks corresponding to T_β and T_δ are detected after 6 hours. Peaks in the C1-C1' region of all spectra acquired during heating were deconvoluted, and the sums of peak areas of T_α , T_δ , and T_β were calculated. These areas are

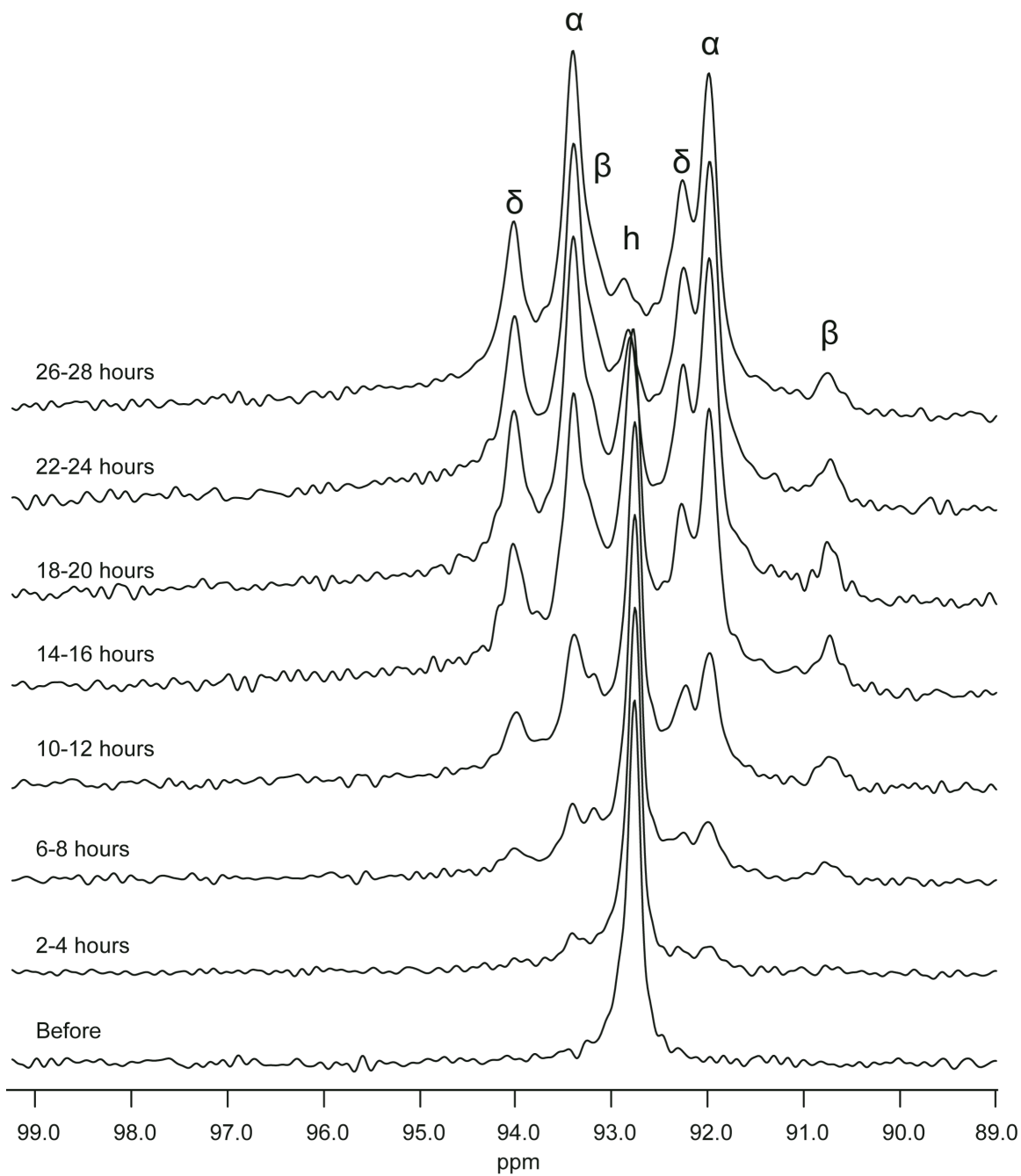


Figure 5.7. ^{13}C SSNMR spectra of a sample of T_n as it was held at 68 °C in the magnet (Sample J in Table 5.1). Spectra were normalized to the same maximum peak height.

plotted in Figure 5.8. Due to the asymmetry of the amorphous peak, it could not be deconvoluted and its area was not plotted. It is important to note that these results are not quantitative; a short pulse delay was chosen so that spectra with a sufficient signal-to-noise ratio could be collected and analyzed. ^1H T_1 relaxation times of T_h and T_β are at least five times longer than those of T_α and T_δ , leading to saturation of the signals from T_h and T_β . This ultimately results in underestimation of the quantities of these two forms and explains why the total area early in the experiment does not equal the total area near the end of the experiment. Regardless, because the ^1H T_1 relaxation times of T_α and T_δ are close, making semi-quantitative statements about the amounts of these two components of the mixture is possible. The decrease in the area of the T_h peak appears to be linear, and the increases in the areas of T_α and T_δ peaks are also approximately linear. Growth of T_α and T_δ occurs throughout the experiment, and the amount of T_α increases faster than the amount of T_δ . In contrast, the amount of T_β plateaus after about ten hours. Under these conditions, the presence of T_β does not facilitate crystallization of the metastable forms to the most stable anhydrous polymorph. At 68 °C, the sample is about 50 °C below the T_g of amorphous trehalose, and the sample is not expected to be very mobile. This may inhibit crystallization of metastable forms to T_β . It is unclear why certain regions of the T_h sample transform to the most stable polymorph and others do not, but it appears that the mechanism of water loss leading to formation of T_α and T_δ is different from the mechanism of water loss that leads to formation of T_β . Dupray et al. showed that different anhydrous forms of trehalose could be formed within a single particle of T_h during dehydrations,¹⁵ and it is possible that this sample is behaving similarly. Dehydration of T_h is discussed in more detail in Chapters 6 and 7.

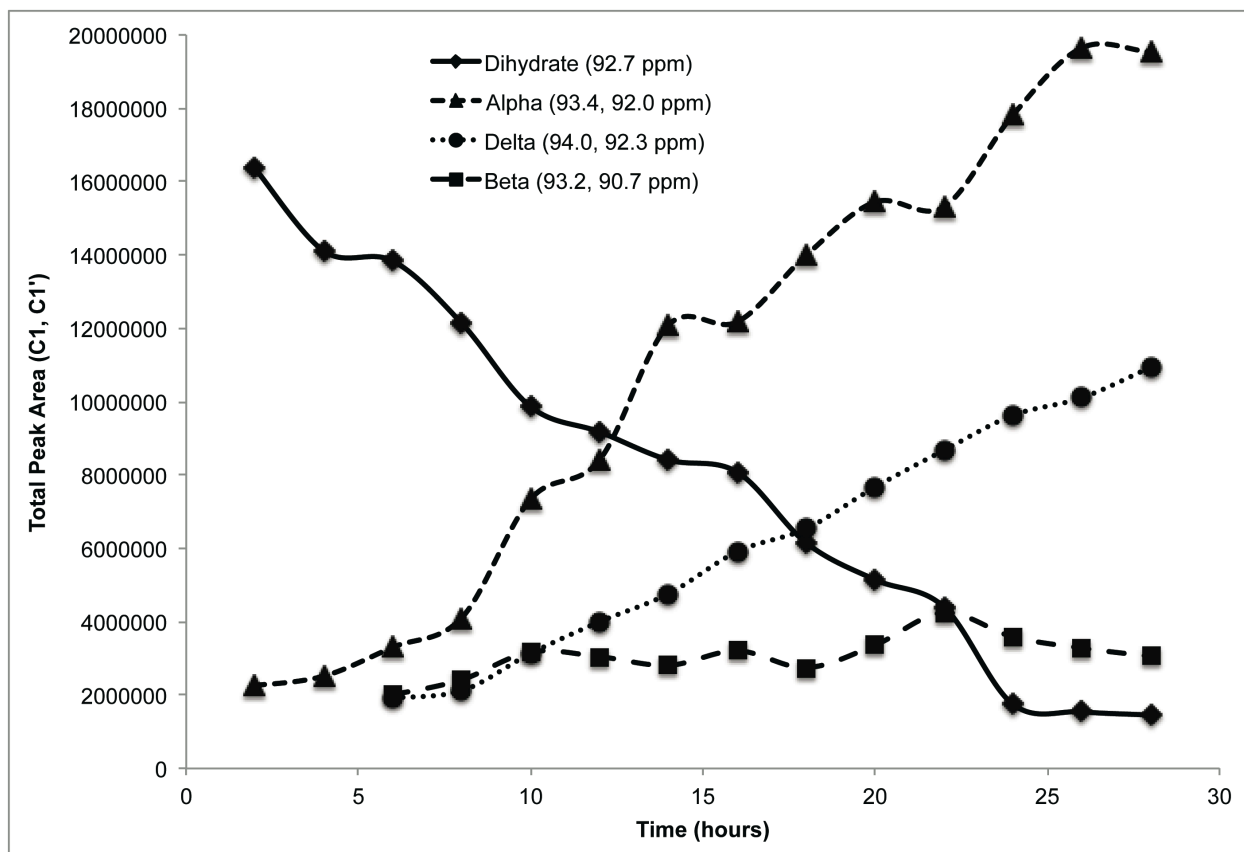


Figure 5.8. Plot of deconvoluted peak areas from the ^{13}C SSNMR spectra shown in Figure 5.7. These results are not quantitative due to the differences in ^1H T_1 relaxation times among the forms and the selection of a short pulse delay, and therefore, T_h and T_β are underreported.

5.4 Discussion

5.4.1 Identification of Unknown Peaks

Table 5.3 lists the ^{13}C SSNMR chemical shifts of T_δ and the four other solid forms of trehalose, and Figure 5.9 shows the ^{13}C SSNMR spectrum of a sample that contains the five solid forms of trehalose (Sample G in Table 5.1). In the C1, C1' region, each form is easily detected, highlighting the power of SSNMR to study this complicated system. For T_δ , only three chemical shifts are listed for C2–C5 and C2'–C5', and eight peaks would be expected if each carbon were represented by a separate resonance. Due to the number of peaks in the region, it is probable that other T_δ peaks are present but overlap with peaks assigned to other forms of trehalose. It is also possible that two or more carbons in T_δ may resonate at the same frequency, resulting in peak overlap. If a pure sample of this material could be analyzed, more peaks would likely be detected.

T_δ is not the same as the T_ϵ form.¹⁶ PXRD patterns of T_ϵ are haloed and contain peaks at about $20.5^\circ 2\theta$ and $22.5^\circ 2\theta$, both characteristic of T_β ; the PXRD pattern of a sample containing T_δ does not contain peaks at these diffraction angles. The DSC thermograms of T_ϵ samples do not contain specific thermal events that can be attributed to transitions of T_ϵ . The results for T_δ are not consistent with those observed for T_ϵ , and we believe that T_ϵ may be a mixture of T_{am} and T_β . PXRD patterns of T_ϵ are very similar to PXRD patterns we obtained when analyzing mixtures of T_{am} and T_β , and thermograms are consistent with DSC thermograms that are obtained in which T_h dehydrates to form a mixture of T_{am} and T_β . If this could be confirmed, it would not be the first time that misidentification of trehalose forms has occurred. Previously, mixtures of T_h and T_β were proposed to be a new form, T_γ .¹⁷ A report on the κ form of trehalose, T_κ , was published, but

Table 5.3. ^{13}C SSNMR chemical shifts of all solid forms of trehalose.

Assignment	T_h		T_β			T_α		T_{am}	T_δ
	this work	Gil et al. ⁷	this work	Gil et al. ⁷	Shao et al. ¹⁸	this work	Gil et al. ⁷	this work	this work
C1, C1'	92.7	93.1	93.2	93.8	93.1 (C1')	93.4	93.5	108–88	94.0
			90.7	*	90.5 (C1)	92.0	91.9-92.1	Max: 92.7	92.3
C2–C5 and C2'–C5'	74.2	74.1	75.5	76.0	75.3 (C3)	74.7	74.7-75.0	82–66.5	71.9
	73.7	73.6	73.7	74.4	73.6 (C4)	73.2	73.2	Max: 72.7	71.3
	73.4	73.3	73.3	73.9	73.1 (C5, C2')	72.9	72.8		69.0
	73.3	72.8	72.9	73.5	72.7 (C2)	70.4	70.2		
	72.8	71.5	72.4	73.1	72.2 (C3')	70.3	69.7		
	71.6	68.7	71.6	72.2	71.4 (C5')	69.7			
	68.7		69.0	69.5	68.8 (C4')	69.6			
C6, C6'	63.0	63.0	63.3	63.7	63.2 (C6)	59.7	59.6	66.5–54	63.8
	61.5	61.7	60.8	61.4	60.7 (C6')	59.5		Max: 63.4, 61.1	60.8

*Spectrum shows two peaks, but only one resonance is listed.

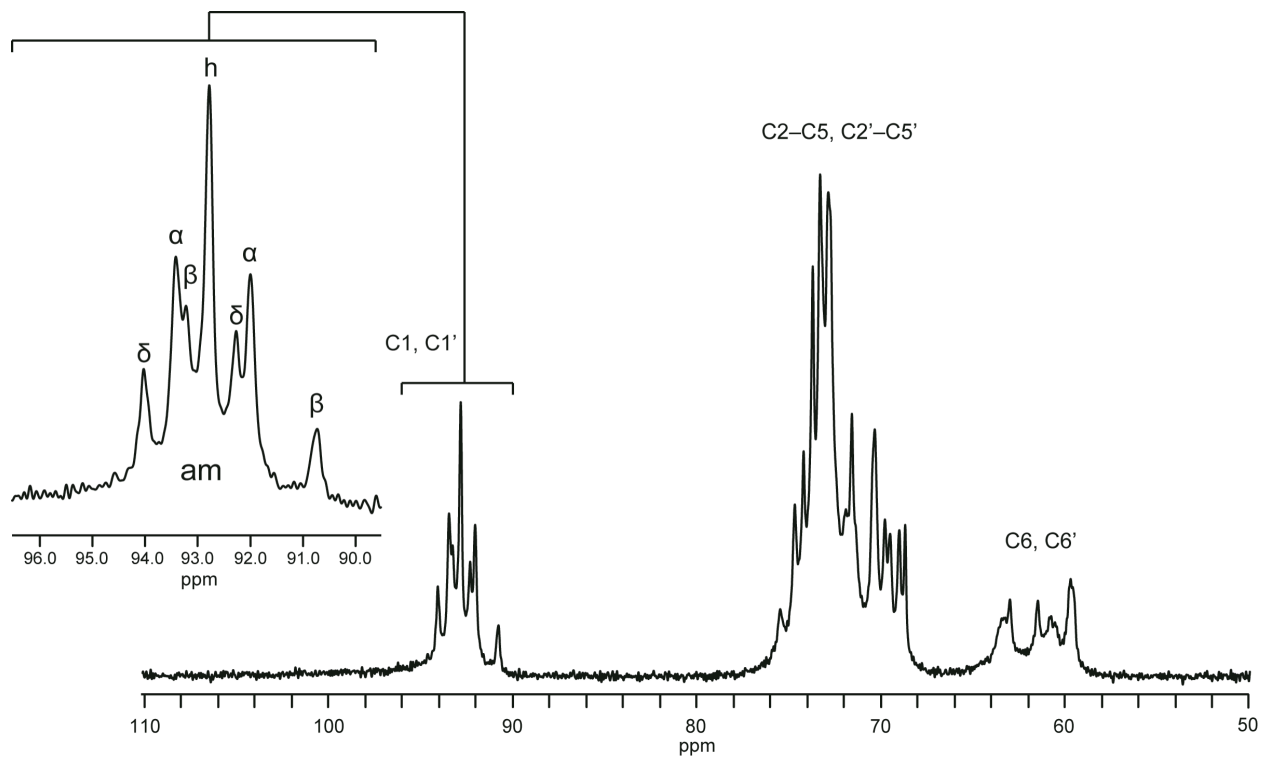


Figure 5.9. ^{13}C SSNMR spectrum of a sample containing the five solid forms of trehalose (Sample G in Table 5.1). All forms are easily identified by examining the C1, C1' region.

the authors concluded that it was actually T_α .¹⁴

T_δ is not a thermal degradant. Trehalose is one of the most stable sugars and is not prone to thermal degradation at low temperatures;¹⁹ however, it was considered that hydrolysis of trehalose to form two molecules of glucose is the most likely degradation pathway. If hydrolysis had occurred, endotherms corresponding to the melting of glucose would appear in the thermograms. DSC thermograms of samples containing T_δ do not contain endotherms at ~ 150 or ~ 162 °C (α and β anomers, respectively). Additionally, the unknown peaks are not observed in SSNMR spectra of T_h samples that are dehydrated above 100 °C, where thermal degradation is more likely to occur. If the T_δ peaks in the SSNMR spectra resulted from a thermal degradation product generated at 75 °C, they might be expected to grow upon exposure to temperatures above this. Instead, the opposite was observed: the peaks began to disappear at only 90 °C. Upon exposure to temperatures between 90 and 110 °C, SSNMR shows that the unknown peaks disappear and no new peaks appear, demonstrating that either T_{am} or T_α is formed from T_δ . This transition, as well as the reversion of T_δ to T_h upon exposure to ambient temperature humidity, would not be expected from anything other than a metastable form of trehalose.

5.4.2 Structure of T_δ and Its Role in the Solid-state Chemistry of Trehalose

Although a pure sample of T_δ could not be made, the data allow for speculation on the structure of T_δ and its relationship to the other solid forms. As was discussed in §3.2.1, the orientations of the primary alcohol groups (O5-C5-C6-O6 and O5'-C5'-C6'-O6' angles) are gauche-trans and gauche-gauche in T_h and T_β ,^{8, 20, 21} and they are both gauche-gauche in T_α .²²

Chemical shifts of C6 and C6' in T_δ are similar to those of T_h and T_β , suggesting that the arrangements of the two C5–C6 rotamers in T_δ are gauche-trans and gauche-gauche.

The peak positions indicate that there are structural differences between T_δ and T_α , but the ^1H T_1 relaxation times and stability studies highlight the similarities between these two forms. The ^1H T_1 relaxation times of T_α and T_δ are 15 and 12 seconds, respectively, which is shorter than those of T_h and T_β by at least a factor of five and longer than that of amorphous trehalose by only a factor of two. For the trehalose system, it appears that the ^1H T_1 relaxation times are related to the relative stabilities of the forms, with the less stable crystalline forms, T_α and T_δ , displaying the shorter relaxation times. The shorter relaxation times show that the trehalose molecules in T_α and T_δ are significantly more mobile than those in T_h or T_β , and this faster mobility may help explain why the structure of T_α collapses below its melting point to form T_{am} . The molecules in T_δ are slightly more mobile than those in T_α , which suggests that the transformation of T_δ between 80 and 110 °C could also be a spontaneous amorphization. Evidence of this transition was not detected in DSC thermograms, but DSC thermograms also do not contain an event corresponding to the conversion of T_α to T_{am} . Instead, the melting of T_α is seen at about 132 °C. In a monotropic system, the melting temperature is related to the stability of the forms,²³ and therefore it is possible that the ^1H T_1 relaxation times could also be related to the stability of the forms. If so, this could indicate that the melting temperatures of T_δ and T_α might also be similar. If they have similar melting temperatures, it is unlikely that the melting of T_δ will be detected unless a pure sample is generated.

The growth of both T_α and T_δ is approximately linear while growth of T_β plateaued (Figure 5.8), suggesting that the formation of T_δ is more similar to the formation of T_α than T_β . The mechanism of T_α formation has not yet been determined, though a few theories have been

proposed. Willart et al. concluded that T_α was formed from T_h in a one-step process in which T_α formed as anhydrous areas developed, and they believed that the growth of T_α was not governed by nucleation and growth models.²⁴ Kilburn et al. observed that growth of T_α occurred after water was removed from T_h , and they proposed that dehydration of T_h and formation of T_α are not simultaneous.²⁵ In the two-step process that they describe, water is first removed to form a more open structure, and then the molecules rearrange to form T_α . Nagase et al. showed that the T_α crystal is less stable than hypothetical crystals of T_h when both water molecules are removed (T_h -W1-W2), although the conformation of the molecules in T_α is more stable.²² It is possible that T_δ is representative of this hypothetical T_h -W1-W2, and it could form T_α by undergoing a slight change in conformation to make the molecule more stable and the crystal structure less stable, which is consistent with the mechanism that Kilburn et al. proposed. If this mechanism is correct and T_δ represents T_h -W1-W2, we might expect to detect T_δ before T_α , but that has not been observed. We also did not observe growth of T_α peaks at the expense of T_δ peaks during the dehydration of T_h at 68 °C. However, SSNMR shows that T_δ transitions to either T_α or T_{am} between 90 and 110 °C and so we are unable to rule out the theory that T_δ is a transient form along the pathway from T_h to T_α .

The SSNMR relaxation experiments clearly show that dehydrated samples contain distinct regions corresponding to T_{am} , T_α , and T_δ , and therefore it is more accurate to describe this system using the two-state model of crystallinity.²⁶ Previously, it was suggested that the one-state model of crystallinity could be used to describe mixtures of T_{am} and T_α .²⁷ In this model, the order in a perfect lattice decreases steadily until a completely disordered lattice, i.e. the amorphous state, is reached. In the two-state model of crystallinity, there are either ordered or disordered regions of the lattice. The relaxation time of T_α is longer than the relaxation time of

T_{am} , providing evidence that T_{am} is more mobile than T_{α} . Kilburn et al. suggested that T_{α} is more mobile than T_{am} due to the greater free volume resulting from the holes in the T_{α} structure;²⁵ the shorter relaxation times that were observed for T_{am} indicate that this is incorrect.

5.5 Conclusion

Using ^{13}C SSNMR, a previously undiscovered form of trehalose, T_{δ} , has been identified and characterized. This form was not detected using either DSC or PXRD. T_{δ} is generated in dehydrations of T_h that occur at or below 100 °C, and it is accompanied by the formation of T_{α} and T_{am} . In these mixtures, T_{δ} is always the minor product. T_{δ} easily reverts to T_h , and above 90 °C, it transforms to T_{am} or T_{α} . Relaxation time measurements show that T_{δ} is probably more similar to T_{α} than T_{β} , though structurally, the orientations of the primary alcohol groups are more similar to T_{β} and T_h . It is possible that T_{δ} may have been generated, but not detected, in the many studies that have been performed on trehalose. The fact that it has only been generated in mixtures of at least three forms of trehalose makes its detection more challenging, and it highlights the utility of SSNMR in studying this system.

5.6 References

1. Bielecki, A.; Burum, D. P. Temperature Dependence of ^{207}Pb MAS Spectra of Solid Lead Nitrate. An Accurate, Sensitive Thermometer for Variable-Temperature MAS. *J. Magn. Reson. Ser. A* **1995**, *116*, 215-220.
2. Andrew, A. R.; Bradbury, A.; Eades, R. G. Removal of dipolar broadening of nuclear magnetic resonance spectra of solids by specimen rotation. *Nature* **1958**, *183*, 1802-1803.
3. Barich, D. H.; Gorman, E. M.; Zell, M. T.; Munson, E. J. 3-Methylglutaric acid as a ^{13}C solid-state NMR standard. *Solid State Nucl. Magn. Reson.* **2006**, *30*, (3-4), 125-129.
4. Dixon, W. T.; Schaefer, J.; Sefcik, M. D. Total suppression of sidebands in CPMAS carbon-13 NMR. *J. Magn. Reson.* **1982**, *49*, (2), 341-345.
5. Fung, B.; Khittrin, A.; Ermolaev, K. An improved broadband decoupling sequence for liquid crystals and solids. *J. Magn. Reson.* **2000**, *142*, (1), 97-101.
6. Pines, A.; Gibby, M. G.; Waugh, J. S. Proton-enhanced NMR of Dilute Spins. *J. Chem. Phys.* **1973**, *59*, 569-590.
7. Gil, A. M.; Belton, P. S.; Felix, V. Spectroscopic studies of solid α - α trehalose. *Spectrochim. Acta A* **1996**, *52*, 1649 - 1659.
8. Jeffrey, G. A.; Nanni, R. The Crystal Structure of Anhydrous α,α -Trehalose at -150° . *Carbohydr. Res.* **1985**, *137*, 21-30.
9. Xu, M.; Harris, K. D. M. Altering the Polymorphic Product Distribution in a Solid-State Dehydration Process by Rapid Sample Rotation in a Solid-State NMR Probe. *J. Am. Chem. Soc.* **2005**, *127*, 10832-10833.
10. Dempah, K. E.; Barich, D. H.; Kaushal, A. M.; Zong, Z.; Desai, S. D.; Suryanarayanan, R.; Kirsch, L.; Munson, E. J. Investigating Gabapentin Polymorphism Using Solid-State NMR Spectroscopy. *AAPS PharmSciTech* **2012**.

11. Lubach, J. W.; Xu, D.; Segmuller, B. E.; Munson, E. J. Investigation of the effects of pharmaceutical processing upon solid-state NMR relaxation times and implications to solid-state formulation stability. *J. Pharm. Sci.* **2007**, *96*, (4), 777-787.
12. Offerdahl, T. J.; Salsbury, J. S.; Dong, Z.; Grant, D. J. W.; Schroeder, S. A.; Prakash, I.; Gorman, E. M.; Barich, D. H.; Munson, E. J. Quantitation of Crystalline and Amorphous Forms of Anhydrous Neotame using ^{13}C CPMAS NMR Spectroscopy. *J. Pharm. Sci.* **2005**, *94*, (12), 2591-2605.
13. Zumbulyadis, N.; Antalek, B.; Windig, W.; Scaringe, R. P.; Lanzafame, A. M.; Blanton, T.; Helber, M. Elucidation of Polymorph Mixtures Using Solid-State ^{13}C CP/MAS NMR Spectroscopy and Direct Exponential Curve Resolution Algorithm. *J. Am. Chem. Soc.* **1999**, *121*, 11554–11557.
14. Nagase, H.; Endo, T.; Ueda, H.; Nakagaki, M. An anhydrous polymorphic form of trehalose. *Carbohydr. Res.* **2002**, *337*, 167-173.
15. Dupray, V.; Berton, B.; Ossart, S.; Atmani, H.; Petit, M.-N. Concomitant dehydration mechanisms in single crystals of α, α -trehalose. *Carbohydr. Res.* **2009**, *344*, 2539-2546.
16. Furuki, T.; Kishi, A.; Sakurai, M. De- and rehydration behavior of α, α -trehalose dihydrate under humidity-controlled atmospheres. *Carbohydr. Res.* **2005**, *340*, 429-438.
17. Sussich, F.; Urbani, R.; Cesáro, A.; Princivalle, F.; Bruckner, S. New Crystalline and Amorphous Forms of Trehalose. *Carbohydr. Lett.* **1997**, *2*, 403-408.
18. Shao, L.; Yates, J. R.; Titman, J. J. Carbon-13 Chemical Shift Tensors of Disaccharides: Measurement, Computation and Assignment. *J. Phys. Chem. A* **2007**, *111*, 13126-13132.
19. Shafizadeh, F.; Lai, Y. Z. Thermal Rearrangements of Cellobiose and Trehalose. *Carbohydr. Res.* **1973**, *31*, 57-67.
20. Brown, G. M.; Rohrer, D. C.; Berking, B.; Beevers, C. A.; Gould, R. O.; Simpson, R. The Crystal Structure of α, α -Trehalose Dihydrate from Three Independent X-ray Determinations. *Acta Crystallogr. B* **1972**, *B28*, 3145-3158.

21. Taga, T.; Senma, M.; Osaki, K. The Crystal and Molecular Structure of Trehalose Dihydrate. *Acta Crystallogr. B* **1972**, *28*, 3258-3263.
22. Nagase, H.; Ogawa, N.; Endo, T.; Shiro, M.; Ueda, H.; Sakurai, M. Crystal Structure of an Anhydrous Form of Trehalose: Structure of Water Channels of Trehalose Polymorphism. *J. Phys. Chem. B* **2008**, *112*, 9105-9111.
23. Burger, A.; Ramberger, R. On the polymorphism of pharmaceuticals and other molecular crystals. II. *Microchim. Acta* **1979**, *72*, (3-4), 273-316.
24. Willart, J. F.; De Gusseme, A.; Hemon, S.; Descamps, M.; Leveiller, F.; Rameau, A. Vitrification and Polymorphism of Trehalose Induced by Dehydration of Trehalose Dihydrate. *J. Phys. Chem. B* **2002**, *106*, 3365-3370.
25. Kilburn, D.; Sokol, P. E. Structural Evolution of the Dihydrate to Anhydrate Crystalline Transition of Trehalose as Measured by Wide-angle X-ray Scattering. *J. Phys. Chem. B* **2009**, *113*, 2201-2206.
26. Suryanarayanan, R.; Mitchell, A. G. Evaluation of two concepts of crystallinity using calcium gluceptate as a model compound. *Int. J. Pharm.* **1985**, *24*, (1), 1-17.
27. Rani, M.; Govindarajan, R.; Surana, R.; Suryanarayanan, R. Structure in Dehydrated Trehalose Dihydrate—Evaluation of the Concept of Partial Crystallinity. *Pharm. Res.* **2006**, *23*, (10), 2356-2367.

Chapter 6

Dehydration of Trehalose Dihydrate: Part I

6.1 Introduction

The initial results described in Chapter 4 suggested that the dehydration of trehalose dihydrate (T_h) is affected by source and lot-to-lot variability; different anhydrous forms of trehalose were obtained from dehydrations of trehalose dihydrate from two sources and two lots. In this chapter, variability of T_h is investigated by analyzing sixteen samples of T_h from five sources using differential scanning calorimetry (DSC), thermogravimetric analysis (TGA), polarized light microscopy (PLM) with a hot stage, and ^{13}C solid-state NMR spectroscopy (SSNMR). First, the DSC and TGA thermograms of three sieved samples are discussed in detail. From the DSC thermograms, critical thermal events were identified and analyzed for all samples, and a classification system was developed to describe the different ways that T_h can dehydrate. Images from hot-stage polarized light microscopy (PLM) are then used to illustrate the possible transformations that T_h undergoes during dehydration at 10 °C/minute. Finally, potential causes of the observed differences in dehydration behavior are investigated using DSC and SSNMR.

6.2 Experimental

6.2.1 Materials

Sixteen samples of D-(+)-trehalose dihydrate were purchased from Acros (Geel, Belgium), Alfa Aesar (Ward Hill, MA), Fluka (Buchs, Switzerland), Life Sciences Advanced Technologies Inc. (St. Petersburg, FL), and Sigma (St. Louis, MO). The sample identities, sources, and lot numbers are listed in Table 6.1.

Table 6.1. Sample identities, sources, and lot numbers.

Sample ID	Manufacturer	Product Code	Lot Number
Acros 18255-1	Acros	18255	A0252515
Acros 18255-2	Acros	18255	A0264819
Acros 18255-3	Acros	18255	A0285874
Alfa Aesar A19434-1	Alfa Aesar	A19434	10131165
Alfa Aesar A19434-2	Alfa Aesar	A19434	10143600
Fluka 90208	Fluka	90208	1357383
Fluka 90210-1	Fluka	90210	1401913
Fluka 90210-2	Fluka	90210	1383659
Fluka 90210-3	Fluka	90210	BCBC1043
Life Science	Life Science	TDH033	61821T0905
Sigma T9449-1	Sigma	T9449	099K7351
Sigma T9449-2	Sigma	T9449	099K7352
Sigma T9449-3	Sigma	T9449	114K7064
Sigma T9531-1	Sigma	T9531	058K7357
Sigma T9531-2	Sigma	T9531	127K7350
Sigma T9531-3	Sigma	T9531	127K7355

6.2.2 Sieving

Bulk materials were sieved to obtain particle size fractions of <75 μm , 75–125 μm , 125–180 μm , 180–425 μm , 425–850 μm , and >850 μm . A set of U.S.A. Standard Test Sieves (Hogentogler&Co., Inc., Columbia, MD) was stacked and shaken manually or using a Performer III Model SS-3 mechanical sieve shaker (Gilson Company, Inc., Lewis Center, OH).

6.2.3 Differential Scanning Calorimetry

Differential scanning calorimetry (DSC) experiments were performed using a Thermal Analysis DSC Q2000 (TA Instruments; New Castle, DE). Approximately 5–7 mg of dihydrate samples were weighed into open aluminum pans. All samples were analyzed using a standard ramp method and were heated from 25 °C to 250 °C at a rate of 10 °C/minute under a dry nitrogen purge at 50 mL/min. Samples were analyzed in triplicate when sufficient material was available. When smaller amounts of material or fewer replicates were analyzed, this is noted with the result.

6.2.4 Thermogravimetric Analysis

Thermogravimetric analysis (TGA) experiments were performed using a Thermal Analysis Q50 (TA Instruments; New Castle, DE). Samples were heated in open aluminum pans from 25 °C to 250 °C at a rate of 10 °C/min under a dry nitrogen purge at 40 mL/minute.

6.2.5 Polarized Light Microscopy

Samples were viewed using an Olympus microscope (Center Valley, PA). Hot stage microscopy (HSM) was performed using the Linkam CI94 and Linkam LTS350 attachments (Linkam Scientific Instruments, Surrey, UK) with the Olympus microscope.

6.2.6 ^{13}C Solid-State NMR Spectroscopy

^{13}C SSNMR spectroscopy was performed using either a Chemagnetics CMX-300 spectrometer (Varian, Inc.) or a Tecmag Redstone spectrometer (Tecmag, Inc.), both operating at approximately 300 MHz for ^1H and 75 MHz for ^{13}C . Samples were packed into zirconia rotors and spun at the magic angle.¹ The spinning speed was 4 kHz. Peaks were referenced to the methyl peak of 3-methylglutaric acid, which was set to 18.84 ppm.² Spectra were acquired using ramped cross polarization, Spinal 64 decoupling, and sideband suppression.³⁻⁵ A contact time of 1 ms was used for all samples.

^1H T_1 relaxation times were measured using a saturation recovery experiment. Integrated peak areas were fit to the following monoexponential equation:

$$I_{\tau} = I_{\infty} \left(1 - e^{-\frac{\tau}{T_1}} \right) \quad (\text{Equation 6.1})$$

where I_{τ} is the integrated peak area at a saturation recovery time, τ ; I_{∞} is the maximum signal; and T_1 is the ^1H spin-lattice relaxation time. Data were plotted and fitted to Equation 6.1 using KaleidaGraph (Version 4.01, Synergy Software), which employs a Levenberg-Marquardt algorithm for curve fitting.

6.3 Results and Discussion

6.3.1 DSC and TGA Thermograms: Fluka 90210-1

Figure 6.1 shows DSC and TGA thermograms of sieved particles from the Fluka 90210-1 T_h sample. The first thermal event in the DSC thermograms in Figure 6.1a is a broad endotherm that begins below 50 °C and ends at about 90 °C (**A**). The nature of this event is determined by examining the TGA thermograms in Figure 6.1b, which show that water loss begins between 50 and 60 °C. Therefore, the broad endotherm in the DSC thermograms (**A**) is associated with water loss. Dehydration requires breaking of hydrogen bonds,⁶ and below 90 °C, water loss likely occurs from sites where it is loosely bound, such as defect sites and particle surfaces. Smaller particles have a much larger surface area to volume ratio, and it is expected that they would lose more water than the larger particles in this temperature range. Accordingly, water loss is fastest, evidenced by the steepest slope in the TGA thermograms (Figure 6.1b), and greatest for the smallest particle size fraction, and both the rate and amount of water loss decrease as the particle size increases.

The second thermal event in the DSC thermograms in Figure 6.1a is a large endotherm at ~100 °C (**B**). This endotherm is usually assigned to dehydration of T_h ,^{7, 8} although it has been assigned to melting of T_h .^{9, 10} Again, the nature of this event in the DSC thermogram can be determined from the TGA thermogram (Figure 6.1b): at approximately 95 °C, the rate of water loss sharply increases for all fractions indicating that the endotherm in the DSC thermogram can be assigned to dehydration. At that temperature, it appears that sufficient energy has been supplied to initiate dehydration from more tightly bound sites within the particles. For particles smaller than 180 μm , the rate of water loss slows significantly at about 110 °C, but at that

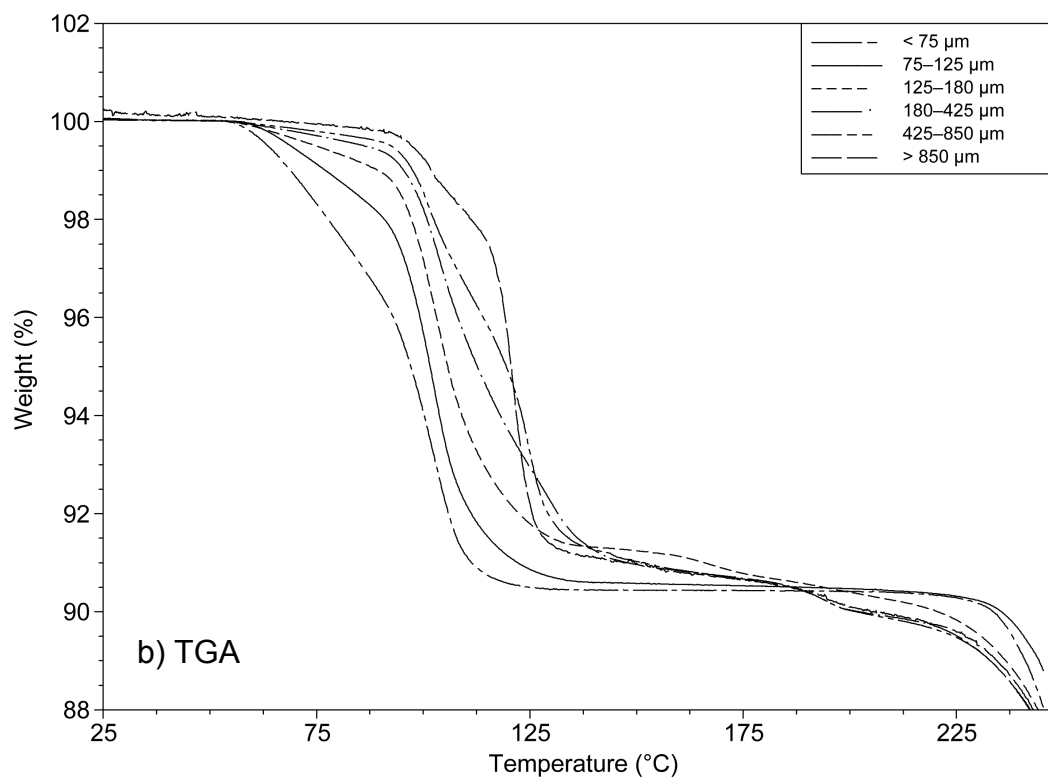
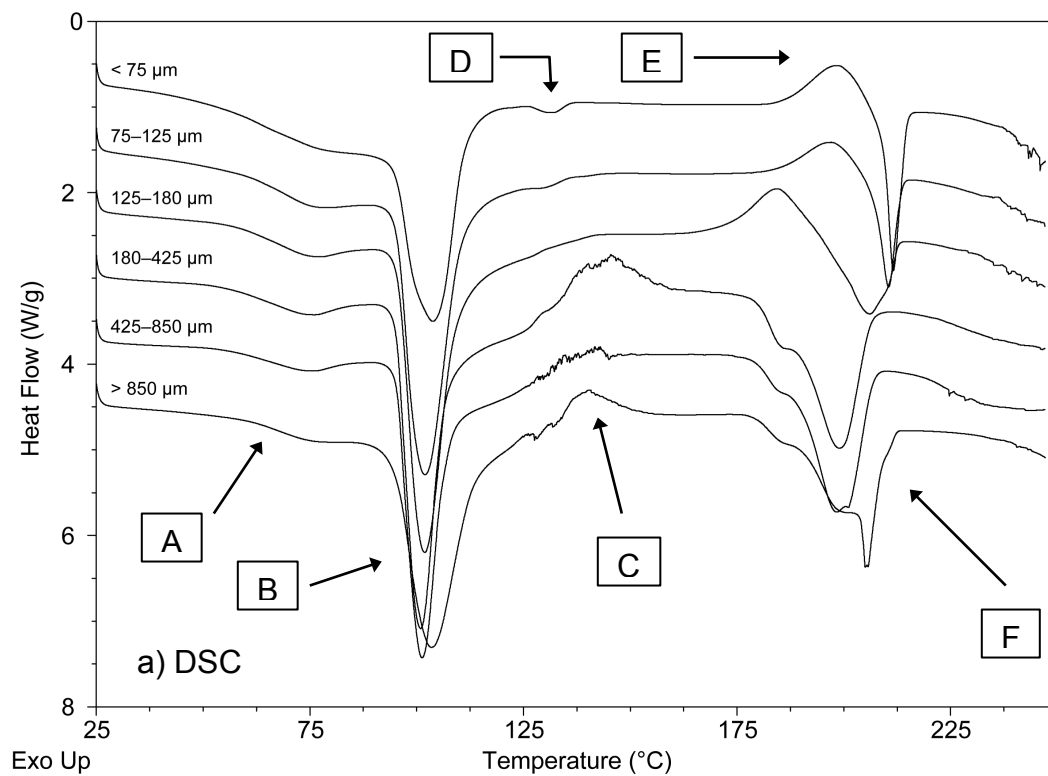


Figure 6.1. DSC (a) and TGA (b) thermograms of particles from the Fluka 90210-1 sample.

temperature, only particles smaller than 75 μm have undergone the 9.5% weight loss that corresponds to the loss of two molecules of water per molecule of trehalose. Particles in the 125–180- μm range have lost about 6% of their weight at this temperature, but particles larger than 180 μm have lost <5%. This demonstrates that while the endotherm near 100 °C (**B**) is complete by about 115 °C, the dehydration process of larger particles continues at temperatures higher than this.

In Figure 6.1a, a third event (**C**) is observed in thermograms of particles larger than 180 μm ; this irregular, “noisy” region extends from about 125 °C to about 160 °C. As mentioned in the previous paragraph, these particles still contain water at 125 °C, and thus, it appears that the irregular event is associated with further dehydration. Particles larger than 425 μm experience a second region of faster weight loss between 120 and 140 °C (Figure 6.1b), and surprisingly, the largest particles undergo this weight loss at the lowest temperature. Water loss appears to occur via a two-step process in larger particles, and it has been reported that the outer layer of a large particle dehydrates to form an impermeable layer and then dehydration of the core follows.⁸ The data suggest that irregular regions between 125 and 160 °C (**C**) in the DSC thermograms of the larger particles are caused by the loss of trapped water that remains in the dihydrate core after partial dehydration of a large particle. An 850- μm particle will contain more trapped water molecules than a 425- μm particle and will therefore experience higher pressures as the molecules are loosened from the crystal structure. This could result in bursting of water vapor from these larger particles at lower temperatures, and this results in the TGA thermogram of the >850- μm particles crossing over the TGA thermogram of the 425–850- μm particles.

The fourth thermal event in the DSC thermograms in Figure 6.1a is a small endotherm at ~132 °C (**D**). This event corresponds to the melting of T_α , and its presence indicates that T_α was

formed upon dehydration of T_h . This endotherm is clearly visible in the thermogram of the <75- μm particles and may be present as a shoulder on the dehydration endotherm of the 75–125- μm particles. A disadvantage of DSC is that overlapping thermal events can mask transitions and, for particles larger than 180 μm , the melting endotherm of T_α , if present, would almost certainly be masked by events corresponding to dehydration. Therefore, the absence of this event in the thermograms of larger particles does not necessarily show that T_α was not formed.

The fifth thermal event in the DSC thermograms in Figure 6.1a is an exotherm between 150 and 210 °C (E) that corresponds to crystallization of T_β . Thermograms of the <75- μm and 75–125- μm fractions contain exotherms with peaks at ~200 °C. The presence of a crystallization exotherm in the DSC thermogram of the 75–125- μm fraction indicates that T_{am} and/or T_α must have been generated in this sample despite the absence of a distinct glass transition corresponding to T_{am} and a melting endotherm for T_α . The thermogram of the 125–180- μm sample also contains an exotherm, but its onset is lower and its peak is at about 185 °C. The lower onset of crystallization suggests that T_β , or nuclei of T_β , may have been formed from dehydration of T_h in this sample and are able to facilitate crystallization of T_β .

The final thermal event in the DSC thermograms in Figure 6.1a is a melting endotherm between 180 and 215 °C (F). Reported melting temperatures of T_β range from 197 °C to 218 °C,^{11, 12} indicating that this endotherm corresponds to melting of T_β . The thermograms of particles smaller than 125 μm contain relatively sharp endotherms at about 215 °C, and the thermogram of the 125–180- μm sample contains a broader endotherm with a peak at about 210 °C. Each of the thermograms of particles larger than 180 μm contains a large, broad endotherm spanning from about 180 to 210 °C that is also attributed to melting of T_β . Because, for particles larger than 180 μm , formation of T_β via crystallization is not evidenced by a well-defined

exotherm as discussed in the previous paragraph, it can be concluded that T_{β} must have been formed directly from dehydration of T_h . Melting endotherms of T_{β} for particles smaller than 125 μm are much smaller than the melting endotherms of T_{β} for particles larger than 180 μm , indicating that crystallization to T_{β} from smaller particles of T_h was incomplete.

Although the large variation in the melting temperature of T_{β} is unusual, large ranges of melting temperatures have been reported for other sugars.¹³ It was shown that the heating rate affects the melting temperature, with slower heating rates resulting in lower melting temperatures. The difference in melting temperatures was attributed to the influence of a kinetic process, likely to be thermal decomposition, on the loss of crystalline structure: at slower heating rates, the sample is held at higher temperatures longer than when heated at a faster heating rate, and therefore the kinetic process can occur to a greater extent. Though DSC thermograms presented here correspond to T_h samples that were all heated at the same rate, the data suggest that the melting temperature is related to the temperature at which T_{β} is formed. When T_{β} forms upon dehydration of T_h , it is exposed to temperatures between 100 and 180 °C, and the kinetic decomposition processes can occur; this results in a lower apparent melting temperature. This is analogous to a slower heating rate. If T_{β} is formed from crystallization of T_{am} , it may not be formed until 180 °C, resulting in a higher melting temperature due to the smaller contribution of the kinetic process to the loss of crystalline order. This is analogous to a faster heating rate. It has also been suggested that a lower melting temperature of T_{β} results from lower quality crystals, i.e. smaller or more defective crystals;¹⁴ this cannot be determined from the DSC thermograms.

6.3.2 DSC and TGA Thermograms: Sigma T9449-3

Figure 6.2 shows DSC and TGA thermograms of particles from the Sigma T9449-3 sample. As the thermal events were discussed in great detail in §6.3.1, the primary purpose of this section is to highlight the differences between the previously discussed sample (Fluka 90210-1) and this sample (Sigma T9449-3). Similar to the Fluka 90210-1 sample (Figure 6.1a), events **A**, **B**, and **C** in Figure 6.2a correspond to dehydration. All DSC thermograms in Figure 6.2a contain a more defined endotherm below 90 °C (**A**) than is observed in Figure 6.1a, though an explanation for this is not immediately apparent. The TGA thermograms (Figure 6.2b) indicate that the rate of water loss increases significantly at approximately 80 °C, about 15 degrees below temperature at which the rate of water loss increased for the Fluka 90210-1 sample. The peak temperature of the dehydration endotherm near 100 °C (**B**) for the Sigma T9449-3 particles decreases slightly as the particle size decreases; this was not observed for the Fluka 90210-1 sample. DSC thermograms of particles that are larger than 180 µm contain irregular regions that begin between 105 and 120 °C and continue for at least 40 degrees (**C**). For particles larger than 425 µm, the shape of the event suggests that the spikes are possibly superimposed on an endotherm. In §6.3.1, the irregular regions were attributed to bursting of trapped water from the interior of large T_h particles in the second step of a two-step dehydration process. The two-step nature of the water loss in larger particles, evidenced by the shape of the TGA thermograms, is much more pronounced for the Sigma T9449-3 particles (Figure 6.2b) than in the Fluka 90210-1 particles (Figure 6.1b), and TGA shows that at least half of the expected 9.5% water in these larger particles of T_h is still present at 105 °C. This provides additional support for the conclusion that the irregular regions in the thermograms of larger

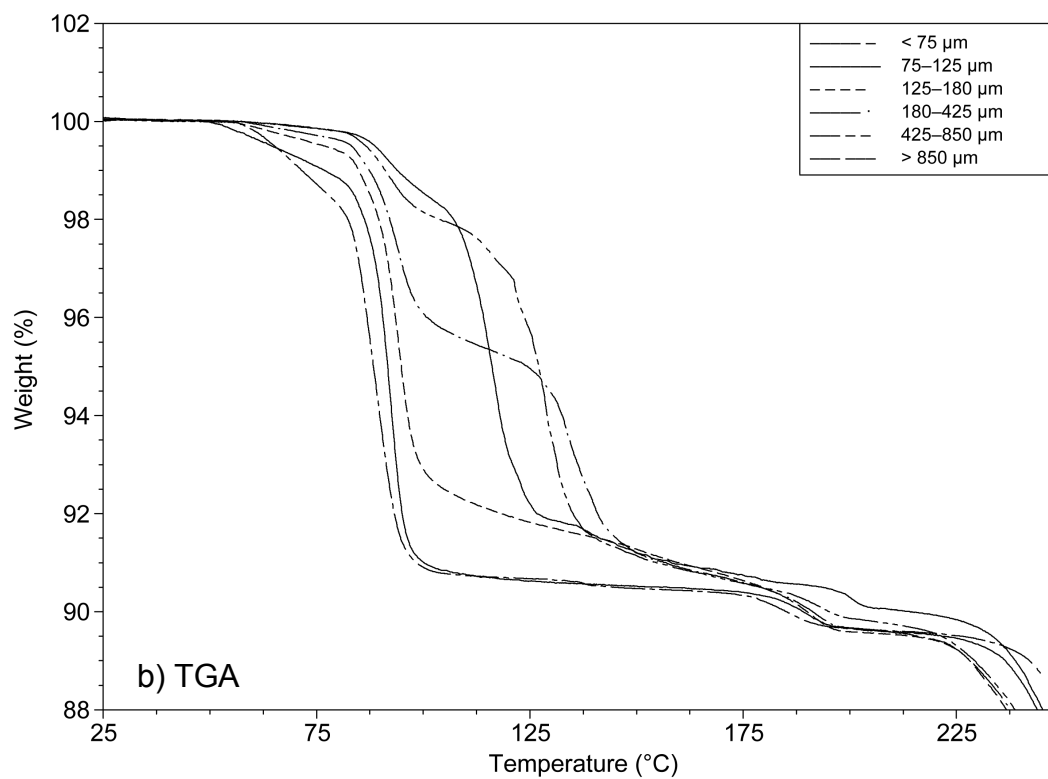
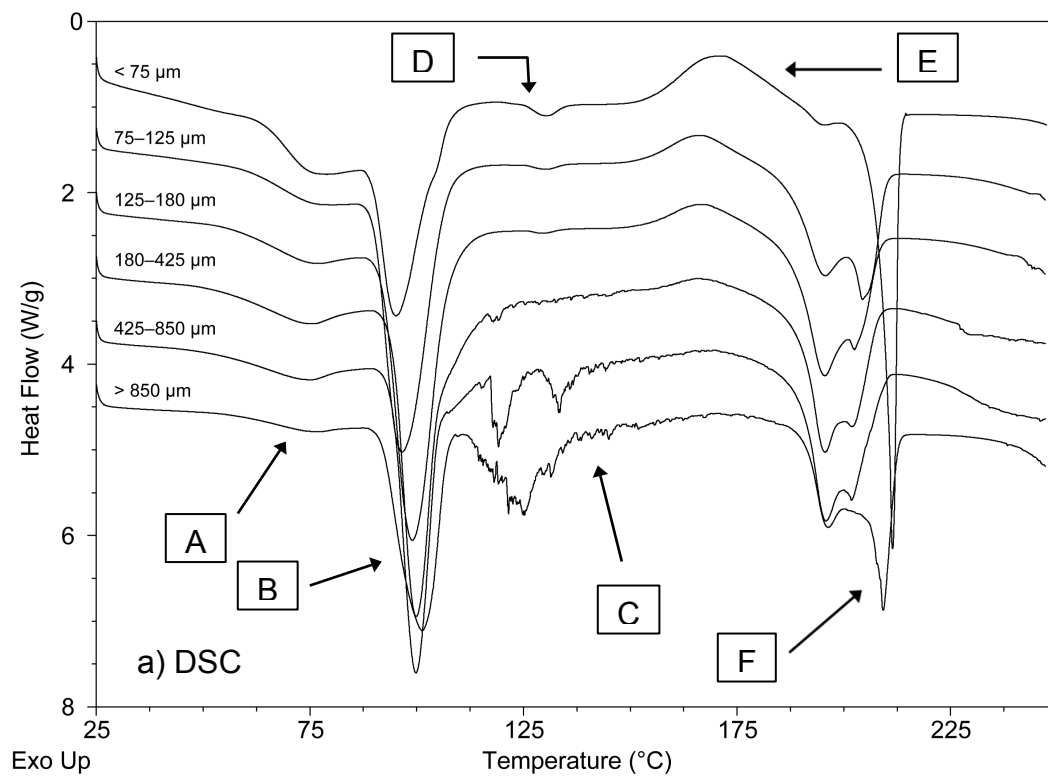


Figure 6.2. DSC (a) and TGA (b) thermograms of particles from the Sigma T9449-3 sample.

particles correspond to the loss of trapped water. Weight loss continues until about 175 °C, and the spikes, although less frequent, are apparent at temperatures as high as 180 °C. The loss of trapped water is expected to be more powerful in larger particles due to the amount of water present in the particle, and accordingly, the spikes present in DSC thermograms of the largest particles are much larger than those observed in the DSC thermograms of the 180–425- μm particles. They are also larger than the irregular spikes observed in thermograms of the Fluka 90210-1 particles.

A well-defined endotherm corresponding to melting of T_α (**D**) is visible in the three thermograms of particles smaller than 180 μm , whereas this endotherm could only be detected in the thermogram of the <75- μm particles of the Fluka 90210-1 sample. This results from the lower dehydration temperature of the Sigma T9449-3 particles: the endothermic event near 100 °C is completed by about 115 °C, and overlap of this event with the melting of T_α is significantly less than that observed in the Fluka 90210-1 samples.

Events **E** and **F** in Figure 6.2a correspond to crystallization and melting, respectively, of T_β . Exotherms corresponding to crystallization of T_β (**E**) are present in thermograms of particles smaller than 425 μm . All have approximately the same onset temperature of about 150 °C, which is significantly lower than the onset of about 180 °C that was observed for Fluka 90210-1 particles that were smaller than 125 μm (Figure 6.1a). The lower onset of crystallization can be explained by the presence of more T_β (or more T_β nuclei) in these samples, though it is not clear why more T_β would be formed in this sample than the Fluka 90210-1 sample. Endotherms corresponding to melting of T_β (**F**) are present in DSC thermograms of all particle sizes. For particles larger than 75 μm , the onset of melting occurs at about 180 °C, similar to what was observed for Fluka 90210-1 particles that are larger than 180 μm . All thermograms of Sigma

T9449-3 particles that are larger than 75 μm contain melting endotherms with two well-defined maxima near 190 and 202 $^{\circ}\text{C}$. The endotherm of the $<75\text{-}\mu\text{m}$ particles contains one sharp endotherm with a peak temperature near 215 $^{\circ}\text{C}$.

6.3.3 DSC and TGA Thermograms: Acros 18255-1

Figure 6.3 shows DSC and TGA thermograms of particles from the sieved Acros 18255-1 sample. Due to insufficient material, a $<75\text{-}\mu\text{m}$ sample could not be analyzed. As with §6.3.2, the purpose of this section is to highlight differences in the thermograms in Figure 6.3 as compared to those in Figures 6.1 and 6.2, and detailed descriptions of thermal events are not repeated. Like the previously described samples, events **A**, **B**, and **C** in Figure 6.3a correspond to dehydration. Overall, DSC and TGA thermograms of the Acros 18255-1 sample are more similar to those observed for the Fluka 90210-1 sample than they are to the Sigma T9449-3 sample, though there are still several differences. While thermograms of the Fluka 90210-1 and Sigma T9449-3 materials contain broad endotherms below 90 $^{\circ}\text{C}$, thermograms of the Acros 18255-1 particles contain only a slight downward drift in the baseline (**A**). Like the Fluka 90210-1 sample, the peak temperature of the dehydration endotherm does not decrease as the particle size decreases, and it remains relatively sharp for all particle sizes (**B**). Irregular regions between 130 and 190 $^{\circ}\text{C}$ (**C**) are only observed in thermograms of particles that are larger than 425 μm , but the spikes are much larger than were observed in the Fluka 90210-1 or Sigma T9449-3 thermograms. The TGA thermograms of the Acros 18255-1 particles are more gently sloped, and an explanation for this is not immediately apparent. For the 75–125- μm particles of the Acros 18255-1 sample, TGA

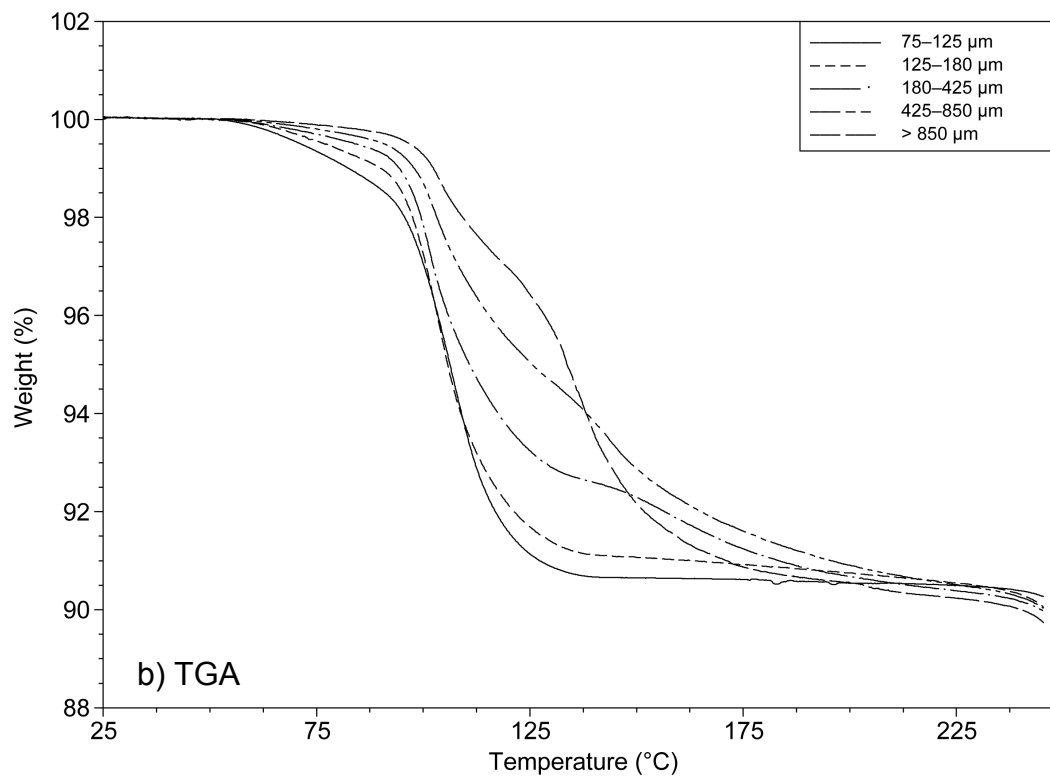
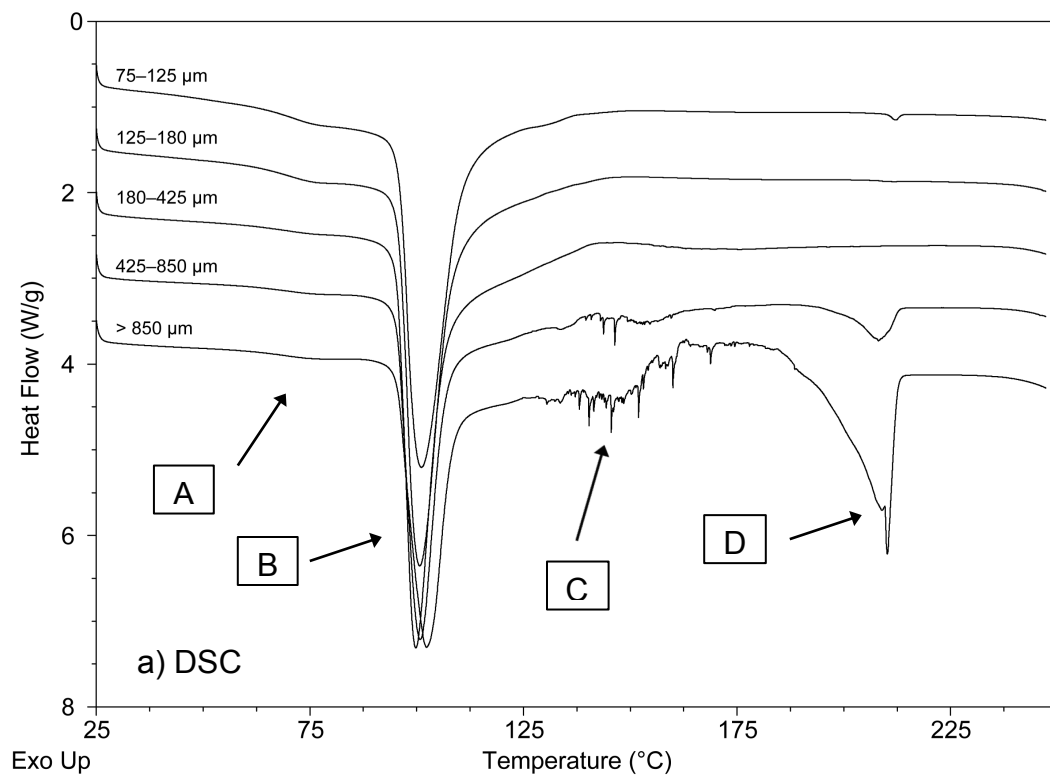


Figure 6.3. DSC (a) and TGA (b) thermograms of particles from the Acros 18255-1 sample.

shows that complete dehydration, or weight loss of 9.5%, does not occur until above 125 °C; for the other samples, the dehydration of this particle size fraction was complete by 125 °C. It may be that morphological or surface differences affect the way that water leaves the crystal structure, even when particle sizes are the same. Several thermograms of Acros 18255-1 particles contain no significant thermal events above 125 °C. The absence of a melting endotherm for T_{α} is likely caused by the higher-temperature water loss experienced by the Acros 18255-1 sample and the overlap of dehydration events with the expected melting of T_{α} at about 132 °C. For Sigma T9449-3 particles, dehydration was completed by about 100 °C, and melting endotherms for T_{α} were easily detected (Figure 6.2a). Distinct exotherms corresponding to crystallization of T_{β} are also not observed in any of the thermograms in Figure 6.3a. In contrast to small particles from the Fluka 90210-1 and Sigma T9449-3 samples, small particles from the Acros 18255-1 sample do not undergo significant crystallization to T_{β} . T_{β} was not generated from dehydration or heating of small Acros 18255-1 T_h particles, and therefore, though there is no direct evidence of the formation of T_{am} (glass transition) or T_{α} (melting endotherm), one or both of these forms must have been generated. If T_{am} were generated during dehydration, the thermogram would be expected to contain a glass transition near 120 °C, but its glass transition may overlap with thermal events corresponding to dehydration and the endotherm for melting of T_{α} . Although none of the thermograms contain a glass transition, it cannot be assumed that T_{am} was not formed. The thermogram of the <75- μm contains a very small melting endotherm for T_{β} , but replicates do not contain this endotherm. The thermograms of larger Acros 18255-1 particles contain endotherms corresponding to melting of T_{β} .

6.3.4 DSC and TGA Summary

Results from DSC and TGA analyses of the Fluka 90210-1, Sigma T9449-3, and Acros 18255-1 particles demonstrate that for T_h from different sources, water loss occurs at different temperatures, different anhydrous forms are generated upon water loss, and crystallization to T_β may or may not be observed. This suggests that the inconsistencies observed in Chapter 4 and in the literature result from variability of T_h . In order to support this hypothesis, thirteen additional samples were subjected to DSC analyses after sieving. Differences among all samples were apparent, but each DSC sample set resembled Figure 6.1a, Figure 6.2a, or Figure 6.3a. The following sections describe the quantitation of the observed differences and classification of the sixteen T_h samples through the identification of critical thermal events in the DSC thermograms.

6.3.5 Analysis of Endotherm Near 100 °C

Figure 6.4 is a plot showing the average peak temperatures of the well-defined endotherm near 100 °C for the sixteen sieved samples that were analyzed. This endotherm is the only thermal event that is present in each thermogram of each fraction from every sample. Results from TGA show that this endotherm accounts for near complete dehydration of smaller particles, but for larger particles, it accounts for only partial dehydration. Four of the sixteen samples (Sigma T9449-3, Sigma T9531-2, Fluka 90208, and Life Science) show a decrease in the peak temperature of the dehydration endotherm as the particle size decreases, with Fluka 90208 particles showing the steepest decline. For clarity, the group of samples that show this decrease will be referred to as “Group A” samples, and the other group will be referred to as “Group B” samples.

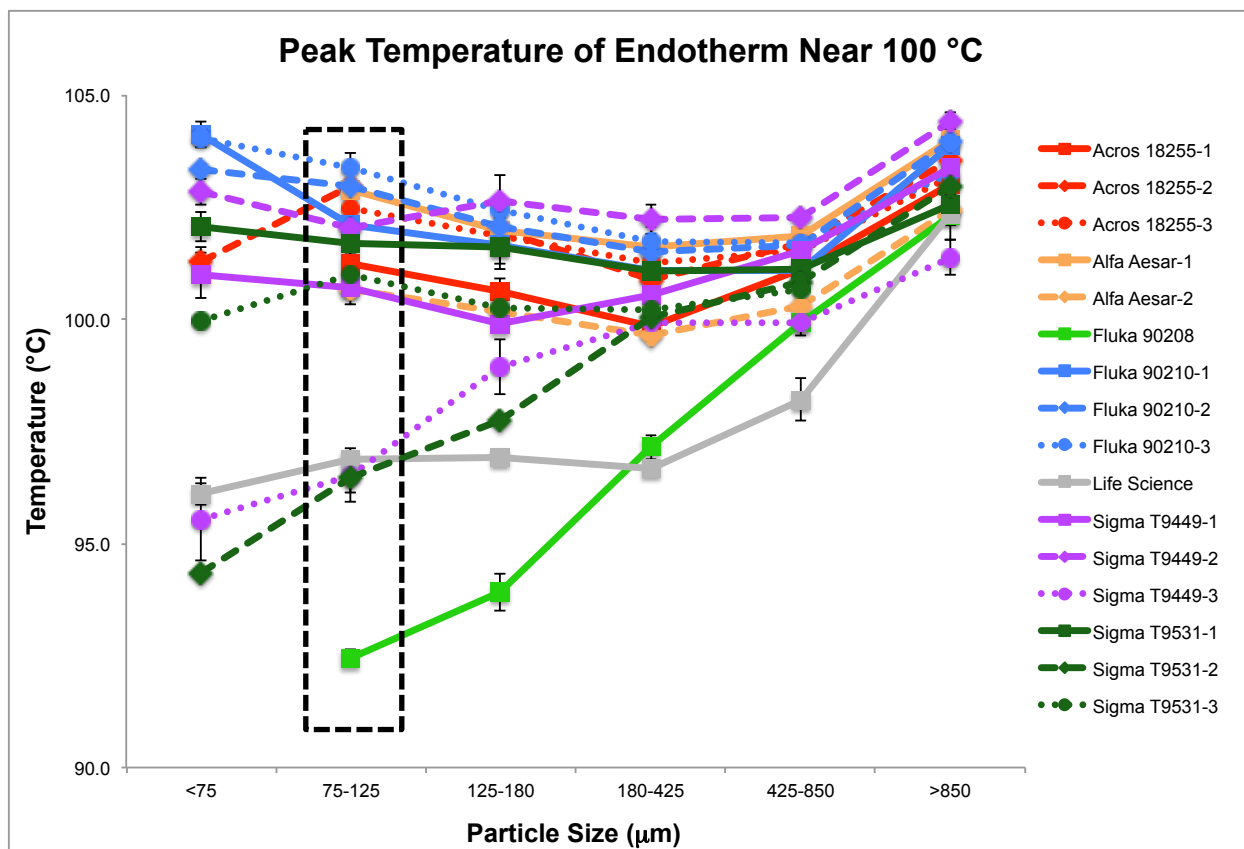


Figure 6.4. Plot of the average peak temperature of the endotherm near 100 °C versus the particle size range. For most samples, at least three replicates were analyzed, and the error bars represent the standard deviations. Missing data points indicate that sufficient material was not available for analysis. For the Sigma T9531-2 sample (<75- μ m fraction), there was only enough material to analyze one sample. Four samples (Sigma T9449-3, Sigma T9531-2, Fluka 90208, and Life Science) show a decrease in the peak temperature as the particle size decreases and are designated “Group A.” The remaining twelve samples are designated “Group B.” The 75–125- μ m fraction is highlighted: despite the narrow range of particle sizes, the peak temperatures vary by about 10 °C, and these particles were selected for additional analyses.

The differences between the two groups become apparent with particle sizes between 125 and 180 μm . For particles larger than this, most peak temperatures fall within a fairly narrow range: 101–105 $^{\circ}\text{C}$ for $>850\text{-}\mu\text{m}$ particles, 101–103 $^{\circ}\text{C}$ for 425–850- μm particles, and 99–102 $^{\circ}\text{C}$ for 180–425- μm particles. Peak temperatures for four samples with particle sizes between 125 and 180 μm are less than 99 $^{\circ}\text{C}$ (Group A), and the remaining twelve samples have peak temperatures greater than 100 $^{\circ}\text{C}$. The differences among the samples are even clearer when the particle size is smaller than 125 μm . Particles between 75 and 125 μm from Group A samples have peak temperatures below 97 $^{\circ}\text{C}$, and Group B particles in this size range have peak temperatures above 100 $^{\circ}\text{C}$. Peak temperatures of Group B samples containing particles smaller than 75 μm are between 100 and 105 $^{\circ}\text{C}$, and peak temperatures for Group A samples are between 94 and 96 $^{\circ}\text{C}$. While the peak temperatures for Group A samples decrease as the particlesize decreases from 180 μm to smaller than 75 μm , the peak temperatures for Group B samples increase. This increase is unexpected and may result from the different processes, e.g. loosening of water molecules and evaporation, that occur during the temperature region encompassed by the dehydration endotherm. While all Acros and Alfa Aesar samples belong to Group B, both Sigma products (T9449 and T9531) have one sample that is classified as Group A and two that are classified as Group B. This demonstrates that both source-to-source variability and lot-to-lot variability impact the temperature at which water leaves the crystal structure of T_h . Compared to Group B samples, small Group A particles lose the water of crystallization at lower temperatures. Potential explanations for this difference, such as the presence of crystal defects in Group A samples, are discussed in §6.3.8.

6.3.5 Crystallization and Melting of T_{β}

Figure 6.5 shows representative thermograms of the 75–125- μm sieved fractions from two Group A samples and four Group B samples. This range of particle sizes was chosen for additional analysis of the crystallization and melting of T_{β} for two reasons. First, for a narrow range of particle sizes, the variation in DSC thermograms due to particle size should be minimized, and the influence of other factors should be emphasized. Second, for small particles, dehydration is nearly complete by 125 °C, and there is therefore little overlap of dehydration thermal events and other transitions. As a result, events occurring at temperatures greater than 125 °C are slightly better resolved in these thermograms when compared to thermograms of larger particles. The thermograms in Figure 6.5 show that crystallization and melting of T_{β} occurs at different temperatures in different samples, and they also show the significant variation among the magnitudes of the crystallization exotherms and melting endotherms corresponding to T_{β} . Integrating these exotherms and endotherms results in $\Delta H_{\text{crystallization}}$ and $\Delta H_{\text{melting}}$ values for each sample.

Figure 6.6a is a plot of the average $\Delta H_{\text{crystallization}}$ and $\Delta H_{\text{melting}}$ for each 75–125- μm sample, and Figure 6.6b is a plot of the average $\Delta H_{\text{melting}}$ versus the differences between the average $\Delta H_{\text{crystallization}}$ and $\Delta H_{\text{melting}}$. It should be noted that the true values for these transitions are about 10% higher than what is reported because these enthalpies were calculated from the weight of the dihydrate: approximately 10% of the original sample weight is lost when the water molecules leave the crystal structure. The four samples that are assigned to Group A (Fluka 90208, Sigma T9449-3, Sigma T9531-2, and Life Science) have the largest melting endotherms (>120 J/g), and the differences between the magnitudes of the crystallization exotherm and

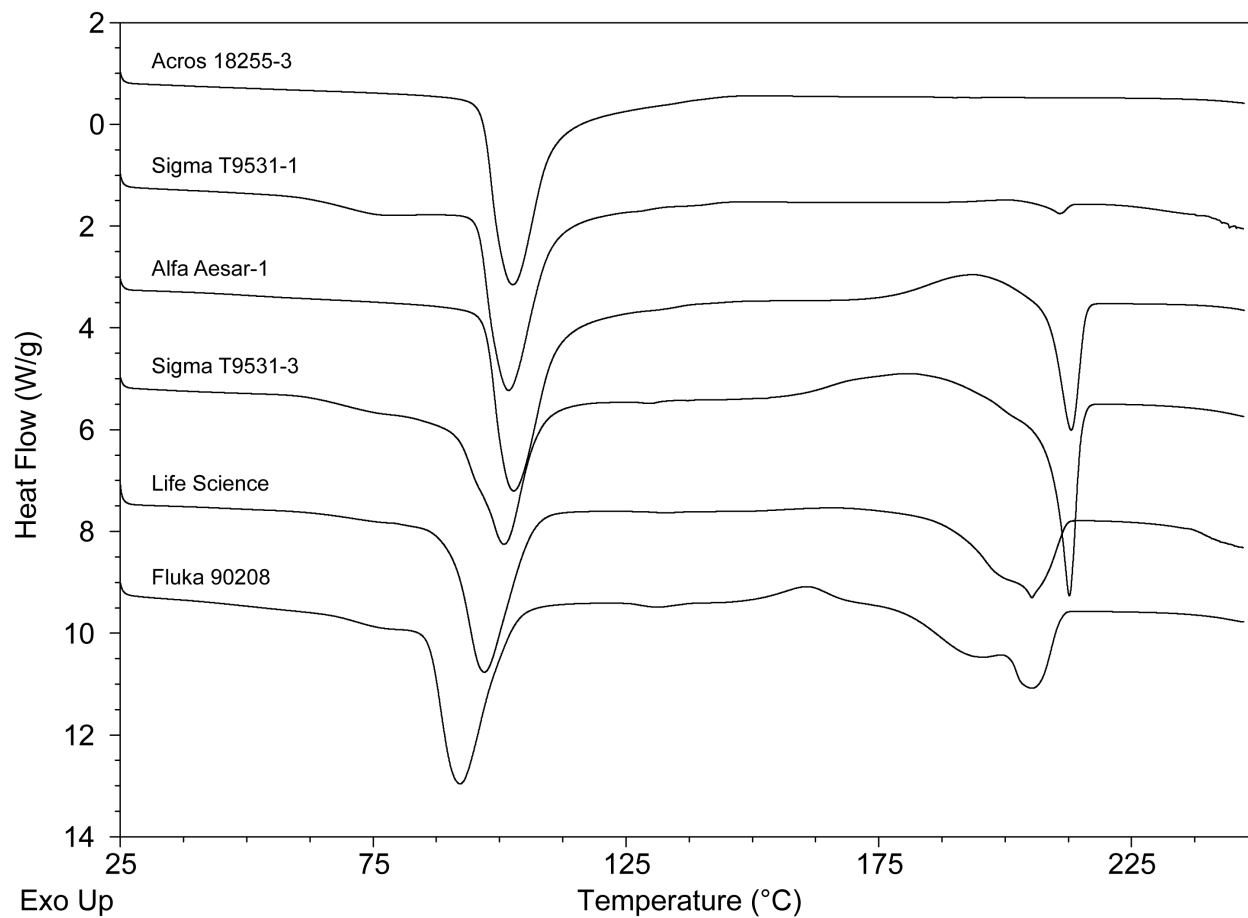


Figure 6.5. DSC thermograms of the 75–125- μm fraction from six samples of T_h .

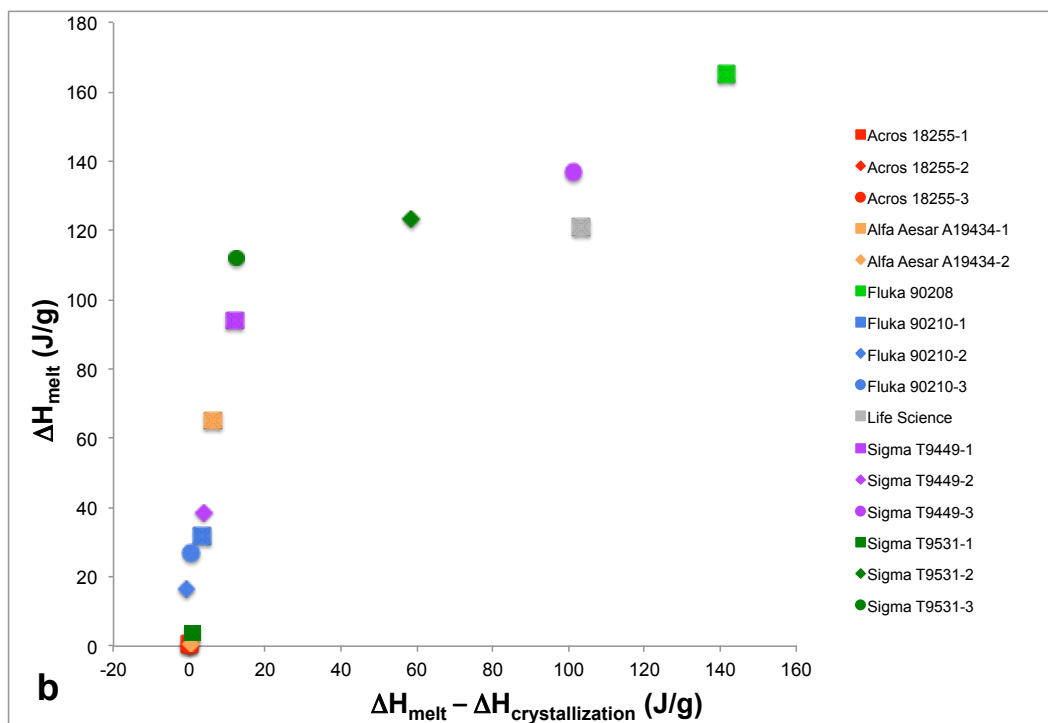
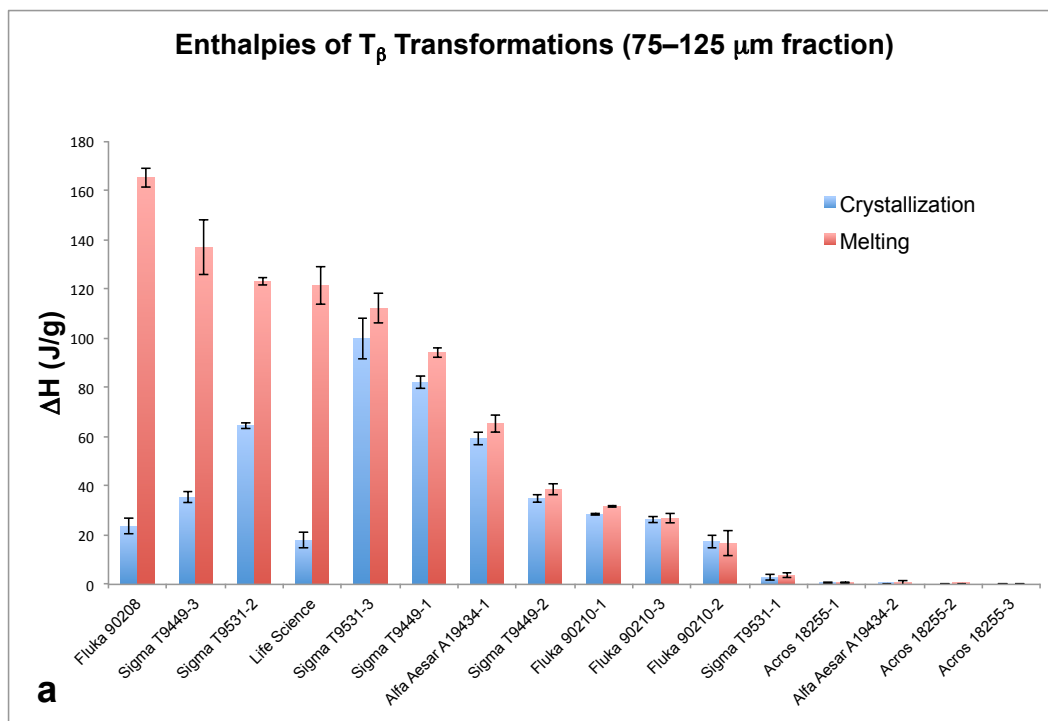


Figure 6.6. Plots of the enthalpies of T_β crystallization and melting (a) and the enthalpy of melting versus the difference between the enthalpies of crystallization and melting (b).

melting endotherm are more than 50 J/g. For the remaining twelve samples, $\Delta H_{\text{melting}}$ ranges from 0 J/g to about 115 J/g, and the difference between the magnitudes of the crystallization exotherm and melting endotherm is less than 20 J/g.

Examining the energetics of a crystalline-amorphous-liquid system (Figure 6.7) is helpful in assigning a physical meaning to the values in Figure 6.6b. For a fully amorphous sample that crystallizes, it is expected that $\Delta H_{\text{crystallization}}$ will be similar to, but slightly less than, $\Delta H_{\text{melting}}$. According to Figure 6.7, as the difference between the crystallization and melting temperatures increases, the difference between the magnitudes of the crystallization exotherm and melting endotherm will also increase. For Group A samples, crystallization to T_{β} occurs at a lower temperature than for Group B samples: the peak temperatures of the crystallization exotherms for Group A samples are between 160 and 170 °C. These samples have the largest differences between the magnitudes of the crystallization exotherm and melting endotherm. For Group B samples, the peak temperatures of the crystallization exotherms, if present, are between 180 and 201 °C, and the differences between the magnitudes of the crystallization exotherm and melting endotherm are small. The behavior of Group B samples appears to be consistent with Figure 6.7; however, despite the lower crystallization temperatures, the behavior of Group A samples does not appear to be consistent with Figure 6.7. This suggests that Group A samples are not fully amorphous when crystallization of T_{β} occurs and that T_{β} was formed directly from dehydration of T_h . The difference in magnitude between the crystallization exotherm and melting endotherm can therefore be used to determine how T_{β} forms during dehydration of T_h . Ergo, the y-axis in Figure 6.6b describes *how much* T_{β} is forming, and the x-axis describes *how* T_{β} is forming. The clear break in the data (Figure 6.6b) that occurs when the difference between the average $\Delta H_{\text{crystallization}}$ and $\Delta H_{\text{melting}}$ is about 20 J/g indicates a change in the mechanism of T_{β} formation:

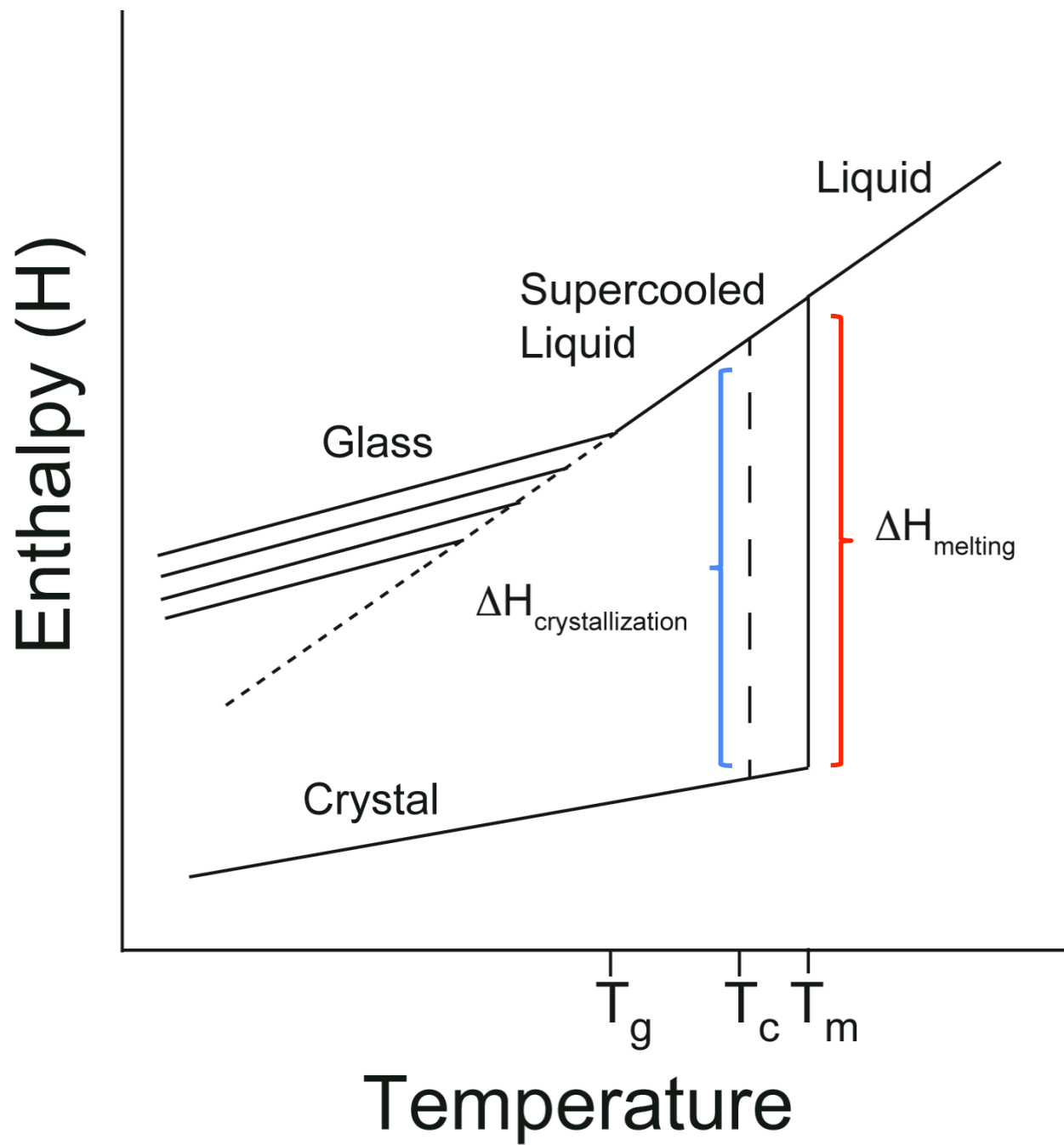


Figure 6.7. Energetics of a crystalline-amorphous-liquid system.

$T_h \rightarrow T_\beta$ (Group A) or $T_h \rightarrow T_{am} \rightarrow T_\beta$ (Group B). This information allows the categorization of T_h samples to be refined and a quantitative classification system to be developed.

6.3.6 Classification of Trehalose Dihydrate Samples

Based on data from Figures 6.4 and 6.6, a system was developed to classify and describe the dehydration behavior of T_h when heated at 10 °C/minute:

Type 1. The peak temperature of the endotherm near 100 °C decreases as particle size decreases. For a 75–125- μm sample, the difference between $\Delta H_{\text{crystallization}}$ and $\Delta H_{\text{melting}}$ is greater than 50 J/g. T_h dehydrates to form T_β . (Fluka 90208, Life Science, Sigma T9449-3, Sigma T9531-2)

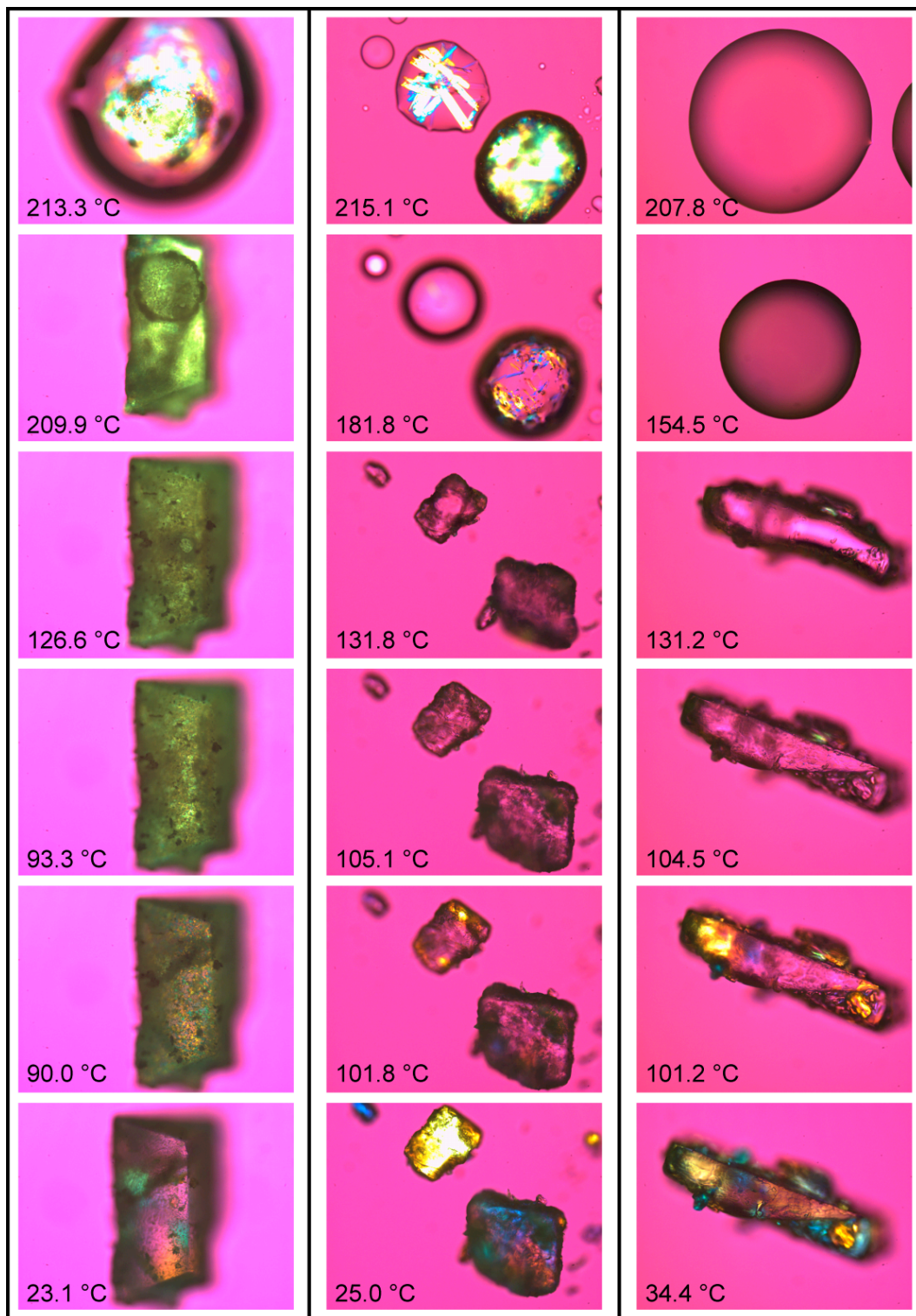
Type 2. The peak temperature of the endotherm near 100 °C decreases slightly as the particle size decreases from $>850 \mu\text{m}$ to $180 \mu\text{m}$ and then increases slightly as the particle size decreases to $<75 \mu\text{m}$. For a 75–125- μm sample, the difference between $\Delta H_{\text{crystallization}}$ and $\Delta H_{\text{melting}}$ is less than 20 J/g and $\Delta H_{\text{melting}}$ is greater than 5 J/g. T_h dehydrates to form T_{am} that crystallizes to T_β . (Alfa Aesar A19434-1; Fluka 90210-1, 2, 3; Sigma T9449-1, 2; Sigma T9531-3)

Type 3. The peak temperature of the endotherm near 100 °C decreases slightly as the particle size decreases from $>850 \mu\text{m}$ to $180 \mu\text{m}$ and then increases slightly as the particle size decreases to $<75 \mu\text{m}$. For a 75–125- μm sample, the difference between $\Delta H_{\text{crystallization}}$ and $\Delta H_{\text{melting}}$ is less than 20 J/g and $\Delta H_{\text{melting}}$ is less than 5 J/g. T_h dehydrates to form T_{am} that does not crystallize to T_β . (Acros 18255-1, 2, 3; Alfa Aesar A19434-2; Sigma T9531-1)

These descriptions are only intended to capture the general behavior that was observed when dehydrating T_h at 10 °C/minute, and they do not account for all transformations that may occur. For example, the DSC thermograms of 75–125- μm particles of Type 1 samples contain a melting endotherm for T_α and a crystallization exotherm for T_β . As a result, it can be concluded that some T_α , and possibly T_{am} , must also form upon dehydration of Type 1 samples. It is also possible that T_δ is formed during dehydration of T_h , but as was shown in Chapter 5, T_δ is not detected with DSC. In Chapter 7, SSNMR is used to unambiguously detect which anhydrous forms of trehalose are generated as T_h is dehydrated. Additionally, the effect of particle size is not accounted for in these descriptions. Previously, it was concluded that the dehydration of large particles ($>425 \mu\text{m}$) leads to T_β , and the dehydration of small particles ($<75 \mu\text{m}$) leads to T_{am} .⁸ The results presented in this chapter have shown dehydration of small particles to form T_β , as well as dehydration of large particles to form T_{am} . The particle size influences which forms are generated upon dehydration, but the effect can be different depending on which type of material is being analyzed. The behavior of Type 2 samples most closely resembles the previously published description.^{8, 15, 16} For Type 1 samples, all particle sizes form T_β directly from T_h , but smaller particles show evidence that T_α and/or T_{am} were also formed. For Type 3 samples, all particle sizes form T_α and T_{am} upon dehydration.

6.3.7 Visualization of Solid Form Changes During Dehydration of T_h Using Polarized Light Microscopy (PLM)

Figure 6.8 shows PLM images of three T_h samples as they were heated at 10 °C/minute and illustrates the possible transformation of T_h upon heating: $T_h \rightarrow T_\beta$ (Type 1), $T_h \rightarrow T_{\text{am}} \rightarrow T_\beta$ (Type 2), or $T_h \rightarrow T_{\text{am}}$ (Type 3). Figure 6.8a shows six images from the heating of a single



a. Sigma T9449-3

b. Fluka 90210

c. Acros

Figure 6.8. HSM images of 75–125- μm particles of trehalose dihydrate.

particle from the Sigma T9449-3 sample (Type 1). Prior to heating (23.1 °C), the particle has a well-defined prismatic morphology. Some areas within the particle are birefringent, and it is not a single crystal. Upon heating, the birefringence of the particle changes (90.0 °C) as many small single crystals form within the larger particle. A single greenish particle is observed at 93.3 °C, and continued heating to 126.6 °C does not change the appearance of the particle. The particle appears to get brighter (209.9 °C) before melting at about 213 °C. This melting temperature is consistent with the melting temperature of T_{β} . These observations demonstrate that a Type 1 particle undergoes a T_h to T_{β} transformation upon dehydration, confirming the conclusions from the analysis of the DSC thermograms.

Figure 6.8b shows particles from a Fluka 90210 sample (Type 2). Before heating (25.0 °C), the largest particle has areas of blue and yellow, indicating that it is not a single crystal. Other particles appear to have been milled or ground and are single crystals, as they are brightly colored and either blue or yellow. Unlike the Sigma T9449-3 particle, the Fluka 90210 particles lose birefringence upon heating (101.8 °C and 105.1 °C), and the change occurs at a higher temperature. This is consistent with the TGA and DSC data that showed dehydration of Type 1 samples at lower temperatures than Type 2 or Type 3 samples. The loss of birefringence by Fluka 90210 particles suggests that these particles of T_h form T_{am} upon dehydration. In the image captured at 131.8 °C, the material appears to be melting, and the original morphology of the particles is lost. This is about 10 degrees above the T_g of amorphous trehalose, and the “melt” likely corresponds to softening of the glassy material and its transformation to the more mobile rubbery state. This temperature is also close to the melting temperature of T_{α} , but it has been reported that this form is not birefringent.¹² However, it is possible that small amounts of T_{α} could also have been formed upon dehydration. At 181.8 °C, single crystals are present within

the amorphous material (possibly on the surface), and they continue to grow into brightly colored blue and yellow needles (215.1 °C). Crystallization is incomplete before melting occurs above 215.1 °C (T_{β}). The crystals of T_{β} formed from dehydration of Type 2 material appear to be larger and higher quality than those formed from dehydration of Type 1 material, possibly providing support for the suggestion that the crystal quality affects the melting temperature.¹⁴ These images illustrate and support conclusions reached from analysis of the DSC data of Type 2 samples: T_h transforms to T_{am} which then crystallizes to T_{β} .

Figure 6.8c shows particles from an Acros sample (Type 3). This particle is narrower than the Sigma T9449-3 particle, and unlike the Fluka 90210 particles, it does not appear to have undergone grinding. The different morphologies of the particles may impact the dehydration of T_h , and this is discussed in §6.3.8.1. Prior to heating, there are brightly colored birefringent regions within the large, elongated particle (34.4 °C). The loss of birefringence begins at about 100 °C and is completed by 104.5 °C, demonstrating that T_{am} was formed upon dehydration. Like the Fluka 90210 particles (Figure 6.8b), the Acros particle retains its morphology until about 131 °C. This material shows no evidence of crystallization as it is heated to about 208 °C. As before, these images confirm the description of the dehydration of a Type 3 sample: T_h dehydrates to form T_{am} that does not crystallize to T_{β} .

6.3.8 Cause(s) of Differences in the Dehydration Behavior of Trehalose Dihydrate

It was speculated that the observed differences in dehydration behavior may result from different particle morphologies, the presence of defect sites, or physical impurities (T_{β}). PLM and SSNMR were used to investigate each of these sources.

6.3.8.1 Particle Morphology and Crystal Defects (PLM)

Figure 6.9 shows PLM images of 75–125- μm particles from eight samples of T_h ; these particles are representative of the range of appearances of 75–125- μm particles. These images were obtained in order to assess morphological differences among the samples that could be correlated with the dehydration behavior of T_h . There are variations in the apparent particle size, e.g. the particles in Figure 6.9a appear much larger than the particles in Figure 6.9c, which may result from particles with different morphologies passing through the sieves with different orientations. Some samples contain particles that are long and narrow (Figure 6.9a and Figure 6.9b), while others contain particles that are prismatic (Figure 6.9g and Figure 6.9h). Some particles are brightly colored (Figure 6.9e), but others are not (Figure 6.9d). The particles in Figure 6.9e and Figure 6.9f appear to have been ground during the manufacturing process while others have well-defined morphologies.

The particles in Figure 6.9a and Figure 6.9b are from the Acros 18255-3 and Alfa Aesar A19434-1 samples, respectively. These particles are similar in shape to the particles that were observed by Ohashi et al.¹⁷ In Figure 6.9a, a smaller particle is clearly visible within the larger particle, demonstrating that it is not a single crystal. These particles have an elongated shape, are brightly colored, and do not appear to have been subjected to grinding or milling. Although they may not be single crystals, these particles do not appear to have high concentrations of defects. While the particles in Figure 6.9a and Figure 6.9b have similar morphologies, the Acros 18255-3 sample displayed Type 3 behavior, and the Alfa Aesar A19434-1 sample displayed Type 2 behavior. Type 2 and Type 3 samples of T_h dehydrate similarly but display different tendencies to crystallize to T_β . Above 140 °C, where crystallization occurs, the original morphology of the

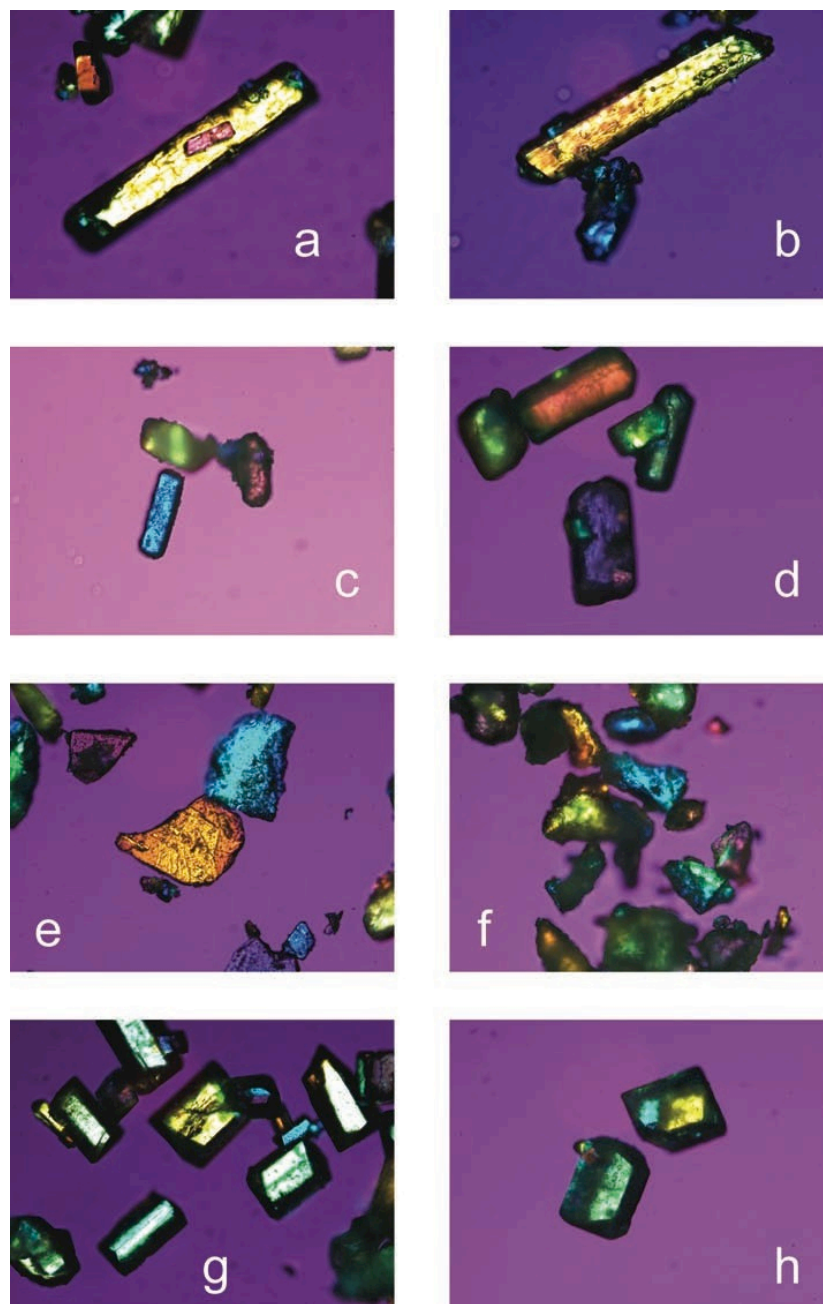


Figure 6.9. PLM images of 75–125- μm particles of trehalose dihydrate: Acros 18255-3 (a), Alfa Aesar A19434-1 (b), Fluka 90208 (c), Sigma T9531-2 (d), Fluka 90210-1 (e), Fluka 90210-3 (f), Sigma T9449-1 (g), and Sigma T9531-1 (h).

particle has been lost and may not influence the crystallization. Therefore, it is possible that the morphology influences the way that water is lost but not the extent of crystallization.

The particles in Figures 6.9c and Figure 6.9d are from the Fluka 90208 and Sigma T9531-2 samples, respectively, both of which were identified as Type 1 material. Some particles from the Fluka 90208 sample may be single crystals, as evidenced by the bright blue color. The particles from the Sigma T9531-2 sample, shown in Figure 6.9d, have a well-defined morphology, but they are not as brightly colored as the particles from the other samples. While they do not appear to have been milled, the Sigma T9531-2 particles may have a higher number of defects than the other samples. Type 1 samples undergo dehydration at lower temperatures, which could be explained by the smaller apparent size or defective nature of these particles.

The particles shown in Figure 6.9e and Figure 6.9f are from the Fluka 90210-1 and Fluka 90210-3 samples, respectively, both of which were classified as Type 2. The particles from both samples are irregularly shaped and appear to have undergone grinding during the manufacturing process. These images are similar to those that were published by Taylor and York.⁸ They are brightly colored and either blue or yellow, indicating that they are single crystals. We suggested that grinding could lead to lower dehydration temperatures; however, lower dehydration temperatures are characteristic of Type 1 samples, and the particles that show evidence of grinding did not display this dehydration behavior.

The particles shown in Figure 6.9g and Figure 6.9h are from the Sigma T9449-1 and Sigma T9531-1 samples, respectively. The particles from both samples have prismatic morphologies, and the particles have very sharp edges. This morphology has been reported several times.^{11, 18, 19} Although the particles from the Sigma T9449-1 and Sigma T9531-1 samples have very similar morphologies, the Sigma T9449-1 sample was classified as Type 2,

and the Sigma T9531-1 sample was classified as Type 3. This is similar to what was observed for the particles in Figure 6.9a and Figure 6.9b, indicating that factors other than morphology may be responsible for the extent of crystallization that is observed. Though significant differences in the shapes of the T_h particles were observed, a particular morphology could not be assigned to each type of dehydration behavior.

6.3.8.2 Physical Impurities and Crystal Defects (SSNMR)

Figure 6.10 shows ^{13}C SSNMR spectra of seven of the sixteen samples of T_h . All spectra contain peaks that are consistent with the published spectrum of T_h ; however, the spectrum of the Life Science T_h (Figure 6.10b) also contains peaks corresponding to T_β . Of the sixteen samples that were analyzed, the spectrum of the Life Science material is the only spectrum that shows the presence of a physical impurity, as evidenced by the small T_β peaks at 90.7 and 93.2 ppm. The Life Science sample is one of four Type 1 samples that transitioned directly to T_β from T_h upon dehydration, but the absence of T_β peaks in the spectra of the other Type 1 samples indicates that the presence of T_β as a physical impurity does not direct the dehydration behavior of T_h . The absence of T_β peaks in spectra of Type 2 samples (Figure 6.10c, d, and e) suggests that crystallization of T_β above the T_g of amorphous trehalose is not facilitated by the presence of T_β in the starting material. However, it is possible that nuclei or crystals of T_β are formed as water leaves the crystal structure of T_h ; this is investigated in Chapter 9.

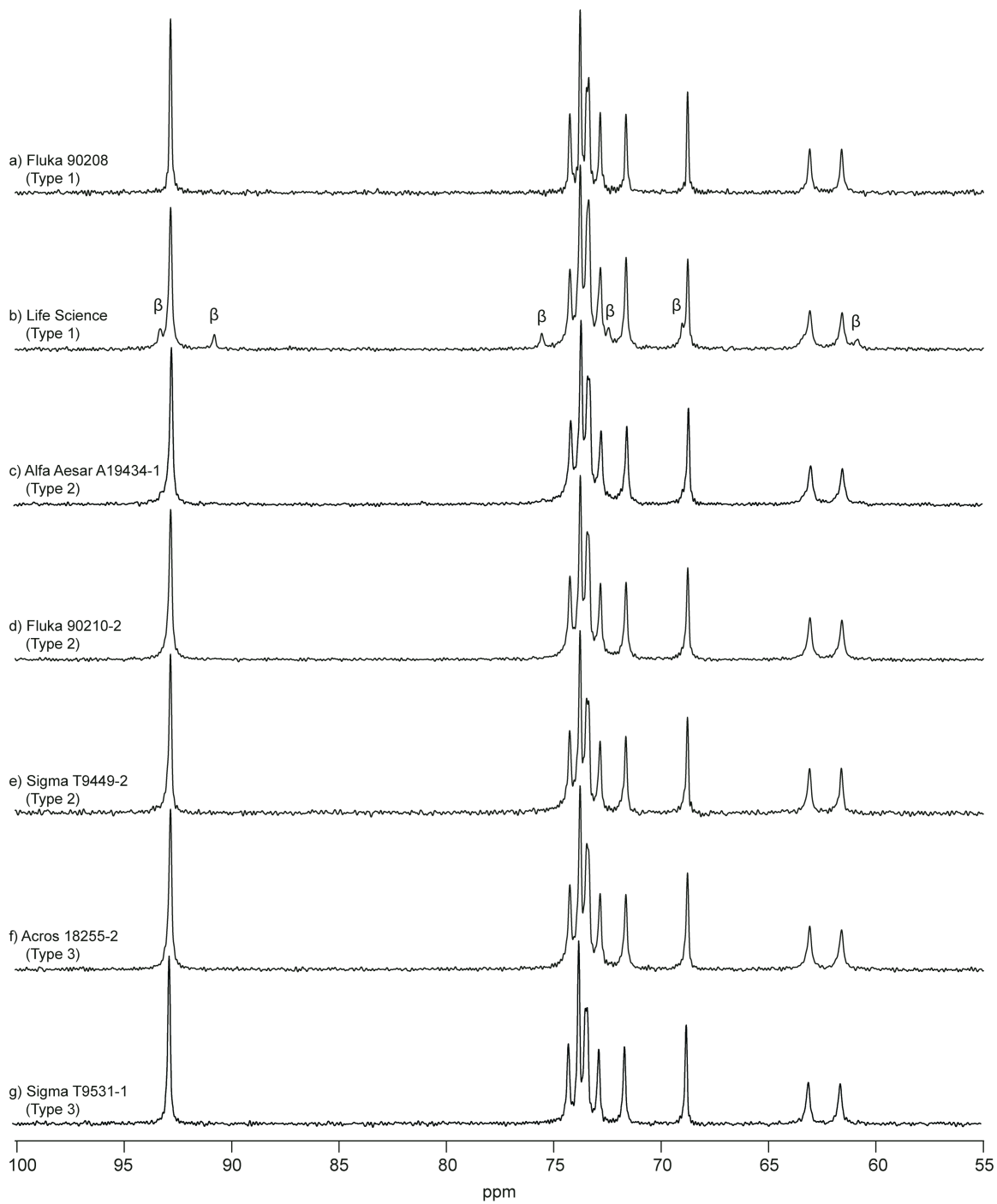


Figure 6.10. ^{13}C SSNMR spectra of trehalose dihydrate samples. Peaks corresponding to T_β are marked with “ β ,” and all other peaks correspond to T_h .

The ^1H T_1 relaxation times of several samples are listed in Table 6.2. Measured ^1H T_1 relaxation times ranged from about 100 seconds to more than 500 seconds, but as was observed for the particle morphologies, the differences do not appear to be correlated to the dehydration behavior of T_h . For example, the two samples with the longest relaxation times (>400 seconds), Fluka 90208 and Sigma T9531-1, were classified as Type 1 and Type 3, respectively. It was suggested that the lower dehydration temperature of Type 1 samples could be due to a high concentration of crystal defects and manifested as a shorter ^1H T_1 relaxation time for those samples,²⁰ but that does not appear to be consistent with the results.

6.3.8.3 Sample Purity

The purity of each sample, as reported by the manufacturer, is listed in Table 6.3. The samples are grouped by their classification in order to more clearly identify any possible correlations. Per the USP, the purity of trehalose must be between 97.0% and 102.0%, and all samples meet this specification. The purities range from 98.7% to 100.0 %, and there is no obvious correlation between purity and dehydration behavior. Some of the lower purities are reported for the Type 3 samples, but one Type 3 sample has a reported purity of 99.9%. The theoretical water content of T_h is about 9.5%, so it might be expected that the Life Science sample, with an anhydrous impurity (T_β), might have one of the lower water contents. At 9.2%, the water content is lower than expected, but the water content of the Acros 18255-3 sample, which does not contain or crystallize to T_β , is only 8.6%. The optical rotations range from 177° to 183° with no apparent correlation to the dehydration behavior. Although it is possible that the sample purity contributes to the dehydration behavior of T_h , an exhaustive search for the

Table 6.2. ^1H T_1 Relaxation Times of Trehalose Dihydrate Samples. The sample classifications and peak temperatures of the dehydration endotherms near 100 °C are included in order to demonstrate the absence of a correlation with the relaxation times.

Sample ID	Type	Particle Size (μm)	Peak Temp. ($^{\circ}\text{C}$)	^1H T_1 (s)
Fluka 90208	1	75–125	92.44	506.3 (21.7)
Life Science	1	75–125	96.87	202.4 (7.2)
Sigma T9449-3	1	180–425	99.92	125.6 (1.9)
Alfa Aesar A19434-1	2	180–425	101.59	138.1 (3.2)
Fluka 90210-2	2	75–125	102.07	125.6 (5.4)
Fluka 90210-3	2	180–425	101.73	124.7 (3.1)
Sigma T9449-1	2	180–425	100.53	118.2 (4.8)
Acros 18255-2	3	75–125	102.98	173.8 (5.7)
Acros 18255-3	3	180–425	101.26	94.1 (1.4)
Alfa Aesar A19434-2	3	180–425	99.64	101.8 (2.9)
Sigma T9531-1	3	75–125	101.7	445.7 (15.8)

Table 6.3 Information from the manufacturer-supplied Certificates of Analysis. Water contents were determined either by a loss-on-drying method (LOD) or by Karl Fischer titrimetry (KF). The purity was measured by HPLC. Trace metals were measured by Inductively Coupled Plasma Mass Spectrometry.

Sample ID	Type	Water Content	Optical Rotation (°)	Purity (%)	Trace Metals (ppm)
Fluka 90208	1	8.6% (LOD)		100.0	<2 Al, <2 Ba, <3 Ca, <1 Fe, <1 Ni, <1 Zn
Life Science	1	9.29% (KF)	181.91	99.7	0.290 Fe, 0.0048 Cu, 0.0083 Ni, 0.088 Zn, 0.004 Co, <0.0007 Cd, 0.0135 Mn, <0.0076 As, 0.0019 Pb, 0.0048 Ba, 3.49 Ca
Sigma T9449-3	1		183	99.7	
Sigma T9531-2	1	10% (KF)	+177	100	<2 Ba, 1 Ca, <5 Fe, <2 Zn, <1 Pb, 1 Cu
Alfa Aesar A19434-1	2	9.9% (KF)	179.3	99.0	
Fluka 90210-1	2		181.2	100.0	<200 Ca; <5 Cd, Co, Cr, Cu, Fe, Mn, Ni, Pb; <10 Mg, Zn; <50 K, Na
Fluka 90210-2	2		178.9	100.0	<200 Ca; <5 Cd, Co, Cr, Cu, Fe, Mn, Ni, Pb; <10 Mg, Zn; <50 K, Na
Fluka 90210-3	2		181.4	99.1	<200 Ca; <5 Cd, Co, Cr, Cu, Fe, Mn, Ni, Pb; <10 Mg, Zn; <50 K, Na
Sigma T9449-1	2	9.3% (KF)	179	100	
Sigma T9449-2	2	10.2% (KF)	178	99	
Sigma T9531-3	2	10% (KF)	+181	100	<2 Ba, <3 Ca, <5 Fe, <2 Zn, <1 Pb, 1 Cu
Acros 18255-1	3	9.1% (KF)	+180.3	98.79	<10 (as Pb)
Acros 18255-2	3	9.95% (KF)	+180.8	99.5	2.1 (as Pb)
Acros 18255-3	3	8.57% (KF)	+178.5	98.7	<5 (as Pb)
Alfa Aesar A19434-2	3	9.9% (KF)	+178.7	99.2	
Sigma T9531-1	3	9.8% (KF)	+177	99.9	<1 Ba, <3 Ca, <5 Fe, <1 Zn, <1 Pb, <1 Cu

identity and concentration of the critical impurity (or impurities) is beyond the scope of this dissertation.

6.4 Conclusions

Results from DSC, TGA, and HSM experiments show that both source variability and lot-to-lot variability impact the way in which T_h dehydrates when heated at 10 °C/minute. Across and Fluka samples show less lot-to-lot variability than Sigma samples. Based on these results, a classification system for T_h was developed.

Type 1: The peak temperature of the endotherm near 100 °C decreases as particle size decreases. For a 75–125 μ m sample, the difference between $\Delta H_{\text{crystallization}}$ and $\Delta H_{\text{melting}}$ is greater than 50 J/g. Upon dehydration, T_h tends to form T_β .

Type 2: For a 75–125 μ m sample, the difference between $\Delta H_{\text{crystallization}}$ and $\Delta H_{\text{melting}}$ is less than 20 J/g and $\Delta H_{\text{melting}}$ is greater than 5 J/g. Upon dehydration, T_h tends to form T_{am} that crystallizes to T_β .

Type 3: For a 75–125 μ m sample, the difference between $\Delta H_{\text{crystallization}}$ and $\Delta H_{\text{melting}}$ is less than 20 J/g and $\Delta H_{\text{melting}}$ is less than 5 J/g. Upon dehydration, T_h tends to form T_{am} that does not crystallize to T_β .

It is likely that one or more factors influences the way that water leaves the crystal structure of T_h (distinguishing Type 1 material from Types 2 and 3) and other factors influence the crystallization tendency of the amorphous material (distinguishing Type 2 from Type 3).

The results also clearly demonstrate that there are two pathways to the formation of T_β : directly from T_h upon dehydration or via crystallization of T_{am} . The first pathway has been

excluded from some descriptions of the dehydration of T_h ,²¹⁻²³ but in the future, comprehensive discussions of the solid-state transformation of trehalose must account for direct formation of T_β from T_h . However, when considering the influence of source variability and lot-to-lot variability on the dehydration of T_h , it is likely that authors who did not account for the $T_h \rightarrow T_\beta$ transformation were not analyzing samples that undergo this transition. Conflicting reports are found throughout the literature (as summarized in Chapter 3), and in Chapter 7, the influence of sample type on dehydrations performed at different scan rates and at different isothermal dehydration temperatures is explored.

6.5 References

1. Andrew, A. R.; Bradbury, A.; Eades, R. G. Removal of dipolar broadening of nuclear magnetic resonance spectra of solids by specimen rotation. *Nature* **1958**, *183*, 1802-1803.
2. Barich, D. H.; Gorman, E. M.; Zell, M. T.; Munson, E. J. 3-Methylglutaric acid as a ¹³C solid-state NMR standard. *Solid State Nucl. Magn. Reson.* **2006**, *30*, (3-4), 125-129.
3. Dixon, W. T.; Schaefer, J.; Sefcik, M. D. Total suppression of sidebands in CPMAS carbon-13 NMR. *J. Magn. Reson.* **1982**, *49*, (2), 341-345.
4. Fung, B.; Khitritin, A.; Ermolaev, K. An improved broadband decoupling sequence for liquid crystals and solids. *J. Magn. Reson.* **2000**, *142*, (1), 97-101.
5. Pines, A.; Gibby, M. G.; Waugh, J. S. Proton-enhanced NMR of Dilute Spins. *J. Chem. Phys.* **1973**, *59*, 569-590.
6. Galwey, A. K. Structure and order in thermal dehydrations of crystalline solids. *Thermochim. Acta* **2000**, *355*, (1-2), 181-238.
7. Shafizadeh, F.; Lai, Y. Z. Thermal Rearrangements of Cellobiose and Trehalose. *Carbohydr. Res.* **1973**, *31*, 57-67.
8. Taylor, L. S.; York, P. Characterization of the Phase Transitions of Trehalose Dihydrate on Heating and Subsequent Dehydration. *J. Pharm. Sci.* **1998**, *87*, (3), 347-355.
9. Richards, A. B.; Krakowka, S.; Dexter, L. B.; Schmid, H.; Wolterbeek, A. P. M.; Waalkens-Berendsen, D. H.; Shigoyuki, A.; Kurimoto, M. Trehalose: a review of properties, history of use and human tolerance, and results of multiple safety studies. *Food Chem Toxicol.* **2002**, *40*, 871-898.
10. Furuki, T.; Abe, R.; Kawaji, H.; Atake, T.; Sakurai, M. Effect of Atmospheric Pressure on the Phase Transitions of α,α -Trehalose Dihydrate: DTA study of the dehydration behavior in open systems. *J. Therm. Anal. Calorim.* **2008**, *93*, (2), 561-567.

11. Ohashi, T.; Yoshii, H.; Furuta, T. Innovative crystal transformation of dihydrate trehalose to anhydrous trehalose using ethanol. *Carbohydr. Res.* **2007**, *342*, 819-825.
12. Reisener, H. J.; Goldschmid, H. R.; Ledingham, G. A.; Perlin, A. S. Formation of Trehalose and Polyols by Wheat Stem Rust (*Puccinia Graminis Triticis*) Uredospores. *Can. J. Biochem. Phys.* **1962**, *40*, 1248-1251.
13. Lee, J. W.; Thomas, L. C.; Schmidt, S. J. Investigation of the Heating Rate Dependence Associated with the Loss of Crystalline Structure in Sucrose, Glucose, and Fructose Using a Thermal Analysis Approach (Part I). *J. Agr. Food Chem.* **2011**, *59*, 684-701.
14. Sussich, F.; Cesáro, A. Transitions and Phenomenology of α,α -Trehalose Polymorphs Inter-conversion. *J. Therm. Anal. Calorim.* **2000**, *62*, 757-768.
15. Taylor, L. S.; Williams, A. C.; York, P. Particle size dependent molecular rearrangements during the dehydration of trehalose dihydrate in situ FT-Raman spectroscopy. *Pharm. Res.* **1998**, *15*, (8), 1207-14.
16. Taylor, L. S.; York, P. Effect of particle size and temperature on the dehydration kinetics of trehalose dihydrate. *Int. J. Pharm.* **1998**, *167*, 215-221.
17. Ohashi, T.; Yoshii, H.; Furuta, T. Effect of Drying Methods on Crystal Transformation of Trehalose. *Dry. Technol.* **2007**, *25*, 1305-1311.
18. Jones, M. D.; Beezer, A. E.; Buckton, G. Determination of Outer Layer and Bulk Dehydration Kinetics of Trehalose Dihydrate Using Atomic Force Microscopy, Gravimetric Vapor Sorption and Near Infrared Spectroscopy. *J. Pharm. Sci.* **2008**, *97*, 4404-4415.
19. Surana, R.; Pyne, A.; Suryanarayanan, R. Effect of preparation method on physical properties of amorphous trehalose. *Pharm. Res.* **2004**, *21*, (7), 1167-76.
20. Lubach, J. W.; Xu, D.; Segmuller, B. E.; Munson, E. J. Investigation of the effects of pharmaceutical processing upon solid-state NMR relaxation times and implications to solid-state formulation stability. *J. Pharm. Sci.* **2007**, *96*, (4), 777-787.

21. Kilburn, D.; Sokol, P. E. Structural Evolution of the Dihydrate to Anhydrate Crystalline Transition of Trehalose as Measured by Wide-angle X-ray Scattering. *J. Phys. Chem. B* **2009**, *113*, 2201-2206.
22. Sussich, F.; Skopec, C.; Brady, J.; Cesáro, A. Reversible dehydration of trehalose and anhydrobiosis: from solution state to an exotic crystal? *Carbohydr. Res.* **2001**, *334*, 165-176.
23. Willart, J. F.; Danede, F.; De Gusseme, A.; Descamps, M.; Neves, C. Origin of the Dual Structural Transformation of Trehalose Dihydrate upon Dehydration. *J. Phys. Chem. B* **2003**, *107*, 11158-11162.

Chapter 7

Dehydration of Trehalose Dihydrate: Part II

7.1 Introduction

In this chapter, the classification system described in Chapter 6 is challenged by dehydrating samples of T_h under a variety of conditions designed to yield slower and faster rates of water loss. In Chapter 6, it was shown that source variability and lot-to-lot variability affect the dehydration behavior of trehalose dihydrate (T_h) when samples are heated at 10 °C/minute. Type 1 samples tend to form the β -anhydrate form of trehalose (T_β) upon dehydration while Type 2 and Type 3 samples tend to form amorphous trehalose (T_{am}). When heated above the glass transition temperature (T_g) of T_{am} , Type 2 samples crystallize to form T_β , and Type 3 samples remain amorphous.

In §3.3.2.2, the effects of heating rate on the dehydration of T_h were summarized. While Sussich et al. observed the formation of amorphous trehalose (T_{am}) when T_h was heated at slower rates,¹ Willart et al. determined that the α -anhydrate (T_α) was formed at slower rates and T_{am} was formed at faster rates.² In this chapter, two samples of T_h with very different dehydration behaviors (Type 1 and Type 3) were heated at 2 °C/minute and 20 °C/minute via differential scanning calorimetry (DSC) in order to determine if heating T_h at different rates produces results that are consistent with the classification system.

In §3.3.1, the anhydrous forms of trehalose produced from isothermal dehydrations of T_h were discussed. In general, lower isothermal dehydration temperatures (≤ 85 °C) result in a slower rate of water loss and are reported to produce T_α ,²⁻⁵ but mixtures of T_α and T_{am} have also been observed following dehydration between 40 and 85 °C.⁶ In Chapter 4, two samples were dehydrated at 75 °C for 48 hours (§4.3.5): one sample contained T_α , T_{am} , T_δ , and T_β after dehydration, and the other contained T_α , T_{am} , and T_δ . Low temperature dehydrations of T_h in a vacuum oven were also performed in Chapter 5, and mixtures of T_α , T_{am} , and T_δ were

consistently produced. Dehydration of T_h at 100 °C is reported to generate T_{am} ,⁷ but in Chapter 4, dehydration of four samples at 100 °C yielded mixtures of T_{am} and T_β . Also in Chapter 4, dehydration of T_h at 125 °C resulted in mixtures of T_{am} and T_β , with different proportions of each in the mixtures. As shown in §3.3.1, isothermal dehydration of T_h near 125 °C has been reported to form T_β ⁸ and T_{am} ⁹. In this chapter, isothermal dehydrations at 75 °C, 100 °C, and 125 °C are repeated on samples of each type, and the composition of each sample is analyzed using DSC and ¹³C solid-state NMR (SSNMR) in order to determine if the classification system can be used to predict isothermal dehydration behavior of T_h .

Finally, isothermal dehydrations of each type of T_h were performed as samples were held at 68 °C in the magnet and SSNMR spectra were acquired. A disadvantage of the previous isothermal dehydration experiments is that only the final composition of the dehydrated sample is analyzed, which may not indicate how the anhydrous forms are generated. By acquiring SSNMR spectra as water leaves the crystal structure of T_h , it can be determined, for example, if T_β forms via a metastable intermediate or directly upon dehydration of T_h .

7.2 Experimental

7.2.1 Materials

Sixteen samples of D-(+)-trehalose dihydrate were purchased from Acros (Geel, Belgium), Alfa Aesar (Ward Hill, MA), Fluka (Buchs, Switzerland), Life Sciences Advanced Technologies Inc. (St. Petersburg, FL), and Sigma (St. Louis, MO). The sample identities, sources, lot numbers, and classification (as determined in Chapter 6) are listed in Table 7.1.

Table 7.1. Sample identities, classification (from Chapter 6), sources, and lot numbers.

Sample ID	Type	Manufacturer	Product Code	Lot Number
Acros 18255-1	3	Acros	18255	A0252515
Acros 18255-2	3	Acros	18255	A0264819
Acros 18255-3	3	Acros	18255	A0285874
Alfa Aesar A19434-1	2	Alfa Aesar	A19434	10131165
Alfa Aesar A19434-2	3	Alfa Aesar	A19434	10143600
Fluka 90208	1	Fluka	90208	1357383
Fluka 90210-1	2	Fluka	90210	1401913
Fluka 90210-2	2	Fluka	90210	1383659
Fluka 90210-3	2	Fluka	90210	BCBC1043
Life Science	1	Life Science	TDH033	61821T0905
Sigma T9449-1	2	Sigma	T9449	099K7351
Sigma T9449-2	2	Sigma	T9449	099K7352
Sigma T9449-3	1	Sigma	T9449	114K7064
Sigma T9531-1	3	Sigma	T9531	058K7357
Sigma T9531-2	1	Sigma	T9531	127K7350
Sigma T9531-3	2	Sigma	T9531	127K7355

7.2.2 Sieving

Bulk materials were sieved to obtain particle size fractions of <75 μm , 75–125 μm , 125–180 μm , 180–425 μm , 425–850 μm , and >850 μm . A set of U.S.A. Standard Test Sieves (Hogentogler&Co., Inc., Columbia, MD) was stacked and shaken manually or using a Performer III Model SS-3 mechanical sieve shaker (Gilson Company, Inc., Lewis Center, OH).

7.2.3 Dehydration

Samples of trehalose dihydrate (not sieved) were isothermally dehydrated in a Baxter DP-32 vacuum drying oven (Deerfield, IL) under the following conditions: 75 °C for 48 hours, 100 °C for 24 hours, and 125 °C for one hour. Each sample (~2 g) was spread in single layer in a Pyrex dish and placed in the oven for the designated period of time. The oven temperature was verified with a calibrated thermometer.

7.2.4 Differential Scanning Calorimetry

Differential scanning calorimetry was performed using a Thermal Analysis DSC Q100 or Q2000 (TA Instruments; New Castle, DE). T_h samples were weighed into open aluminum pans, and dehydrated trehalose samples were weighed into aluminum hermetic pans with 3 pinholes in each lid. All samples were analyzed using a standard ramp method and were heated from 25 °C to 250 °C under a dry nitrogen purge at 50 mL/min: T_h samples were heated at 2 and 20 °C/minute, and dehydrated trehalose samples were heated at 10 °C/minute.

7.2.5 ^{13}C Solid-state NMR Spectroscopy

^{13}C SSNMR spectra were acquired using a Tecmag Redstone spectrometer (Tecmag Inc., Houston, TX) operating at approximately 300 MHz for ^1H and 75 MHz for ^{13}C . Dehydrated samples and T_h samples were packed into 7.5-mm zirconia rotors, but for T_h , the rotors were fitted with a top endcap with a small hole ($\sim 2\text{mm}$) to allow water vapor to escape. Rotors were spun at the magic angle at a spinning speed of 4kHz.¹⁰ Peaks were referenced to the methyl peak of 3-methylglutaric acid, which was set to 18.84 ppm.¹¹ Spectra were acquired using ramped cross polarization, Spinal 64 decoupling, and sideband suppression.¹²⁻¹⁴ A contact time of 1 ms and a pulse delay of 120 seconds were used to acquire spectra of dehydrated trehalose samples. T_h samples were heated to 68 °C in the magnet and allowed to equilibrate for about 10 minutes. After equilibration, multiple data sets of 512 acquisitions with a pulse delay of 14 seconds were collected until the dehydration was complete. These conditions yielded spectra that represented the composition of the material over a 2-hour period.

7.3 Results and Discussion

7.3.1 Non-Isothermal Dehydration of Trehalose Dihydrate

Differences in dehydration behavior of T_h samples were identified when the samples were heated at 10 °C/minute (Chapter 6), and in this section, slower (2 °C/minute) and faster (20 °C/minute) dehydrations of T_h are performed. Due to the known influence of particle size on the dehydration of T_h ,^{8, 15, 16} both small (75–125- μm) and large (425–850- μm) particle size fractions were analyzed.

7.3.1.1 Dehydration of Trehalose Dihydrate at 2 °C/minute

Figure 7.1 shows DSC thermograms of 75–125- μm particles of T_h from the Sigma T9449-3 (Type 1: tends to form T_β upon dehydration) sample and Acros 18255-1 sample (Type 3: tends to form T_{am} that does not crystallize to T_β) as they were heated at 2 °C/minute. Both thermograms contain broad endotherms with peak temperatures of about 75 °C and sharper endotherms with peak temperatures near 100 °C. The lower temperature endotherm is significantly larger in the thermogram of the Sigma T9449-3 material, and its onset temperature is lower. The higher temperature endotherm is significantly larger in the thermogram of the Acros 18255-1 sample. When heated at 10 °C/minute, the Sigma T9449-3 sample dehydrated at a lower temperature than the Acros 18255-1 sample (§6.3.2 and §6.3.3), and the results at a slower heating rate are consistent with this observation. If water is able to leave the Sigma T9449-3 particles at a lower temperature, it suggests that the water molecules in these particles are either more loosely bound or have an easier path to escape the crystal structure of T_h . Both the level of crystal defects and particle morphologies of the different samples were investigated in §6.3.8, but a clear correlation between either of these factors and the dehydration behavior was not observed.

In both DSC thermograms (Figure 7.1), a small endotherm at about 130 °C follows the two dehydration endotherms. This endotherm corresponds to melting of T_α . It has been shown that the formation of T_α from T_h is favored for dehydration of small particles and via slow heating rates,² and the presence of the endotherm in both thermograms confirms these conclusions. Both thermograms also contain an exotherm corresponding to crystallization of T_β , though they occur at different temperatures. For the Sigma T9449-3 sample, the onset of

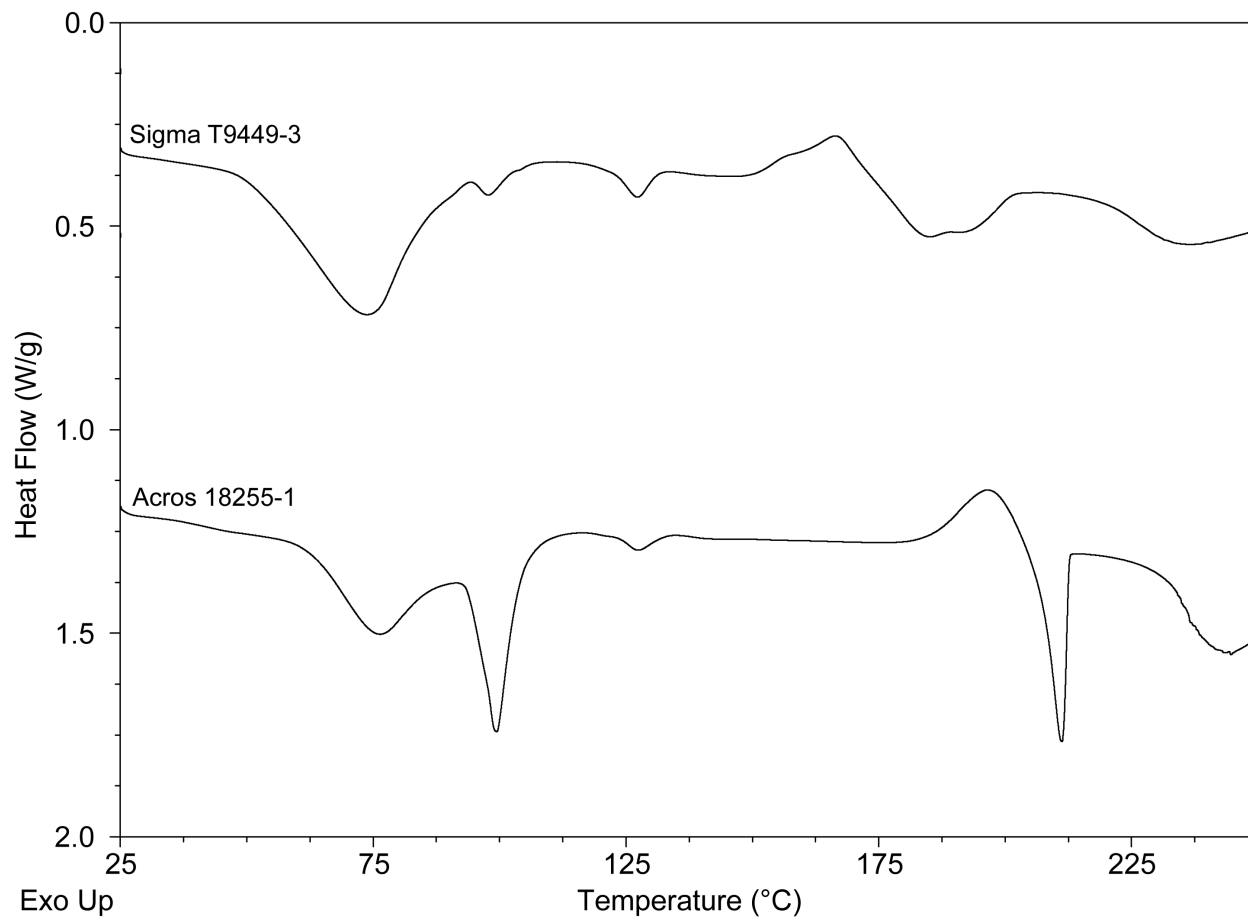


Figure 7.1. DSC thermograms of 75–125- μm particles from a Type 1 sample (Sigma T9449-3) and a Type 3 sample (Acros 18255-1) as they are heated at 2 °C/minute.

crystallization occurs at about the same temperature (150 °C) as it did when the sample was heated at 10 °C/minute (§6.3.2), suggesting that T_{β} or nuclei of T_{β} were formed upon dehydration. Crystallization of the Acros 18255-1 sample was not observed when heated at 10 °C/minute, but when heated at 2 °C/minute, crystallization begins at about 175 °C. When heated at 2 °C/minute, the sample spends 20 minutes between 140 and 180 °C; when heated at 10 °C/minute, the sample only spends 4 minutes in the same temperature range. Therefore, when allowed enough time, the Acros 18255-1 sample is able to crystallize to T_{β} , which may make it less likely that something in the Acros 18255-1 sample prevents it from crystallizing and more likely that something in the Sigma T9449-3 sample facilitates crystallization.

Each exotherm corresponding to crystallization of T_{β} is immediately followed by an endotherm corresponding to melting of T_{β} (Figure 7.1). Both the shapes and temperatures of the melting event are different: melting in the Sigma T9449-3 samples occurs over a broader, lower temperature range than that of the Acros 18255-1 sample. In fact, at ~180 °C, different transitions are occurring in the samples: T_{β} in the Sigma T9449-3 sample is melting, and T_{am} in the Acros 18255-1 sample is crystallizing to T_{β} . It has been shown that the heating rate can affect the melting temperature of other sugars,¹⁷ but as in Chapter 6, these samples were heated at the same rate. This provides additional support for the conclusion that T_{β} formed at a lower temperature will melt at a lower temperature because kinetic decomposition processes can occur prior to and concurrently with melting (§6.3.1). In both thermograms, $\Delta H_{\text{crystallization}}$ and $\Delta H_{\text{melting}}$ are approximately equal, suggesting that T_{β} was not formed upon dehydration of either sample. In accordance with the classification system, the Type 1 sample (Sigma T9449-3) displayed a higher tendency to crystallize to T_{β} than the Type 3 sample even though only T_{α} appears to have

been formed upon dehydration of both samples at 2 °C/minute. The difference in crystallization tendency is addressed in Chapter 9.

Figure 7.2 shows thermograms of 425–850- μm particles from the Sigma T9449-3 and Acros 18255-1 samples as they were heated at 2 °C/minute. Like the smaller particles, whose thermograms were shown in Figure 7.1, the thermograms of larger particles have a broad endotherm centered at about 75 °C and a sharper endotherm near 100 °C. Neither thermogram contains a well-defined endotherm at ~ 130 °C that would correspond to the melting of T_α . The thermogram of the Sigma T9449-3 particles contains an irregular, spiky region between 125 and 150 °C that corresponds to the loss of trapped water from a large particle with an anhydrous shell. For the Acros 18255-1 sample, there are very small spikes at about 175 °C. Both thermograms contain exotherms that correspond to crystallization of T_β , but the difference between the temperatures at which the events occur is not as significant as it was for smaller particles. As was observed for smaller particles, the endotherms for melting of T_β immediately follow the crystallization exotherms; however, for the Sigma T9449-3 sample, $\Delta H_{\text{melting}} > \Delta H_{\text{crystallization}}$, which indicates that T_β was formed upon dehydration of this sample (§6.3.5). Because $\Delta H_{\text{crystallization}}$ and $\Delta H_{\text{melting}}$ are approximately equal for the Acros 18255-1 sample, it appears that metastable forms of trehalose (T_{am} , T_α , and/or T_δ) were generated upon dehydration even though the thermograms do not indicate their presence. This may provide an explanation for the much larger spikes in the thermogram of the Sigma T9449-3 sample: Water loss from within a particle with a crystalline outer layer (Sigma T9449-3) is likely more difficult than water loss from within a particle with a rubbery amorphous outer layer (Acros 18255-1), because water molecules can potentially diffuse through the amorphous outer layer. This may explain why large spikes are only observed in the thermogram of the Sigma T9449-3 sample.

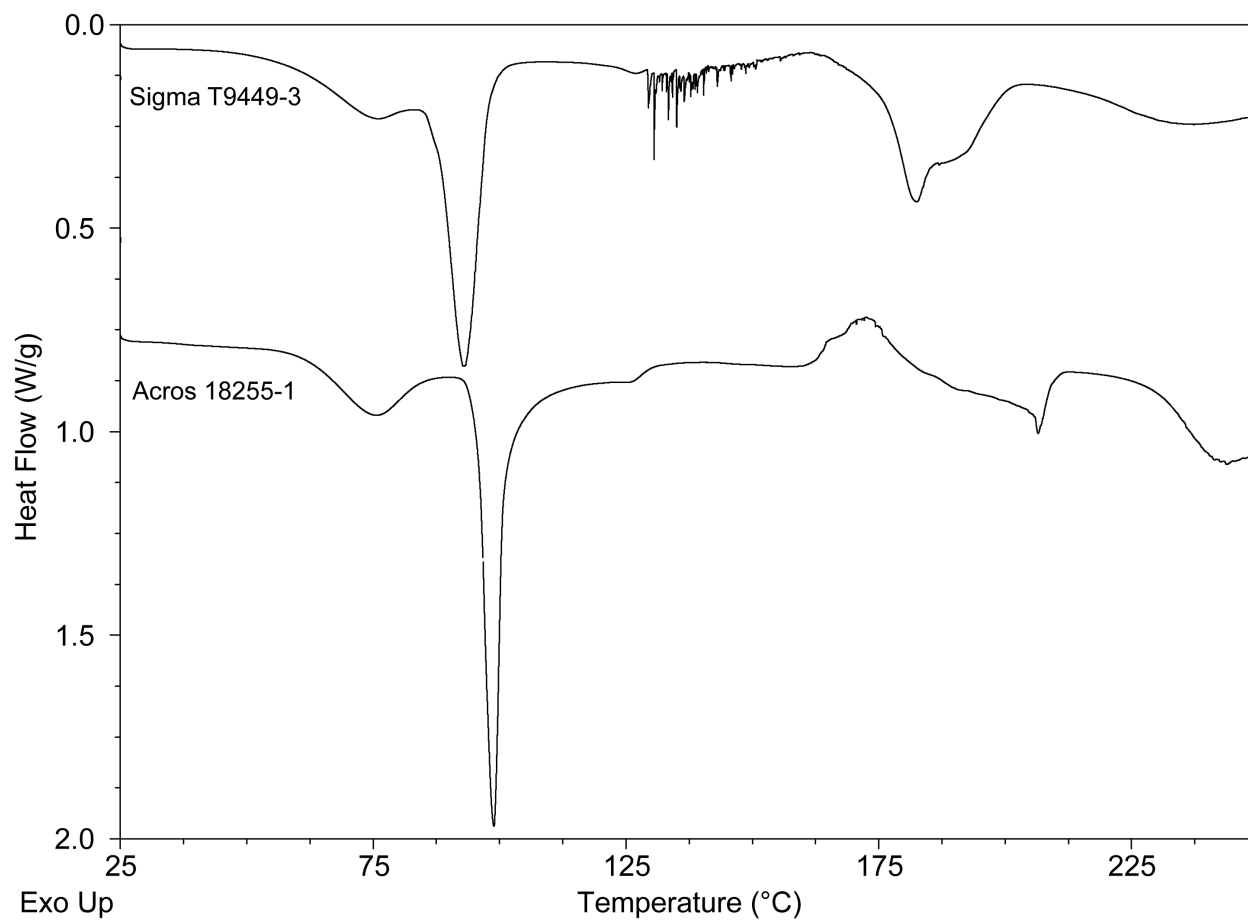


Figure 7.2. DSC thermograms of 425–850- μm particles from a Type 1 sample (Sigma T9449-3) and a Type 3 sample (Acros 18255-1) as they are heated at 2 °C/minute.

Additionally, any trapped water vapor in the Acros 18255-1 particles may be able to more easily move through the less viscous amorphous material and reach the surface.

In summary, dehydration of small particles of Type 1 T_h at 2 °C/minute leads to formation of T_α and possibly other metastable forms of trehalose that could not be determined from the thermograms. Crystallization of T_β begins at about 150 °C, suggesting that nuclei of T_β may be formed upon slow dehydration of Type 1 T_h . It is also possible that the nuclei of T_β are present in the starting material, but the way that water leaves the crystal structure at a slow heating rate (via channels¹⁸) does not allow for the direct formation of T_β from Type 1 T_h . T_β was not detected in the starting material (§6.3.8.2), but it is possible that nuclei of T_β escaped detection. The detection of crystal nuclei is the subject of Chapter 9. Dehydration of small particles of Type 3 T_h at 2 °C/minute also leads to formation of T_α and, most likely, other metastable forms of trehalose as well. This material crystallized to T_β at a higher temperature than the Type 1 sample. Crystallization of this sample was not observed when heated at 10 °C/minute, and this is due to the shorter amount of time that the material remains between the T_g of T_{am} and the melting temperature of T_β when heated at a faster rate.

7.3.1.2 Dehydration of Trehalose Dihydrate at 20 °C/minute

Figure 7.3 shows thermograms of the 75–125- μm samples when heated at 20 °C/minute. Until about 90 °C, the thermograms are very similar: there is a downward drift in both baselines, and onset temperatures of the dehydration endotherms near 100 °C are within a few degrees of each other. However, the dehydration endotherm that follows is about twice as broad in the

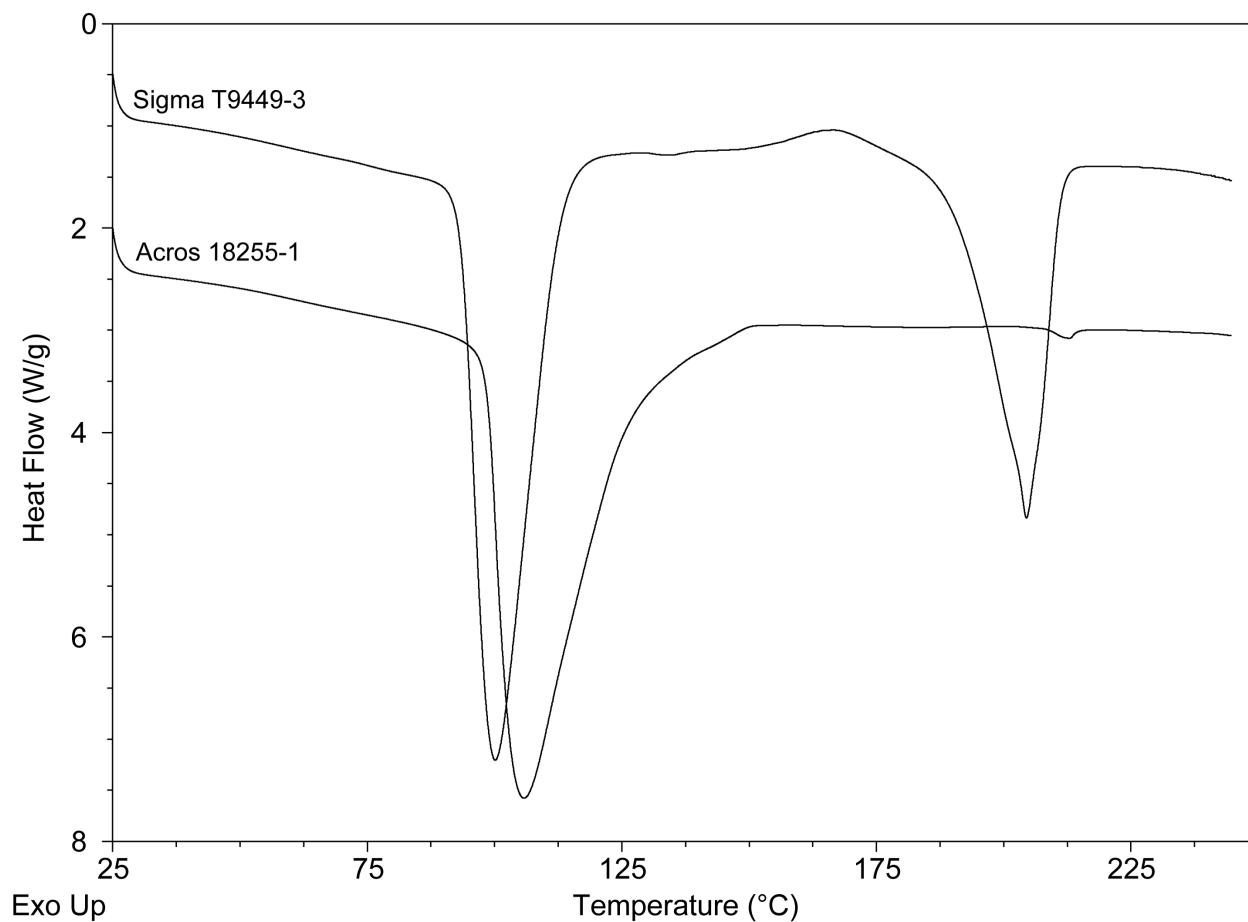


Figure 7.3. DSC thermograms of 75–125- μm particles from a Type 1 sample (Sigma T9449-3) and a Type 3 sample (Acros 18255-1) as they are heated at 20 °C/minute.

thermogram of the Acros 18255-1 sample as it is in the thermogram of the Sigma T9449-3 sample. This suggests that more energy is required for dehydration of small Acros 18255-1 particles than for small Sigma T9449-3 particles. In the thermogram of the Sigma T9449-3 sample, the small endotherm near 130 °C shows that T_{α} was formed in this sample, demonstrating that the formation of T_{α} is possible at high scanning rates. This endotherm is not present in the thermogram of the Acros 18255-1 sample, but as was described in Chapter 6, this does not necessarily mean that T_{α} was not formed because dehydration thermal events could overlap with the endotherm associated with melting of T_{α} . As was observed at heating rates of 2 °C/minute and 10 °C/minute, crystallization of the Sigma T9449-3 sample to T_{β} begins at about 150 °C. Thus, it appears that the kinetics of crystallization of this sample are independent of heating rate. Little crystallization of the Acros 18255-1 sample is observed, most likely because the two minutes that the sample spends between 140 and 180 °C are not long enough for crystallization to occur. Although direct evidence of the formation of T_{am} or T_{α} was not found in the thermogram of the Acros 18255-1 sample, it must be concluded that one or both of these forms was generated upon dehydration of T_{h} . T_{δ} may also have been formed, but DSC is unable to detect the presence of this form (§5.3.4).

Figure 7.4 shows thermograms of 425–850- μm particles that were heated at 20 °C/minute. Like the thermograms of the smaller particles (Figure 7.3), the thermograms of the two samples are similar at lower temperatures. Both thermograms contain a relatively sharp dehydration endotherm with a peak temperature of about 105 °C, but the endotherm for the Acros 18255-1 particles is broader. For the Sigma T9449-3 sample, irregular thermal events are superimposed on a large endotherm centered near 125 °C. Irregular thermal events in the thermogram of the Acros sample are much larger and continue until almost 200 °C.

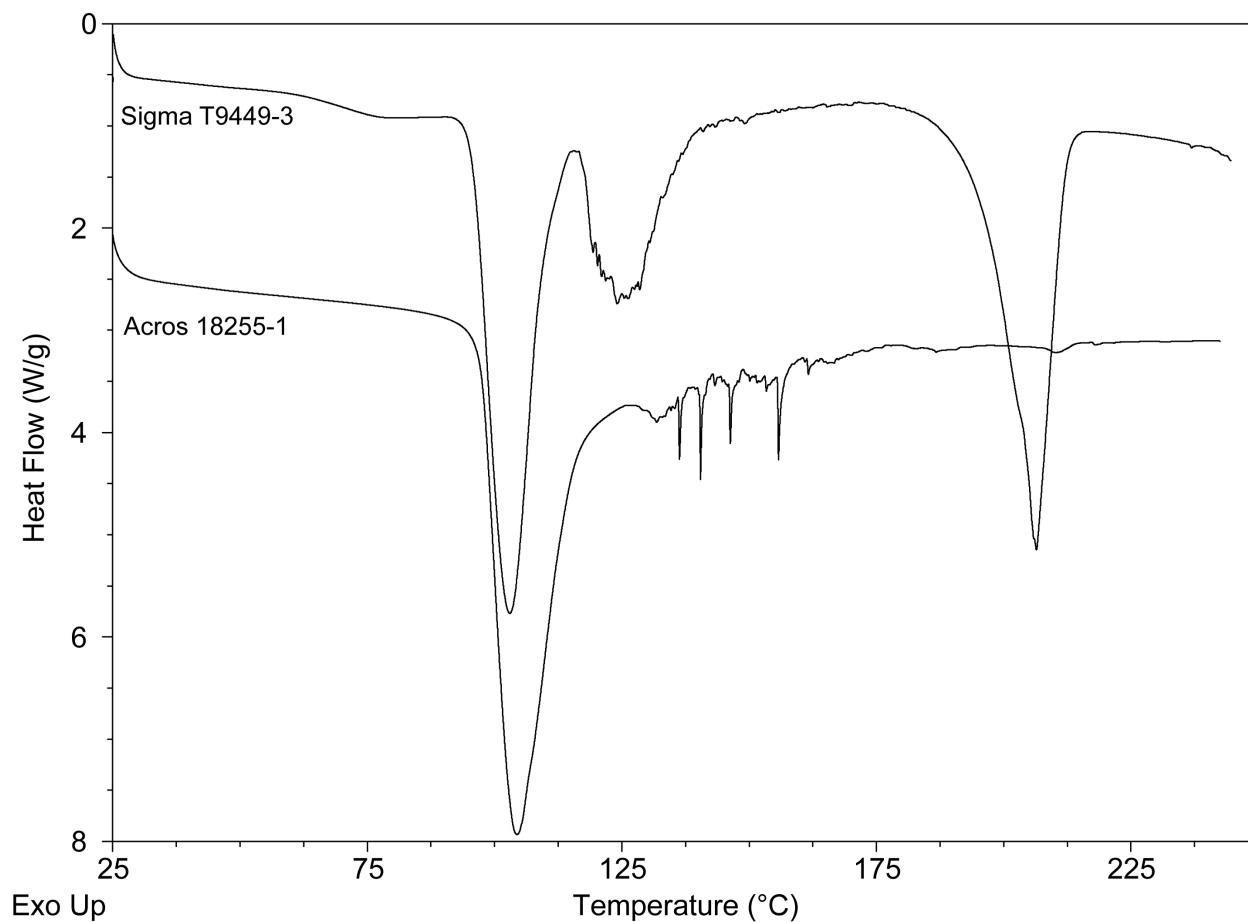


Figure 7.4. DSC thermograms of 425–850- μm particles from a Type 1 sample (Sigma T9449-3) and a Type 3 sample (Acros 18255-1) as they are heated at 20 °C/minute.

Crystallization exotherms are not observed in either thermogram, but the thermogram of the Sigma T9449-3 sample contains a large endotherm corresponding to melting of T_β . Therefore, T_β must have formed directly from dehydration of the Sigma T9449-3 T_h , and the “noisy endotherm” near 125 °C represents trapped water bursting from a large particle with a crystalline T_β surface. The absence of a melting endotherm for T_β in the thermogram of the Acros 18255-1 samples suggests that metastable forms of trehalose were formed upon dehydration of this sample. Therefore, the spiky region in the thermogram of this sample represents trapped water vapor bubbles escaping from the rubbery T_{am} after diffusing through the amorphous material. These results confirm that the classification system that was developed to describe small particles of T_h that were heated at 10 °C/minute can also be used to describe particles of T_h that were heated at 20 °C/minute: regardless of particle size, the Type 1 sample forms T_β , and the Type 3 sample forms T_{am} that does not crystallize to form T_β . As before, the classification describes the general dehydration behavior and not the subtleties of each dehydration.

7.3.2 Isothermal Dehydrations of Trehalose Dihydrate: Vacuum Oven

Isothermal dehydrations of T_h were performed in Chapters 4 and 5, and unexpected mixtures of forms were generated. Dehydration at 75 °C for 48 hours was expected to produce T_α , but mixtures of T_α , T_{am} , T_δ , and sometimes T_β were produced. Dehydration at 100 °C for 24 hours was expected to produce T_{am} , but mixtures of T_{am} and T_β were produced. Dehydration at 125 °C was expected to produce either T_{am} or T_β , but mixtures of these forms were generated. After determining that variability of T_h impacts the dehydration at several heating rates, the isothermal dehydrations were repeated on samples of each type in order to determine if sample variability impacts the forms that are generated from isothermal dehydrations. Dehydrated

samples were analyzed using both DSC and SSNMR to conclusively identify all forms of trehalose that are present.

7.3.2.1 Isothermal Dehydration of Trehalose Dihydrate in a Vacuum Oven: 75 °C

Figure 7.5 shows DSC thermograms of three samples, one of each type, following dehydration at 75 °C for 48 hours. Each thermogram contains an exotherm at about 132 °C that corresponds to the melting of T_{α} . The heat capacity of the three samples changes upon melting (shift in the baseline), indicating that T_{am} is present and that the glass transition of T_{am} , near 120 °C, is superimposed on this endotherm. The thermograms of the Type 1 and Type 2 samples contain exotherms above 150 °C that correspond to crystallization of T_{β} . For the Type 1 sample, the onset of crystallization to T_{β} occurs at about 155 °C, and for the Type 2 sample, crystallization to T_{β} begins at about 190 °C. No crystallization is observed for the Type 3 sample. Melting of T_{β} (endotherm above 200 °C) occurs immediately after its formation. These thermograms suggest that isothermal dehydration of the three types of T_h at 75 °C results in the formation of T_{α} and T_{am} . However, the dehydrated samples display different tendencies to crystallize to T_{β} , and these tendencies (higher for Type 1, very low for Type 3) are consistent with the classification.

Figure 7.6 shows ^{13}C SSNMR spectra (C1, C1' region) of the samples that were dehydrated at 75 °C. The spectra are nearly identical and show that each dehydrated sample is composed of T_{am} , T_{α} , and T_{δ} . All spectra contain a small peak at about 92.8 ppm. This is consistent with the presence of T_h , most likely resulting from the adsorption of water by the metastable, hygroscopic materials during sample packing. Peaks corresponding to T_{β} are not present in any of the spectra. Therefore, the higher tendency of the Type 1 sample to crystallize

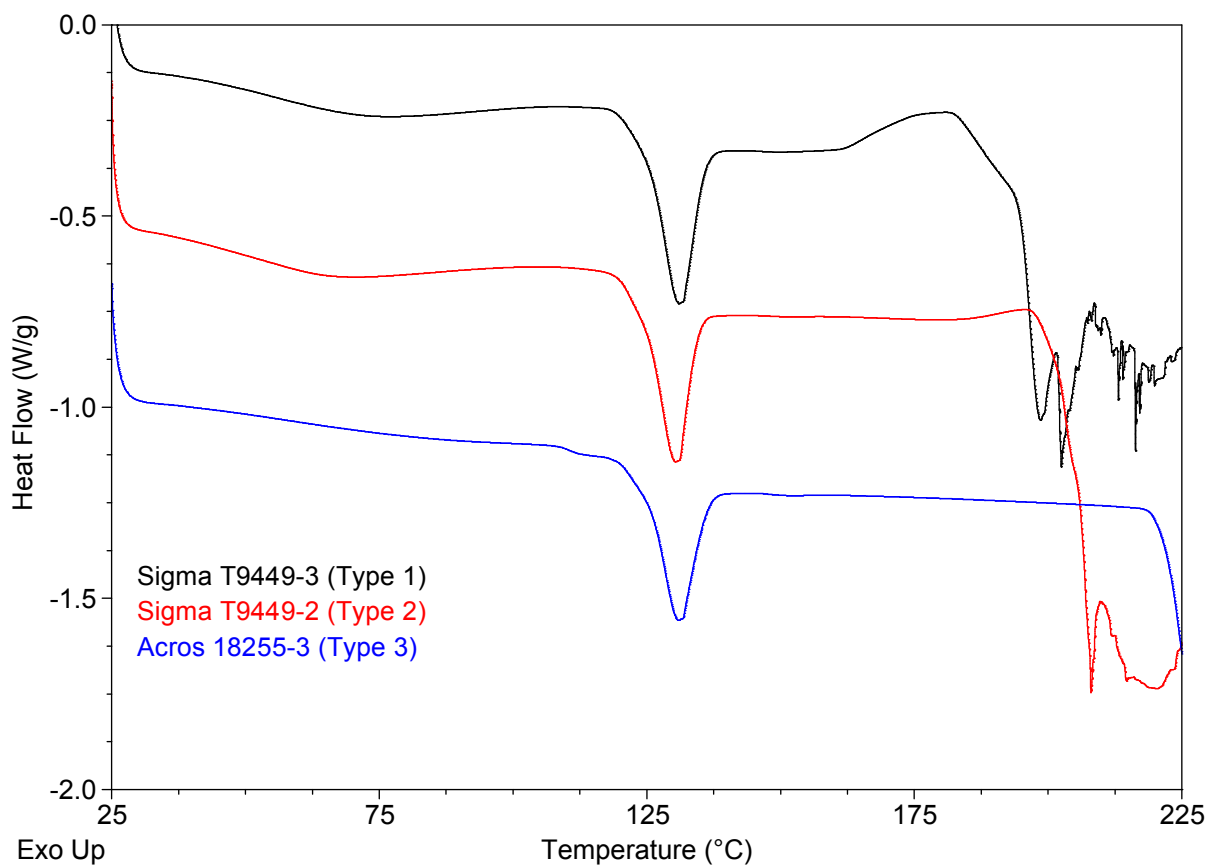


Figure 7.5. DSC thermograms of three samples that were dehydrated at 75 °C.

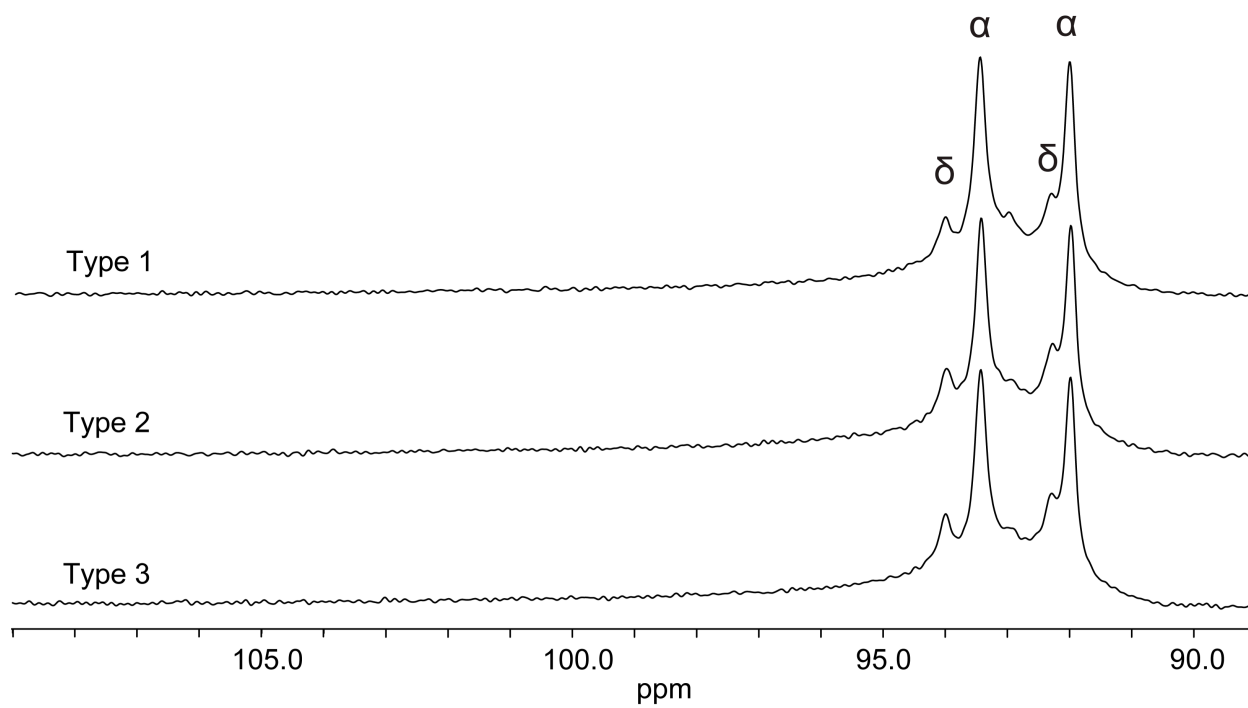


Figure 7.6. ^{13}C SSNMR spectra (C1, C1' region) of samples that were dehydrated at 75 °C.

to T_β , as evidenced by the lower onset temperature and larger magnitude of the crystallization exotherm in the DSC thermogram, is not related to the presence of T_β in this sample. These results are analogous to those observed when T_h was heated slowly (§7.3.1.1): similar mixtures of metastable forms of trehalose are generated, but they have different tendencies to crystallize. Data for three samples is presented in this section, but other samples of T_h have also been subjected to low-temperature dehydrations. SSNMR spectra of an additional Type 1 sample and an additional Type 3 sample following dehydration at 75 °C were shown in Figure 4.7. The three metastable forms (T_{am} , T_α , and T_δ) are present in both samples, but the Type 1 sample also contained T_β , and the Type 3 sample also contained T_h . The dehydration of T_h is extremely sensitive to many factors, and the differences may result from the use of a different oven or different particle sizes within the samples. Although there were differences, it is reassuring that they are consistent with the classification: the Type 1 sample formed T_β upon dehydration. In Chapter 9, SSNMR spectra of an additional Type 1 sample and an additional Type 3 sample after dehydration at 75 °C are presented. For these two samples, mixtures of T_{am} , T_α , and T_δ were formed, and the Type 1 sample showed a higher tendency to crystallize to T_β .

It has been shown that mixtures of T_α and T_{am} can be generated simultaneously,^{2, 6} but low-temperature dehydrations in which water loss from T_h is slow are often thought to yield only T_α .^{2-5, 19-22} In the literature, the techniques most often used to characterize dehydrated trehalose samples are DSC and PXRD. In Chapter 5, it was established that neither DSC nor PXRD can be used to detect T_δ . If amorphous material is present in a mixture of solid forms, it may be difficult to detect the corresponding amorphous halo in a PXRD pattern. Due to the overlap between the glass transition of T_{am} and the melting endotherm of T_α , it may be difficult to determine that both forms are present in a mixture without a deep understanding of the thermal events in the DSC

thermograms. The SSNMR spectra in Figure 7.6 show that mixtures of metastable forms of trehalose are generated, and the generation of pure T_α has not been observed in these investigations. This suggests that the number of trehalose forms that will be detected in a mixture is limited by the characterization method. However, it should also be noted that the DSC thermograms provided information about the thermal behavior of the sample (crystallization tendency) while the SSNMR spectra did not. Therefore, it is important to use a combination of techniques in order to fully characterize the system.

7.3.2.2 Isothermal Dehydration of Trehalose Dihydrate in a Vacuum Oven: 100 °C

Figure 7.7 shows the DSC thermograms of Type 1, Type 2, and Type 3 samples following dehydration at 100 °C for 24 hours. These conditions have been reported to form T_{am} ,⁷ but the results in Chapter 4 showed that significant amounts of T_β were formed under these conditions. The thermogram of the Type 1 sample contains a small, broad glass transition and a small crystallization exotherm, indicating that some T_{am} was formed during the dehydration. However, the sample appears to be largely composed of T_β . The thermogram of the Type 2 sample contains a glass transition with enthalpic recovery and an endotherm at about 130 °C, demonstrating that both T_{am} and T_α were formed in this sample. The dehydration temperature of 100 °C is about 20 degrees below the T_g of T_{am} , and any amorphous material that is generated early in the dehydration is expected to age as the sample is heated, resulting in a peak for enthalpic recovery. It appears that T_β may have been formed in the Type 2 sample because $\Delta H_{melting} > \Delta H_{crystallization}$. The thermogram of the dehydrated Type 3 material contains a glass transition with an enthalpic recovery peak, a small crystallization exotherm, and a small crystallization endotherm. This thermogram is consistent with the published thermogram of

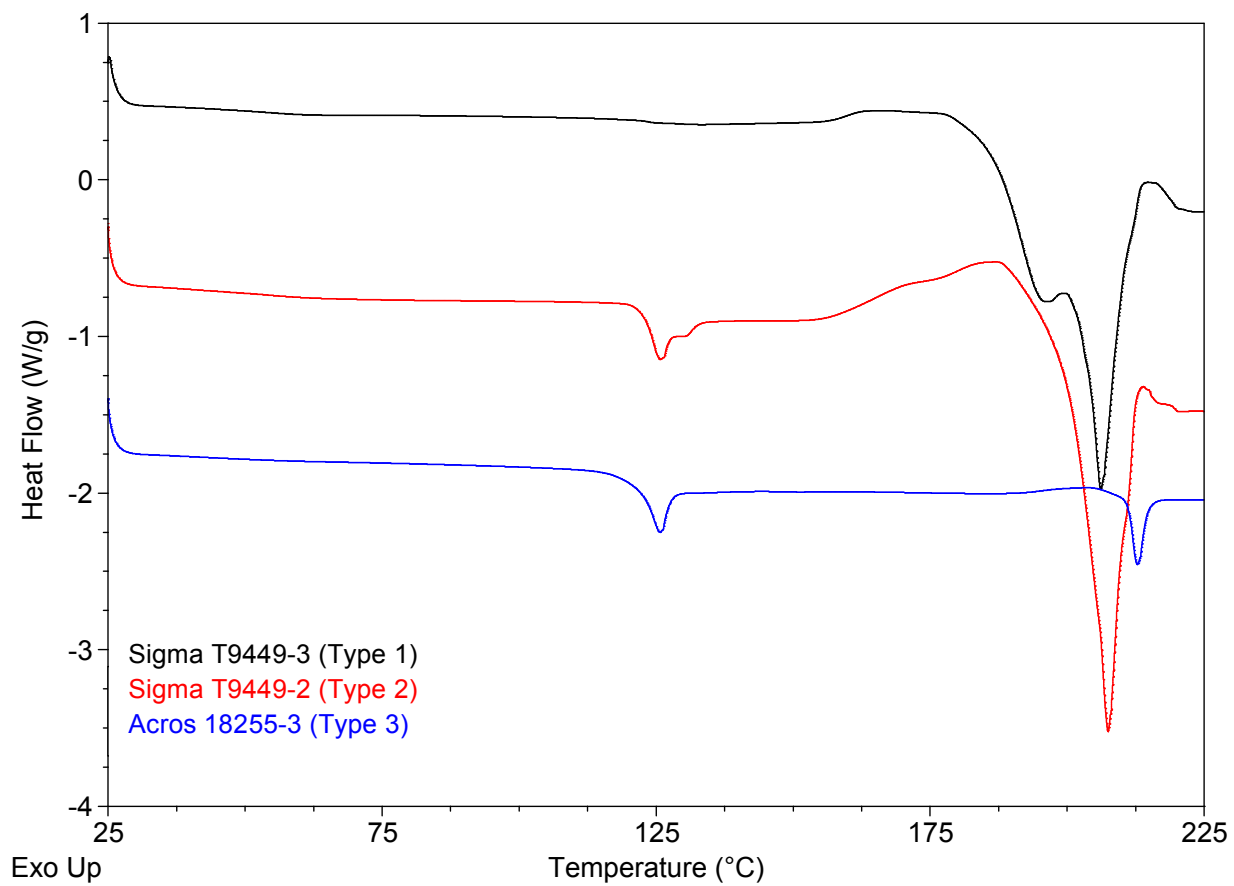


Figure 7.7. DSC thermograms of three samples that were dehydrated at 100 °C.

dehydrated T_{am} ,⁷ although this sample displays a much lower tendency to crystallize to T_{β} . The DSC results indicate that amorphous trehalose can be prepared from dehydration of Type 3 T_h samples at 100 °C.

Figure 7.8 shows the ^{13}C SSNMR spectra (C1, C1' region) of the samples that were dehydrated at 100 °C. As expected from the DSC thermograms, the spectrum of the Type 1 sample contains large T_{β} peaks. Interestingly, it also contains a small peak at 92.0 ppm that corresponds to T_{α} ; the presence of T_{α} in this sample was not indicated by DSC. Peaks corresponding to T_{am} are not detected, but low levels of amorphous materials are more difficult to detect using SSNMR due to their breadth of amorphous peaks. Low levels of amorphous material may be detected using SSNMR with the use of special acquisition conditions or processing techniques.²³ The spectrum of the dehydrated Type 2 sample shows that it is a mixture of four forms: T_{am} , T_{α} , T_{δ} , and T_{β} . Of these forms, all but T_{δ} were indicated by the DSC thermogram. The spectrum of the dehydrated Type 3 material shows that it is largely amorphous, but the small peaks at 92.0 and 93.4 ppm show that T_{α} is also present in this sample. For both the Type 1 and Type 3 samples, SSNMR, but not DSC, was able to detect the presence of T_{α} . The detection of small amounts of T_{α} with DSC may be difficult due to its small heat of fusion which results in a small endotherm for melting.^{6, 22, 24} It may also be difficult to detect low levels of T_{α} using PXRD, the technique that was used to confirm the amorphous nature of T_{am} prepared by dehydration at 100 °C,⁷ due to the broad diffraction peaks displayed by T_{α} .²⁰

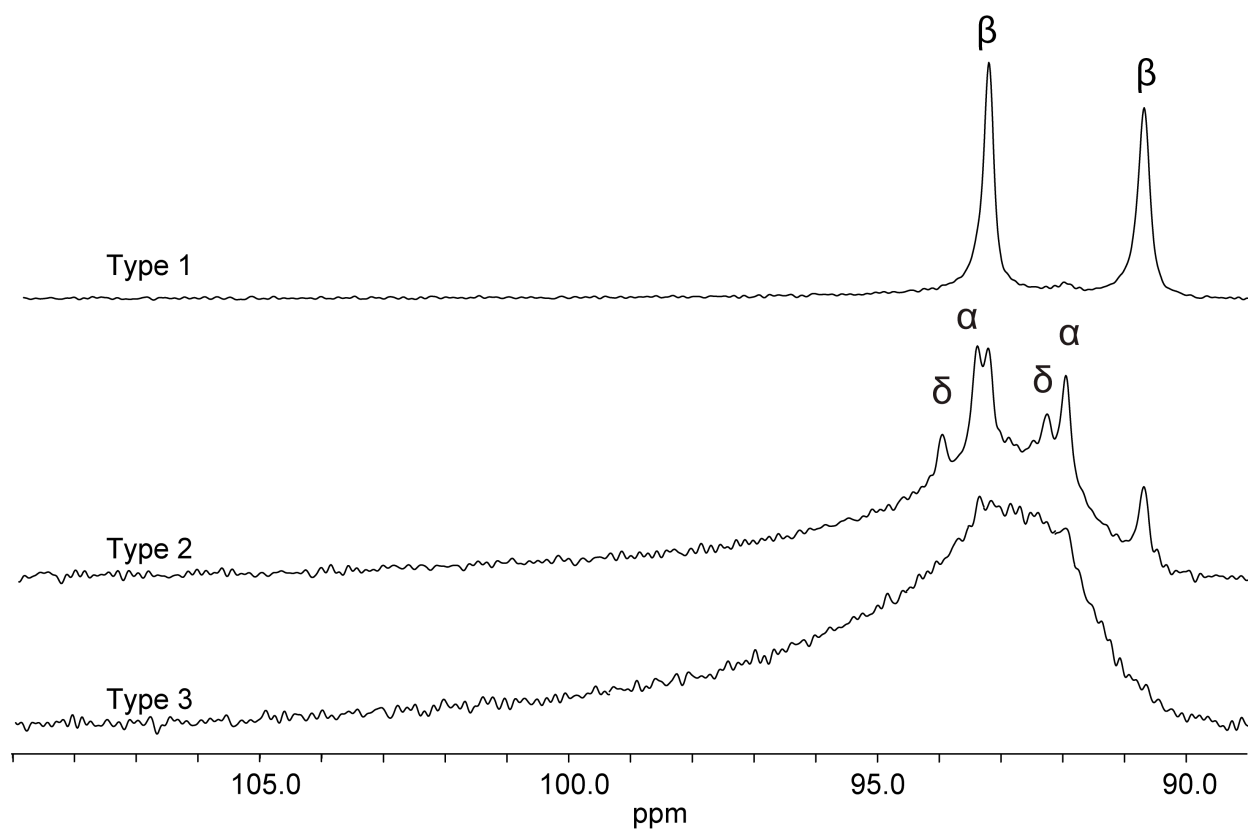


Figure 7.8. ^{13}C SSNMR spectra (C1, C1' region) of samples that were dehydrated at 100 °C.

7.3.2.3 Isothermal Dehydration of Trehalose Dihydrate in a Vacuum Oven: 125 °C

Figure 7.9 shows the DSC thermograms of Type 1, Type 2, and Type 3 samples following dehydration at 125 °C for one hour. The thermogram of the Type 1 sample does not contain a glass transition or a crystallization exotherm, suggesting that metastable forms are not present. The thermograms of the Type 2 and Type 3 samples both contain a glass transition, however, the glass transition of the Type 3 material is broader than that of the Type 2 material, and the change in heat capacity is larger. The magnitude of the change in heat capacity is related to the amorphous content, and it appears that the Type 2 sample is not fully amorphous. The width of the glass transition of T_{am} is discussed in Chapter 8. The thermogram of the dehydrated Type 1 sample contains an irregular region between 145 °C and 190 °C that is reminiscent of the irregular regions that were observed in thermograms of large particles of T_h (Figures 7.2 and 7.4). This may indicate that the dehydration of these samples was incomplete due to the trapping of water by an outer shell of T_β . Melting of T_β from this sample is evidenced by a broad endotherm with maxima at about 190 °C and 205 °C. Crystallization of the Type 2 sample begins at about 155 °C, approximately 20 degrees below the onset of crystallization of the Type 3 sample, suggesting that the presence of T_β may facilitate crystallization of the Type 2 sample. Accordingly, $\Delta H_{melting}$ is larger than $\Delta H_{crystallization}$. T_β formed from the Type 3 material melts at the highest temperature: the peak of the melting endotherm is at about 213 °C. From the DSC thermograms, it appears that the Type 1 sample is composed of T_β and T_h , the Type 2 sample is composed of T_{am} and T_β , and the Type 3 sample is composed of T_{am} .

Figure 7.10 shows the ^{13}C SSNMR spectra (C1, C1' region) of the samples that were dehydrated at 125 °C. The observations from the DSC thermograms in Figure 7.7 are confirmed,

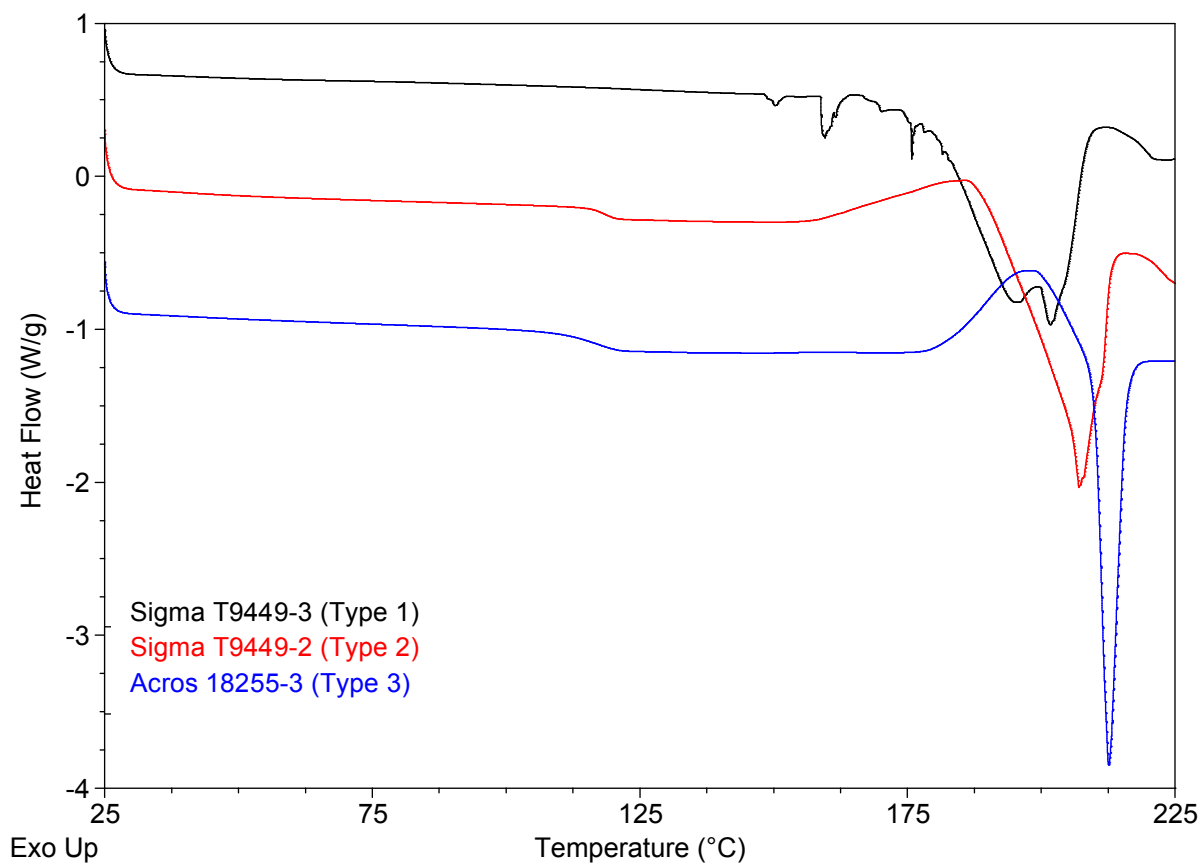


Figure 7.9. DSC thermograms of samples that were dehydrated at 125 °C.

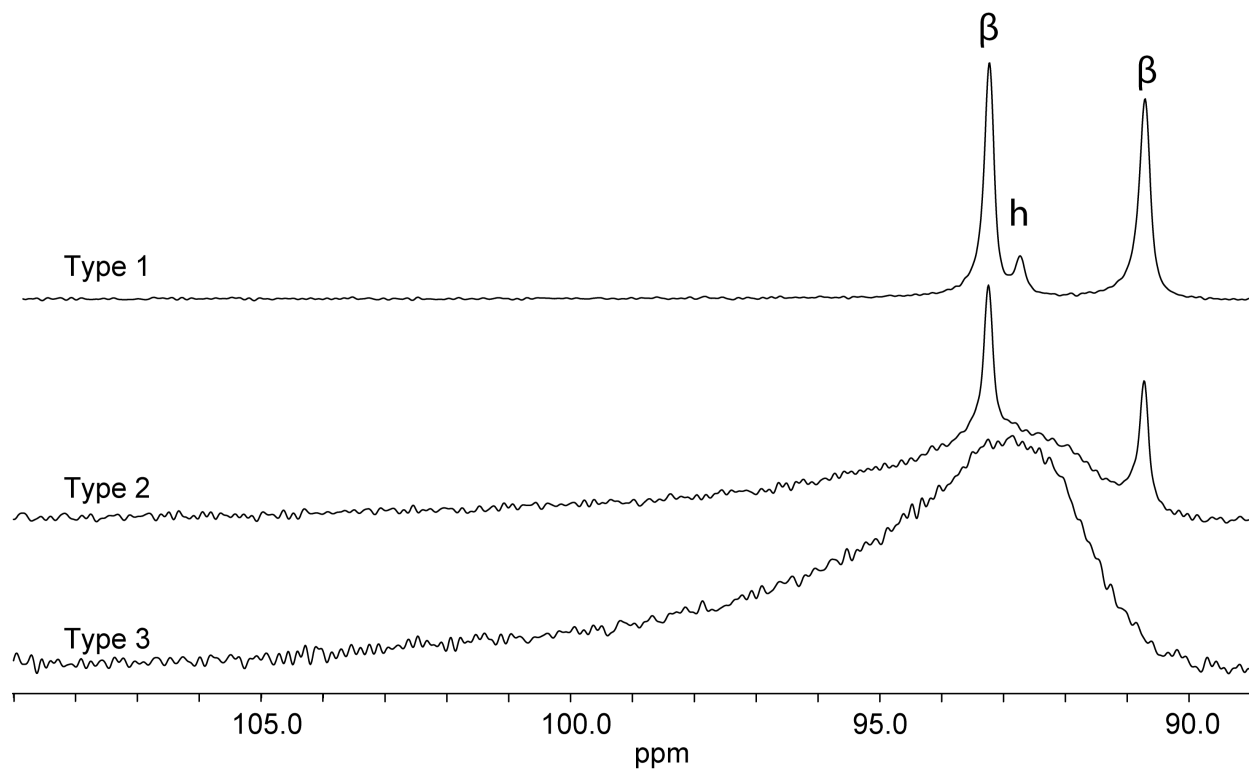


Figure 7.10. ¹³C SSNMR spectra (C1, C1' region) of samples that were dehydrated at 125 °C.

and the SSNMR spectrum of the Type 1 material shows that it is a mixture of T_{β} and T_h . The presence of T_h in this sample provides additional support for the conclusion that the irregular regions in DSC thermograms of large particles of T_h result from water loss. The SSNMR spectrum of the Type 2 material shows that it is a mixture of T_{am} and T_{β} , as was expected based on the DSC thermogram. The SSNMR spectrum of the Type 3 material shows that it is completely amorphous.

Additional dehydrations of these samples and of other samples have been performed at 125 °C, and the results are largely consistent with the results presented in this section. SSNMR spectra of one additional Type 1 and two additional Type 2 samples after dehydration at 125 °C were shown in Figure 4.6. Each of these three dehydrated sample is a mixture of T_{am} and T_{β} . The amount of T_{am} formed in the additional Type 1 sample is about the same as was formed in the Type 2 samples, but again, differences could result from the oven or the particle sizes. The SSNMR spectrum of an additional Type 3 sample is shown in Chapter 9 and shows that T_{am} was formed upon dehydration at 125 °C. Because the formation of T_{am} upon dehydration of T_h is of particular interest, this behavior was verified for all Type 3 samples; however, while all samples formed T_{am} , the samples display different tendencies to crystallize to T_{β} during DSC experiments. This is investigated in Chapter 9.

These results, as well as those presented in §7.3.2.1 and §7.3.2.2, clearly show that the classification system developed in Chapter 6 can be used to predict the dehydration behavior and crystallization tendency of bulk samples of trehalose dihydrate. The anhydrous forms of trehalose generated from isothermal dehydrations are highly dependent on the source and lot of the material, but the differences are more apparent at faster rates of water loss, such as what occurs at a higher heating rate (20 °C/minute) or a higher isothermal dehydration temperature

(125 °C). The results also reveal two pathways to the formation of T_{am} from T_h . First, any sample of T_h can be made amorphous by first dehydrating at a low temperature to form a mixture of metastable forms and then annealing below the T_g (§5.3.4). Second, a T_h sample that is identified as “Type 3” can be rapidly dehydrated at a higher temperature to form T_{am} .

7.3.3 Dehydration of Trehalose Dihydrate at 68 °C: Variable-temperature ^{13}C SSNMR

Variable-temperature SSNMR studies of T_h enable the anhydrous forms resulting from dehydration of T_h to be monitored directly, allowing for the determination of not just *which* anhydrous forms are generated as T_h is heated, but *how* they are generated. Due to the relaxation dynamics of these samples, it is not possible to acquire SSNMR spectra while a sample of T_h is heated at 2, 10, or 20 °C/minute; however, SSNMR spectra can be acquired as a sample is held at an elevated temperature. Unfortunately, it was also not possible to hold the samples at either 75 °C or 125 °C because the dehydration proceeded too quickly at these temperatures, and multiple SSNMR spectra could not be acquired. Because VT-SSNMR dehydrations performed at 68 °C are completed within a reasonable amount of time (1–3 days), and spectra with sufficient signal-to-noise to detect all forms in a mixture can be acquired, this temperature was used to acquire the following data.

Figure 7.11 shows the C1, C1' region of SSNMR spectra of 180–425- μ m particles from the Sigma T9449-3 sample (Type 1) at room temperature (Before) and as they are held at 68 °C. The decrease in intensity of the T_h peak at 92.7 ppm, corresponding to the loss of the crystalline structure of T_h , is accompanied by the appearance and growth of peaks corresponding to anhydrous forms of trehalose. In the first two hours of the experiment, a significant portion of the sample has been dehydrated to form T_β , and growth of T_β appears to stop after only four hours.

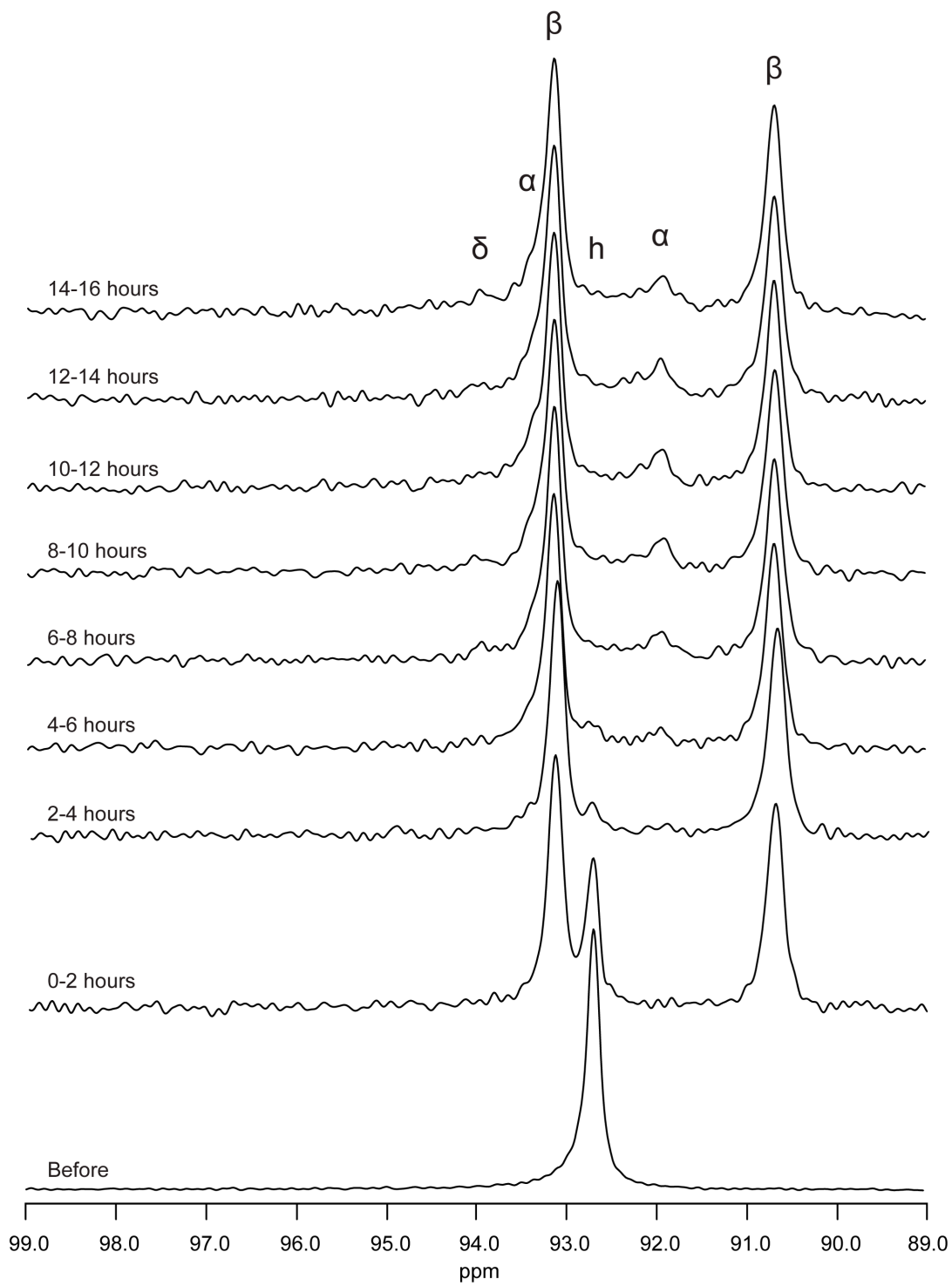


Figure 7.11. ^{13}C SSNMR spectra (C1, C1' region) of a Type 1 sample (180–425- μm) as it was held at 68 °C.

After six hours, the peak for T_h is no longer detected, and very small peaks corresponding to T_α are detected. Peaks corresponding to T_α continue to slowly grow until the experiment was stopped after 16 hours. The T_δ peak at 94.0 ppm may be observed in a few of the spectra, but its intensity is very low.

Figure 7.12 shows the C1, C1' region of SSNMR spectra of 180–425- μm particles from the Alfa Aesar A19434-1 sample (Type 2) at room temperature (Before) and as they are held at 68 °C. For this sample, small peaks corresponding to T_α and T_β are present after four hours, and peaks corresponding to T_δ can be detected after eight hours. While the T_h peak was no longer detected after only six hours for the Sigma T9449-2 sample, it could still be detected after the Type 2 sample was held for 24 hours at 68 °C. Peaks corresponding to T_β , T_α , and T_δ grow over the course of the experiment, but growth of T_β slows after about 20 hours. Dehydration of this sample required almost 24 hours at 68 °C.

Figure 7.13 shows the C1, C1' region of SSNMR spectra of 180–425- μm particles from the Acros 18255-3 sample at room temperature (Before) and as they are held at 68 °C. Peaks corresponding to T_α are easily detected after eight hours, and peaks corresponding to T_δ are detected after 12 hours. Both T_α and T_δ grow throughout the experiment. Additionally, the broad peak corresponding to amorphous trehalose can be detected in these spectra. T_β was not formed in this sample. Even after 40 hours, the peak corresponding to T_h can still be detected, but the experiment was stopped at this point.

The SSNMR spectra show that the dehydration of the Type 1 sample (Figure 7.9) proceeded much faster than the dehydration of the Type 2 (Figure 7.10) and Type 3 (Figure 7.11) samples, which is consistent with the DSC and TGA results presented in Chapter 6. For both the Type 1 and Type 2 samples, the growth of the T_β peaks plateaued as the growth of peaks

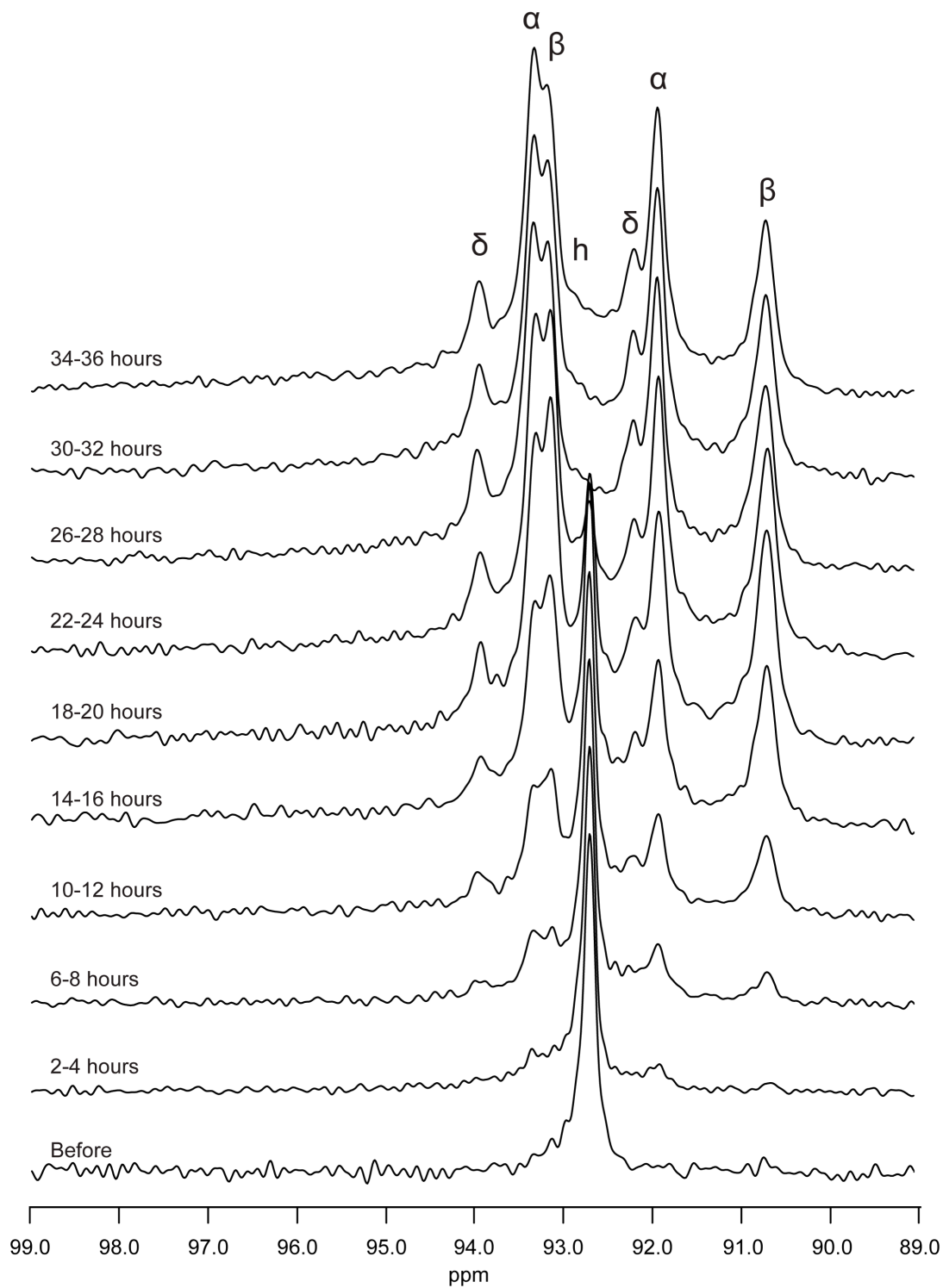


Figure 7.12. ^{13}C SSNMR spectra (C1, C1' region) of a Type 2 sample (180–425- μm) as it was held at 68 °C.

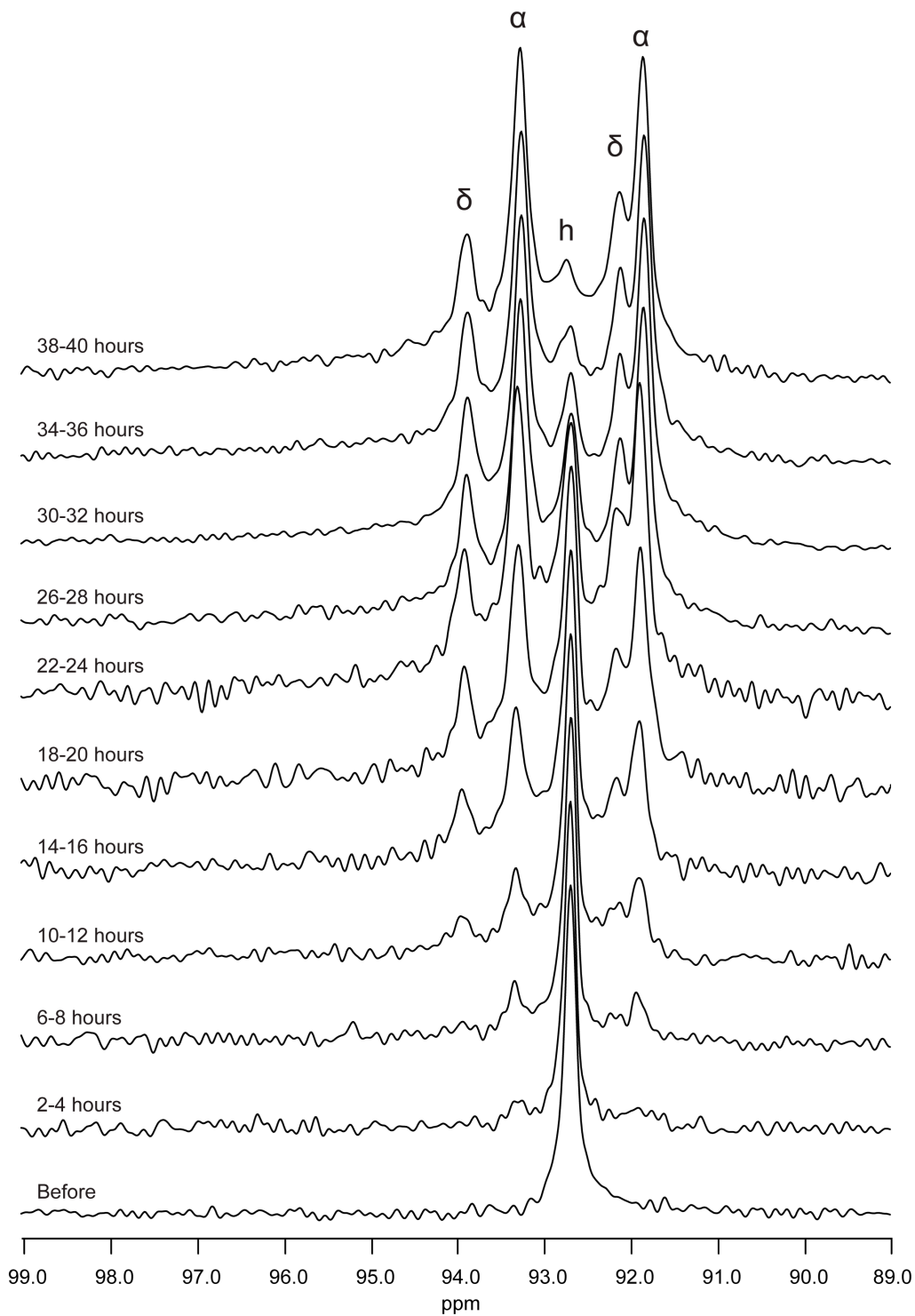


Figure 7.13. ^{13}C SSNMR spectra (C1, C1' region) of a Type 3 sample (180–425- μm) as it was held at 68 °C.

corresponding to metastable forms continued. The loss of water from T_h and concurrent crystallization of T_β seems to occur via a faster process than the loss of water and formation of the metastable forms. It is unclear if the formation of T_β results in water loss at lower temperatures, i.e. crystallization of T_β helps to force water out of the crystal, or if the way that water leaves T_h causes T_β to be formed. Additional characterization of the starting materials will be necessary to determine this. It should be noted that SSNMR spectra of samples following VT-SSNMR dehydration at 68 °C (Figures 7.11, 7.12, and 7.13) are very different from the SSNMR spectra of samples following dehydration in a vacuum oven at 75 °C. Although it was concluded that lower temperature dehydrations of T_h lead to the formation of mixtures of metastable forms (T_{am} , T_α , and T_δ), it is clear that the sample environment and method of heating must also be considered and that T_β can also be formed under certain low-temperature dehydration conditions. In a vacuum oven, the water is able to freely escape from the sample, but in a SSNMR rotor, the sample, and therefore the evolved water vapor, is more constrained (even with a hole in the endcap).

7.4 Conclusion

The classification system that was developed in Chapter 6 to describe the dehydration behavior of T_h at 10 °C can be used to predict the dehydration behavior and crystallization tendency of T_h when dehydrated at other heating rates and when dehydrated isothermally. When the rate of water loss is slow, mixtures of metastable forms of trehalose are generated, but these mixtures show different tendencies to crystallize to T_β that are in accordance with the classification system. When the rate of water loss is fast, Type 1 samples form T_β and Type 3 samples form T_{am} , also in accordance with the classification system.

7.5 References

1. Sussich, F.; Urbani, R.; Princivale, F.; Cesáro, A. Polymorphic Amorphous and Crystalline Forms of Trehalose. *J. Am. Chem. Soc.* **1998**, *120*, 7893-7899.
2. Willart, J. F.; De Gusseme, A.; Hemon, S.; Descamps, M.; Leveiller, F.; Rameau, A. Vittrification and Polymorphism of Trehalose Induced by Dehydration of Trehalose Dihydrate. *J. Phys. Chem. B* **2002**, *106*, 3365-3370.
3. Chakravarty, P.; Bhardwaj, S. P.; King, L.; Suryanarayanan, R. Monitoring Phase Transformations in Intact Tablets of Trehalose by FT-Raman Spectroscopy. *AAPS PharmSciTech* **2009**, *10*, (4), 1420-1426.
4. Gil, A. M.; Belton, P. S.; Felix, V. Spectroscopic studies of solid α - α trehalose. *Spectrochim. Acta A* **1996**, *52*, 1649 - 1659.
5. Reisener, H. J.; Goldschmid, H. R.; Ledingham, G. A.; Perlin, A. S. Formation of Trehalose and Polyols by Wheat Stem Rust (*Puccinia Graminis Tritici*) Uredospores. *Can. J. Biochem. Phys.* **1962**, *40*, 1248-1251.
6. Rani, M.; Govindarajan, R.; Surana, R.; Suryanarayanan, R. Structure in Dehydrated Trehalose Dihydrate—Evaluation of the Concept of Partial Crystallinity. *Pharm. Res.* **2006**, *23*, (10), 2356-2367.
7. Surana, R.; Pyne, A.; Suryanarayanan, R. Effect of preparation method on physical properties of amorphous trehalose. *Pharm. Res.* **2004**, *21*, (7), 1167-76.
8. Taylor, L. S.; York, P. Characterization of the Phase Transitions of Trehalose Dihydrate on Heating and Subsequent Dehydration. *J. Pharm. Sci.* **1998**, *87*, (3), 347-355.
9. Dranca, I.; Bhattacharya, S.; Vyazovkin, S.; Suryanarayanan, R. Implications of Global and Local Mobility in Amorphous Sucrose and Trehalose as Determined by Differential Scanning Calorimetry. *Pharm. Res.* **2009**, *26*, 1064.
10. Andrew, A. R.; Bradbury, A.; Eades, R. G. Removal of dipolar broadening of nuclear magnetic resonance spectra of solids by specimen rotation. *Nature* **1958**, *183*, 1802-1803.

11. Barich, D. H.; Gorman, E. M.; Zell, M. T.; Munson, E. J. 3-Methylglutaric acid as a ^{13}C solid-state NMR standard. *Solid State Nucl. Magn. Reson.* **2006**, *30*, (3-4), 125-129.
12. Dixon, W. T.; Schaefer, J.; Sefcik, M. D. Total suppression of sidebands in CPMAS carbon-13 NMR. *J. Magn. Reson.* **1982**, *49*, (2), 341-345.
13. Fung, B.; Khittrin, A.; Ermolaev, K. An improved broadband decoupling sequence for liquid crystals and solids. *J. Magn. Reson.* **2000**, *142*, (1), 97-101.
14. Pines, A.; Gibby, M. G.; Waugh, J. S. Proton-enhanced NMR of Dilute Spins. *J. Chem. Phys.* **1973**, *59*, 569-590.
15. Taylor, L. S.; Williams, A. C.; York, P. Particle size dependent molecular rearrangements during the dehydration of trehalose dihydrate in situ FT-Raman spectroscopy. *Pharm. Res.* **1998**, *15*, (8), 1207-14.
16. Taylor, L. S.; York, P. Effect of particle size and temperature on the dehydration kinetics of trehalose dihydrate. *Int. J. Pharm.* **1998**, *167*, 215-221.
17. Lee, J. W.; Thomas, L. C.; Schmidt, S. J. Investigation of the Heating Rate Dependence Associated with the Loss of Crystalline Structure in Sucrose, Glucose, and Fructose Using a Thermal Analysis Approach (Part I). *J. Agr. Food Chem.* **2011**, *59*, 684-701.
18. Sussich, F.; Skopec, C.; Brady, J.; Cesáro, A. Reversible dehydration of trehalose and anhydrobiosis: from solution state to an exotic crystal? *Carbohydr. Res.* **2001**, *334*, 165-176.
19. Ballirano, P.; Sadun, C. Thermal behavior of trehalose dihydrate (Th) and b-anhydrous trehalose (Tb) by in-situ laboratory parallel-beam X-ray powder diffraction. *Struct. Chem.* **2009**, *20*, 815-823.
20. Nagase, H.; Endo, T.; Ueda, H.; Nakagaki, M. An anhydrous polymorphic form of trehalose. *Carbohydr. Res.* **2002**, *337*, 167-173.

21. Willart, J. F.; Danede, F.; De Gusseme, A.; Descamps, M.; Neves, C. Origin of the Dual Structural Transformation of Trehalose Dihydrate upon Dehydration. *J. Phys. Chem. B* **2003**, *107*, 11158-11162.
22. Willart, J. F.; Hedoux, A.; Guinet, Y.; Danede, F.; Paccou, L.; Capet, F.; Descamps, M. Metastability Release of the Form α of Trehalose by Isothermal Solid State Vitrification. *J. Phys. Chem. B* **2006**, *110*, 11040-11043.
23. Schieber, L. Methods for Increasing Sensitivity and Throughput of Solid-State NMR Spectroscopy of Pharmaceutical Solids. **2010**.
24. Sussich, F.; Cesáro, A. Transitions and Phenomenology of α,α -Trehalose Polymorphs Inter-conversion. *J. Therm. Anal. Calorim.* **2000**, *62*, 757-768.

Chapter 8

Characterization of Amorphous Trehalose Prepared by Lyophilization and Dehydration of Trehalose Dihydrate

8.1 Introduction

In the previous chapters, the factors influencing the forms of anhydrous trehalose that are generated upon dehydration of trehalose dihydrate (T_h) were discussed. As a result of those experiments, it was discovered that amorphous trehalose (T_{am}) can be generated by dehydrating certain samples of T_h at 125 °C. In addition, it was determined that T_{am} can be prepared from all samples of T_h by first dehydrating T_h at low temperatures to form mixtures of metastable forms and then heating these samples to 110 °C.

Previous studies have shown that dehydrated T_{am} has a higher tendency to crystallize to the β -anhydrate form of trehalose (T_β) than lyophilized T_{am} .^{1, 2} The authors speculated that the difference in crystallization tendencies was due to different extents of nucleation during preparation.¹ Others have suggested that trehalose is polyamorphous, meaning that there are two distinct forms of amorphous trehalose that are separated by a first-order phase transition,³ and that different preparation methods can produce either a non-crystallizable or a crystallizable amorphous form of trehalose.² It has also been shown that aging at 100 °C increases the crystallization tendency of lyophilized T_{am} .⁴ Again, the cause of this was attributed to crystal nuclei, specifically an increase in their concentration during aging. In the published studies, samples were characterized using differential scanning calorimetry (DSC), powder X-Ray diffraction (PXRD), microscopy, and water vapor sorption. Although these techniques are important in the characterization of amorphous materials, they provide little structural information and may be limited in their ability to determine the origin of crystallization differences. ¹³C solid-state NMR spectroscopy (SSNMR) is able to provide information about the structure of materials that lack long-range order and has been used to study conformations in amorphous trehalose.^{5, 6} However, SSNMR has not been used to investigate the factors

influencing the tendency of amorphous trehalose to crystallize. Differences in the SSNMR spectra and relaxation times of various amorphous trehalose samples (if present) could indicate structural differences that are consistent with polyamorphism or the presence of nuclei.

In this chapter, the physical properties of amorphous trehalose prepared by lyophilization and dehydration of T_h are investigated using polarized light microscopy (PLM), DSC, and SSNMR. The effects of aging on each sample are also assessed. Images from PLM show that the samples have different morphologies, and DSC analyses show that lyophilized T_{am} has a lower tendency to crystallize than dehydrated T_{am} . SSNMR spectra and relaxation times indicate that there may be structural differences among the samples.

8.2 Experimental

8.2.1 Materials

D-(+)-trehalose dihydrate was purchased from Acros and used as received. In Chapter 6, this sample was identified as “Type 3,” indicating that it tends to form amorphous trehalose rather than T_β upon dehydration.

8.2.2 Lyophilization

Amorphous trehalose was prepared by lyophilization of a 10 % w/v aqueous solution of trehalose dihydrate using a VirTis AdVantage lyophilizer (SP Scientific, Warminster, PA) and the procedure of Surana et al.¹ Approximately 10 mL of solution was placed in 25 mL scintillation vials and cooled to -45 °C. Samples were subjected to primary drying at -45 °C and ~100 mTorr for 48 hours. The temperature was then increased to 50 °C over the next 24 hours,

and then secondary drying proceeded at 50 °C for 24 hours. The temperature was increased to 60 °C over 24 hours and then held at 60 °C for 24 hours.

8.2.3 Dehydration

Amorphous trehalose was prepared by dehydrating trehalose dihydrate at 125 °C for one hour under vacuum. The sample was spread in single layer in a Pyrex dish and placed in a vacuum oven. A Baxter DP-32 vacuum drying oven (Deerfield, IL) was used for the dehydration, and the temperature was verified with a calibrated thermometer.

8.2.4 Polarized Light Microscopy

Samples were imaged using an Olympus microscope (Center Valley, PA). Hot stage microscopy (HSM) was performed using the Linkam CI94 and Linkam LTS350 attachments (Linkam Scientific Instruments, Surrey, UK) with the Olympus microscope.

8.2.5 Differential Scanning Calorimetry (DSC)

Modulated DSC (MDSC) and conventional DSC experiments were performed using a Thermal Analysis DSC Q100 or a Thermal Analysis DSC Q2000 (TA Instruments, New Castle, DE). All samples were analyzed in aluminum hermetic pans with 3 pinholes in each lid. In MDSC experiments, samples were heated from 25 to 250 °C using a period of 60 s, an amplitude of ± 1 °C, and an underlying heating rate of 2 °C/minute. In conventional DSC experiments, samples were heated at 10 °C/minute.

8.2.6 Solid-state NMR Spectroscopy

Variable-temperature ^{13}C SSNMR spectroscopy was performed using a Chemagnetics CMX-300 spectrometer operating at approximately 75 MHz for ^{13}C . Samples were packed into 7.5-mm zirconia rotors and spun at the magic angle.⁷ The spinning speed was 4kHz. Peaks were referenced to the methyl peak of 3-methylglutaric acid, which was set to 18.84 ppm.⁸ Spectra were acquired using ramped cross polarization, Spinal 64 decoupling, and sideband suppression.⁹⁻¹¹ A contact time of 1 ms and an acquisition length of 256 points were used for all samples. More than 1000 acquisitions with pulse delays of 6–10 seconds were acquired for each sample.

^1H T_1 relaxation times were measured using a saturation recovery experiment. Integrated peak areas were fit to the following monoexponential equation:

$$I_{\tau} = I_{\infty} \left(1 - e^{-\frac{\tau}{T_1}} \right) \quad (\text{Equation 8.1})$$

where I_{τ} is the integrated peak area at a saturation recovery time, τ ; I_{∞} is the maximum signal; and T_1 is the ^1H spin-lattice relaxation time.

8.3 Results

Amorphous trehalose can be prepared in a variety of ways, including lyophilization and dehydration of T_h . The physical characterization of lyophilized T_{am} using PLM, DSC, and SSNMR is described first, and a discussion of the characterization of dehydrated T_{am} using the same techniques follows.

8.3.1 Amorphous Trehalose Prepared by Lyophilization

Figure 8.1 shows an image of amorphous trehalose prepared by lyophilization. The sample consists of thin flakes in various sizes. The lyophilized T_{am} is largely non-birefringent, but the presence of brightly colored areas on the edges of the flakes suggests birefringence due to a crystalline component. If the birefringence were indicative of the presence of T_{β} , these areas would be expected to grow as the material is held between the T_g and the melting temperature of T_{β} . Figure 8.2 shows images of a lyophilized sample as it is heated at 10 °C/minute. The birefringent areas disappear as the glassy material softens and transitions to the rubbery state, demonstrating that the areas of birefringence do not correspond to T_{β} . Another source of birefringence could be T_h . If this were the case, it would indicate that T_h was formed during the lyophilization cycle; formation of T_h during lyophilization has been reported,¹²⁻¹⁴ but it dehydrated to form T_{am} before the cycle was completed (below room temperature). Therefore, it is unlikely that T_h formed in this manner would be present in the lyophilized sample shown in Figure 8.1. While it was shown in Chapter 6 that water can remain in large particles of T_h at temperatures as high as 180 °C, the lyophilized material in Figure 8.2a consists of thin flakes and would likely be dehydrated at temperatures lower than 120 °C. If T_h were formed and dehydration was incomplete, the birefringence could result from T_{α} or T_{δ} . The melting temperature of T_{α} is about 132 °C, and this is consistent with the temperature at which the birefringence disappears. Though the melting temperature of T_{δ} could not be determined, it does not appear to be greater than 132 °C. As was shown in Chapter 7, other techniques such as SSNMR and DSC are able to conclusively determine if crystalline forms are present; results from these techniques are presented in the following paragraphs.

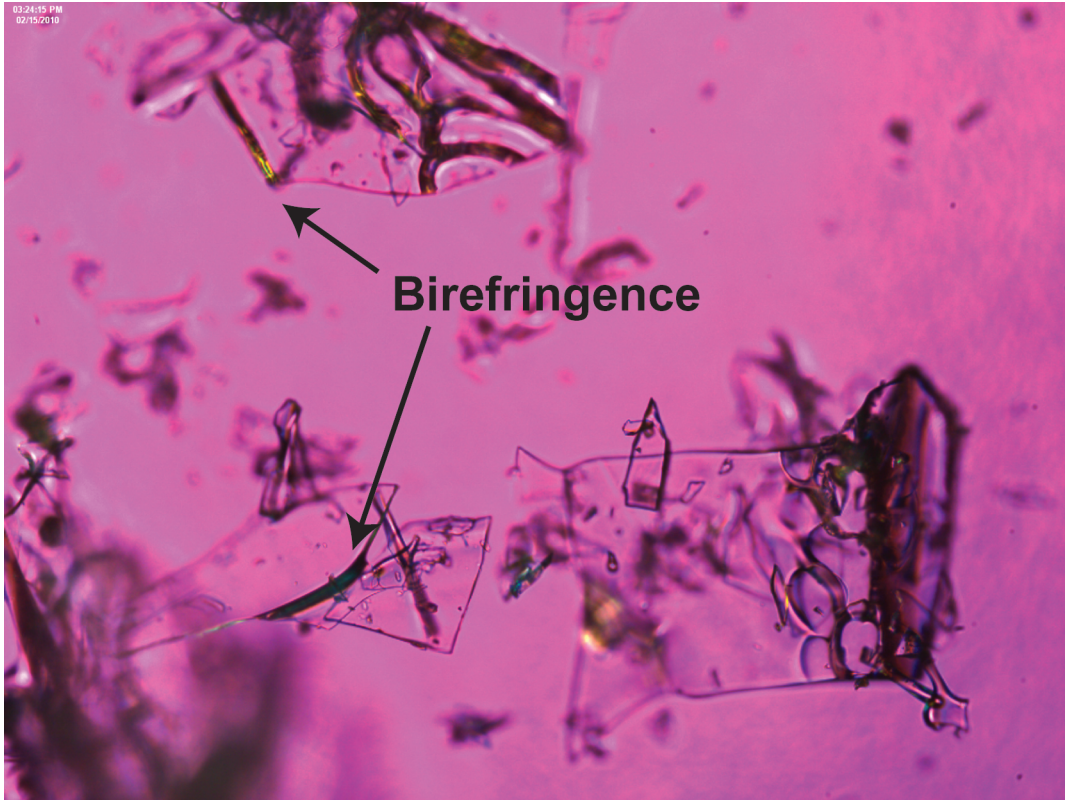


Figure 8.1. Image of lyophilized amorphous trehalose (T_{am}) from polarized light microscopy.

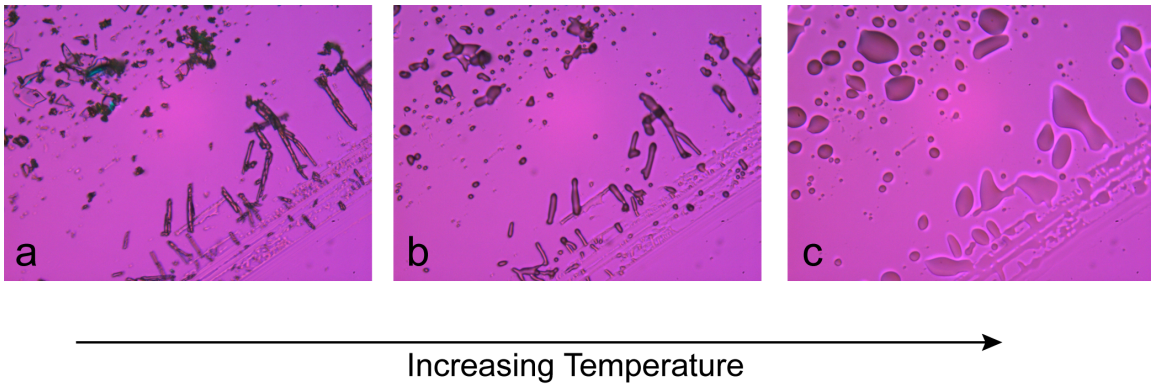


Figure 8.2. PLM Images of amorphous trehalose as it is heated through the glass transition temperature. The material transitions from the glassy state (a, $T \approx 120$ °C) to the rubbery state (c, $T \approx 150$ °C), areas of birefringence are lost. This indicates that birefringence does not result from T_{β} .

Figure 8.3 shows an image of melted trehalose at >220 °C. There are faint blue and yellow areas within the image of the material. These areas are not defined and appear to be on the surface. Up to this point, it has been assumed that birefringence indicates crystallinity, but the images showing birefringence of liquid trehalose suggest that this assumption may not always be accurate. It is possible that the numerous -OH groups on trehalose molecules can form a hydrogen-bonded network that is organized enough to exhibit birefringence, even in the liquid state. If this can occur in the liquid state, then it is possible that it can also occur in the supercooled liquid or glassy states, providing an alternative explanation for the birefringence in the images in Figure 8.1.

Figure 8.4 shows the reversible and non-reversible heat flow signals from MDSC experiments performed on lyophilized trehalose, both before and after aging at 100 °C for 24 hours. A glass transition (A) is present in each reversible signal, and the midpoints of the glass transitions differ by about 1.5 °C. The endpoint temperature of each is about 123 °C, but the onset temperature increases by about 2.5 °C after aging. The width of the glass transition may be related to the range of conformations that exists in the amorphous state. Some conformations are less stable than others, and the highest energy conformations are likely to be the most mobile and would begin to transition from the glassy state to the rubbery state at lower temperatures. As the material is aged, the molecules have enough energy to relax to more energetically favorable conformations, leading to an increase in the onset of the glass transition.¹⁵ During aging, the free volume decreases, which likely results in the strengthening of intermolecular interactions, such as hydrogen bonds.¹⁶ Stronger hydrogen bonding could inhibit the mobility of the trehalose



Figure 8.3. PLM image of melted trehalose (temperature > 220 °C). Even though the material is in the liquid state, the translucent blue and yellow areas indicate birefringence.

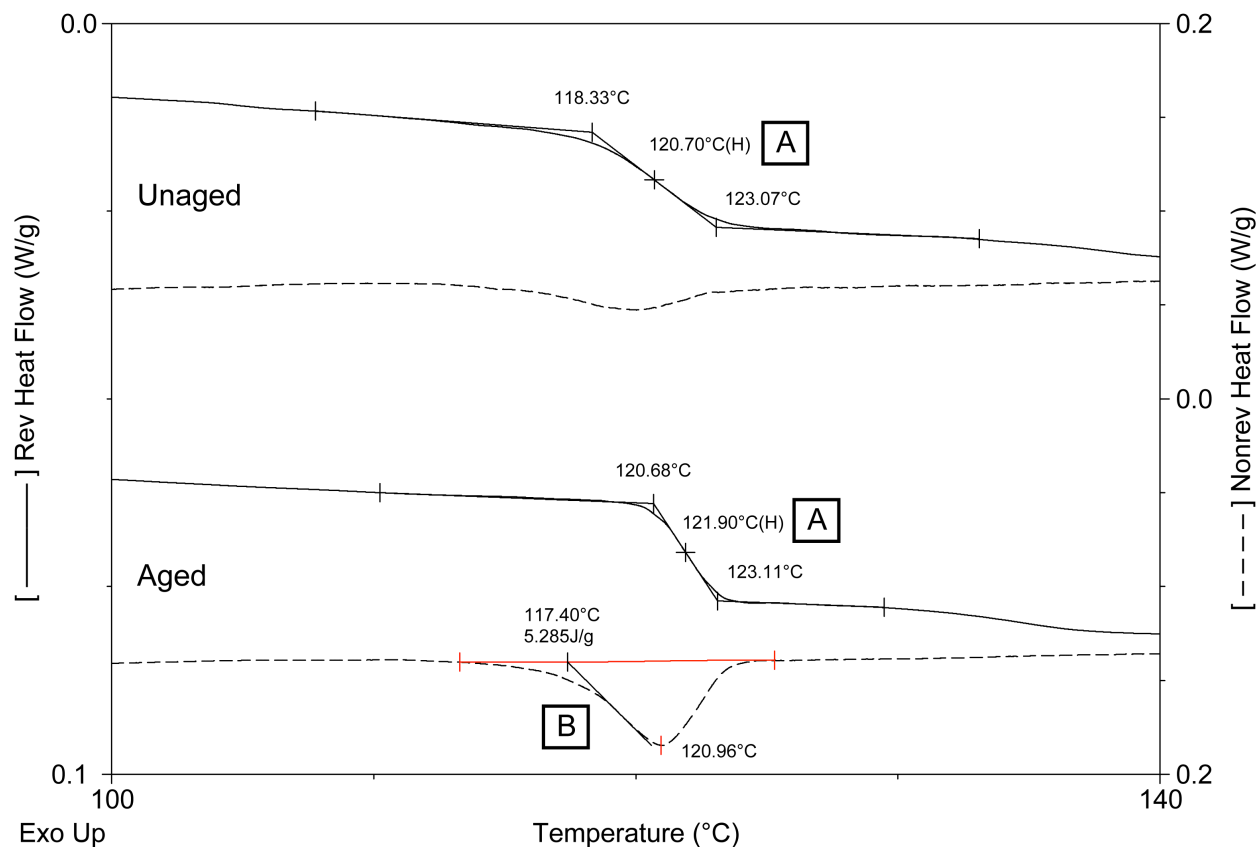


Figure 8.4. MDSC thermograms containing the reversible and non-reversible heat flow signal of lyophilized trehalose both before and after aging at 100 °C for 24 hours. The glass transition (A) is found in the reversible signal, and the enthalpic recovery (B) is found in the nonreversible signal.

molecules and also contribute to an increase in the T_g . An enthalpic recovery peak accompanies the glass transition of aged amorphous trehalose and is found in the non-reversible signal. (B). For this sample, the magnitude of the enthalpic recovery is about 5 J/g.

Figure 8.5 shows the crystallization exotherms (A) and melting endotherms (B) in the total heat flow signal from MDSC experiments performed on lyophilized T_{am} , both before and after aging at 100 °C. After aging, the onset temperature of crystallization decreases by about 10 °C, from 182.5 °C to 172.2 °C. Additionally, the enthalpy of the transition increases from ~90 J/g to ~140 J/g. Both the decrease in the temperature at which the material crystallizes and the increase in the ΔH of the transition demonstrate that aging increases the crystallization tendency of lyophilized trehalose. For both samples, $\Delta H_{crystallization} \approx \Delta H_{melting}$. The relationship between these two thermal events was examined in Chapter 6, and it was found that when $\Delta H_{crystallization} \approx \Delta H_{melting}$, T_β is not formed upon dehydration of T_h . The similar magnitudes of the crystallization exotherm and melting endotherm suggest that T_β is not present in either sample and that formation of T_β during aging is not the cause of the increased crystallization tendency. It is generally thought that heating an amorphous material through the T_g erases the effects of aging; if this were true, the crystallization tendency would not be affected by aging.⁴ At 20 °C below the T_g of amorphous trehalose, there is not enough energy or mobility for crystallization during aging, but it is possible for the concentration of nuclei to increase.⁴ These results support the suggestion that heating an aged amorphous material through the T_g may not erase the effects of nucleation during aging, resulting in an increased tendency to crystallize.

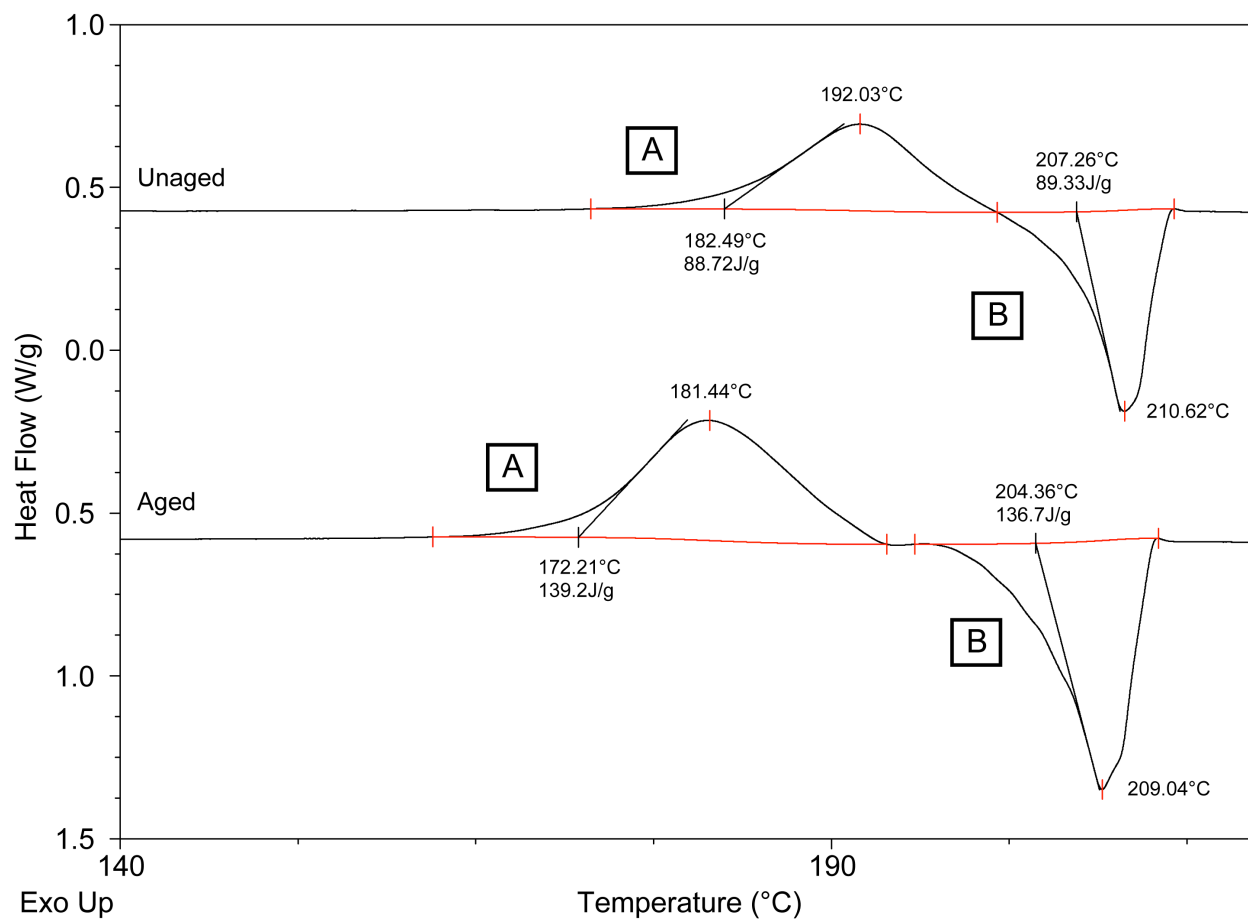


Figure 8.5. MDSC thermograms containing the total heat flow signal of lyophilized trehalose both before and after aging at 100 °C for 24 hours. Crystallization exotherms (A) and melting endotherms (B) corresponding to T_{β} are labeled.

Figure 8.6 shows ^{13}C SSNMR spectra of a lyophilized T_{am} sample. The spectrum of the unaged material at room temperature (Figure 8.6a) is consistent with previously published spectra of amorphous trehalose and does not contain peaks corresponding to T_{h} , T_{β} , or T_{α} . This demonstrates that birefringence of lyophilized T_{am} (Figure 8.1a) does not result from a crystalline component. In the spectrum of the material undergoing aging at 100 °C (Figure 8.6b), the shapes of peaks corresponding to C1–C5 and C1'–C5' are similar to the peaks observed at room temperature. These carbons are located in the two rings, and in the glassy state, the ring structures may still be too rigid to undergo significant conformational changes. In Figure 8.6a, the peaks for C6 and C6' are not baseline-resolved, but two maxima are clearly detected; however, at 100 °C, the peaks for C6 and C6' have begun to coalesce, and only one maximum is detected. This demonstrates that there is mobility outside the rings at 20 °C below the T_{g} . The spectrum of the material after aging (Figure 8.6c) is consistent with the spectrum that was acquired prior to aging (Figure 8.6a), suggesting that little structural change occurred during aging. A spectral subtraction, in which the spectrum of the aged material was subtracted from the spectrum of the unaged material, was performed and the resulting spectrum is shown in Figure 8.6d. The presence of peaks in this spectrum indicates that there are structural differences between the samples before and after aging. The peaks in the subtracted spectrum are not much larger than the noise level, demonstrating that these differences are very small. The broad peak between 65 and 80 ppm represents eight carbons, and differences between the aged and unaged sample are most apparent by examining this region. In this region, the subtracted spectrum contains a “+ – +” shape, where the signal is positive, decreases, and then increases. This shape indicates that this peak is slightly narrower in the spectrum of the aged material. A similar

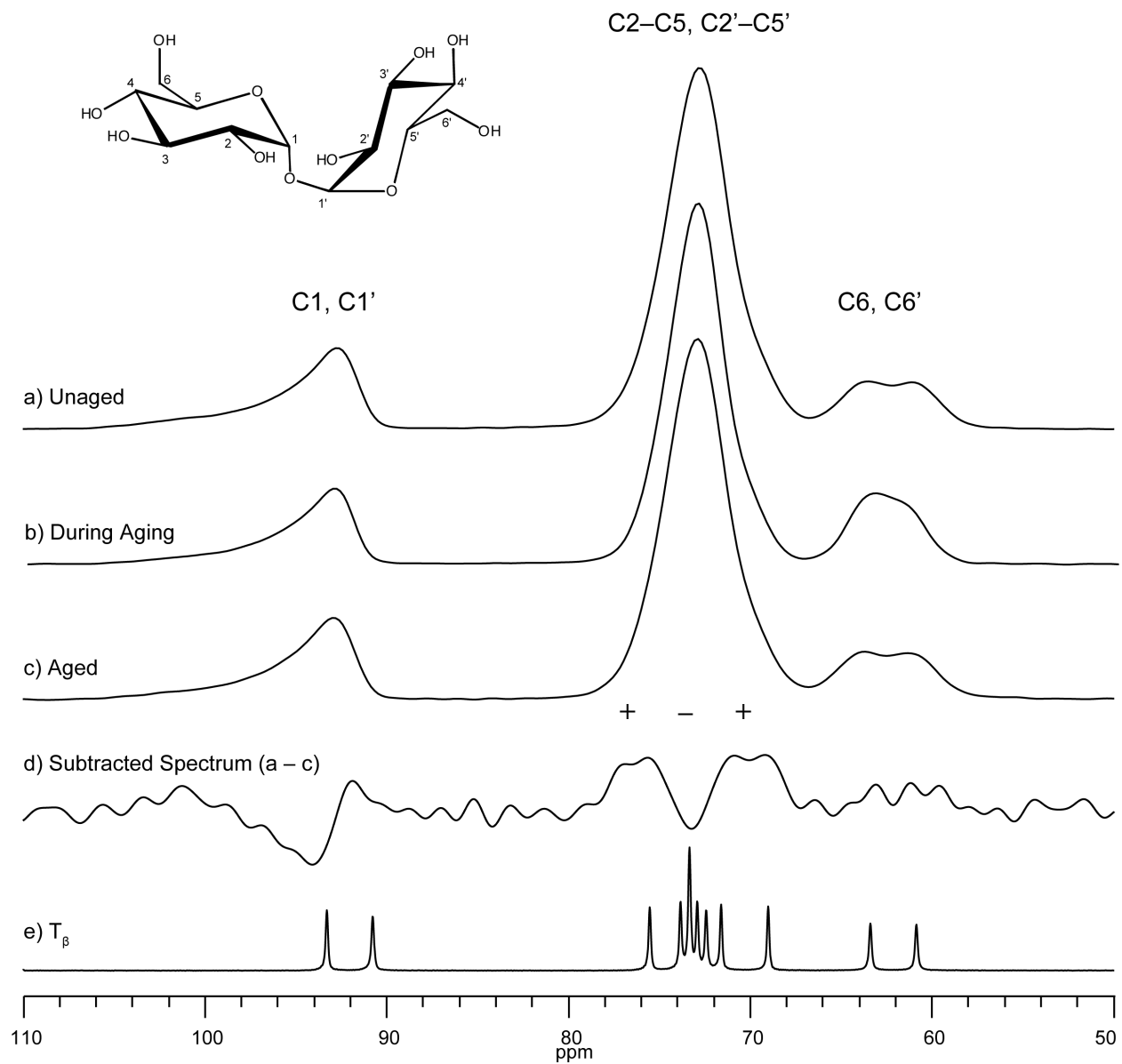


Figure 8.6. ^{13}C SSNMR spectra of amorphous trehalose prepared by lyophilization (a, b, c), the spectrum that results when the spectrum of the aged sample is subtracted from the spectrum of the unaged sample (d), and the spectrum of T_β (e). Spectra a, c, and e were acquired at room temperature, and spectrum b was acquired at 100 °C.

“+ – +” shape is observed in the region of the C1 and C1' carbons (90–110 ppm), showing a decrease in signal intensity between 90 and 92 ppm for the aged sample. After aging, there is an increase in the tendency of the material to crystallize to T_{β} , which might be expected to result in an increase in signal intensity near the chemical shifts of the T_{β} peaks in Figure 8.6c. In T_{β} , there is a peak at 90.7 ppm, and it is therefore surprising that there is a decrease in the signal intensity in this region for the aged sample. This suggests that if nuclei are present, either the spectra have not been acquired in a way that shows evidence of the nuclei or the nuclei are present at very low levels. This topic is addressed in Chapter 9. In a ^{13}C SSNMR spectrum, peaks from amorphous materials are broad due to the range of conformations and electronic environments of molecules in the amorphous state.⁵ Because the signal intensity is directly proportional to the number of carbons resonating at that frequency, the shape of an amorphous peak represents the population distribution of the molecules in these different conformations and environments. Depending on the thermal history of an amorphous sample, which includes both the preparation method and the storage conditions, some of these conformations may be more or less accessible to the molecules. Few molecules occupy the states that are represented by the chemical shifts at the edges of these broad peaks, suggesting that these states are not as energetically favorable. During aging, these molecules are expected to relax to more stable conformations. The narrowing of SSNMR peaks that was observed after aging translates to fewer molecules in the conformations/environments that are less favorable and is consistent with the narrowing of the glass transition.

In addition to changes in conformation, the ^1H T_1 relaxation time also changes. Prior to aging, the ^1H T_1 relaxation time of lyophilized T_{am} is 4.6 seconds, and after aging, it increases to 7.2 seconds. The error of the fit was less than 0.1 seconds. After aging and the structural relaxation that accompanies it, the trehalose molecules are less mobile. The increase in the ^1H T_1

relaxation time is consistent with this description of aging, and it is also consistent with an increase in the onset temperature of the glass transition. Molecules in the glassy state that are less mobile will require more energy (higher temperature) to transition to the rubbery state. The MDSC and SSNMR analyses of lyophilized T_{am} are consistent with each other and with expectations of how an amorphous material behaves after aging.

8.3.3 Amorphous Trehalose Prepared by Dehydration of Trehalose Dihydrate

Figure 8.7 shows an image of amorphous trehalose prepared by dehydration of T_h . T_{am} prepared by dehydration of T_h at 125 °C retains the morphology of the original T_h particles whereas T_{am} prepared by lyophilization was flaky (Figure 8.1). Results from the hot-stage microscopy experiments presented in Chapter 6 showed that softening of the glassy material occurs at temperatures closer to 135 °C; therefore, dehydration at 125 °C is high enough to quickly dehydrate the sample and destroy the crystal lattice, but it is not high enough for the material to soften and lose its morphology. Like lyophilized T_{am} , dehydrated T_{am} is largely non-birefringent, but there are brightly colored blue and yellow areas in the center of the dehydrated T_{am} . Upon closer inspection, there appears to be an air bubble in the middle of the dehydrated particle, and the birefringent areas are on the surface of the bubble. The presence of this bubble, and many others that have been observed during dehydrations at 125 °C, is consistent with the trapping of water vapor in the interior of partially dehydrated T_h particles. Other groups have observed the formation and migration of bubbles through particles of T_h upon heating.¹⁷⁻¹⁹ As described in §8.3.2, it is possible that the birefringence on the surface of the bubbles does not result from a crystalline component and instead is due to an ordered network of surface molecules.

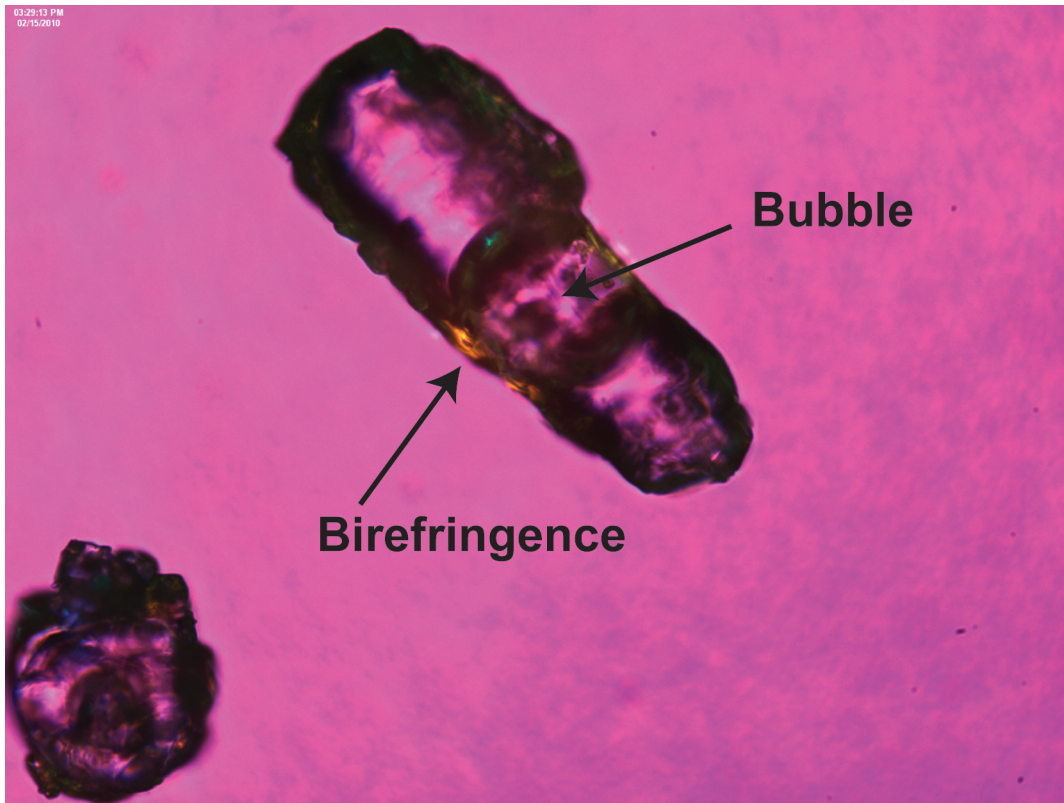


Figure 8.7. Image of dehydrated amorphous trehalose (T_{am}) from polarized light microscopy.

Figure 8.8 shows the reversible and non-reversible heat flow signals from MDSC experiments performed on dehydrated T_{am} , both before and after aging at 100 °C for 24 hours. Thermograms of both samples contain a glass transition (A), with midpoints at about 118 °C (unaged) and 120 °C (aged). Like lyophilized T_{am} , the endpoint temperature of each glass transition is about 123 °C, but the onset temperatures of about 114 °C (unaged) and 116.5 °C (aged) are several degrees lower than what was observed for lyophilized T_{am} . The thermogram of the aged sample contains an enthalpic recovery peak in the non-reversible signal; this peak is unusually broad and appears to consist of two poorly resolved peaks. Its magnitude of about 5 J/g is similar to the extent of relaxation in aged lyophilized T_{am} . To the best of our knowledge, a similarly broad glass transition of T_{am} has not been reported in the literature. As a result, additional experiments were performed in order to investigate this unusual glass transition.

Figure 8.9 shows the conventional DSC thermograms of a dehydrated T_{am} sample immediately after preparation and after storage for four days at room temperature in a desiccator. After preparation, the width of the glass transition is less than 6 degrees and is similar to the shape that was observed for lyophilized T_{am} in Figure 8.4. After four days, the width has increased to almost 15 degrees and resembles the shape of the glass transition for dehydrated T_{am} (Figure 8.8). The change in the glass transition suggests that dehydrated T_{am} undergoes structural changes even when stored ~ 100 °C below its T_g .

Figure 8.10 shows conventional DSC thermograms of aged dehydrated T_{am} samples over a 10-day period. In order to provide additional insight into the differences between dehydrated T_{am} and lyophilized T_{am} , conventional DSC thermograms of aged lyophilized T_{am} subjected to the same treatment are also shown in Figure 8.10. The appearances of the glass transition and

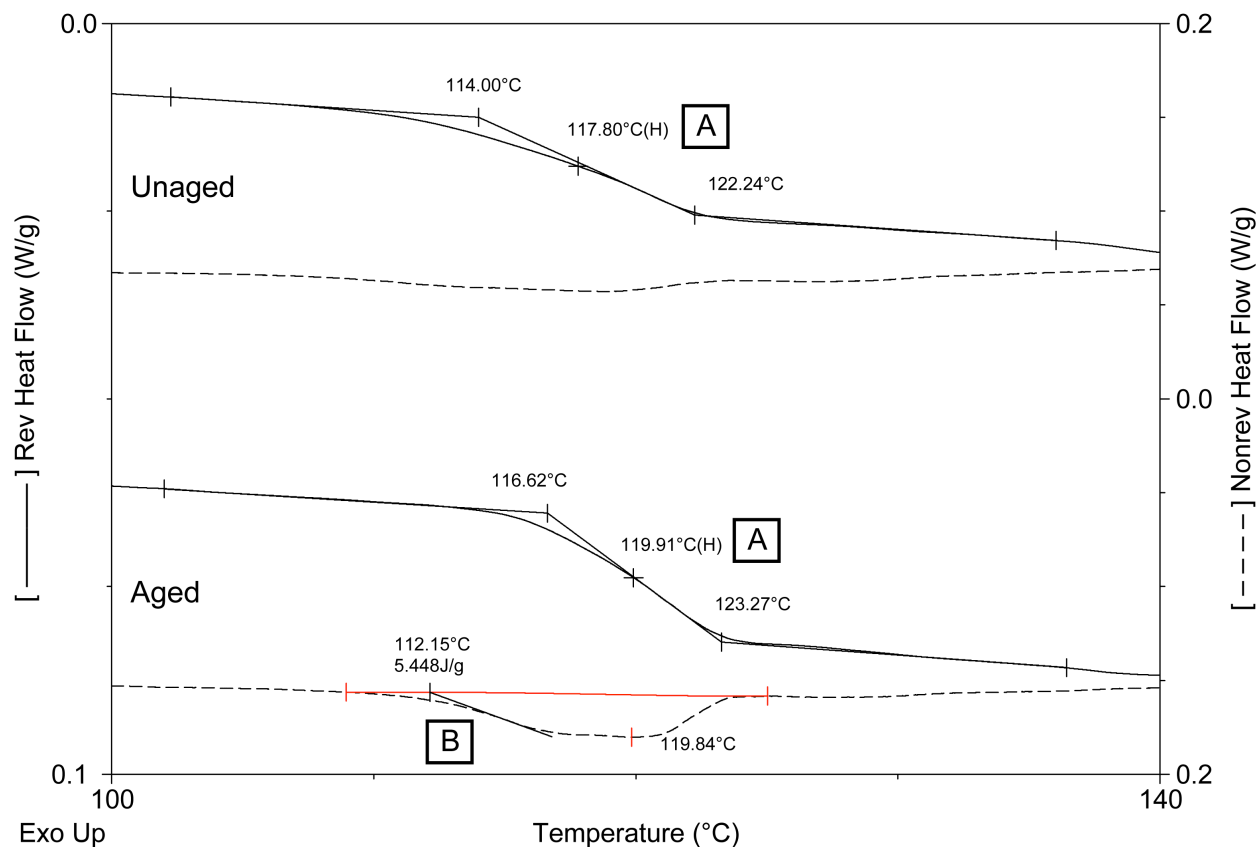


Figure 8.8. MDSC thermograms containing the reversible and non-reversible heat flow signal of amorphous trehalose prepared by dehydration of T_h . Thermograms of the material both before and after aging at 100 °C for 24 hours are shown. The glass transition (A) is found in the reversible signal, and the enthalpic recovery (B) is found in the nonreversible signal.

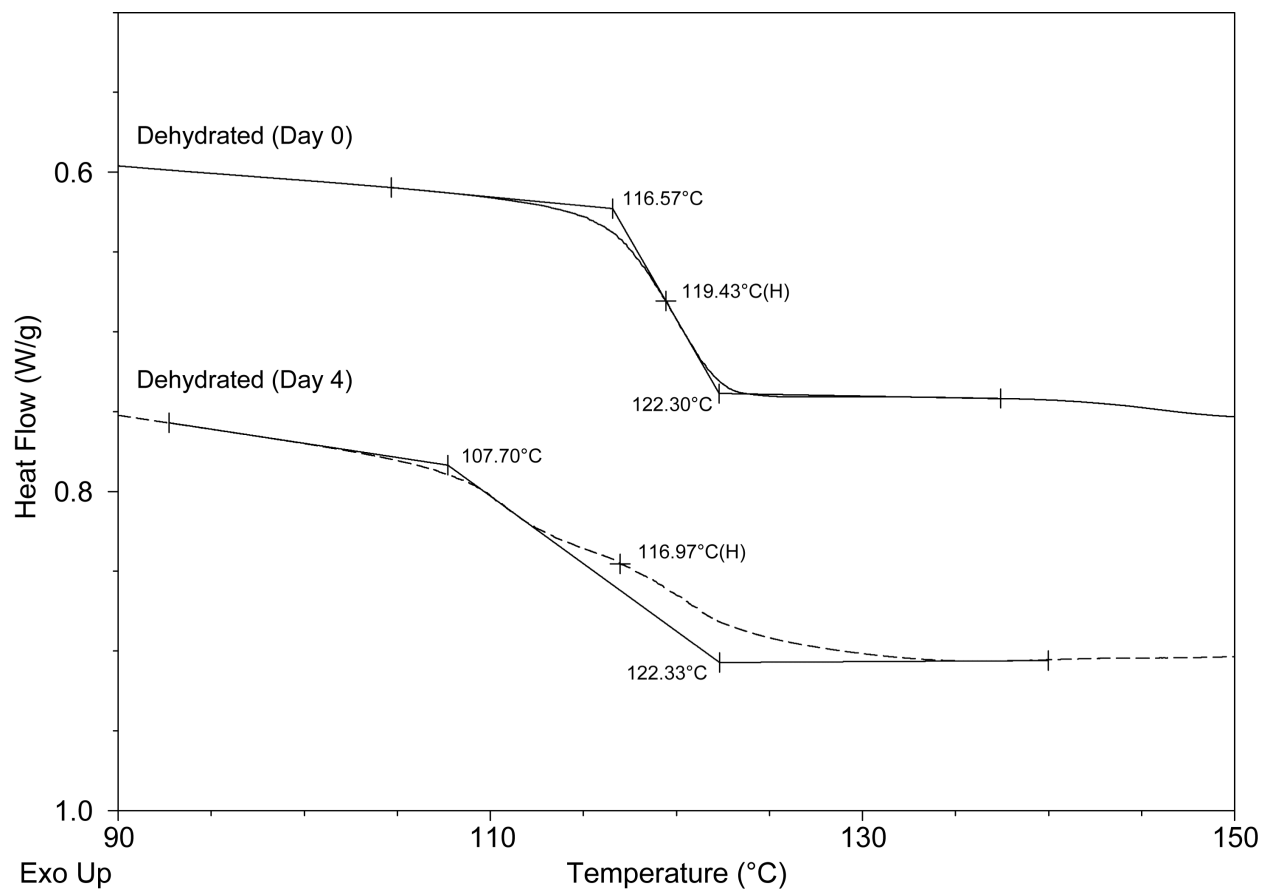


Figure 8.9. DSC thermograms of amorphous trehalose prepared by dehydration of trehalose dihydrate on an aluminum weighing dish in a vacuum oven at 125 °C for 15 minutes. After storing the material for four days in the presence of desiccant, the onset and midpoint temperatures decrease, resulting in a broader glass transition.

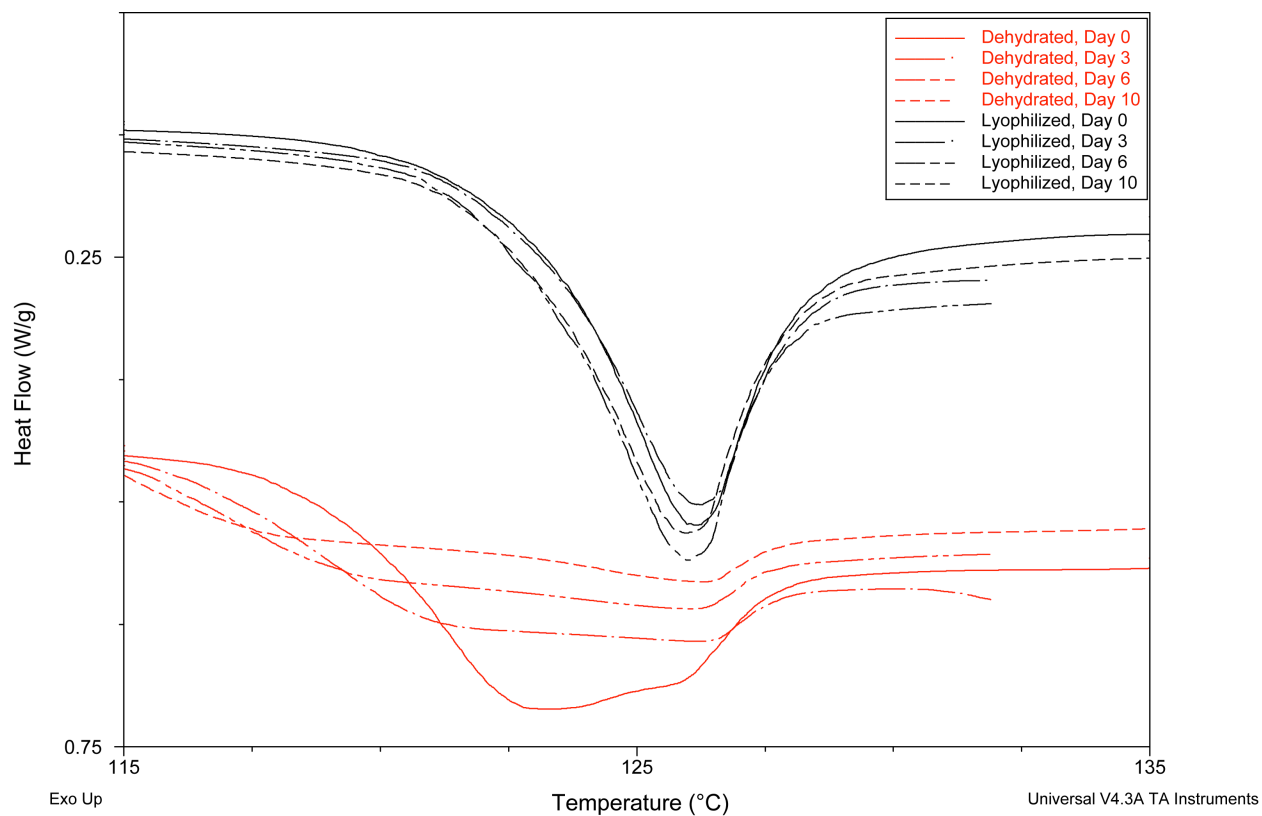


Figure 8.10. DSC thermograms of aged amorphous trehalose prepared by lyophilization and dehydration of trehalose dihydrate. The glass transitions with enthalpic recovery are shown. Over ten days, there is no change in the appearance of these events for the lyophilized sample. For the dehydrated sample, the glass transition becomes broader and the enthalpic recovery peak becomes shallower.

enthalpic recovery peak of the lyophilized sample do not change after ten days, suggesting that this material does not undergo structural changes during storage at room temperature. However, the appearance of the glass transition of the dehydrated sample changes dramatically, with a progressively lower onset temperature over time. The endpoint of the transition does not change, and so the enthalpic recovery peak becomes much shallower. The changes shown in Figures 8.9 and 8.10 suggest that the heterogeneity of dehydrated T_{am} increases as it is stored at room temperature, indicating that the molecules are mobile nearly 100 °C below the T_g . This increase in heterogeneity is not observed for lyophilized T_{am} and is further explored in §8.4.1.

Figure 8.11 shows the crystallization exotherms (A) and melting endotherms (B) in the total heat flow signal from MDSC experiments performed on dehydrated T_{am} , both before and after aging at 100 °C. After aging, the onset temperature of crystallization decreases by about 9 °C, from ~168 °C to ~159 °C. This indicates that, like lyophilized trehalose, aging increases the crystallization tendency of dehydrated amorphous trehalose. Crystallization of dehydrated T_{am} begins about 15 °C below crystallization of lyophilized T_{am} . For the dehydrated samples, the enthalpies of crystallization and melting do not change significantly after aging, and $\Delta H_{melting} > \Delta H_{crystallization}$. In Chapter 6, this seemed to indicate that T_β was present prior to crystallization from the rubbery state. If present, crystalline T_β should be detected with SSNMR.

Figure 8.12 shows the ^{13}C SSNMR spectra of dehydrated T_{am} samples. The spectra of the sample prior to aging, during aging, and after aging (Figure 8.12a–c) are consistent with the spectra of lyophilized T_{am} in Figure 8.6a. Despite the lower onset of crystallization observed for dehydrated T_{am} samples, the SSNMR spectra in Figure 8.12 do not indicate that T_β is present in these samples. It is possible that T_β nuclei are present and are not detected under these acquisition conditions; this is addressed in Chapter 9. Also shown in Figure 8.12 is the subtracted

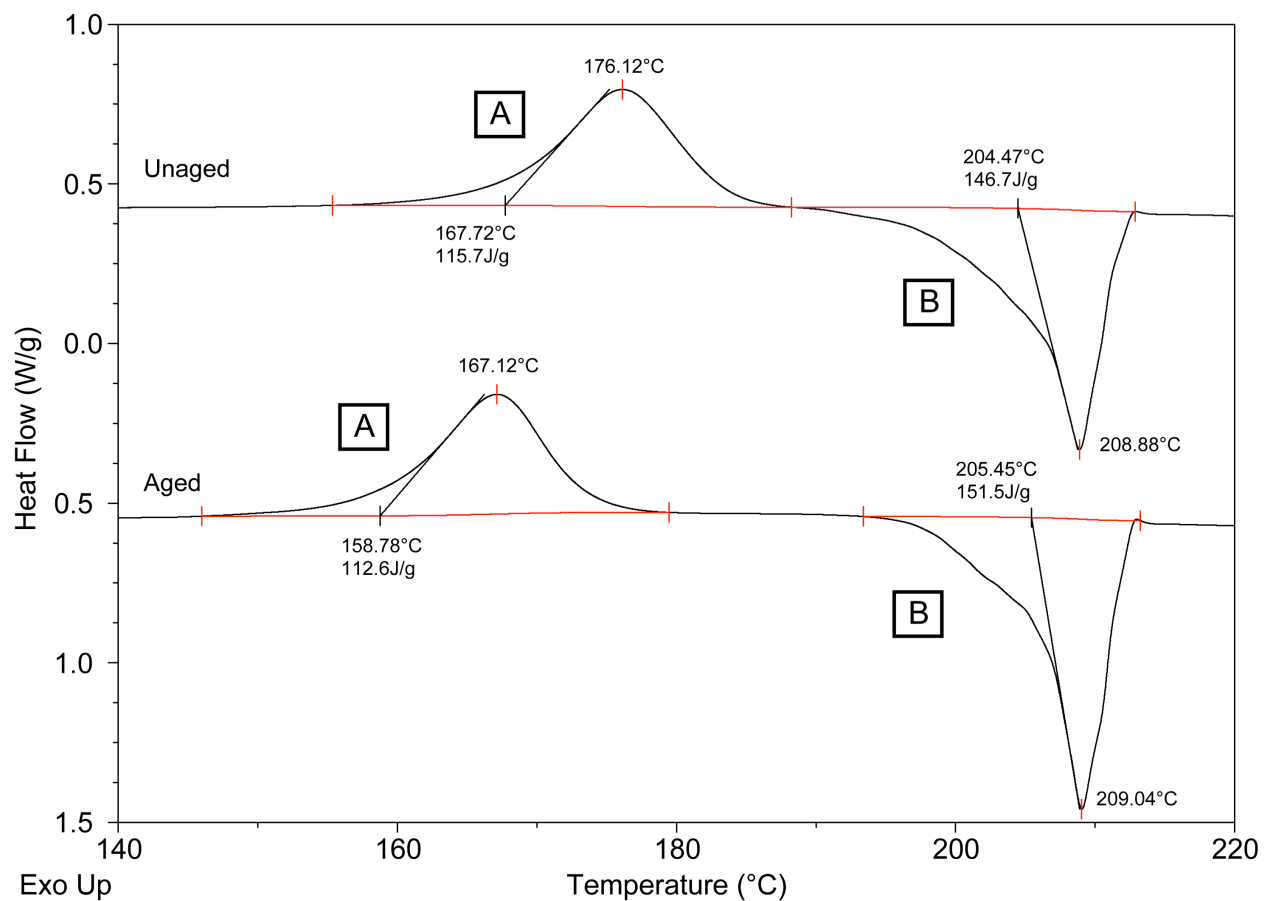


Figure 8.11. MDSC thermograms containing the total heat flow signal of amorphous trehalose prepared by dehydration of trehalose dihydrate both before and after aging at 100 °C for 24 hours. Crystallization exotherms (A) and melting endotherms (B) corresponding to T_{β} are labeled.

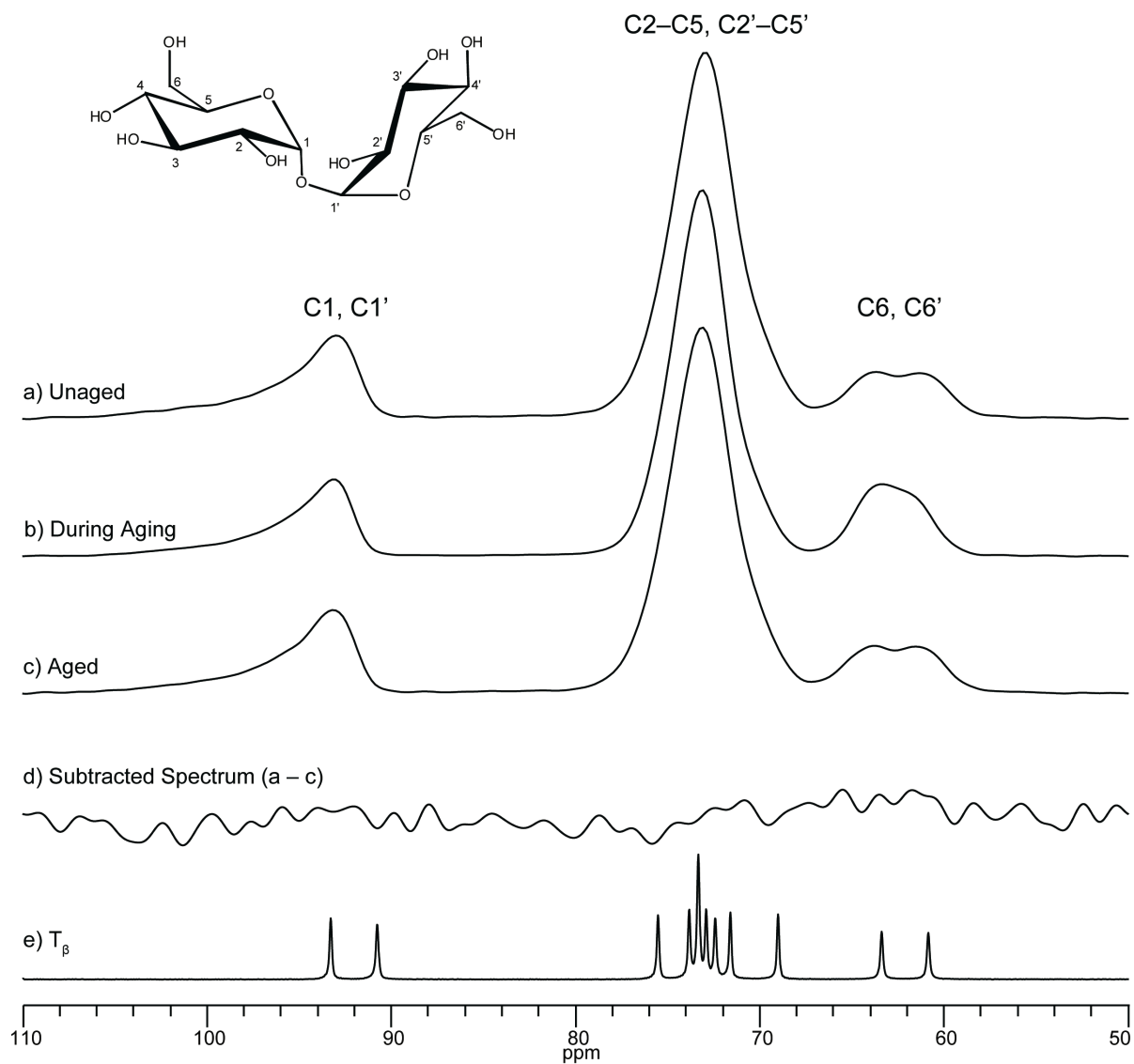


Figure 8.12. ^{13}C SSNMR spectra of amorphous trehalose prepared by dehydration (a, b, c), the spectrum that results when the spectrum of the aged sample is subtracted from the spectrum of the unaged sample, and the spectrum of T_β (e). Spectra a, c, and e were acquired at room temperature, and Spectrum d was acquired at 100 °C.

spectrum (d) that results when the spectrum in Figure 8.12c (aged) is subtracted from the spectrum in Figure 8.12a (unaged). This subtracted spectrum contains no features above the noise level, indicating that there are no structural differences between unaged and aged amorphous trehalose prepared by dehydration of T_h .

Prior to aging, the ^1H T_1 relaxation time is 7.8 ± 0.1 seconds, and after aging, it decreases slightly to 7.4 ± 0.1 seconds. Unlike lyophilized T_{am} , the ^1H T_1 relaxation time of dehydrated T_{am} does not increase after aging. The results from the MDSC experiments indicated that the dehydrated material changed during aging: enthalpic relaxation occurred, the glass transition became narrower, and the crystallization tendency increased. Despite these changes in the thermal behavior, results from SSNMR experiments do not indicate that any structural changes occurred during aging.

8.3.3 Comparison of ^{13}C SSNMR Spectra of Amorphous Trehalose

Figure 8.13 contains the ^{13}C SSNMR spectra of dehydrated T_{am} , lyophilized T_{am} , and the result when the spectrum of lyophilized T_{am} is subtracted from the spectrum of dehydrated T_{am} . Between 58 and 66 ppm (C6 and C6'), the subtracted spectrum contains only noise, but in other regions, there are features that may be considered broad peaks. There is a “- + -” shape between 80 and 66 ppm, indicating that the peak in the spectrum of lyophilized T_{am} is broader than that in the spectrum of dehydrated T_{am} . These small differences in the peak shapes do not appear to show that there are structural differences corresponding to different amorphous states of trehalose with different physical properties. However, they may indicate molecular reorganization of dehydrated T_{am} that is suggestive of pre-nucleation events.

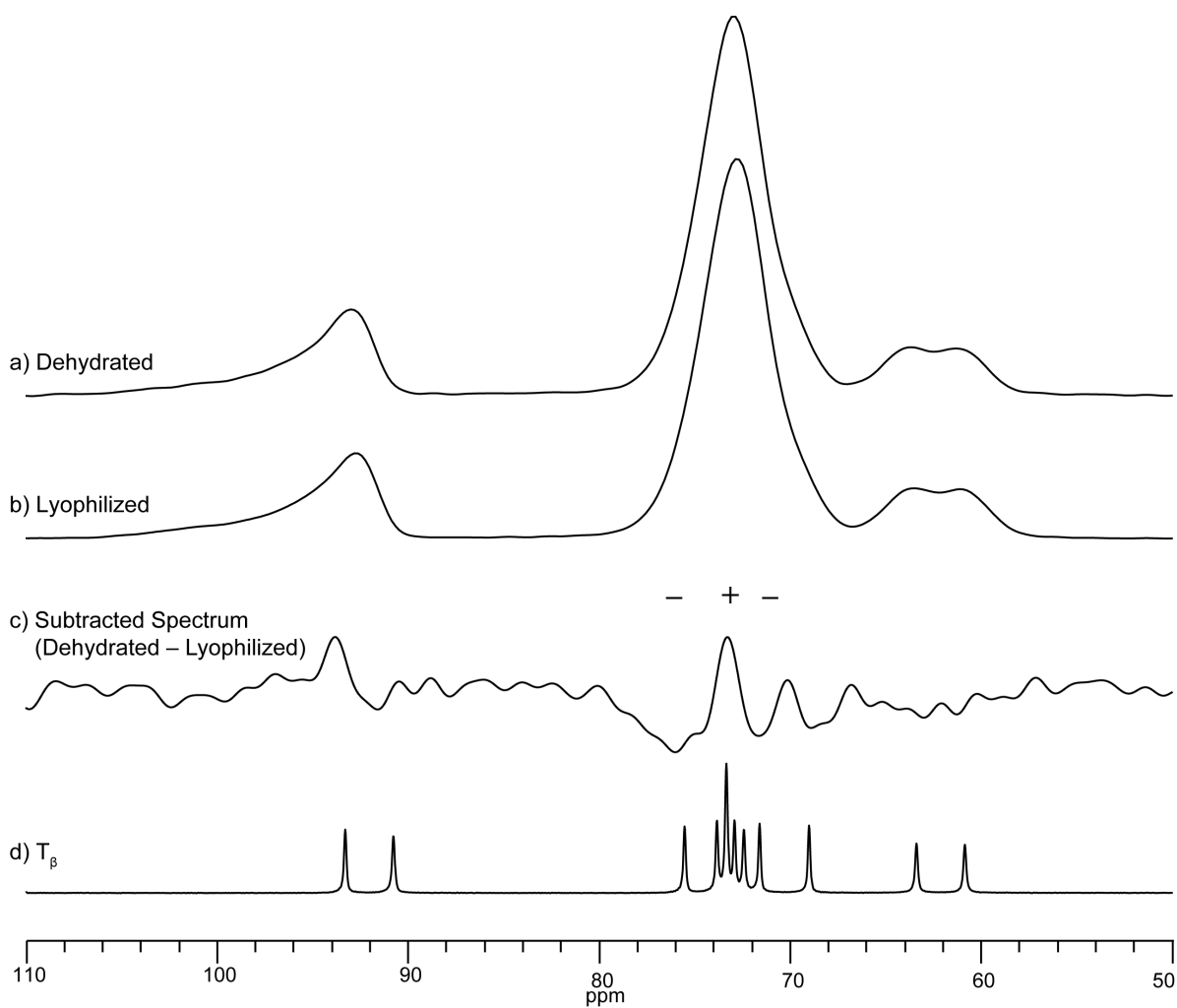


Figure 8.13. ^{13}C SSNMR spectra of amorphous trehalose prepared by dehydration (a) and lyophilization (b), the spectrum that results when the spectrum of the lyophilized sample is subtracted from the spectrum of the dehydrated sample, and the spectrum of T_β (d).

8.4 Discussion

Lyophilization and dehydration of T_h both result in amorphous trehalose, and samples of T_{am} prepared using these techniques exhibit many similarities:

1. PLM images show that the samples are largely non-birefringent with some areas of birefringence that could indicate organization of surface molecules.
2. MDSC experiments show that the thermal behavior of both samples responds similarly to aging: the magnitude of each enthalpic recovery peak is about 5 J/g, the T_g shifts to a higher temperature, and the crystallization onset decreases by about 9 °C.
3. ^{13}C SSNMR spectra of lyophilized and dehydrated materials are nearly identical, and after aging, their ^1H T_1 relaxation times are the same.

These observations suggest that there do not appear to be structural differences that are indicative of two distinct forms of amorphous trehalose. However, some of the results show that dehydrated T_{am} and lyophilized T_{am} differ in several ways:

1. PLM images show that dehydrated T_{am} and lyophilized T_{am} have different morphologies.
2. MDSC experiments show that dehydrated T_{am} undergoes its glass transition over a broader, lower temperature range than lyophilized T_{am} and crystallizes to T_β at lower temperatures than lyophilized T_{am} . Additionally, broadening of the glass transition and enthalpic recovery peak of dehydrated T_{am} occurs over time, while these transitions remain unchanged in lyophilized T_{am} . Also, for dehydrated T_{am} , $\Delta H_{\text{melting}} > \Delta H_{\text{crystallization}}$, but for lyophilized T_{am} , $\Delta H_{\text{crystallization}} \approx \Delta H_{\text{melting}}$.
3. The SSNMR ^1H T_1 relaxation time of unaged lyophilized T_{am} is shorter than that of unaged dehydrated T_{am} , and the ^{13}C SSNMR spectra do not exhibit the same response to

aging: peaks in the spectrum of lyophilized T_{am} become slightly narrower, and peaks in the spectrum of dehydrated T_{am} do not change.

The next paragraphs focus on explanations for the differences in thermal behavior, specifically the width of the glass transition and the onset of crystallization, and how those explanations relate to the SSNMR data.

8.4.1 Differences in the Glass Transitions of Amorphous Trehalose

The lower glass transition temperature of dehydrated T_{am} may result from higher water content. Water can act as a plasticizer to increase the mobility and lower the glass transition temperature of an amorphous material, and discrepancies in the reported glass transition temperatures of T_{am} of nearly 50 °C were suspected to be due to residual moisture.^{20, 21} More recently, Green et al. showed that T_{am} with 0% water has a T_g of about 116 °C while T_{am} with 1.5% water has a T_g of about 98 °C.¹⁵ Thermogravimetric analyses show very similar water contents of dehydrated T_{am} and lyophilized T_{am} (both <0.7%), and the water content of the dehydrated T_{am} was slightly lower than that of lyophilized T_{am} . Consequently, it does not appear that the difference in the glass transition temperatures can be explained by the presence of water. Additional support is provided by the observation that dehydrated T_{am} has a longer 1H T_1 relaxation time than lyophilized T_{am} : increased mobility due to the presence of water might also be expected to lower the 1H T_1 relaxation time.

The glass transition of dehydrated T_{am} occurs over a temperature range that can be more than twice as large as that of lyophilized T_{am} , suggesting that the dehydrated sample is more heterogeneous. Unexpectedly, the heterogeneity of dehydrated T_{am} appears to increase during

storage at room temperature. In reaching the amorphous state directly from the solid state, such as by dehydrating a hydrate, it is possible that the amorphous material retains the heterogeneity of the original solid. It has been shown that vacuoles form in particles of T_h as water leaves the crystal structure,¹⁷ and vacuoles formed during the dehydration at 125 °C may also contribute to the microscopic heterogeneity of the amorphous material. It is expected that a more homogeneous amorphous material will be produced when starting with a solution of trehalose, as occurs when T_{am} is prepared by lyophilization. If the dehydrated T_{am} sample is more heterogeneous, the SSNMR peaks for this sample are expected to be broader. However, the subtracted spectrum in Figure 8.13c shows that the peak between 80 and 66 ppm for lyophilized T_{am} is broader.

The SSNMR relaxation times do not appear to correlate with the MDSC data. It is surprising that lyophilized T_{am} has the second highest T_g onset and the shortest 1H T_1 relaxation time because faster mobility is usually associated with a shorter relaxation time: a higher onset temperature of the glass transition suggests slower mobility. When lyophilized T_{am} was aged, a higher T_g onset was accompanied by an increase in 1H T_1 relaxation time. 1H T_1 relaxation times of dehydrated T_{am} (before and after aging) and aged lyophilized T_{am} are all approximately the same, yet these samples differ in their thermal behavior. It may be that the types of motion influencing the T_g near 120 °C are unrelated to the 1H T_1 relaxation times that are measured at room temperature.

It is possible that the DSC and SSNMR results are contradictory because the two methods measure different properties of the amorphous material. The homogeneity of the lyophilized T_{am} is reflected in its narrow glass transition, and the heterogeneity of the dehydrated T_{am} is reflected in its broad glass transition. While the lyophilized T_{am} is homogeneous, it is also in a higher

energy state; its shorter $^1\text{H } T_1$ relaxation time is representative of this. Because the lyophilized T_{am} was exposed to temperatures less than or equal to $60\text{ }^\circ\text{C}$ during the lyophilization cycle, it did not have the opportunity to undergo structural relaxation during preparation. Conversely, dehydrated T_{am} was formed at $125\text{ }^\circ\text{C}$, and the extra energy available at this temperature enabled the formation of lower energy regions; this is demonstrated by its longer $^1\text{H } T_1$ relaxation time. However, the lower energy regions are likely surrounded by voids that result from the evacuation of water from the crystalline particles. Effectively, the result is an amorphous material with a higher concentration of surface molecules, which have been shown to lower the glass transition temperature.²² The widening of the glass transition of dehydrated T_{am} at room temperature suggests that the higher energy molecules near the voids in the particle are mobile and can undergo motions that reduce the concentration of the voids.

Figure 8.14 contains images depicting the possible heterogeneity of dehydrated T_{am} and homogeneity of lyophilized T_{am} . Immediately after preparation, the lyophilized T_{am} is quite homogeneous and the dehydrated T_{am} contains vacuoles on the order of a few molecules resulting from the loss of water (Figure 8.14a). While both lyophilized T_{am} and dehydrated T_{am} appear to be macroscopically homogeneous, the dehydrated T_{am} is heterogeneous on a molecular level. This molecular-level heterogeneity is too small to be reflected in the DSC thermograms,²³ i.e. both glass transitions are narrow after preparation. Upon storage at room temperature, the free volume and enthalpy of the lyophilized T_{am} may decrease slightly (Figure 8.14b–d). As dehydrated T_{am} is stored, small motions occur that serve to form larger vacuoles from the smaller vacuoles and decrease the surface area within the material. Because the material is “locked in” to the morphology of the particle, as is seen in Figure 8.7, a traditional decrease in free volume cannot occur. Eventually, the dehydrated T_{am} becomes macroscopically heterogeneous, which

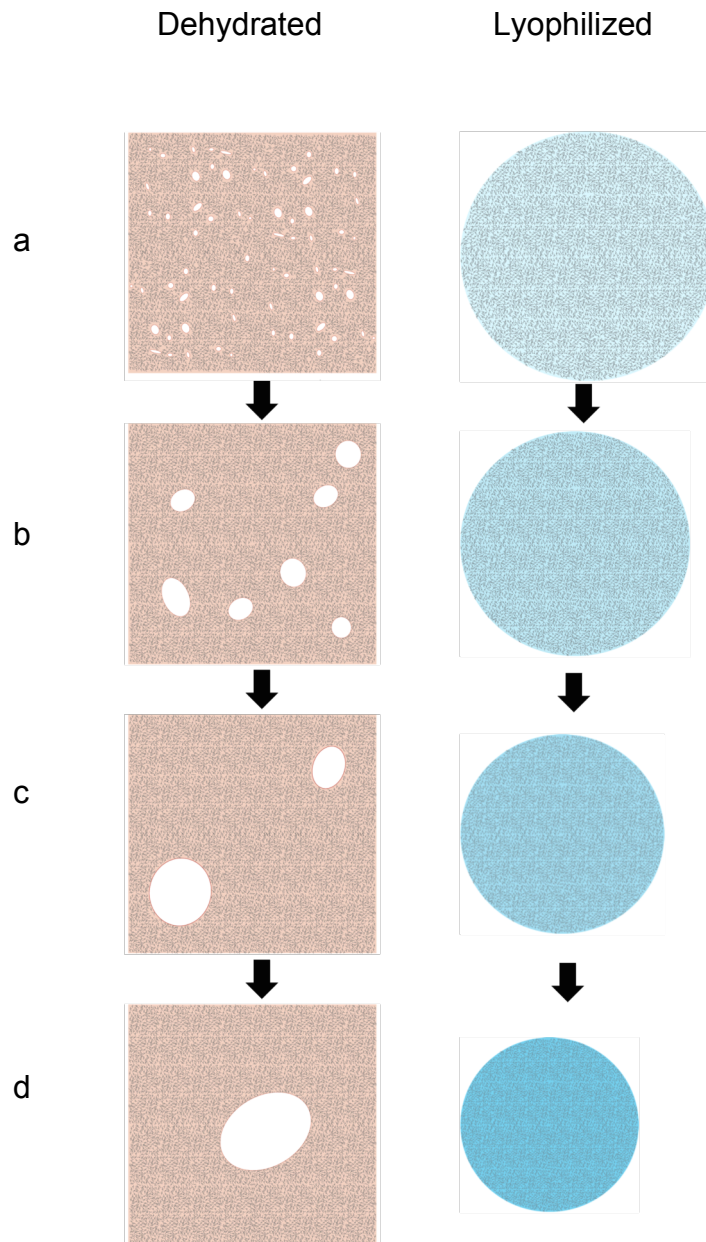


Figure 8.14. Representation of the heterogeneity of dehydrated T_{am} and lyophilized T_{am} . Upon storage (a–d), the macroscopic heterogeneity of dehydrated T_{am} increases as larger vacuoles form from the smaller vacuoles that are created upon dehydration.

is reflected in the broadening of the glass transition. In the proposed model in Figure 8.14, the enthalpy of the dehydrated T_{am} does not decrease upon storage at room temperature because the material likely underwent structural relaxation during preparation.

8.4.2 Differences in the Crystallization Tendencies of Amorphous Trehalose

Crystallization takes place in the rubbery state, where molecules have enough energy to undergo the translational and rotational motions that are required for crystallization.¹⁶ Dehydrated T_{am} has a lower glass transition temperature than lyophilized T_{am} , and so it enters the rubbery state at a lower temperature than lyophilized T_{am} . It is possible that increased mobility of dehydrated T_{am} at lower temperatures results in crystallization at a lower temperature. Dehydrated T_{am} spends more time in the rubbery state, potentially allowing for more crystallization to occur. However, the thermal behavior that is observed after aging is inconsistent with this idea: aging causes an increase in the glass transition onset temperature and a decrease in the crystallization onset temperature. Therefore, it may be that the effects of aging are not the same as the effects of preparation method, and one cannot be used to explain the other.

The higher tendency of dehydrated T_{am} to crystallize may result from a higher concentration of nuclei; however, it is unclear if crystal nuclei can be directly detected using DSC or SSNMR. Nuclei are more ordered than amorphous material, and they are expected to be less mobile. Therefore, the presence of nuclei could affect the surrounding amorphous material and its glass transition temperature. Figure 8.15 illustrates the possible differences in mobility that may be observed when nuclei are present in an amorphous sample. For comparison, mobility

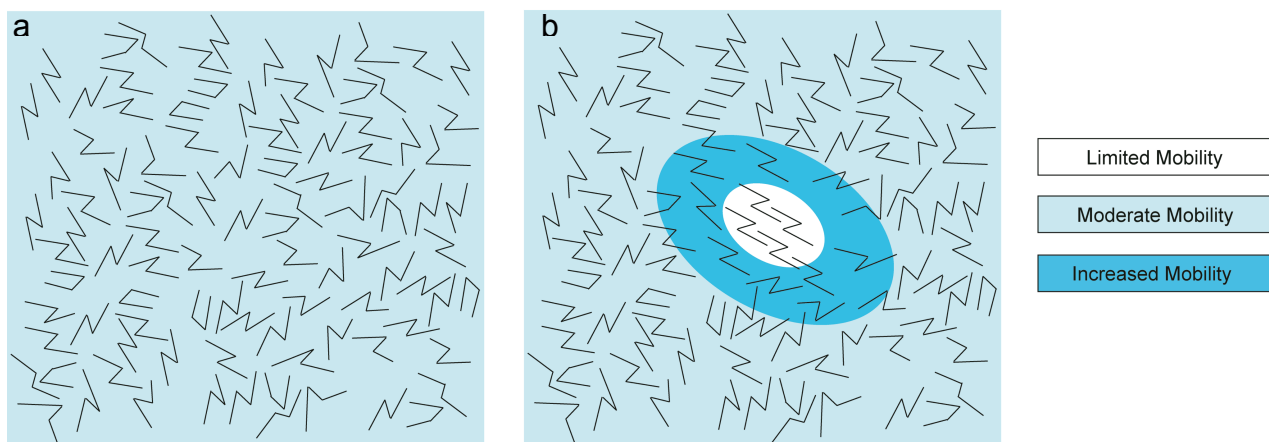


Figure 8.15. Illustration of molecular mobility in an amorphous material (a) and an amorphous material with a crystal nucleus (b) The molecules surrounding a nucleus may experience increased mobility as they find the correct conformation and reversibly add to and leave from the nucleus.

in a sample without nuclei is also illustrated. It should be noted that this is not an alternative to the model proposed in Figure 8.14, and both may occur in the same sample. The T_g onset is lower for dehydrated samples, indicating that the disordered molecules surrounding the nuclei may actually be more mobile than those in completely disordered regions. Molecules near nuclei could undergo many small molecular motions in order to orient themselves properly to add to the nuclei. Addition of molecules to nuclei is reversible,²⁴ and so enhanced motion of molecules that are adding to and leaving the nuclei is possible. However, this motion would result in a decrease in the T_g onset after aging (assuming that nuclei form during the aging process), and this was not observed. Because nuclei are more ordered, they are expected to result in longer ^1H T_1 relaxation times and narrower lines in SSNMR spectra. In Chapter 9, SSNMR techniques to detect the presence of crystal nuclei and low levels of crystalline material are explored.

8.5 Conclusions

Using two methods, lyophilization and dehydration of T_h , samples of amorphous trehalose with different tendencies to crystallize were prepared. Dehydrated T_{am} samples crystallize at lower temperatures than lyophilized T_{am} samples, which is consistent with the literature. Subtle differences between the SSNMR spectra of lyophilized T_{am} and dehydrated T_{am} are too small to indicate that the system is polyamorphous. The glass transition of dehydrated T_{am} is significantly broader than that of lyophilized T_{am} , an observation that has not been previously reported. The larger width of the glass transition of dehydrated T_{am} is attributed to heterogeneity resulting from vacuoles formed upon dehydration and enhanced motion surrounding crystal nuclei. Both lyophilized T_{am} and dehydrated T_{am} undergo structural relaxation during aging at 100 °C, and they both display an increased tendency to crystallize

following aging. However, while the SSNMR results indicated changes in the lyophilized T_{am} after aging that indicate a decrease in less stable conformations (decreased line width, increased relaxation time), there were no SSNMR-detected changes in the dehydrated T_{am} . The reasons for the different tendencies to crystallize remain unclear and are further addressed in Chapter 9.

8.6 References

1. Surana, R.; Pyne, A.; Suryanarayanan, R. Effect of preparation method on physical properties of amorphous trehalose. *Pharm. Res.* **2004**, *21*, (7), 1167-76.
2. Sussich, F.; Cesáro, A. Trehalose amorphization and recrystallization. *Carbohydr. Res.* **2008**, *343*, 2667-2674.
3. Shalaev, E.; Zografí, G. The Concept of 'Structure' in Amorphous Solids from the Perspective of the Pharmaceutical Sciences. *Roy. Soc. Ch.*, 11-30.
4. Surana, R.; Pyne, A.; Suryanarayanan, R. Effect of aging on the physical properties of amorphous trehalose. *Pharm. Res.* **2004**, *21*, (5), 867-74.
5. Lefort, R.; Bordat, P.; Cesáro, A.; Descamps, M. Exploring the conformational energy landscape of glassy disaccharides by cross polarization magic angle spinning ^{13}C nuclear magnetic resonance and numerical simulations. II. Enhanced molecular flexibility in amorphous trehalose. *J. Chem. Phys.* **2007**, *126*, (1), 014511.
6. Zhang, P.; Klymachyov, A. N.; Brown, S.; Ellington, J. G.; Grandinetti, P. J. Solid-state ^{13}C NMR investigations of the glycosidic linkage in α,α' trehalose. *Solid State Nucl. Magn. Reson.* **1998**, *12*, 221-225.
7. Andrew, A. R.; Bradbury, A.; Eades, R. G. Removal of dipolar broadening of nuclear magnetic resonance spectra of solids by specimen rotation. *Nature* **1958**, *183*, 1802-1803.
8. Barich, D. H.; Gorman, E. M.; Zell, M. T.; Munson, E. J. 3-Methylglutaric acid as a ^{13}C solid-state NMR standard. *Solid State Nucl. Magn. Reson.* **2006**, *30*, (3-4), 125-129.
9. Dixon, W. T.; Schaefer, J.; Sefcik, M. D. Total suppression of sidebands in CPMAS carbon-13 NMR. *J. Magn. Reson.* **1982**, *49*, (2), 341-345.
10. Fung, B.; Khitritin, A.; Ermolaev, K. An improved broadband decoupling sequence for liquid crystals and solids. *J. Magn. Reson.* **2000**, *142*, (1), 97-101.

11. Pines, A.; Gibby, M. G.; Waugh, J. S. Proton-enhanced NMR of Dilute Spins. *J. Chem. Phys.* **1973**, *59*, 569-590.
12. Sundaramurthi, P.; Patapoff, T. W.; Suryanarayanan, R. Crystallization of Trehalose in Frozen Solutions and its Phase Behavior during Drying. *Pharm. Res.* **2010**, *27*, 2374-2383.
13. Sundaramurthi, P.; Suryanarayanan, R. Trehalose Crystallization During Freeze-Drying: Implications on Lyoprotection. *J. Phys. Chem. Lett.* **2010**, *1*, 510-514.
14. Sundaramurthi, P.; Suryanarayanan, R. Influence of Crystallizing and Non-crystallizing Cosolutes on Trehalose Crystallization During Freeze-Drying. *Pharm. Res.* **2010**, *27*, 2384-2393.
15. Green, J. E.; Sitaula, R.; Fowler, A.; Toner, M.; Bhowmick, S. Enthalpic relaxation of convective desiccated trehalose–water glasses. *Thermochim. Acta* **2007**, *453*, 1-8.
16. Bhugra, C.; Pikal, M. J. Role of Thermodynamic, Molecular, and Kinetic Factors in Crystallization From the Amorphous State. *J. Pharm. Sci.* **2008**, *97*, (4), 1329-1349.
17. Berton, B.; Dupray, V.; Atmani, H.; Coquerel, G. Gas vacuoles formation during the dehydration of trehalose dihydrate: a Raman microspectroscopy approach. *J. Therm. Anal. Calorim.* **2007**, *90*, 325-328.
18. Dupray, V.; Berton, B.; Ossart, S.; Atmani, H.; Petit, M.-N. Concomitant dehydration mechanisms in single crystals of α,α -trehalose. *Carbohydr. Res.* **2009**, *344*, 2539-2546.
19. Taylor, L. S.; York, P. Characterization of the Phase Transitions of Trehalose Dihydrate on Heating and Subsequent Dehydration. *J. Pharm. Sci.* **1998**, *87*, (3), 347-355.
20. Mehl, P. M. Solubility and glass transition in the system α -D-trehalose/water. *J. Therm. Anal.* **1997**, *49*, 817-822.
21. Chen, T.; Fowler, A.; Toner, M. Literature Review: Supplemented Phase Diagram of the Trehalose-Water Binary Mixture. *Cryobiology* **2000**, *40*, 277-282.

22. Forrest, J. A.; Dalnoki-Veress, K.; Stevens, J. R.; Dutcher, J. R. Effect of Free Surfaces on the Glass Transition Temperature of Thin Polymer Films. *Phys. Rev. Lett.* **1996**, *77*, (10), 2002-2005.
23. Newman, A.; Engers, D.; Bates, S.; Ivanisevic, I.; Kelly, R. C.; Zografi, G. Characterization of amorphous API:Polymer mixtures using X-ray powder diffraction. *J. Pharm. Sci.* **2008**, *97*, (11), 4840-4856.
24. Byrn, S. R.; Pfeiffer, R. R.; Stowell, J. G., *Solid-state chemistry of drugs*. SSCI, Inc.: 1999.

Chapter 9

Detection of Low Levels of Crystallinity Using SSNMR

9.1 Introduction

The results presented in Chapter 8 demonstrated that ^{13}C solid-state NMR (SSNMR) and differential scanning calorimetry (DSC) could be used to detect differences in samples of amorphous trehalose (T_{am}) that were prepared by dehydration of trehalose dihydrate (T_{h}) or lyophilization. However, these results could not be used to explain the higher tendency of dehydrated T_{am} to crystallize or the increased tendency of T_{am} to crystallize after aging. It has been suggested that different concentrations of crystal nuclei are responsible for different crystallization tendencies of T_{am} ,^{1, 2} and the methods used in Chapter 8 may not have been appropriate for the detection of crystal nuclei. Crystal nuclei or low levels of crystalline material may facilitate crystallization of an amorphous sample, resulting in the loss of the bioavailability advantage of an amorphous API or a decrease in the ability of an amorphous excipient to act as an effective stabilizer.³ Therefore, it is important to develop analytical techniques that can be used to detect any crystallinity or crystal nuclei as early as possible so that the stability of the amorphous material might be predicted.⁴ Often, crystal nuclei are not detected directly; instead, crystallization is viewed as evidence that nuclei are present.^{1, 2, 5-7} In this chapter, a new SSNMR method for the direct detection of very low levels of ordering in disordered samples is proposed and tested.

9.2 Experimental

9.2.1 Materials

D-(+)-trehalose dihydrate was purchased from Acros (Geel, Belgium), Fluka (Buchs, Switzerland), and Sigma (St. Louis, MO). Amorphous trehalose was prepared in three ways:

rapid dehydration of T_h , slow dehydration of T_h followed by annealing, and lyophilization. More details are provided in the following sections.

9.2.2 Dehydration of T_h

Two samples of T_h from Acros (180–425- μm fraction) were spread in a single layer in an aluminum weighing dish and placed in a vacuum oven at 125 °C for 15 minutes. A VWR Scientific Products vacuum oven (Model 1410M) was used, and the temperature was verified with a calibrated thermometer.

Using the same oven, two samples of T_h , one from Acros and one from Fluka, were dehydrated at 75 °C for two days under vacuum to generate mixtures of T_{am} , T_{α} , and T_{δ} . After acquiring a ^{13}C SSNMR spectrum of each sample, these samples were held at 110 °C in the magnet for about an hour in order to convert T_{α} and T_{δ} to T_{am} .

9.2.3 Lyophilization

Amorphous trehalose was prepared by lyophilization of a 10 % w/v aqueous solution of trehalose dihydrate using a VirTis AdVantage lyophilizer (SP Scientific, Warminster, PA) using the procedure of Surana et al.¹ Approximately 10 mL of solution was placed in 25 mL scintillation vials and cooled to -45 °C. Samples were subjected to primary drying at -45 °C and ~100 mTorr for 48 hours. The temperature was then increased to 50 °C over the next 24 hours, and then secondary drying proceeded at 50 °C for 24 hours. The temperature was increased to 60 °C over 24 hours and then held at 60 °C for 24 hours.

9.2.4 Aging

Two samples, one prepared by lyophilization and one sample produced by rapid dehydration, were aged for 10 hours at 100 °C using a Binder oven.

9.2.5 Differential Scanning Calorimetry (DSC)

DSC analyses were performed using a Thermal Analysis DSC Q2000 (TA Instruments; New Castle, DE). Samples were analyzed in aluminum hermetic pans with 3 pinholes in each lid. All samples were analyzed using a standard ramp method and were heated from 25 °C to 250 °C at a rate of 10 °C/min. under a dry nitrogen purge at 50 mL/min.

9.2.6 Solid-State NMR Spectroscopy

¹³C SSNMR spectra were acquired using a Tecmag Redstone spectrometer (Tecmag Inc., Houston, TX) operating at approximately 300 MHz for ¹H and 75 MHz for ¹³C. Samples were packed into 7.5-mm zirconia rotors and spun at the magic angle.⁸ The spinning speed was 4kHz. Peaks were referenced to the methyl peak of 3-methylglutaric acid, which was set to 18.84 ppm.⁹ Spectra were acquired using ramped cross polarization, Spinal 64 decoupling, and sideband suppression.¹⁰⁻¹² A contact time of 1 ms was used for all samples. 2048 transients were acquired at a pulse delay of 30 seconds and an acquisition length of 3072 points.

9.3 Results and Discussion

9.3.1 SSNMR Parameters

In acquiring SSNMR spectra of trehalose, parameters including the contact time, the acquisition length, and the pulse delay are varied for different solid forms. A contact time of 1 ms is suitable for all solid forms of trehalose, but the acquisition lengths and pulse delays vary greatly depending on which form is being analyzed. Therefore, analyzing a mixture of solid forms of trehalose can present a challenge.

9.3.1.1 Acquisition Length

Figure 9.1 shows typical free induction decays (FIDs) of T_{β} and T_{am} . The acquisition length (x-axis) is shown in units of time, which is calculated by multiplying the dwell time (the length of time between points) by the number of points. The acquisition length is related to the width of the peaks in a SSNMR spectrum: as peaks become broader, fewer points are required to define them. Amorphous materials are disordered and have very broad SSNMR peaks, and highly ordered crystalline materials have narrow peaks. For T_{β} , long acquisition lengths of ≥ 3072 points are used (Figure 9.1a), and for T_{am} , shorter acquisition lengths of 256 points are used (Figure 9.1b).

Figure 9.2 shows 256-point and 3072-point FIDs of T_{β} and the spectra that are obtained after the fourier transform (FT) is performed. When the proper number of points is used (Figure 9.2a), the resulting spectrum contains narrow peaks at specific chemical shifts. If too few points are used to acquire the spectrum of T_{β} (Figure 9.2b), the majority of the data in the FID is lost. Processing the shortened FID results in a spectrum with broad peaks and Gibbs

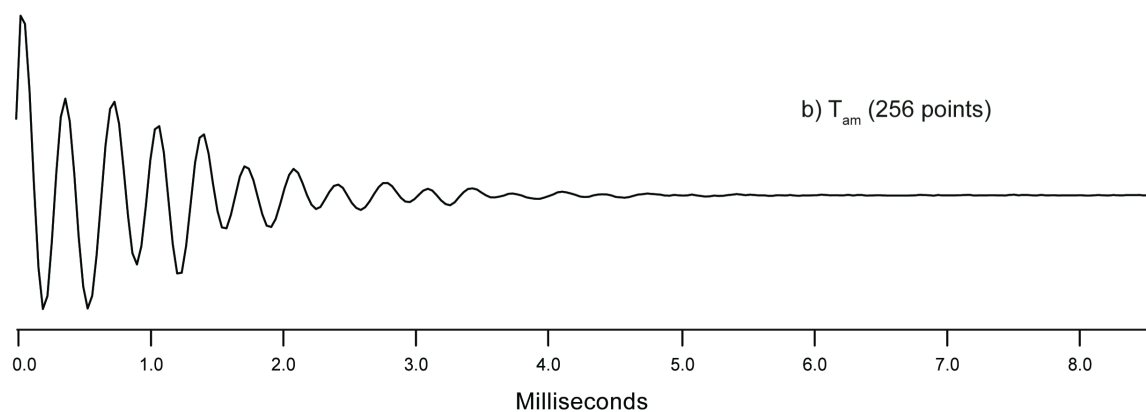
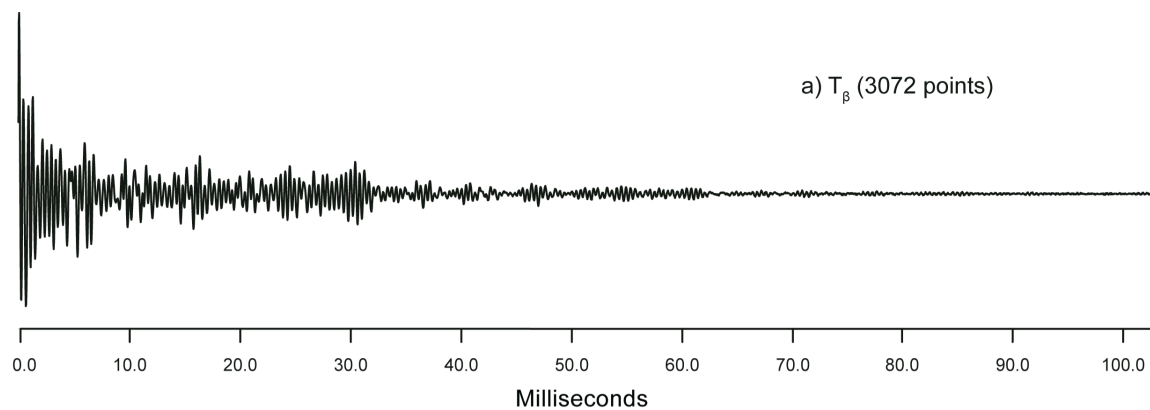


Figure 9.1. Typical free induction decays (FIDs) of T_{β} (a) and T_{am} (b). More points, and therefore more time, are required to acquire the signal from the crystalline material.

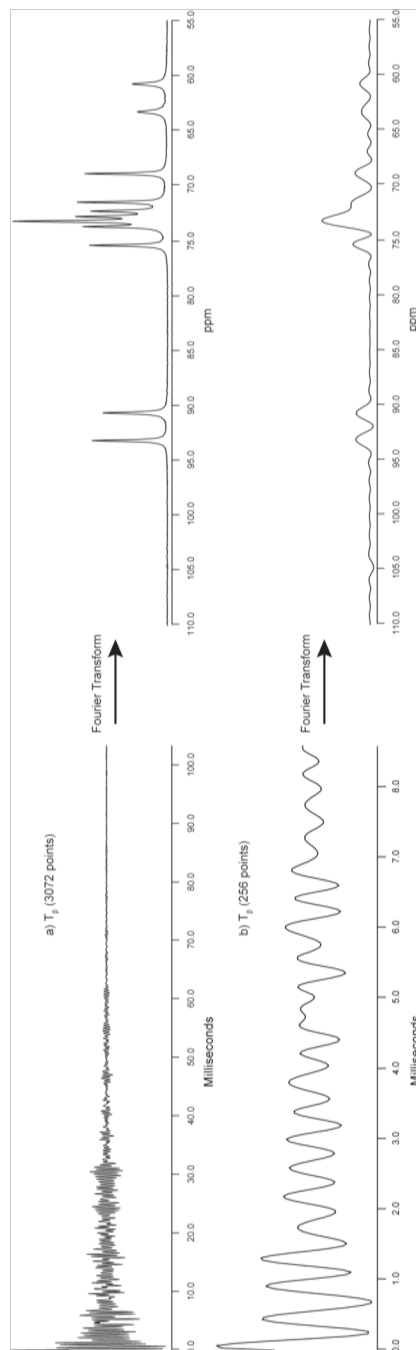


Figure 9.2. Comparison of FIDs and processed spectra of T_{β} when 3072 points (a) and 256 points (b) are acquired.

wiggles. This spectrum gives an approximate idea of where peaks might be located but nothing more.

Figure 9.3 shows 256-point and 3072-point FIDs of T_{am} and the spectra that are obtained after the fourier transform (FT) is performed. If too many points are used to acquire the spectrum of T_{am} , the result is a spectrum with excessive noise (Figure 9.3a). If very low levels of T_{β} are present, it could be difficult to differentiate these peaks from the noise. When the proper number of points is acquired, the result is a high quality spectrum of T_{am} , but indications of low levels of crystalline material may not be present.

9.3.1.2 Pulse Delay

Figure 9.4 shows simulated ^1H T_1 relaxation time curves that represent T_{am} and T_{β} . The curves were calculated using a ^1H T_1 relaxation time of 8 seconds for T_{am} and 90 seconds for T_{β} . The pulse delay is determined from the ^1H T_1 relaxation time, and it is related to the mobility of the sample. In the absence of a natural relaxation sink, as is the case for trehalose, crystalline forms typically have longer relaxation times than the amorphous form.¹³ When a pulse delay of 10 seconds is used to analyze a mixture of T_{am} and T_{β} , only about 10% of the T_{β} signal and about 70% of the T_{am} signal are detected (red line in Figure 9.4). When a pulse delay of 80 seconds is used, about 60% of the T_{β} signal and nearly 100% of the T_{am} signal is recovered (blue line in Figure 9.4). For T_{β} , long pulse delays (>100 seconds) are typically used, and for T_{am} , shorter pulse delays (<10 seconds) are typically used. If a shorter pulse delay is chosen to analyze an amorphous sample, the amount of signal recovered for the crystal nuclei or crystalline material (if present) may not sufficient for detection. However, using a long pulse delay when

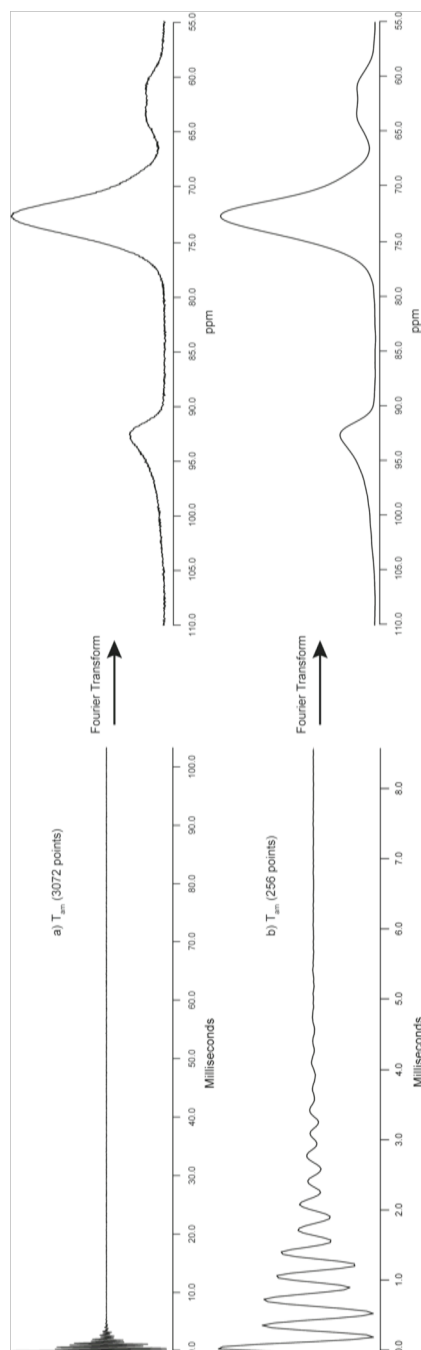


Figure 9.3. Comparison of FIDs and processed spectra of amorphous trehalose when 3072 points (a) and 256 points (b) are acquired.

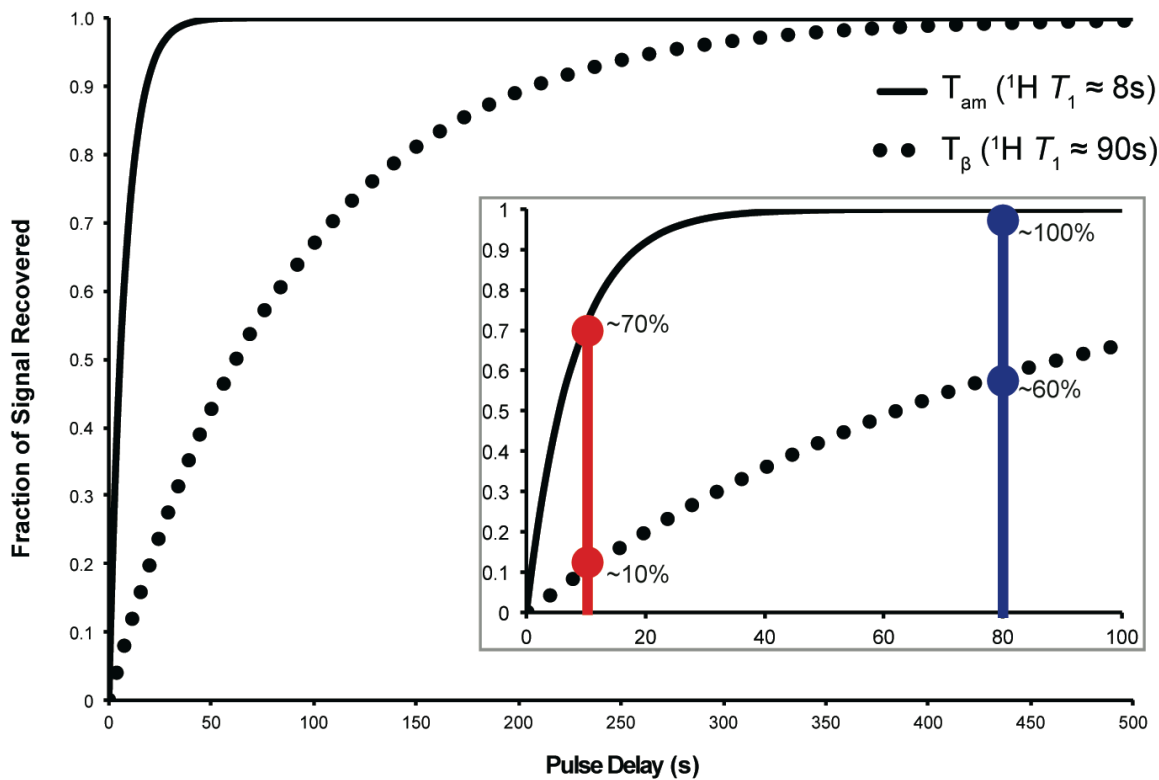


Figure 9.4. Hypothetical $^1H T_1$ curves for amorphous trehalose and the β -anhydrate. In the inset, the percent of signal recovered for each form is shown for two pulse delays.

analyzing T_{am} is inefficient because the signal intensity does not increase significantly when using a pulse delay longer than 30 seconds. In other words, the amount of signal recovered after 40 seconds is the same as after 80 seconds, yet the experiment is twice as long. Because the peaks corresponding to T_{am} are so broad, more acquisitions are needed to achieve the same signal-to-noise ratio that is expected from the spectra of T_{β} . Therefore, while using a longer-than-necessary pulse delay to analyze T_{am} may allow for the detection of crystalline material in the sample, it also results in a lower quality spectrum of the amorphous material. In addition, using a long pulse delay could lead to experiments that are prohibitively long.

9.3.1.3 Detection of Crystal Nuclei Using SSNMR

The SSNMR properties of crystal nuclei are unknown, making the detection of crystal nuclei in amorphous samples difficult. Crystal nuclei consist of 10–1000 molecules, and though they do not have the long-range order of a crystal, they do possess short-range order. Therefore, the peaks corresponding to crystal nuclei are expected to have narrower lines than those observed for amorphous material. It is expected that the FID resulting from crystal nuclei will more closely resemble the FID in Figure 9.1a, and therefore a longer acquisition length is most likely needed to properly analyze crystal nuclei. Ongoing work in the Munson lab shows that for rigid molecules without an internal relaxation sink, the ^1H T_1 relaxation time decreases as particle size decreases. A T_{β} nucleus of 1000 molecules is in the nanometer range, and its relaxation time is expected to be shorter than what has been measured for crystalline T_{β} . An intermediate pulse delay may be most appropriate to recover sufficient signal for detection of crystal nuclei.

Because the ideal SSNMR acquisition parameters for T_{am} , T_{β} , and crystal nuclei are not the same, acquiring a high-quality SSNMR spectrum of T_{am} that allows for analysis of the

amorphous material and detection of crystal nuclei (or low levels of crystalline material) in a reasonable amount of time presents a challenge. There are several analytical approaches that could be used to analyze a sample of amorphous trehalose that may contain crystal nuclei, but most techniques sacrifice one or more of these criteria. First, if one were interested only in seeing the possible contribution from T_β or T_β nuclei in a sample of amorphous trehalose, a long contact time could be used with a pulse delay and acquisition length optimized for T_β . T_β has a $^1\text{H } T_{1\rho}$ relaxation time of more than 300 milliseconds, and T_{am} has a $^1\text{H } T_{1\rho}$ of about 5 milliseconds. Using a contact time of 1 millisecond is sufficient to detect both, but a contact time of 25 milliseconds would suppress the T_{am} signal and show only the T_β signal. Similarly, if one were interested only in observing the amorphous signal, a very short pulse delay could be used to saturate the T_β signal and minimize the appearance of crystalline peaks. If the goal is to detect and analyze both components, as it is here, these options are not applicable. Finally, two spectra of an amorphous trehalose sample, one optimized for T_β and one optimized for T_{am} , can be acquired; however, it is impractical to consider acquiring multiple spectra for each sample due to the analysis times.

Figure 9.5 illustrates an alternative method that utilizes a spectral subtraction. In this method, one spectrum is acquired with a long acquisition length and an intermediate pulse delay of 30 seconds. The first step is to process the 3072-point FID in order to generate a “noisy” spectrum of T_{am} (Figure 9.5a). Small peaks corresponding to crystal nuclei or crystalline material may be hidden in the noise. The second step is to replace points 257–3072 in the original FID with zeroes and then process this altered FID to generate a nearly noise-free spectrum of T_{am} (Figure 9.5b). The last step is to subtract the noise-free spectrum from the “noisy” spectrum (Figure 9.5c). This subtracted spectrum contains very small peaks that are consistent with the

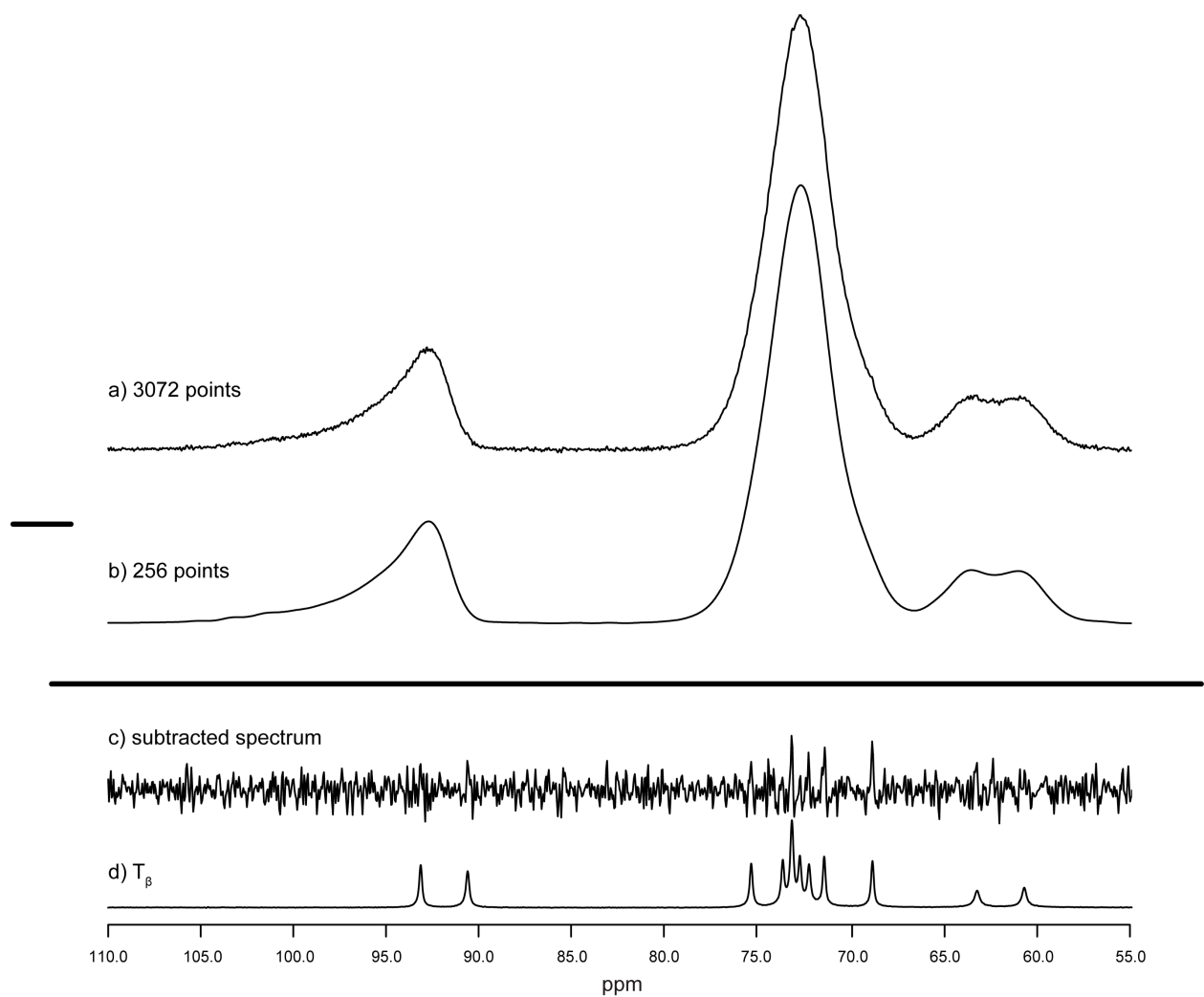


Figure 9.5. ^{13}C SSNMR spectra of amorphous trehalose using 3072 points (a) and 256 points (b) and the result of the spectral subtraction (c). Small peaks in the subtracted spectrum at about 69, 72, and 73 ppm are consistent with peaks in the spectrum of T_β .

chemical shifts characteristic of T_{β} (Figure 9.5d). This approach can only be successful for samples with very low levels of crystalline material. The signal due to crystalline material is still present in the shortened FID, but it has been manipulated in such a way that it disappears. If higher levels of T_{β} were present, the distorted spectrum that is seen in Figure 9.2b would be superimposed on the spectrum of the amorphous material. Collecting one spectrum with a long acquisition length and intermediate-to-long pulse delays offers a more efficient method of detection for low levels of crystalline material and structural differences in amorphous materials. After assessing the crystallization tendency of various samples of T_{am} using DSC, this SSNMR method was applied to several samples of T_{am} .

9.3.2 Assessment of Crystallization Tendency

Listed in Table 9.1 are the temperatures and enthalpies associated with the crystallization exotherms and melting endotherms (T_{β}) observed in DSC thermograms of various samples of T_{am} . The results for Samples 2 and 4 refer to the sample before annealing at 110 °C. When heated at 10 °C/minute, crystallization was observed in four of the seven samples. The lowest onset temperature, about 155 °C, was measured for Sample 4; this is more than 20 °C below the temperatures at which other samples begin to crystallize. Interestingly, the enthalpies of crystallization and melting for this sample were approximately equal and were less than half of the measured enthalpies for samples dehydrated at 125 °C. This suggests that crystallization of sample 4 was incomplete even though it was initiated at a much lower temperature. During other dehydration experiments, this sample often formed T_{β} directly from T_{h} . In this sample, T_{β} was formed at a lower temperature than in other samples, and it also melted at a lower temperature.

Table 9.1 Sample identifications, preparations, and crystallization results from DSC experiments. (DNC = Did Not Crystallize)

ID	Sample	Preparation	Aging/Annealing	Crystallization Onset (°C)	$\Delta H_{\text{crystallization}}$ (J/g)	Melting Peak (°C)	$\Delta H_{\text{melting}}$ (J/g)
1	Acros A0264819	125 °C/15min/vacuum		181.3 (0.6)	108.1 (8.6)	213.3 (0.1)	111.3 (1.4)
1A	Acros A0264819	125 °C/15min/vacuum	10 hrs at 100 °C	178.2	124.3	213.2	129.2
2	Acros A0285874	75 °C/2days/vacuum	~1 hr at 110 °C	DNC	DNC	DNC	DNC
3	Acros A0285874	125 °C/15min/vacuum		178.8 (0.4)	96.8 (0.8)	212.8 (0.1)	112.8 (2.5)
4	Fluka 90208	75 °C/2days/vacuum	~1 hr at 110 °C	155.1 (0.4)	45.9 (1.4)	201.1 (0.1)	44.4 (3.7)
5	Sigma 114K7064	Lyophilized		DNC	DNC	DNC	DNC
5A	Sigma 114K7064	Lyophilized	10 hrs at 100 °C	DNC	DNC	DNC	DNC

Aging of Sample 1, which was prepared by dehydrating T_h at 125 °C, resulted in a slight decrease in the crystallization onset temperature and an increase in the amount of T_β that was formed; this was also observed in Chapter 8, though the effect was more significant. Sample 5, which was prepared by lyophilization, did not crystallize under these experimental conditions, and aging of Sample 5 did not result in an increased tendency to crystallize. While this may appear to contradict the results presented in Chapter 8, the DSC experiments were performed under different conditions. The faster heating rate used in the experiments described in this chapter may not have allowed the lyophilized T_{am} sample enough time to crystallize.

9.3.2 SSNMR: Detection of Crystal Nuclei

Figure 9.6 shows the SSNMR analysis of Sample 1. The spectra in Figures 9.6a and 9.6b are consistent with the spectrum of amorphous trehalose and show no evidence of crystalline material. The subtracted spectrum (Figure 9.6c) contains three very small peaks at 90.7, 73.7, and 73.3 ppm. These chemical shifts correspond to carbons C5/C2', C4, and C1, respectively, in T_β . Crystallization of sample 1 during the DSC experiment began at about 181 °C and may have been facilitated by the presence of low levels of T_β in this sample.

Figure 9.7 shows the SSNMR analysis of Sample 1A. This is the same sample that was shown in Figure 9.6, but it was subjected to aging for 10 hours at 100 °C prior to analysis. The spectra in Figures 9.7a and 9.7b are consistent with the spectrum of amorphous trehalose; however, the spectrum in Figure 9.7a contains a slight irregularity at 69.0 ppm. Using only the spectrum in Figure 9.7a, it is difficult to conclusively determine if this irregularity is indicative of crystalline material. The subtracted spectrum shown in Figure 9.7c contains six small peaks at

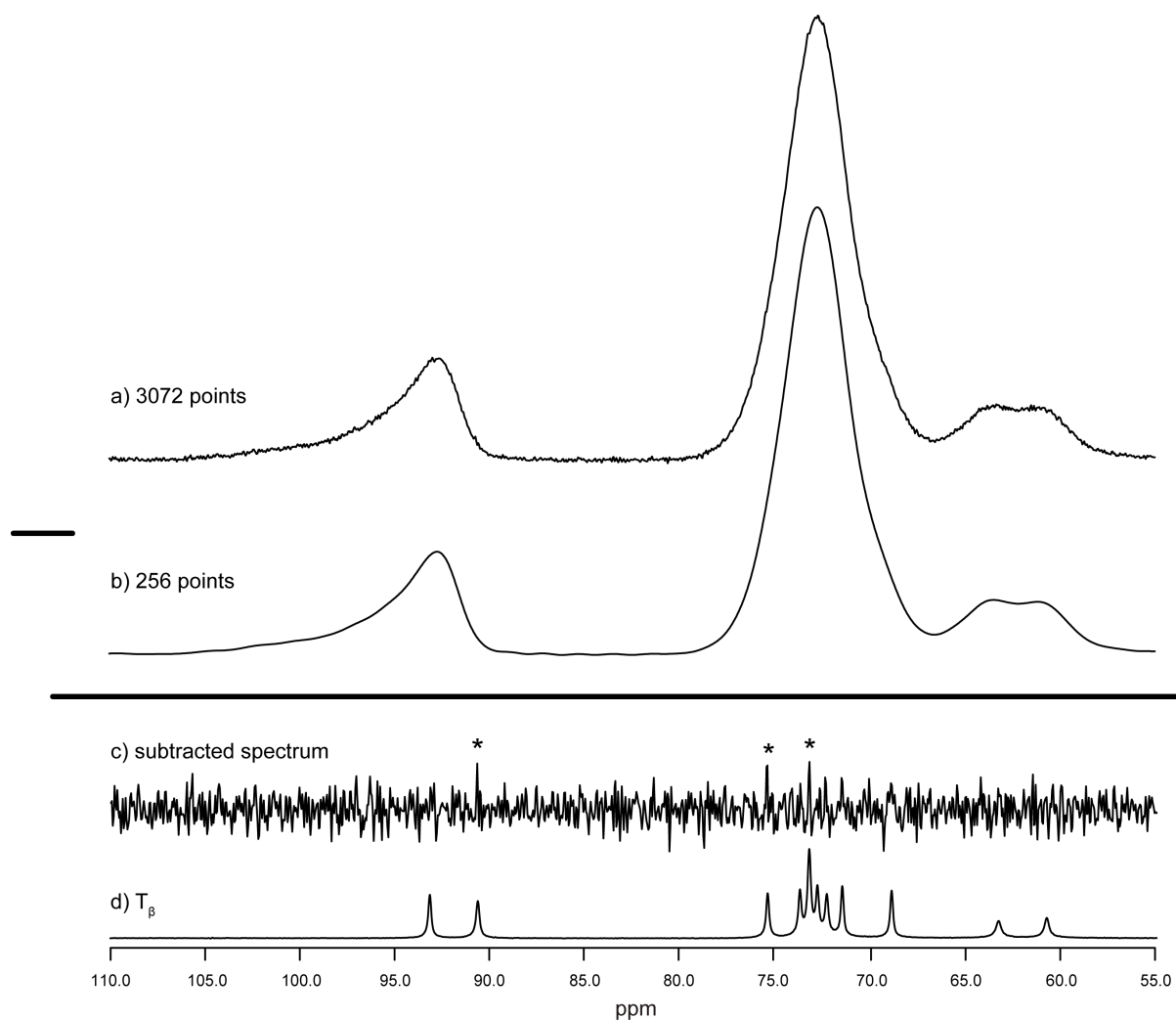


Figure 9.6. ^{13}C SSNMR spectra and spectral subtraction of Sample 1. Peaks in the subtracted spectrum corresponding to T_β are labeled with an asterisk (*).

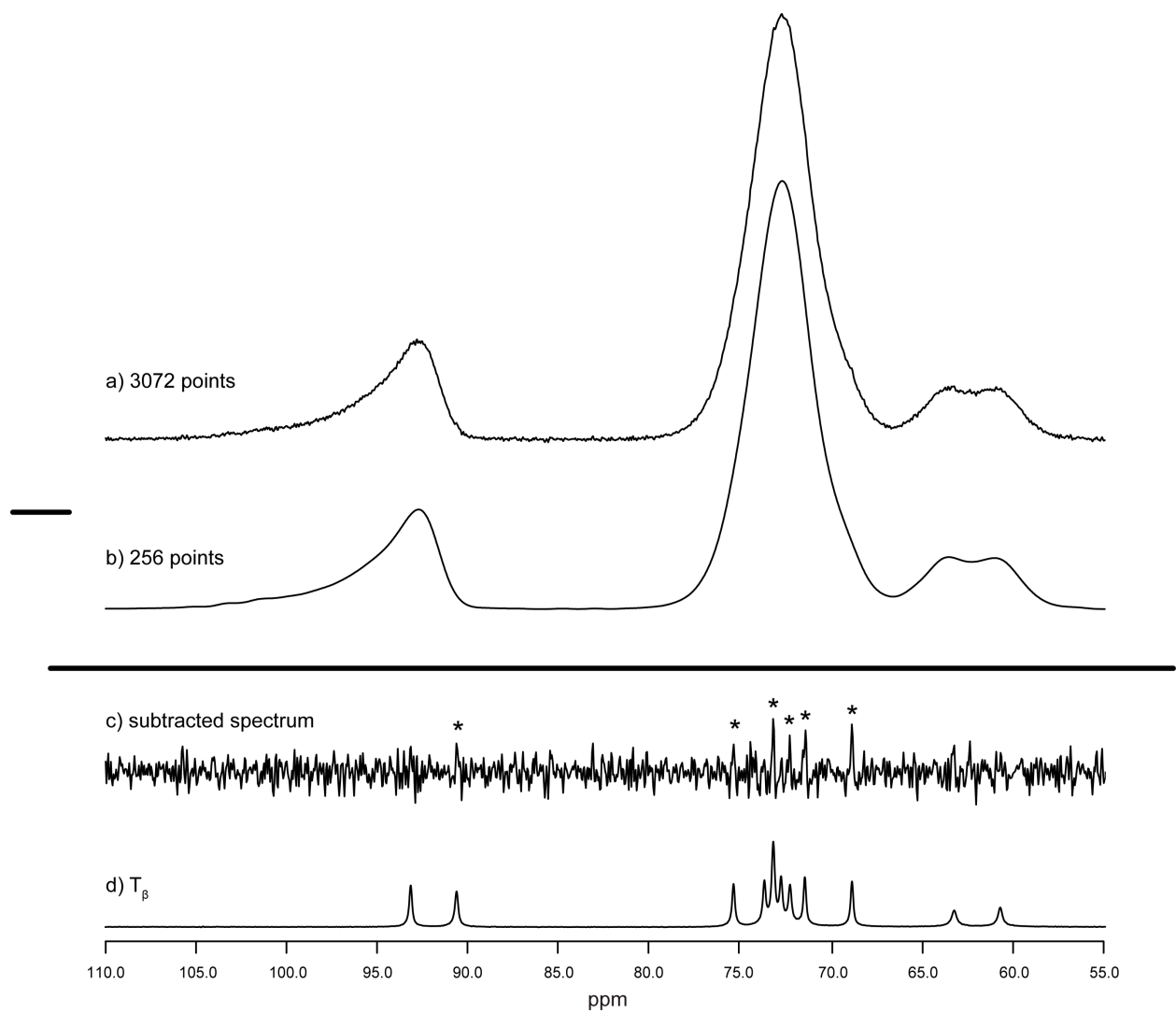


Figure 9.7. ^{13}C SSNMR spectra and spectral subtraction of Sample 1A. Peaks in the subtracted spectrum corresponding to T_β are labeled with an asterisk (*).

69.0, 71.6, 72.4, 73.3, 75.5, and 90.7 ppm, all of which correspond to carbons in T_β . Three of these peaks were detected in the subtraction that was performed on the sample prior to aging. The aged sample has a higher tendency to crystallize to T_β , as evidenced by a lower onset of crystallization and an increase in $\Delta H_{\text{crystallization}}$ and $\Delta H_{\text{melting}}$. The subtracted spectrum suggests that the concentration of T_β increases during aging, providing a reasonable explanation for the higher tendency to crystallize.

Figure 9.8 shows the SSNMR analysis of Sample 2, a sample that did not crystallize during the DSC experiment. The spectrum of the material prior to annealing at 110 °C shows that it is a mixture of T_α , T_δ , and T_{am} (Figure 9.8a). After annealing, the spectra (Figures 9.8b and 9.8c) are consistent with the spectrum of T_{am} , demonstrating that the mixture of metastable forms has completely transformed to the amorphous state. The subtracted spectrum in Figure 9.8d contains two small peaks at about 69.7 and 72.9 ppm. These locations correspond to carbons in T_α , indicating that the annealing time was not sufficient to transform all T_α to T_{am} . The subtracted spectrum does not contain peaks that correspond to T_β , which is consistent with the absence of crystallization during the DSC experiment.

Figure 9.9 shows the SSNMR analysis of Sample 3. Like sample 1, this material was prepared by rapidly dehydrating the dihydrate, though different starting materials were used. Interestingly, though this sample crystallized at a lower temperature than Sample 1 during the DSC experiment, there are no detectable peaks corresponding to T_β in the subtracted spectrum in Figure 9.9c. There are several possible reasons that could explain this. First, if crystalline material rather than nuclei has been detected in the previous samples, then the SSNMR acquisition conditions needed to detect crystal nuclei may not have been determined. Undetected

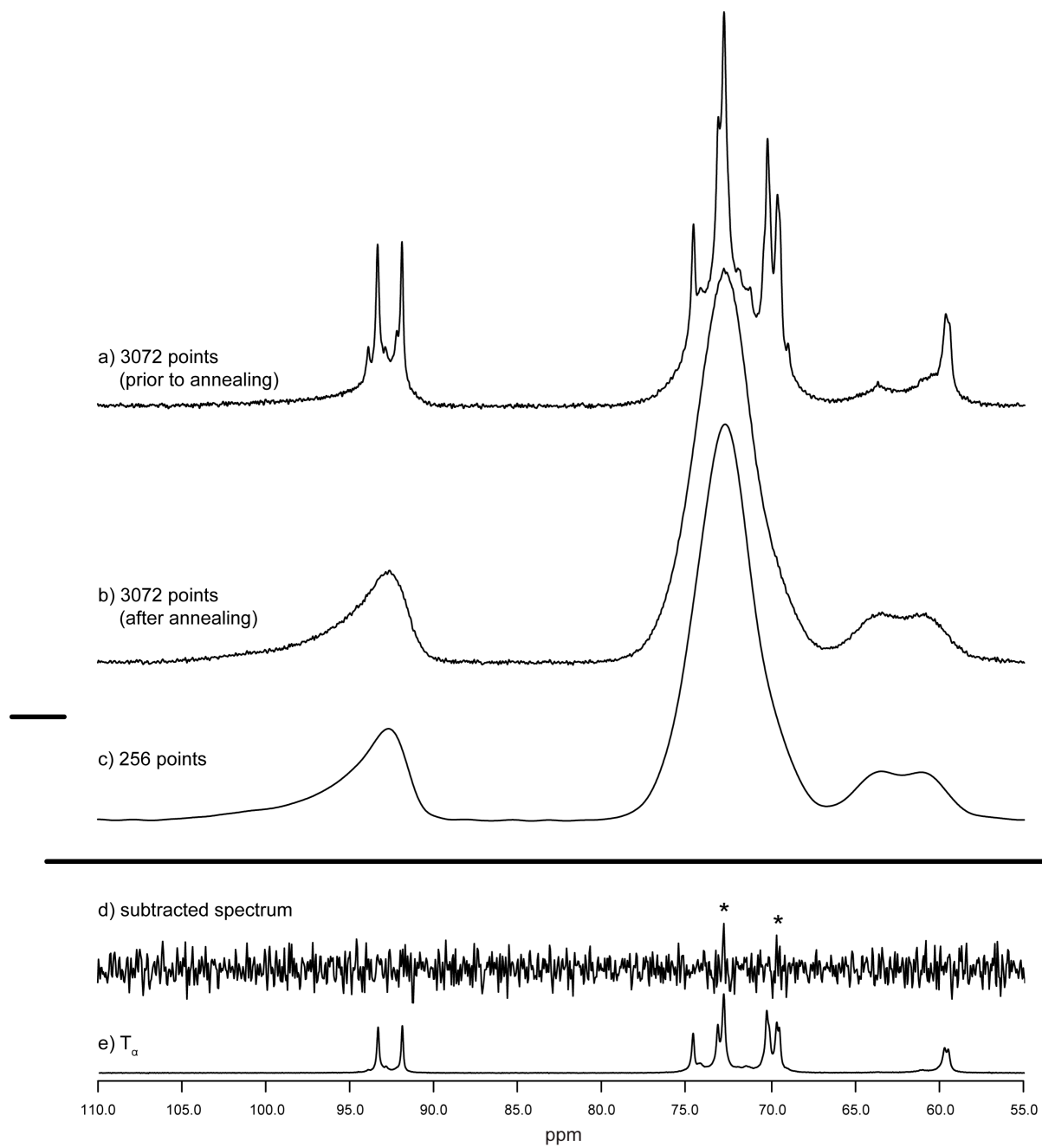


Figure 9.8. ^{13}C SSNMR spectra and spectral subtraction of Sample 2. Peaks in the subtracted spectrum corresponding to T_α are labeled with an asterisk (*).

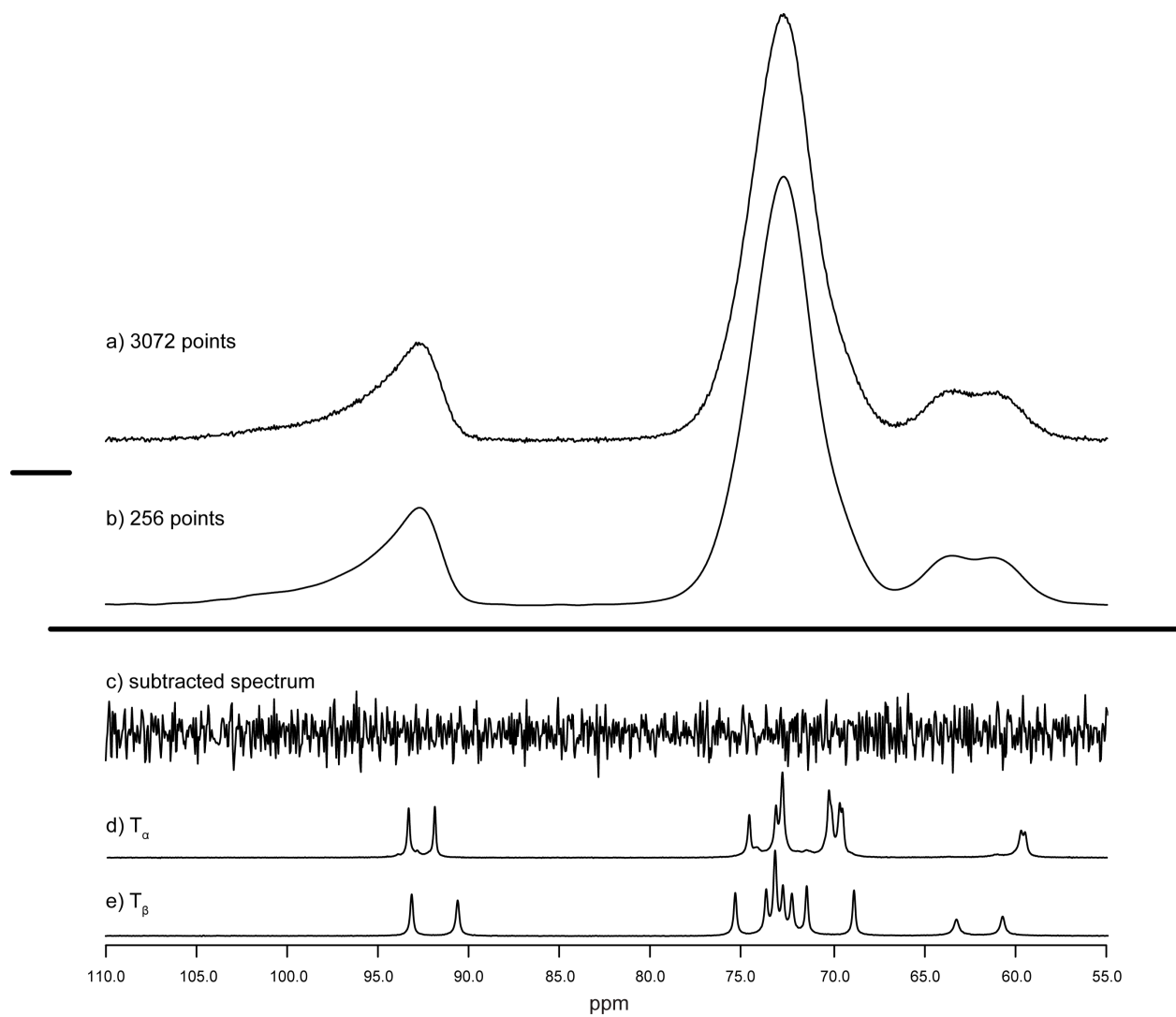


Figure 9.9. ^{13}C SSNMR spectra and spectral subtraction of Sample 3. No peaks are detected in the subtracted spectrum.

crystal nuclei of T_β may be present in this sample, and these could facilitate crystallization. Crystallization of this sample could also be promoted by something other than T_β , such as a greater concentration of defects. Even in disordered materials, higher-energy sites that promote crystallization can be present.

Figure 9.10 shows the SSNMR analysis of Sample 4. Like Sample 2, this sample was prepared by slowly dehydrating T_h to form a mixture of metastable forms (Figure 9.10a) and then annealed at 110 °C to convert the metastable forms to T_{am} (Figures 9.10b and 9.10c). The absence of peaks corresponding to T_β in the spectrum in Figure 9.10a shows that T_β was not formed directly, though it was shown in Chapter 6 that the Fluka 90208 sample of T_h (which was used to prepare Sample 4) shows a high tendency to convert to T_β directly under other dehydration conditions. In Figure 9.10b, there appears to be a small peak at 93.4 ppm, corresponding to one of the C1/C1' positions in T_α , and the subtracted spectrum in Figure 9.10d contains several peaks corresponding to both T_β and T_α . The T_α peaks indicate that the conversion of metastable forms to T_{am} was not complete, and the presence of T_β peaks in Figure 9.10d helps to explain why this sample crystallizes to T_β at the lowest temperature. Previously, crystallization of T_β during the annealing of mixtures of T_{am} and T_α has been observed.¹⁴ An unidentified peak at about 74.5 ppm is also present in the spectral subtraction in Figure 9.10d. This peak is commonly observed in samples that have been dehydrated at lower temperatures, and it can be seen in Figures 9.8a and 9.10a. In Chapter 5, this peak was observed in the spectra of dehydrated samples, and it was suggested that it might correspond to residual T_h . It typically disappears after annealing, but for Sample 4, it did not. This peak does not appear to affect the crystallization of these samples to T_β : it is present in both samples 2 and 4, and these samples have very different crystallization tendencies.

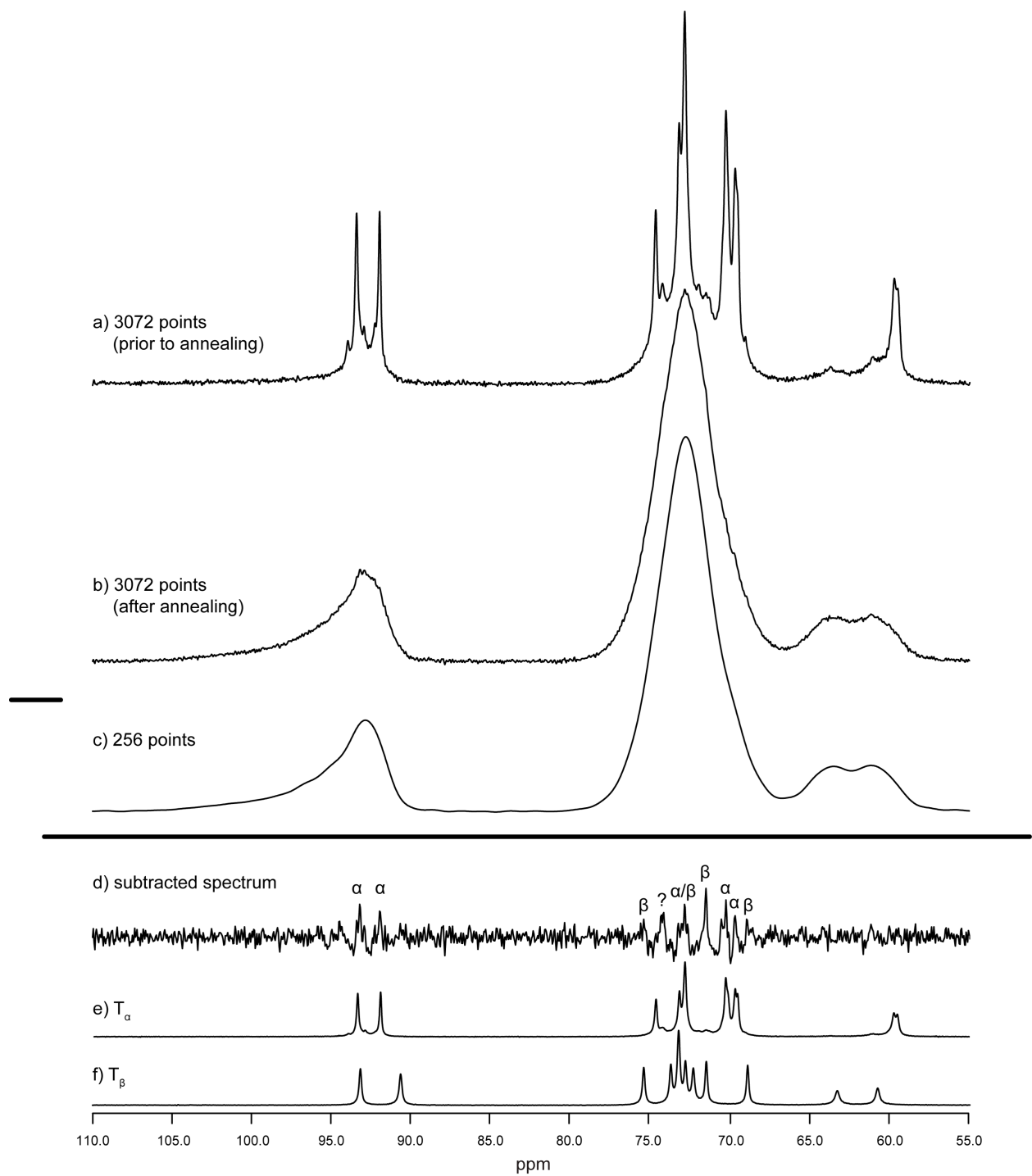


Figure 9.10. ^{13}C SSNMR spectra and spectral subtraction of Sample 4. Peaks in the subtracted spectrum corresponding to T_α and T_β are labeled with an asterisk. An unidentified peak is labeled with a question mark (?).

Figures 9.11 and 9.12 show the SSNMR analyses of samples 5 and 5A, respectively. Neither spectral subtraction (Figures 9.11c and 9.12c) contains peaks that can be distinguished from the noise. These samples did not crystallize to T_{β} during the DSC experiment, and it is therefore unsurprising that the spectral subtractions do not contain evidence of nuclei or low levels of T_{β} .

9.4 Conclusions

Detection of low levels of crystalline material, either T_{β} or T_{α} , in samples of amorphous trehalose, can be facilitated using the technique shown in Figure 9.5. Using this technique, no evidence of T_{β} was detected in three samples that did not crystallize to T_{β} during a DSC experiment performed at 10 °C/minute. For three of the four samples that crystallized during the DSC experiment, peaks corresponding to T_{β} were detected after performing spectral subtractions. For Sample 1, which showed an increased tendency to crystallize after aging, this technique suggested that there was an increase in T_{β} during aging. Most peaks fall below the traditional limit of detection (LOD) of signal-to-noise ratio (SNR) > 3:1; however, if more than one crystalline peak is detected, as was the case for all samples, the SNR requirements may be able to be relaxed. These results are preliminary and additional testing is needed, but this technique shows promise in identifying amorphous samples with low levels of crystalline material or nuclei.

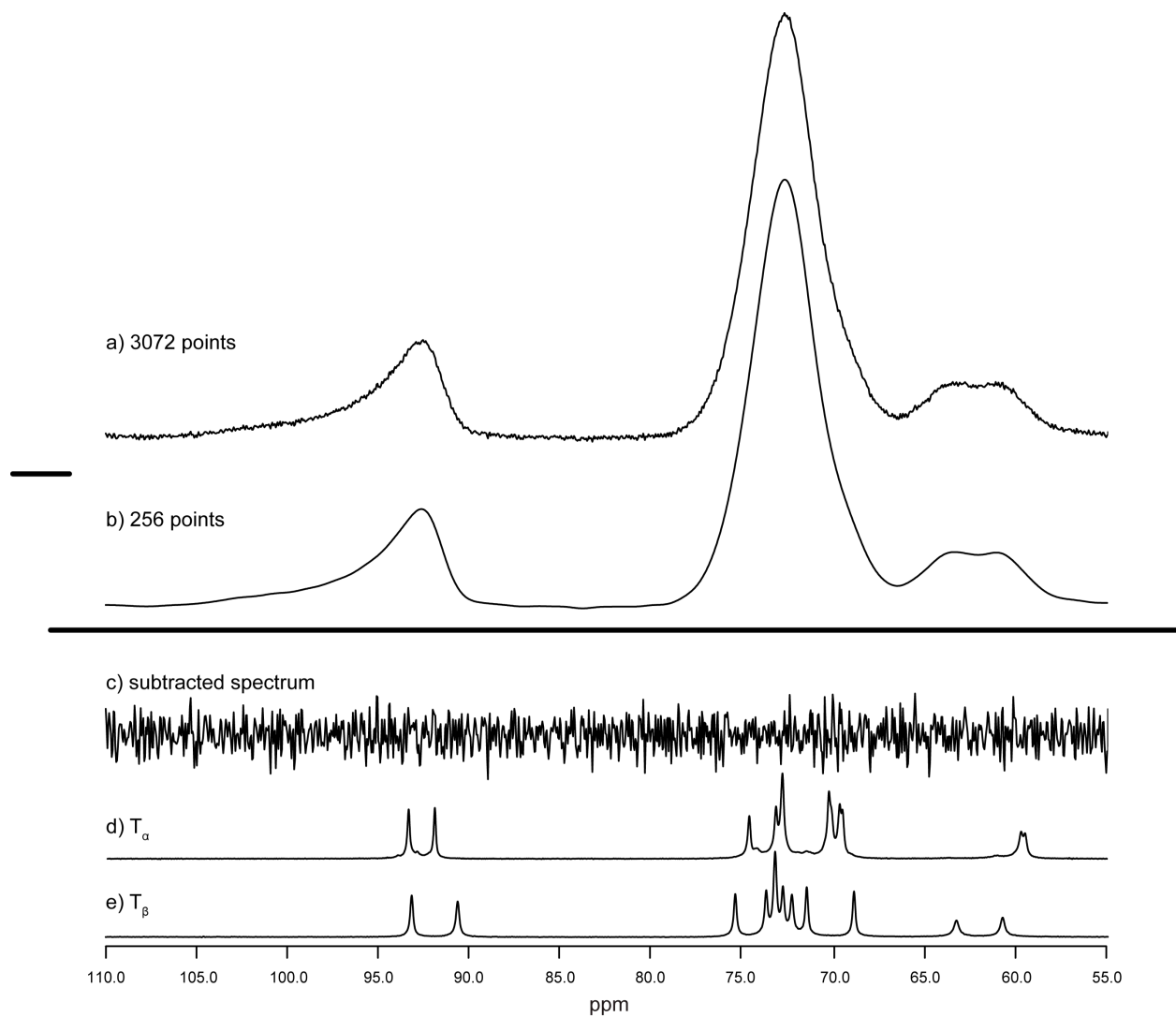


Figure 9.11. ^{13}C SSNMR spectra and spectral subtraction of Sample 5. No peaks are detected in the subtracted spectrum.

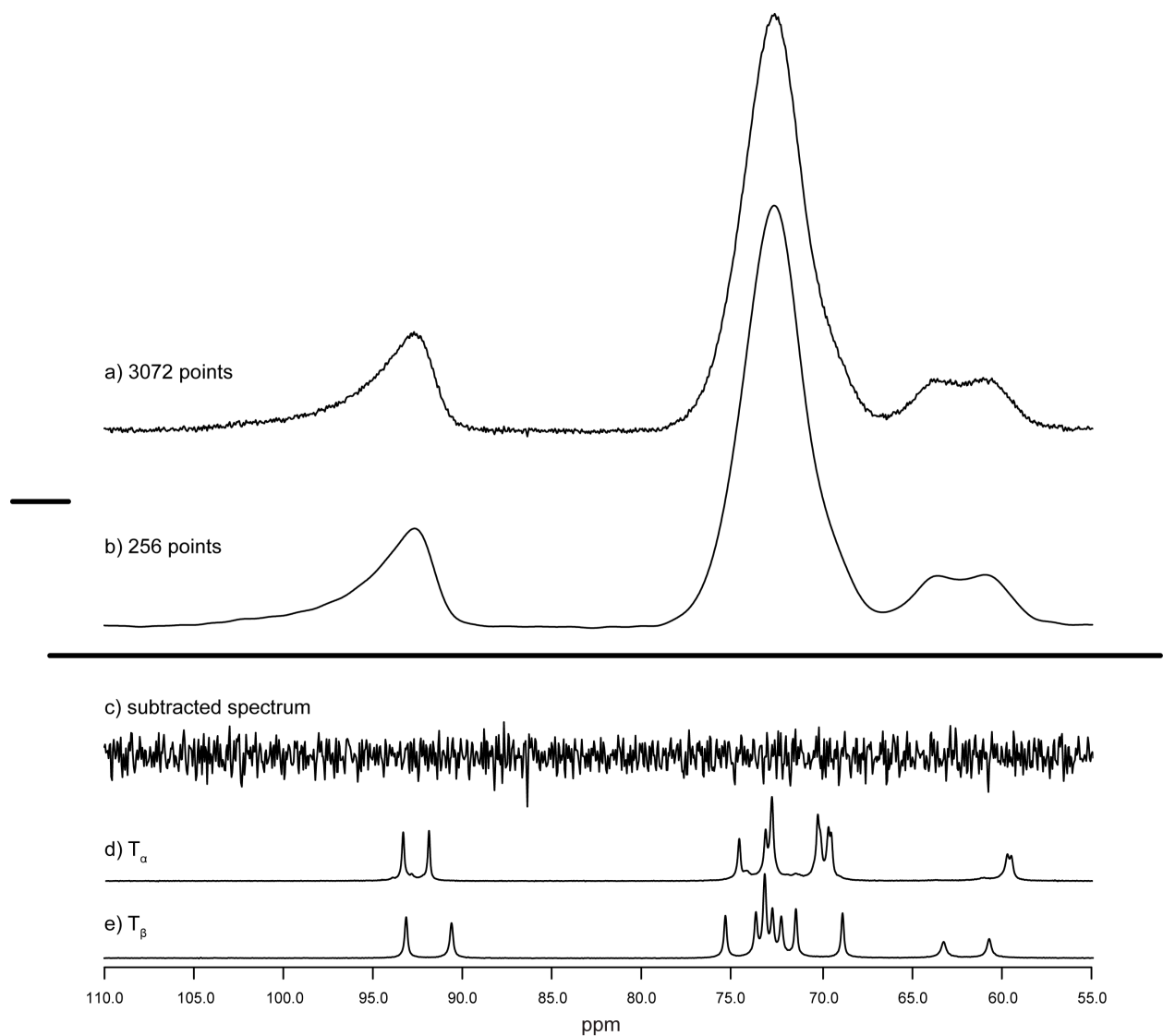


Figure 9.12. ^{13}C SSNMR spectra and spectral subtraction of Sample 5A. No peaks are detected in the subtracted spectrum.

9.5 References

1. Surana, R.; Pyne, A.; Suryanarayanan, R. Effect of preparation method on physical properties of amorphous trehalose. *Pharm. Res.* **2004**, *21*, (7), 1167-76.
2. Surana, R.; Pyne, A.; Suryanarayanan, R. Effect of aging on the physical properties of amorphous trehalose. *Pharm. Res.* **2004**, *21*, (5), 867-74.
3. Bhugra, C.; Pikal, M. J. Role of Thermodynamic, Molecular, and Kinetic Factors in Crystallization From the Amorphous State. *J. Pharm. Sci.* **2008**, *97*, (4), 1329-1349.
4. Nunes, C.; Mahendrasingam, A.; Suryanarayanan, R. Quantification of Crystallinity in Substantially Amorphous Materials by Synchrotron X-ray Powder Diffractometry. *Pharm. Res.* **2005**, *22*, (11), 1942-1953.
5. Andronis, V.; Zografi, G. Crystal nucleation and growth of indomethacin polymorphs from the amorphous state. *J. Non-Cryst. Solids* **2000**, *271*, (3), 236-248.
6. Konno, H.; Taylor, L. S. Influence of different polymers on the crystallization tendency of molecularly dispersed amorphous felodipine. *J. Pharm. Sci.* **2006**, *95*, (12), 2692-2705.
7. Schmitt, E. A.; Law, D.; Zhang, G. G. Z. Nucleation and crystallization kinetics of hydrated amorphous lactose above the glass transition temperature. *J. Pharm. Sci.* **1999**, *88*, (3), 291-296.
8. Andrew, A. R.; Bradbury, A.; Eades, R. G. Removal of dipolar broadening of nuclear magnetic resonance spectra of solids by specimen rotation. *Nature* **1958**, *183*, 1802-1803.
9. Barich, D. H.; Gorman, E. M.; Zell, M. T.; Munson, E. J. 3-Methylglutaric acid as a ^{13}C solid-state NMR standard. *Solid State Nucl. Magn. Reson.* **2006**, *30*, (3-4), 125-129.
10. Dixon, W. T.; Schaefer, J.; Sefcik, M. D. Total suppression of sidebands in CPMAS carbon-13 NMR. *J. Magn. Reson.* **1982**, *49*, (2), 341-345.
11. Fung, B.; Khittrin, A.; Ermolaev, K. An improved broadband decoupling sequence for liquid crystals and solids. *J. Magn. Reson.* **2000**, *142*, (1), 97-101.

12. Pines, A.; Gibby, M. G.; Waugh, J. S. Proton-enhanced NMR of Dilute Spins. *J. Chem. Phys.* **1973**, *59*, 569-590.
13. Lubach, J. W.; Xu, D.; Segmuller, B. E.; Munson, E. J. Investigation of the effects of pharmaceutical processing upon solid-state NMR relaxation times and implications to solid-state formulation stability. *J. Pharm. Sci.* **2007**, *96*, (4), 777-787.
14. Willart, J. F.; Hedoux, A.; Guinet, Y.; Danede, F.; Paccou, L.; Capet, F.; Descamps, M. Metastability Release of the Form α of Trehalose by Isothermal Solid State Vitrification. *J. Phys. Chem. B* **2006**, *110*, 11040-11043.

Chapter 10

Summary and Suggestions for Future Work

10.1 Summary

In this dissertation, several new insights into the solid-state forms and transformation of trehalose were described. Trehalose was previously thought to exist in four solid forms, a crystalline dihydrate (T_h), the β -anhydrate (T_β), the α -anhydrate (T_α), and the amorphous form (T_{am}), but ^{13}C solid-state NMR spectroscopy (SSNMR) was used to identify and characterize a fifth solid form, T_δ . The dehydration of T_h was shown to be significantly affected by the source and lot of the starting material, and a classification system was developed to describe the behavior. A sample of T_h can be classified based on the differential scanning calorimetry (DSC) thermogram of 75–125- μm particles, and this classification can be used to predict its dehydration behavior under various temperatures and scanning rates. Finally, the physical properties of T_{am} prepared via lyophilization and dehydration of T_h were investigated, and a new ^{13}C SSNMR analysis technique was used to identify low levels of T_β in several samples that displayed an increased tendency to crystallize to T_β upon heating.

10.1.1 Generation and Characterization of T_δ (Chapter 5)

T_δ is formed from dehydrations of trehalose dihydrate (T_h) performed at lower temperatures ($\leq 100\text{ }^\circ\text{C}$), and it is generated concurrently with T_α , T_{am} , and occasionally T_β . T_δ was detected using SSNMR but has not been detected with differential scanning calorimetry (DSC) or powder X-ray diffraction (PXRD). Upon exposure to ambient humidity, T_δ quickly reverts to T_h . When heated above $80\text{ }^\circ\text{C}$, T_δ converts to either T_α or T_{am} . The chemical shifts of the carbons in the primary alcohol groups (C6 and C6') suggest that these groups are in the

gauche-trans and gauche-gauche conformations, as they are in T_{β} and T_h . This study highlights the utility of SSNMR in studying the trehalose system.

10.1.2 Impact of Source and Lot-to-Lot Variability on the Dehydration of Trehalose Dihydrate (Chapters 6 and 7)

Variability of T_h strongly influences the anhydrous forms that are generated upon dehydration, providing an explanation for much of the confusion and inconsistencies that are present in the literature. In Chapter 6, a classification system to describe the dehydration behavior of sixteen sieved T_h samples that were heated at 10 °C/minute was developed. Upon dehydration, Type 1 samples tend to form T_{β} , Type 2 samples tend to form T_{am} that crystallizes to T_{β} , and Type 3 samples tend to form T_{am} that remains amorphous. Although differences in particle morphologies, 1H T_1 relaxation times, and sample purities were identified, these factors could not be correlated to the dehydration behavior.

In Chapter 7, the effect of source and lot-to-lot variability of T_h on isothermal dehydrations and dehydrations performed at other heating rates were investigated. Following slow dehydrations (2 °C/minute heating rate or isothermally at 75 °C) of T_h , similar mixtures of metastable forms (T_{α} , T_{δ} , and T_{am}) are generated; however, the mixture formed from dehydration of a Type 1 samples had a higher tendency to crystallize to T_{β} than the mixture formed from dehydration of Type 2 or Type 3 samples. When dehydrated quickly (20 °C/minute heating rate or isothermally at 125 °C), the Type 1 sample formed primarily T_{β} , the Type 2 sample formed a mixture of T_{am} and T_{β} , and the Type 3 sample formed T_{am} . This demonstrates the utility of the classification system to predict the dehydration behavior of T_h . Interestingly, if the first

dehydration of T_h at 100 °C (Chapter 4) had been performed on a Type 3 sample, the results would have been consistent with the literature,¹ and an investigation into the effects of source and lot-to-lot variability on the dehydration of T_h would not have been initiated.

10.1.3 Analysis of Physical Properties of Amorphous Trehalose (Chapters 8 and 9)

Following the development of two methods to prepare amorphous trehalose via dehydration of T_h , the physical properties of T_{am} prepared by rapid dehydration (125 °C) were compared to those of T_{am} prepared by lyophilization. DSC analyses showed that dehydrated T_{am} has a higher tendency to crystallize to T_β than lyophilized T_{am} and that aging at 100 °C increases the crystallization tendency of the amorphous samples. Although there are subtle differences between the SSNMR spectra of dehydrated T_{am} and lyophilized T_{am} , these differences do not indicate two distinct amorphous states of trehalose. Rather, it appears that lyophilization generates a more homogeneous, higher energy material than dehydration of T_h . A SSNMR spectral subtraction method was developed in order to detect low levels of T_β or nuclei of T_β in T_{am} samples and was used to show evidence of ordering in three of four T_{am} samples that crystallized to T_β during a DSC experiment. For three samples of T_{am} that did not crystallize, no evidence of T_β was detected.

10.2 Suggestions for Future Work

The research described in this dissertation has significantly advanced our understanding of the trehalose system, but it also provides motivation for a number of additional studies. A few suggestions for future work are described below.

10.2.1 Additional Characterization of T_{δ}

The ideal solid-state characterization of T_{δ} would include a single crystal X-ray diffraction analysis in order to determine the crystal structure of T_{δ} . However, we were unsuccessful in preparing pure samples of T_{δ} , and it may be impossible to control the dehydration so precisely as to avoid the concurrent formation of T_{am} and T_{α} . A pure sample, or perhaps even a sample containing just T_{am} and T_{δ} , will also be necessary to determine the melting point of the new form. It would be interesting to perform low temperature dehydrations of T_h as powder X-ray diffraction (PXRD) patterns are acquired and then subject these samples to SSNMR analyses. If no new peaks are present in the PXRD pattern but SSNMR indicates that T_{δ} is present, this could provide additional support for the suggestion that T_{δ} is the true isomorphous desolvate of T_h .

10.2.2 Further Investigation of Variability in Trehalose Dihydrate

We were successful in identifying the effects of source and lot-to-lot variability on the dehydration of T_h , but it is still unclear what causes the differences in dehydration behavior. It is likely a combination of several physical and chemical factors, making isolation of each factor challenging. The issue is complicated even further by the fact that different dehydration processes can occur within a single particle,² which may indicate that physical factors are a more likely source of the differences. Gentle grinding prior to dehydration facilitates the formation of metastable forms (§4.3.2), and by subjecting samples of each type to cryogrinding and/or ball-milling, it may be possible to determine if there is a level of disorder that results in different

types of T_h behaving similarly. Could sufficient disorder in a Type 1 sample prevent direct formation of T_β upon dehydration of T_h and prevent crystallization of metastable forms to T_β at lower temperatures? If so, this would suggest that the differences among the types result from physical differences.

Recrystallizations have the advantage of increasing both the chemical and the physical purity of a sample, and it would be of interest to examine the morphologies of T_h after repeated recrystallizations to determine if there is a point at which samples eventually display the same morphology. However, if recrystallization results in crystals with fewer defects and higher chemical purity, it may not be possible to conclusively determine which factor influences the dehydration. Following one recrystallization from water, the Sigma T9449-3 and Alfa Aesar A19434-2 samples maintained the shorter and longer morphologies, respectively. Perhaps some of the samples contain an impurity that preferentially interacts with one or more faces of the crystals, resulting in morphological differences? Possible impurities in T_h include, but are not limited to, reducing sugars, microbes, endotoxin, and heavy metals.³ Initial analyses of the metal content in a few samples did not indicate a trend among the forms, and solution HPLC analyses were also inconclusive.

The DSC thermogram of 75–125- μm particles of T_h allows one to determine if a sample of T_h can be made amorphous via dehydration at 125 °C, which could be of interest to manufacturers who are interested in efficient production of T_{am} for certain dosage forms. However, it is unclear if the different types of T_h will behave differently in lyophilized formulations, when the trehalose is dissolved in solution during manufacturing. The first step will be to continue the investigations from §4.3.3 and determine if T_{am} formed different types of

T_h have different physical properties. The next step would be to incorporate different types of trehalose into protein formulations and examine the properties of these formulations.

10.2.3 Characterization of Amorphous Trehalose

Amorphous trehalose can be prepared using many techniques,^{1, 4} and a logical continuation of the work described in Chapters 8 and 9 is to apply the same characterization methods to T_{am} prepared by spray-drying, milling or grinding of anhydrous forms, etc. The SSNMR subtraction technique described in Chapter 9 shows promise in the identification of substantially amorphous samples of trehalose that contain low levels of T_β or T_β nuclei. Next steps include: 1) examining the utility of this technique in analyzing other amorphous systems, 2) determining if quantitative statements can be made about the concentration of crystalline material in these systems, and 3) further investigating the SSNMR properties of crystal nuclei. The second and third steps pose the greatest challenge since it may be impossible to generate a sample of crystal nuclei for SSNMR analysis. Samples contain mixtures of lyophilized T_{am} (few nuclei) and T_β could be prepared, but these are not a good representation of an amorphous sample with a known quantity of nuclei.

10.2.4 Other Questions from the Literature

It has been suggested that amorphous trehalose dihydrate can be generated by cryogrinding.⁵ The concept of an “amorphous hydrate” implies that water molecules occupy the same positions as they do in the crystal structure of the hydrate, and it differs from the more widely accepted concept of a hydrated amorphous state. The glass transition of “amorphous T_h ”

is about 20 °C, requiring that analyses of its structure be performed at very low temperatures (< –30 °C) in order to prevent recrystallization. Variable-temperature SSNMR experiments would allow us to determine if the structure of “amorphous T_h ” differs from the structure of hydrated T_{am} .

10.3 References

1. Surana, R.; Pyne, A.; Suryanarayanan, R. Effect of preparation method on physical properties of amorphous trehalose. *Pharm. Res.* **2004**, *21*, (7), 1167-76.
2. Dupray, V.; Berton, B.; Ossart, S.; Atmani, H.; Petit, M.-N. Concomitant dehydration mechanisms in single crystals of α,α -trehalose. *Carbohydr. Res.* **2009**, *344*, 2539-2546.
3. Ohtake, S.; Wang, Y. J. Trehalose: Current Use and Future Applications. *J. Pharm. Sci.* **2011**, *100*, (6), 2020-2053.
4. Sussich, F.; Cesáro, A. Trehalose amorphization and recrystallization. *Carbohydr. Res.* **2008**, *343*, 2667-2674.
5. Megarry, A. J.; Booth, J.; Burley, J. Amorphous trehalose dihydrate by cryogenic milling. *Carbohydr. Res.* **2011**, *346*, 1061-1064.